Imperial College London

DESIGN OF PRINTABLE ELECTROACTIVE BIOMATERIALS FOR TISSUE ENGINEERING

Julian Michael Heck

February 2022

A Thesis Submitted for the Degree of

Doctor of Philosophy

At the Imperial College London

Department of Bioengineering

Supervised by Professor Rylie Green

Assistant Supervisor: Dr. Josef Goding

Collaborator Co-Supervisors: Prof. Paul Dalton and Prof. Robert Luxenhofer

Declaration of Originality

I hereby certify that the following work is my own and, to the best of my knowledge, has not been previously published as part of any other degree. All other sources have been referenced with footnotes and listed in a bibliography.

Julian Michael Heck

February 2022

Copyright Declaration

The copyright of this thesis rests with the author. Unless otherwise indicated, its contents are licensed under a Creative Commons Attribution-Non Commercial 4.0 International Licence (CC BY-NC).

Under this licence, you may copy and redistribute the material in any medium or format. You may also create and distribute modified versions of the work. This is on the condition that: you credit the author and do not use it, or any derivative works, for a commercial purpose.

When reusing or sharing this work, ensure you make the licence terms clear to others by naming the licence and linking to the licence text. Where a work has been adapted, you should indicate that the work has been changed and describe those changes.

Please seek permission from the copyright holder for uses of this work that are not included in this licence or permitted under UK Copyright Law.

to my uncles

Norman († 2020) and Paul († 2020)

Acknowledgments

There are a number of people I would like to thank for their support during my PhD. Firstly, I would like to thank my supervisor Rylie Green. Thank you for giving me the opportunity to do my PhD in your group. Even though the PhD period was sometimes ill-starred, I knew that you were behind me 100% at all times and always supported me on every single step of the way. I surpassed myself both as a person and scientifically. Without you, this would not have been possible.

Secondly, I would like to thank Josef "Joe" Goding. As my unofficial/official supervisor, you were involved in every single decision of the project. Thank you for your great ideas and consideration when the crazy German chemist came into the office with a weird idea again. Even outside of research, you were always there as a true friend and I could come to you with any problem, bureaucratic or personal. You are one in a million.

I would also like to thank my two co-supervisors, Paul Dalton and Robert Luxenhofer. Thank you for initially recommending me for this project and for supporting me afterwards. I would also like to thank you for the opportunity to do some part of my project in your labs. And, of course, for the many wonderful hours spent in Würzburg alongside my research.

I would like to thank the entire Rylie Green group. Starting with the Post Docs, namely Omaer Syed, Catalina Vallejo-Giraldo, Chris Chapman, Roberto Portillo-Lara and Bogachan Tahirbegi. Thank you for the great collaboration and support. Thanks also to the other PhDs, Alexey Novikov, Estelle Cuttaz, Sofia Peressotti, Martina Genta, Gilian Koehl and Emmanuel "Manolis" Kanelos. How boring the time would have been without you. I would especially like to thank Estelle, Manolis and Gilian. It all started with the four of us and without you I wouldn't have made it to the end. Many thanks also to Olivia Cauvi and the numerous students who did their work during my time in the group.

I would also like to thank Paul's and Robert's group. Thank you for welcoming me and for the wonderful time in Würzburg. In this context, I would like to mention Lukas Hahn, Dario Polzin, Robin Bissert, Daniel Nahm, Larissa Keßler, Thomas Robinson, Ezgi Bakirici and Christian May. As well as my two project partners Juliane Kade and Jochen Löblein.

Many thanks to my friends who accompanied me on this journey. Above all, I would like to thank Thomas Lorson and Florian Wittmann for taking the journey and visiting me during the difficult phases of the project. Many thanks to my two hockey teams, the Imperial College Mens 1s and Indian Gymkhana Hockey Mens 1s.

I would also like to thank my family, especially my grandmother, my parents and my two brothers for their financial and spiritual support. To Jessy, Samson and Pumba for their mental health support, cuddles and sporting activity during walks.

Lastly, I would like to thank my partner. Thank you for believing in me every single day, even when I didn't do it by myself. Thank you for having my back during the difficult phases. Thank you for accepting the

distance and still giving me love every day. Even when I was working through the night and you were questioning my approach, I knew at all times that I could rely on you. Thank you so much Dani.

Abstract

Conducting polymers (CPs) possess unique electrical and electrochemical properties and hold great potential for a wide range of applications in the field of bioelectronics. However, the widespread implementation of CPs in this field has been critically hindered by their poor processibility. There are four key elements that determine the processibility of CPs, which are thermal tunability, chemical stability, solvent compatibility, and mechanical robustness.

This research aimed to create processible CP-based systems that were compatible with 3D printing techniques. It was hypothesised that by introducing a thiophene ring in the side group of polyoxazolines (POx) and polyoxazines (POzi), would produce a new class of polymers with the processability of POx and POzi, with the electrical functionality of CPs. For this purpose, eight monomers were first prepared by Seeliger and Wittig reactions. Here, the first crystal structures of Ox and Ozi were produced, as four of these monomers were present in solid phase at room temperature.

The polymerisation of these monomers followed a cationic ring-opening polymerisation (CROP). Poly(2-thiophene-3-oxazine) (P2Th3OZi) was obtained at high yield and efficiency. This polymer was further investigated as a feed for 3D printing. P2Th3Ozi was found to have good solubility in many organic solvents including chloroform and toluene. It possessed ideal thermal properties for melt-processing techniques such as melt electrospinning writing (MEW). Post-fabrication treatment of P2Th3Ozi scaffolds with water demonstrated swelling behaviour and amelioration of initially brittle mechanical properties. Since P2Th3Ozi was found to have low conductivity in its native state, further modification via intermolecular crosslinking with thiophene monomers in the presence of ferric chloride was explored, resulting in a 20-fold increase in conductivity.

Cytotoxicity studies demonstrated low toxicity of P2Th3OZi following adequate washing to remove solvents used for polymer synthesis. Printed scaffolds of P2Th3OZi were also found to promote cellular attachment and spreading along the scaffold structures. Future studies will focus on improving the electrical properties of the scaffolds. This new class of monomers have the potential to be a technology platform for the bespoke development of printable scaffolds in tissue regeneration.

Contents

Declaration of Originality III

Copyright Declaration IV

Acknowledgments V

Abstract VII

Contents VIII

List of Figures XII

List of Tables XVIII

Abbreviations XIX

Publications XXIV

journal papers XXIV

planned journal papers XXIV

conferences XXIV

Chapter 1 – Introduction 1

1.1 Motivation 2

1.2 Project Overview, Hypothesis and Aims 3

1.3 Thesis Structure 5

Chapter 2 – Background Information 6

2.1 Conducting Polymers 6

2.1.1 Mechanism of Conduction 7
2.1.2 Fabrication of CPs 9
2.1.3 Properties of CP 13
2.1.4 Chemical stability and influence of dopant counterions 13
2.1.5 Thermal properties of CPs 15
2.1.6 Solubility of CPs 18
2.1.7 Mechanical properties of CPs 20
2.1.8 Limitations of CPs 21
2.1.9 Processability via Chemical Modification 22
2.2 Polyoxazoline and Polyoxazine 24
2.2.1 Synthesis of POx and POzi 26
2.2.2 Physicochemical Properties of POx and POzi 31
2.2.3 Biological Properties of POx and POzi 32
2.2.4 Limitations and Potential of POx and POzi 32
2.3 Processability of CPs via Additive Manufacturing 34
2.3.1 Melt Electrospinning Writing (MEW) 37
2.3.2 MEW Applications of CPs 40
2.4 Conclusion 41
Chapter 3 – Synthesis of Thiophene-based Ox and Ozi 43
3.1 Introduction 43
3.2 Aims and Hypotheses 45

3.3 Results and Discussion 46
3.4 Conclusion 55
3.5 Experimental section 56
3.5.1 Materials and Equipment 56
3.5.2 Characterisation and Analysis of Material 56
3.5.3 Synthesis of thiophene-based Ox and Ozi monomers 58
3.6 Summary of thiophene-based Ox and Ozi monomer properties 60
Chapter 4 – Exploring the Polymer behaviour of thiophene-based Ox and Ozi 63
4.1 Introduction 63
4.2 Aims and Hypotheses 66
4.3 Results and Discussion 67
4.3.1 Synthesis of novel polymer platform 67
4.3.2 Solubility of thiophene-based POx and POzi 80
4.3.3 Swelling properties of P2Th3Ozi 82
4.3.4 Mechanical properties of P2Th3Ozi 84
4.3.5 Electrical properties of P2Th3Ozi 85
4.4 Conclusion 89
4.5 Experimental Section 90
4.5.1 Materials 90
4.5.2 Polymer synthesis and end-group functionalisation 90
4.5.3 Characterisation and Analysis 94

4.6 Summary of POx and POzi properties 102

Chapter 5 – Exploring the polymer platform of P2Th3Ozi 104

5.1 Introduction 104

5.2 Aims and Hypotheses 106

5.3 Experimental Section 107

5.3.1 Materials 107

5.3.2 Characterisation and Analysis 107

5.4 Results and Discussion 115

5.4.1 MEW 3D printing of P2Th3Ozi 115

5.4.2 Swelling studies of printed scaffolds 123

5.4.3 Biological properties of P2Th3Ozi 127

5.4.4 Post-modification of P2Th3Ozi printed scaffolds 133

5.5 Conclusion 137

Chapter 6 – Summary and Outlook 139

Chapter 7 Bibliography 143

Chapter 8 Appendices 160

List of Figures

Figure 2.1 a) Polyacetylene, b) Poly(ethylenedioxythiophene) 7

Figure 2.2 Doping of polythiophene. Reproduced from Le et al.,[58] with permission..... 9

Figure 2.3(a – c) principle of electrodeposition of PPy onto a gold (AU) electrode, Reproduced from Chen et al.[73] with permission, copyright 2018, Elsevier d) electrode setup. , Reproduced from Rao et al.[75] with permission..... 11

Figure 2.4 Example of chemical polymerisation route for thiophene-based monomers. Reproduced from Khalid et al.[79] with permission 12

Figure 2.5 SEM image showing thermal annealing of PANI-base at Rt (a), 160°C(b), 180°C (c), 200 °C (d)). Reproduced from Lu et al.[116], with permission. (e)TGA graph of PANI. Reproduced from Alam et al.,[118] with permission. 18

Figure 2.6 Delamination and cracking of PEDOT coating on stainless steel electrodes. Reproduced from Qu et al.,[143] with permission. 20

Figure 2.7 The effect of DMSO and Zonyl on the mechanical properties of PEDOT:PSS. Reproduced from Savagatrup et al.,[148] with permission. 21

Figure 2.8 Polyurethane/PEDOT:PSS composite electrodes. Exposed electrode sites are 900 µm in diameter. Reproduced from Cuttaz et al.[153] with permission. 22

Figure 2.9 Functionalisation of EDOT monomers with (**a**) imidazolium salts, (**b**) methacrylate (**c**) pyrimidine bases, (**d**) thiole, (**e**) azide, and (**f**) amino group. Reproduced from Mantione et al.,[155] with permission..... 23

Figure 2.10 General structure of polypeptides (left) vs polyoxazoline (right)..... 26

Figure 2.11 Synthesis of Ox and OZi monomers by a) Wenker using Carboxy acid, amino alcohols and a metal catalys, b) by Seeliger and Wittig using carbonitriles, amino alcohols and zinc acetate, c) by α-deprotonation of MeOx or MeOzi..... 27

Figure 2.12 Initiation of polymerisation mechanism of POx 28

Figure 2.13 Propagation of polymerisation mechanism of POx 30

Figure 2.14 Termination propagation of polymerisation mechanism of POx by nucleophilic attack 30

Figure 2.15 Roll-to-roll method for conductive polymer coating. Reproduced from Hu et al.[199] with permission. 35

Figure 2.16 (a) Inkjet printing of PEDOT:PSS; (b) Printable inks made with different concentrations (1 to 10 wt %) of PEDOT:PSS. Reproduced from Yuk et al.[202] with permission. 36

Figure 2.17 (a) Different ratios of PEDOT:PSS/PEGDA used for stereolithographic fabrication; (b) Pristine PEGDA and PEGDA:PEDOT (5:1) hydrogels. Reproduced from Scordo et al.[208] with permission. ... 37

Figure 2.18 (a) Different patterns printed using photocurable PEDOT/PSS hydrogels. (b) Cells derived from dorsal root ganglia encapsulated in GelMA with 3D printed PEDOT/PSS hydrogels. Reproduced from Heo et al.[209] with permission. 37

Figure 2.19 MEW printed scaffold of PCL with a resolution of 100 µm 38

Figure 2.20 Formation of different cone jets[209] 39

Figure 2.21 a) MEW printing setup with the printing head, collector and electrical connections b) processing parameters, which can occur during printing with different printing parameters 39

Figure 2.22 Structure of (a) oligo-EDOT (b) copolymerised with caprolactam, (c) crosslinked with 8-arm PEG. Reproduced from Ritzau-Reid et al.[211] with permission. 41

Figure 3.1 Synthesis of thiophene-based monomers 44

Figure 3.2 Synthesis of EDOT-acetontrile via Kolbe-Ntrile synthesis 46

Figure 3.3 Synthesis of 2-EDOT-2-ethyl-oxazoline with n-BuLi and TMEDA analogous to Taubmann et al.[196] 48

Figure 3.4 H,H-COSY-NMR spectrum of EDOT-6-ethyl-2-oxazoline. A succesful synthesis can be seen by cross peak's („square" formation), which identfies a coupling oft wo nucleis. Here, the coupling of methyl-group in the fourth position of the Chlormethyl-EDOT (~4.3 ppm) and the methyl-group of Ox (~1.9 ppm) was detected 48

Figure 3.5 IR spectrum of 3-thiophene-2-oxazine. Identification of functional groups are presented as red lines 49

Figure 3.6 1H-NMR-Spektrum (CdCl3, 7.26 ppm) of 3-thiophene-2-oxazoline..... 50

Figure 3.7 1H-NMR-Spektrum (CdCl3, 7.26 ppm) of 3-thiophene-2-oxazine..... 51

Figure 3.8 crystal structures of A) 2-thiophene-2-oxazoline, B) 2-thiophene-2-oxazine, C) 2-thiophene-3-oxazoline, D) 2-thiophene-3-oxazine..... 52

Figure 3.9 2-EDOT-2-ethyl-oxazoline..... 58

Figure 4.1 Overview of polymer synthesis approaches..... 66

Figure 4.2 Termination of PEtOx with Methoxy-EDOT..... 67

Figure 4.3 Initiation with of MeOc with Tosyl EDOT and termination with methanol and KOH..... 67

Figure 4.4 a) ^{1}NMR spectrum of PEtOx initiated with EDOT-tosylate for the synthesis of EDOT-P(EtOx)-OH, b) GPC of EDOT-P(EtOx)$_{30}$-OH show monodispers distriution 69

Figure 4.5 a) general polymerisation and copolymerisation of poly(thiopheneoxazoline/oxazines) via CROP and initiated with MeOTF in BCN, b) Representative GPC of poly(2-thiophene-3-oxazine) (P2t3Ozi) shows monodisperse distribution, c) ^{1}H-NMR spectrum of P(2t3Ozi)$_{25}$..... 71

Figure 4.6 MALDI-TOF spectrum of a) P2t2Ox$_{25}$ and b) P2t3Ox$_{25}$. As seen in both graphs, the polymers follow a poison distribution 73

Figure 4.7 a) DSC analysis of various PtOx and PtOzi show peaks at glass transition b) TGA of P2t3Ozi with different chain length. A thermal stability till approx. 350 °C can be seen 74

Figure 4.8 IR spectrums of P2Th3Ozi before and after treating show almost identical peaks 75

Figure 4.9 XRD analysis of P2Th3Ozi before (red) and after treatment with water (black), with water while heated (blue) and only heated (green) show no significant varieties..... 76

Figure 4.10 XRD analysis of crystallinity of untreated (red) and treated P2Th3Ozi with water (black), with water while heated (blue) and only heated (green)..... 77

Figure 4.11 First order kinetics of polymerisation of tOx and tOzi. All polymers show a linearity for the first 6 hours of polymerisation 79

Figure 4.12 Swelling properties of P2Th3Ozi a) swelling vs time, b) swelling vs temperature. The swelling of P2Th3Ozi depends on the temperature of water and most of the swelling was done in the first 10 hours 83

Figure 4.13: Mechanical properties of P2Th3Ozi. a) macroscopic view of mechanical properties of treated (H_2O) P2Th3Ozi, b) Youngs modulus of (un)treated P2Th3Ozi ($n \geq 6$). Literature values are used for PEtOx, PEDOT:PSS hydrogel produced by Lu et al. and PU/PEDOT:SS produced by Cuttaz et al. 85

Figure 4.14 Post-modification of polythiophene oxazines can lead to two different transition structures (1. intermolecular crosslinking, 2. Intramolecular crosslinking) 86

Figure 4.15: DLS measurment of Stokes radius and mass diffusion of thiophene-based POx and POzi (n=8) show a stokes radius between 1,5 and 2 nm and mass diffusivity of ~$2*10^{-6} m^2/s$ 87

Figure 4.16 a) Conductivity values of P2Th3Ozi + FeCl3, b) UV-VIS spectrum of P2Th3Ozi + FeCl3 shows a shift between pure polymer and polymer/$FeCl_3$ 88

Figure 4.17 EDOT-tosylate 90

Figure 4.18 EDOT-P(EtOx)-OH 91

Figure 4.19 Temporal dependence of the interparticle Interference 96

Figure 4.20 Seperation function of GPC measurement against time. Small polymer have a longer retention time than bigger polymers 97

Figure 4.21 Energy level of MO and the excited states. Irradiation of the sample leads to excitation and thus to electron transitions. Excited electron transitions can be $n \rightarrow \pi^*$ and $\pi \rightarrow \pi^*$ 101

Figure 5.1 Setup of a MEW printing device[270] 108

Figure 5.2 Design of printed scaffolds[271] 109

Figure 5.3 Reduction of MTS to form formazan 112

Figure 5.4 Cell alignment and orientation of nuclei[275] 114

Figure 5.5 Images demonstrating the stacking and fibre accuracy of P(3Th3Ozi)25 a) SEM before adjustment, b) light microscope before adjustment. c) SEM before adjustment, d) Light microscope after adjustment. The adjusement was carried out by changing the printing parameters like speed, pressure or voltage. Before adjustment, single fibers can be identified, and agglutination is observed. After adjustment, a clean scaffold with rectangular structure was obtained. 115

Figure 5.6 Fiber diamater fluctuation of P2Th3Ozi40. Before optimising the printing parameters, the printed fibers verified between 10 – 60 µm..... 116

Figure 5.7: Scaffold clumping effect at collector plate temperature > 50°C 118

Figure 5.8 Broken fibers of P2Th3Ozi after printing. Due to the limited mechanical properties of the material and the thin fiber diameter (~35 µm), little forces applied to the fibers can damage them. 119

Figure 5.9 different printing speed and analysis of CTS for P2Th3Ozi. The figure shows printed fibers at 300, 700 and 1000 mm/min. At lower speed, printed fibers were not obtained, while printing and higher speed, straight lines were possible 121

Figure 5.10 a) Printing of P2Th3Ozi through a gap (~ 2mm) was possible (loose of the homogeneous electrical field) and b) fibre stacking properties and diameter of P(2Th3Ozi)25..... 122

Figure 5.11 Swelling behaviour of printed scaffolds at different temperatures. Untreated scaffolds were swelled in water at different temperatures (4 °C, Rt & 37 °C)..... 123

Figure 5.12 SEM images of printed fibre a) without treatment with water and at different temperatures b) 4 °C, c) Rt, d) 37 °C..... 124

Figure 5.13 Cryo-SEM image of water treated fibres. As seen in the figure, water is encapsuled inside the porous structure 125

Figure 5.14 PBS treated P2Th3Ozi scaffolds over time at At and 37 °C. Over time, a loose of the grid structure can be observed. Higher temperature reinforce this observation 126

Figure 5.15 dynamic analysis of printed P2Th3Ozi scaffolds treated in water by light microscopy at At. The grid structure is dissolved and “material clumping centres” were formed 126

Figure 5.16 ^{1}H-NMR-spectrum of different purifications methods..... 128

Figure 5.17 Projected cell numbers of different purification treatments. Error is represented as SE, (N=3, n=3 with a minimum of 15 images analysed for each condition), * ANOVA $p < 0.05$ 129

Figure 5.18 Live/dead assay of C2C12 cells on different treated P2Th3Ozi. a-d) Repreentative confocal images of cells for specific treatments: a) Control 24h, b) Treatment 1, c) Treatment 5, d) Treatment 6. e) Perecentage of live cells. Error is represented es SE (N=3, n=3), *$p<0.05$ f) Live cell density (number of cells per mm^2), Error is represented es SE (N=3, n=3), *$p<0.05$ 131

Figure 5.19 Representative images of cell alignment on P2Th3Ozi scaffolds 132

Figure 5.20 Representative image of elongination analysis of P2Th3Ozi scaffolds 133

Figure 5.21 Histogram of the relative Cell elongiation measurment 133

Figure 5.22 a) macroscopic image of printed scaffold untreated, b) light microscopy image of post-modification synthesis, c) SEM image of post-modification scaffolds 134

Figure 5.23 EDX SEM analysis of post-modification scaffolds 135

Figure 5.24: Initial ratio of Ironcloride vs P2Th3Ozi:Cl ratio measured by EDX analysis after post-modification 135

Figure 5.25 a) printing syringe filled with $FeCl_3$ and P2t3Ozi before and after heating for 2 hours, b) comparison of non-treated and with $FeCl_3$ additive printed fibres 136

Figure 5.26 EDX SEM analysis of coaxial printed fibres with PVDF and P2t3Ozi 137

List of Tables

Table 2.1 Glass transition temperature (T_g) of different conductive polymers. 17

Table 2.2 Conductive polymers in AM fabrication 34

Table 3.1 Conditions (temperature, solvent and nucleophil) of Kolbe nitrile synthesis strategies of EDOT-oxazine 47

Table 3.2 Selected crystallographic data for 2Th2Ox, 2Th2Ozi, 2Th3Ox and 2Th3Ozi 52

Table 3.3 Summary of monomer properties (Yield, MP, Phase and BP) 54

Table 3.4 Overview of synthesised monomers 59

Table 4.1 Number average of Molar Mass, polydispersity, T_g, yield of synthesized polymers 72

Table 4.2 Solubility overview of monomers and polymers 81

Table 4.3 Polymerisation quantities of thiophene-based monomers 91

Table 5.1 Table of different purification treatments 111

Table 5.2 Printing properties of P2t3Ozi15;25;40 and P(3t2Ozi)20-ran-P(n-propyl-2-Ox)5 117

Table 5.3 Fibre size analysis via SEM images and ImageJ ($n \geq 50$) 124

Abbreviations

As a general notation in the scope of this thesis, analogous to the literature, 4,5-dihydrooxazole will be simplified and expressed as oxazoline (Ox) and the higher homologue 5,6-dihydro-4H-1,3-oxazine as oxazine (Ozi)

2At2Ox	2-acetothiophene-2-oxazoline
2At3Ox	2-acetothiophene-3-oxazoline
2At2Ozi	2-acetothiophene-2-oxazine
2At3Ozi	2-acetothiophene-3-oxazine
2Th2Ox	2-thiophene-2-oxazoline
2Th3Ox	2-thiophene-3-oxazoline
2Th2Ozi	2-thiophene-2-oxazine
2Th3Ozi	2-thiophene-3-oxazine
AM	Additive manufacturing
CAD	Computer-aided design
CE	Conductive elastomers
CH	Conductive hydrogels
CP	Conducting polymers
CROP	Cationic ring polymerization
CS	Collector speed
CSC	Charge storage capacity
CV	Cyclic voltammetry

DCM	Dichloromethane
DEP	Diethyl phthalate
DIBP	Diisobutyl phthalate
DLS	Dynamic light scattering
DMSO	Dimethylsulfoxide
DSC	Differential scanning calorimetry
EDOT	3,4-ethylenedioxythiopene
EDOT-Me	3,4-ethylenedioxythiopehene methanol
EIS	Impedance spectroscopy
ESCRM	Electrochemically stimulated conformational relaxation model
EtOx	Ethyl-oxazoline
FD	Fibre distance
FDM	Fused deposition modelling
GelMa	Gelatin methacryloyl
GPC	Gel permeation chromatography
HFIP	Hexafluoro isopropnaol
HSkM	Human skeletal myoblasts
IL	Ionic liquids
LCROP	Living cationic ring polymerisation
LCST	Critical solution temperature
MeOTf	Methyl trifluoromethanesulfonate

MEOx	Methyl-oxazolines
MEW	Melt electrospinning writing
MTS	Metabolic assay
NMR	Nuclear magnetic resonance
NT	Needle temperature
OTs-EDOT	3,4-ethylenedioxythiopene tosylate
Ox	Oxazoline
Ozi	Oxazine
P2At2Ox	Poly(2-acetothiophene-2-oxazoline)
P2At3Ox	Poly(2-acetothiophene-3-oxazoline)
P2At2Ozi	Poly(2-acetothiophene-2-oxazine)
P2At3Ozi	Poly(2-acetothiophene-3-oxazine)
P2Th2Ox	Poly(2-thiophene-2-oxazoline)
P2Th3Ox	Poly(2-thiophene-3-oxazoline)
P2Th2Ozi	Poly(2-thiophene-2-oxazine)
P2Th3Ozi	Poly(2-thiophene-3-oxazine)
PAA	Poly (acrylic acid)
PANI	Polyanilines
PBS	Phosphate-buffered saline
PCL	Polycaprolactam
PDAS	Poly(diphenylamine-4-sulfonic acid)

PDI	Poly dispersity index
PEDOT	Poly(3,4-ethylenedixoythiophene)
PEDOT:PSS	Poly(3,4-ethylenedioxythiophene) polystyrene sulfonate
PEG	Polyethyleneglycol
PEGDA	Poly(ethylene glycol) acrylate
PET	Polyethylene terephthalate
PLLA	Poly-l-lactide
PMeOx	Poly(methyl-oxazoline)
POx	Poly(oxazoline)
POzi	Poly(oxazine)
Ppy	Polypyrroles
PSSA	Polystyrene sulfonic acid
PThOx	Poly(thiophene-oxazoline)
PThOzi	Poly(thiophene-oxazine)
PAtOx	Poly(acetothiophene-oxazoline)
PAtOzi	Poly(acetothiophene-oxazine)
PVA	Poly(vinyl alcohol)
SAXS	Small-angle range of XRD analysis
SEM	Scanning electron microscopy
ST	Syringe temperature
TE	Tissue engineering

T_g	Glass transition temperature
TGA	Thermogravimetric analysis
THF	Tetrahydrofuran
T_M	Melting temperature
ThOx	thiophene-oxazolines
ThOzi	Thiophene-oxazines
XRD	X-ray structure analysis

Publications

journal papers

Heck J., Goding J., Roberto Portillo Lara R., Green R. The Influence of Physicochemical Properties on the Processibility of Conducting Polymers: A Bioelectronics Perspective, Acta Biomaterialia, 2021

planned journal papers

Heck, J; Goding, J.: Luxenhofer R.; Green R. A novel class of Oxazolines and Oxazines for Electroactive

Applications — to be submitted

Heck, J; Goding, J.: Luxenhofer R.; Dalton, P.; Green R. 3D Printing of thiophene-based oxazolines/oxazines — to be submitted

conferences

2020 WBC 2020 11Th World Biomaterials Congress, Poster Presentation, Virtual

2018 International Summerschool on 3D Printing technologies, Poster Presentation, Würzburg

2017 International Symposium on Nano dimensional Polymeric Therapeutics, Mainz

Chapter 1 – Introduction

Accidents happen every day. From small haematomas to complicated bone fractures or even more severe trauma that can result in significant loss of bodily function. More than 25,000 amputations happen in the UK per year.[1] For most of the last 3000 years, limb replacement has mostly taken the form of static or basic mechanical prosthetics.[2] However, the advent of brain-machine interfaces has presented the opportunity to develop highly complex prosthetics such as limb prosthetic or bionic muscles with unprecedented levels of complexity and bio-integration. Recent development in additive manufacturing (AM), also known as 3D printing, has a huge potential to close the gap of mass production of individual medical treatments and devices. However, it is limited due to the ability of useable materials.[3] This presents the need for alternative materials which are compatible with modern AM techniques and capable of imparting smart functionalities to the next generation of bionic prosthetics.

New materials for the next generation of implants should be soft, flexible and have the ability to electrically stimulate the surrounding tissue.[4] While metallic electrodes show poor interactions with the surrounding tissue, conductive polymers (CP) provide an alternative class of materials for biomedical applications.[5] CPs are used in various fields such as photovoltaics, optoelectronics, or bioelectronics.[6] Recently there has been increased attention in the use of poly(3,4-ethylenedioxythiophene) polystyrene sulfonate (PEDOT:PSS) based electrodes for biomedical applications..[7] This poly(thiophene) derivate shows good electrical performance but it is limited due to the mechanical and physicochemical characteristics of being brittle, non-flexible, and minimally processible (as CPs in general lack a melt phase).[8] The need for more flexible materials in tissue engineering (TE) & bionics has driven researchers to look at new ways in which to modify the properties of CPs. Due to the polymeric nature of CPs, they show, in general, low cytotoxicity and are chemically modifiable.[9] This enables functionalisation of materials with high control of the physio-mechanical properties and allows for the modulation of specific properties.

Two major processability challenges for CPs are highlighted in literature: the above-mentioned stiffness, which is normally described to be between 20 to 100 MPa[10,11], and the poor solubility in most common solvents[12]. To overcome these restrictions, research is mainly focused on the synthesis of CP-based organic materials[13]. Among the CP materials, a complex of the thiophene derivative, poly(3,4-ethylenedioxythiophene), and polystyrene sulfonate (PEDOT:PSS), is the most prolific material used in practical applications[14]. First developed by Bayer Ag in the 1980s, this non-toxic material formed a dispersion in water, paving the way for printed CPs to be applied in bioelectronic devices. However, application of these dispersible systems has largely been limited to substrate coating applications and has not yet been realised as a suitable alternative to conventionally conductive materials.

Another possibility for improving the properties of electrically conductive polymers is the use of additives such as hydrogels.[15] Hydrogels have tissue-like properties and are already used in many large-scale technical applications such as implants or contact lenses.[16–18] Electrically conductive hydrogels based on PEDOT are of particular interest.[19,20] Wang et al.[21] was able to improve the properties od PEDOT:PSS by using ionic liquids to such an extent that processability via photolithography was possible. However, pure PEDOT:PSS has the disadvantage that no dimensional stability is guaranteed and a supporting matrix is necessary. In addition, the swelling of hydrogels when implanted can lead to an increase in device volume and thus creates pressure on the surrounding tissue.[15] This makes spatial control difficult, which is significantly important for soft tissue repair.

Improving the processibility, namely flexibility, melting and solubility, of conductive materials is a key challenge for enabling superior AM materials for TE.[22] Polymers based on Ox or Ozi offer an alternative to conventional materials for improving the physicochemical properties of CPs. POx, and POzi are already known to have broad synthetic flexibility in modification opportunities[23]. Also known for having low cytotoxicity, this class of polymers can easily be modified by changing the side groups which have a significant impact on the material properties[24]. Besides solubility, thermal properties can also be controlled by the type of side groups or the synthesis of copolymers. Thermoresponsive behaviour, or inverse hydrogelation are further examples of the versatility of POx and POzi[25,26]. This unique character enables a high tunability of material properties and presents a new opportunity to modify the physical properties of CPs. This high capacity for tailored properties in POx polymer systems also make them ideal feed materials for AM processes such as MEW. Currently there is still a lack of materials that can be processed via MEW.[27] However, this gap has been partially closed in recent years. Polymers such as polyproyplene, poly(vinylidene fluoride) or POx can now be processed with this high-resolution technology. Above all, PEtOx as a hydrophilic polymer could be directly written at temperatures around 200 °C and offers therefore an interesting platform for further research due to its modifiability.[28,29]

1.1 Motivation

CPs have gathered considerable attention over the past twenty years due to their unique combination of electrical and ionic conduction properties. Despite significant research interest, CP-based technologies are yet to make significant impact in clinical translation. The reasons for this are multifaceted, but from current industry perspectives, the potential benefits of these technologies do not yet outweigh the potential risks and regulatory burden associated with adopting new material technologies. Therefore, CP technologies need to offer more than incremental increases in electrochemical performance in order to unseat incumbent industry best practices.

The poor processibility of CPs largely contributes to the risk of adopting these technologies, while also limiting the potential benefits that they can offer. Therefore, overcoming this limitation may help to unlock the full potential of CP-based materials. Understanding the physicochemical properties of CPs and their structure-property relationships is critical to addressing key limitations such as poor solubility, and chemical and thermal instability. Several novel approaches to addressing these limitations have been reported,[4,21,30] including the use of adjuncts such as dopants and plasticizers, the development of novel CP-chemistries, the formation of CP-based complexes and composites, and the adoption of novel manufacturing techniques such as AM. The approaches discussed here permit new synthesis and processing routes, which will also enable the development of novel technologies based on these highly versatile materials. It is hypothesised that this higher degree of control over the physicochemical properties of CP systems can only be achieved through the design of new monomers, which specifically address the limitations of conventional CP systems. This will enable the development of tailored biomaterials with enhanced tissue integration and thus, higher clinical efficacy. In addition, the pairing of these approaches with emerging AM fabrication techniques will enable exciting new functionalities and applications for CPs within the field of bioelectronics.

As such, this work aimed to develop a novel material based on conductive polymer, POx and POzi, which can be processed by AM into bespoke constructs using MEW printing. Three main criteria were used to inform the design of these materials:

1. Processability: Solubility was highly desirable with meltability being critical. The final product must be compatible with modern AM techniques.
2. Functionality: The desired material should combine the properties of thiophenes & POx/POzi to develop an electroactive functional and non-toxic scaffold.
3. Translatability: Straight-forward synthesis that is cost-effective and scalable. Here, approaches should be avoided that require complex preparation, are expensive due to the availability of the materials or have a high toxicity due to the materials used.

1.2 Project Overview, Hypothesis and Aims

This thesis addressed the challenges that arise in the manufacturing and processing of electrically conductive polymers. The focus was on the design and synthesis of a new class of materials based on POx and POzi and poly(thiophenes) and further processing using AM. It was proposed that the development of such a copolymer can be achieved either through end-group functionalization or side group modification. The parameters that are important for AM, such as solubility, thermal stability and flexibility, were examined and the ability to control them was investigated. This approach stands in contrast to the common approach reported in literature where conductive composites are fabricated using

additives, and instead aims to improve the processability of CPs by designing processable copolymer systems at the monomer level.

The ultimate objective of this work was to produce electrically active materials for potential application as muscle tissue scaffolds in limb prostheses or muscle regeneration. In addition to developing a copolymer material, a key focus was on modifying the material properties in a targeted manner so that they are suitable for AM. MEW was chosen as an advanced form of AM with great potential in microfabrication of polymer constructs for TE and bionics. This method has the advantage that structures with a resolution in the micro range can be produced, however limiting factors to the application of MEW have been the amount of material required for the feed. As such the most commonly used material for MEW printing has been polycaprolactam (PCL). PCL has no functional groups and is electrically insulating, resulting in a relatively bioinert construct with limited options for functionalising. POx, POzi and polythiophenes present an opportunity for designing new polymer systems for use with MEW.

Therefore, the overarching hypothesis of this thesis is that a material that combines the electroactive components of polythiophenes with the processibility and functional side groups of POx or POzi, will enable new material technologies for application in MEW.

This research was motivated by the following:

- The physicochemical properties of CPs such as polythiophenes can be controllably tailored by the chemical modification at the monomer level;
- POx or POzi offer an ideal copolymer component for incorporation of CP monomers because of their many functionalisation opportunities, including end-functionalisation, copolymerisation and side group modification; and,
- Copolymers of polythiophenes and POx or POzi will be compatible with AM processes such as MEW printing.

The specific aims of this project were to:

1. Develop and characterise a library of POx and POzi based CPs monomers;
2. Create tailorable copolymer systems and study the influence of monomer chemistry as well as copolymerisation techniques and conditions on the physicochemical properties of the resultant copolymer materials;
3. Investigate the relationship between copolymer chemistry and printability by using MEW; and
4. Examine the biological properties of novel copolymer systems to assess cytotoxicity and cell-material interactions.

1.3 Thesis Structure

The goal of this work was to develop a new copolymer platform based on polythiophene, POx and POzi. This was achieved through 3 major research chapters that broadly address the design and characterisation of monomers, the ability to polymerise such monomers and the printability of polymers using MEW. The chapter structure is detailed as follows:

Chapter 2 reviews the literature on conductive polymer with focusing on the physicochemical properties and processability, the fundamentals on the synthesis of polyoxazolines and oxazines and on 3D printing highlighting MEW.

Chapter 3 explores the synthesis of novel monomers and the up-scaling opportunities. Furthermore, a full analysis is performed and a number of analytical techniques that are not reported in detail in the literature are used therefore.

Chapter 4 develops the end-functionalisation of aliphatic POx and the possibilities to polymerise the novel monomers. A detailed characterisation and analysis of the material and its properties is performed.

Chapter 5 analyses the printing and characterisation of scaffolds based on the developed material based on POx and POzi. In addition, the hydrophilic properties are presented in this chapter and further biomedical investigations are presented in the last part.

Chapter 6 presents the summary of this work and shows possible applications and future research directions.

Chapter 2 – Background Information

Portions of this chapter, written by the candidate, has been published in [Heck J., Goding J., Roberto Portillo Lara R., Green R. The Influence of Physicochemical Properties on the Processibility of Conducting Polymers: A Bioelectronics Perspective, Acta Biomaterialia, 2021]

2.1 Conducting Polymers

Bioelectronic devices such as motor prosthetics, neurostimulators and biosensors have enormous potential to shape the way in which we diagnose and treat a wide range of pathologies. Contemporary devices typically use inert metallic materials to conduct electrical signals and transfer them to biological tissues.[31] However, the use of conventional materials such as metals limits the performance of bioelectronic devices and the design of next generation technologies.[32] While metallic materials make excellent electrical conductors, the mechanical mismatch with soft tissues and their restricted charge transfer capabilities limit their implementation in bioelectronic devices. Despite efforts to develop flexible metallic-based materials, these are usually difficult and expensive to produce. Organic conductors such as CP are a promising alternative to the use of metallic conductors and thus, they have been widely used in the fabrication of soft, flexible and fully organic bioelectronic devices.[33]

First reported by Bolto et al.[34] in 1963, CPs have a conjugated π-electron system that enables electrical conduction. Without further modification, CPs have a conductivity in the range of semiconductors.[35] Contemporary CP systems with optimal doping and stabilized backbone structures have been reported as having conductivities of more than 1000 S cm^{-1}.[36–39] The applications of CPs are diverse, ranging from photovoltaics,[40] organic electronic components,[41–43] electromagnetic shielding,[44] sensors and actuators,[45–47] to implantable bioelectronics.[48] While the potential range of applications of CPs within bioelectronics is vast, the exact design requirements for any given CP component depend heavily on its intended use. Therefore, it is critical to comprehend the fundamental factors which give rise to the physicochemical properties of CPs and thereby determine their processibility. In turn, this increased understanding could enable the intelligent design of novel material systems and devices that can overcome the inherent limitations of this promising class of materials. Processing capability is indispensable to the design 3D bioelectronics and addressing the key challenges for tailoring CP material properties has the potential to create opportunities for application of CPs to the field of AM. Better known as 3D printing, AM is a layer-to-layer technique, which allows the fabrication of cost-effective, complex computer-based designs[49] with individual or personalised batch productions. Combining these techniques with electroactive materials such as CPs is a promising solution for fabrication of bioelectronics or other electrical devices, with a specific utility in personalized medicine.

Bioelectronic applications of CPs have been hindered due to their limited mechanical robustness, substrate dependency and restricted processibility. The development of tailorable and processible CP material systems that address these challenges will enable a vast range of CP applications within bioelectronics, as well as the general field of electronics. Despite the technical advantages provided by CPs, several challenges remain in order to overcome their inherent limitations related to solubility, processability and long-term stability. To address the challenges related to the development of processible CP-based materials, it is necessary to understand their chemistry and structure, which give rise to their unique properties and functionality. Conventional synthesis techniques and the properties of CP-based materials are discussed herein, with a focus on functionality and processibility.

2.1.1 Mechanism of Conduction

The defining characteristic of CPs is their conjugated structure and the associated delocalized π-bonding.[50] Polyacetylene (figure 2.1 a) formed the historical basis and also the simplest system of a straight conjugated system[51]. Two assumptions were made here. On the one hand, a conjugated system should be as long as possible and on the other hand, intramolecular electron hopping between two chains should be possible to ensure conductivity. However, it was soon discovered that the physical properties of the chain molecule changed as the number of double bonds increased. The longer the conjugated system became, the more there was a shift of the absorption band to longer wavelengths (batochromic effect) and the extinction coefficient increased.[52] Therefore, it was concluded that in an ideal infinitely long chain system, the different bond lengths disappear, and an ideal delocalised π-electron system exists. However, the first synthesised PAs had an electrical conductivity in the range of poor semiconductors.[51] It was concluded that this happened due to the lack of electron hopping and disruption of the π-electron system.

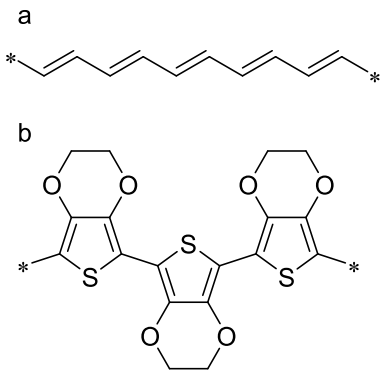


Figure 2.1 a) Polyacetylene, b) Poly(ethylenedioxythiophene)

Looking at a single ethylene molecule in PA, the p_Z-orbital, as the highest energy level of two carbon atoms, splits into a bonding and an antibonding orbital.[53] The highest occupied orbital is called HOMO

and the lowest unoccupied orbital LUMO.[51] The HOMO contains the two electrons for π-bonding. In contrast, the LUMO is unoccupied. Looking at the macroscopic system, the HOMO and LUMO also split here and so-called molecular orbital bands are formed. Here, the individuality of the individual building blocks is abandoned, and they are regarded as one solid body. Through further splitting of the molecular orbitals and as the system grows, an energetic overlapping of the two bands occur. Here, the system changes from an insulator to a semiconductor and, with energetic overlap, to a conductor. However, in PA and other conjugated polymers, the bond lengths are not of equal length.[54] An alternating system is present, as this is the energetically more favourable system due to the Peierls instability. Consequently, there is an energy gap between the occupied π-band (valence band) and the unoccupied π*-band (conduction band). Unlike in the classical band model, the removal of an electron by an oxidising agent (or, conversely, a reducing agent) does not result in the delocalisation of the resulting hole, but rather in the formation of a radical cation, which is localised and must be stabilised by a counter ion. In perspective of energy bands, these defects occupy in the middle of the π-π*-energy gap and consequently a charge transport can be enabled.[52]

Figure 2.2 shows the two types of doping. The result of partial oxidation (reduction) is a distortion of the π-lattice, which forms a charged quasiparticle called a polaron. Two polarons in close proximity can share lattice distortions resulting in the formation of a bipolaron. The formation of stable polaron and bipolaron units is critical to mechanism of conduction of CPs and thus, the choice of dopant and the efficiency of the doping process are critical to the performance of CP-based materials. In practice, most CPs are usually modified by p-doping,[55] as typical n-doping molecules have poor stability in atmospheric conditions as well as low conductivity compared to p-type dopants.[55–57]

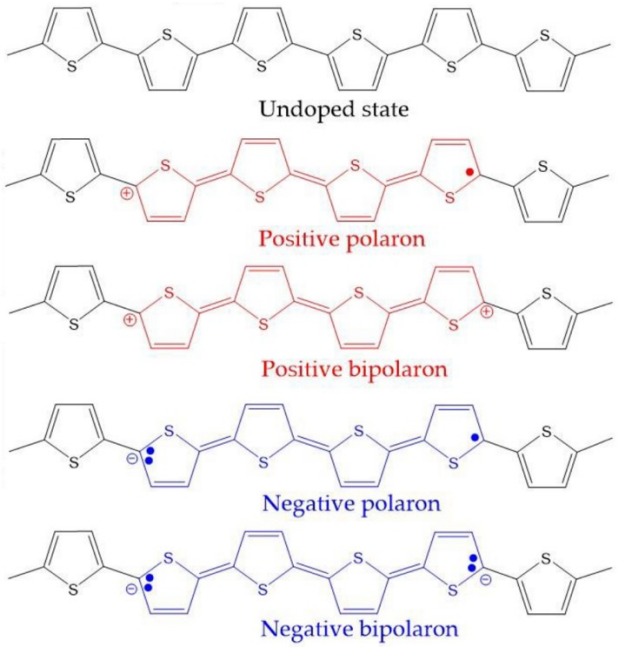


Figure 2.2 Doping of polythiophene. Reproduced from Le et al.,[58] *with permission.*

2.1.2 Fabrication of CPs

Shirakawa et al.[59] synthesized the first CP using chemical oxidative polymerisation of polyacetylene in the mid 1970's. Since then, several techniques for the synthesis of CPs have been developed, including photochemical,[60] metathesis,[61] pyrolysis[62] and plasma polymerisation,[63] among others. However, chemical and electrochemical polymerisation remain the most commonly used approaches. The simplicity of these techniques allow for a high order of control during synthesis, which enables the tailoring of the properties of the resulting CPs. In addition, both methods allow for easy coating of underlying substrates, which is again a useful tool in the fabrication of bioelectronics.

Electrochemical polymerisation (i.e., electrodeposition) is a widely used technique to form CPs, mainly due to the ease of synthesis and the control over the oxidative process.[64] This technique is relatively straightforward, since all materials required are easily accessible, inexpensive, and most of them can be used without further modification. Furthermore, monomer modification can be performed before polymerisation. Early works by Heinze et al.,[65–67] Diaz et al.[68,69] and Chen et al.[70] provide a detailed description of the process of electro polymerisation. In addition, Kumar et al.[71] summarized the main factors that effectively influence the electrodeposition process, namely pH, temperature, current density, time, metal ions, concentration and agitation. The general principles of this technique are shown for PPy in Figure 2.3. Briefly, a three-electrode cell is used (Figure 2.3d) and monomers are dissolved in an electrochemically inert solution in the presence of a charged dopant. Oxidation of the monomer unit forms a radical ion intermediate at the electrode interface, and subsequent step growth results in the formation of oligomers at the electrode surface creating nucleation sites for further growth. The growth of the CP film at this point may be 2-dimensional, 3-dimensional, or both, depending on key

monomer/oligomer concentration and applied potential. This process is initiated by the application of an electronic potential between the working and counter electrodes. Three types of applied potential are typically used, which are potentiodynamic, potentiostatic and galvanostatic potentials.[72] They key differences between these techniques is the way they control different process parameters during electrodeposition, namely polymerisation voltage and current density. CP coatings made using electrodeposition techniques typically have highly nodular surface morphologies, as seen in Figure 2.3a.[73,74]. CPs fabricated using electrochemical polymerisation should be notated as polymer/dopant (for example PEDOT/PSS). This is in contrast to chemically polymerised systems which typically form complexes and are notated as polymer:dopant (for example PEDOT:PSS).

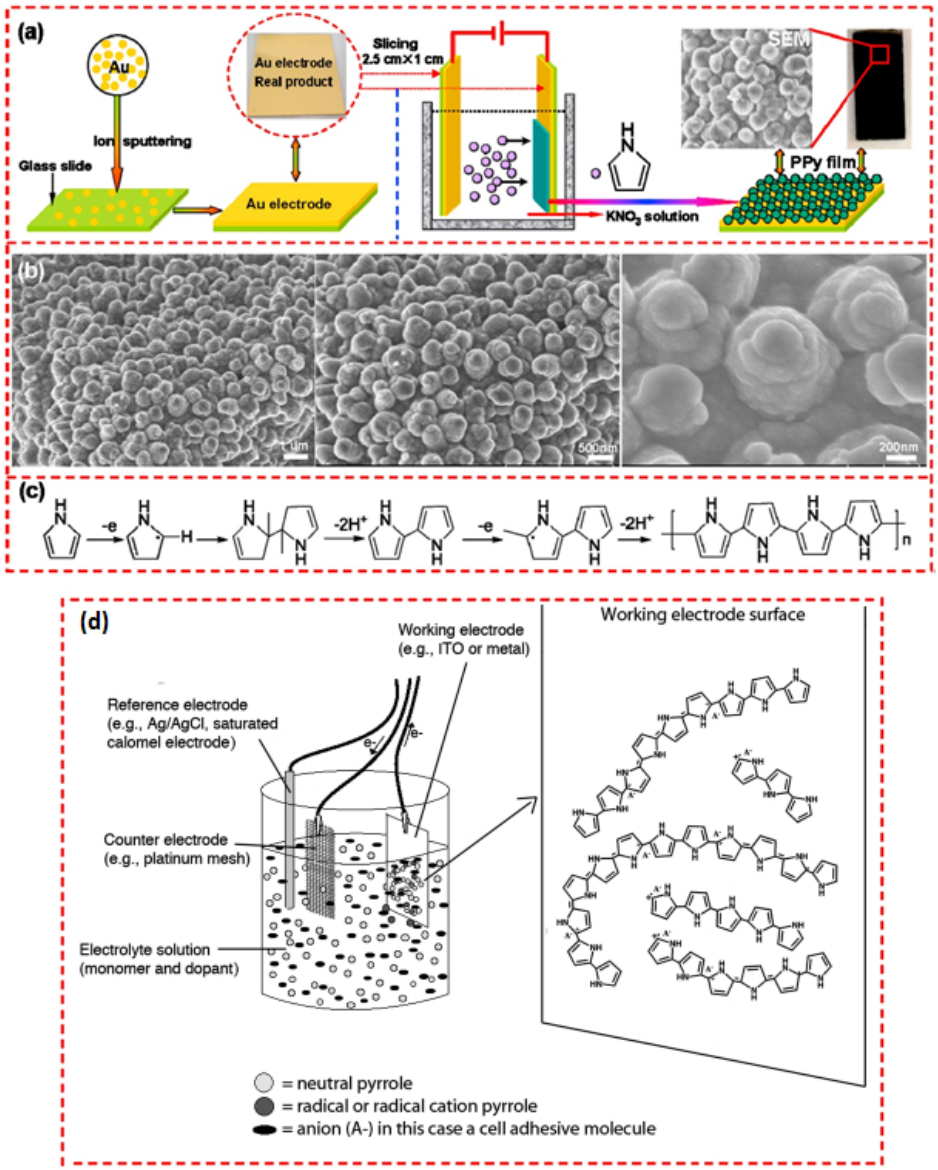


Figure 2.3(a – c) principle of electrodeposition of PPy onto a gold (AU) electrode, Reproduced from Chen et al.[73] with permission, copyright 2018, Elsevier d) electrode setup. , Reproduced from Rao et al.[75] with permission

A wide variety of CPs, such as PPy,[76] poly(thiophene)[77] and PANI[78] have been synthesized chemically. Figure 2.4 shows the mechanism of synthesis with iron chloride as an oxidising agent for the monomer, thiophene. The polymerisation is initiated by oxidation of thiophene monomers with a metal (Fe^{3+} to Fe^{2+}), which is an electron acceptor (i.e., Lewis-acid). A nucleophilic radical is created by cleaving off a hydrogen, which is followed by bonding of a nucleophilic radical to a second monomer to form a dimer. Then, the continuous coupling of monomers yields a polymer chain.

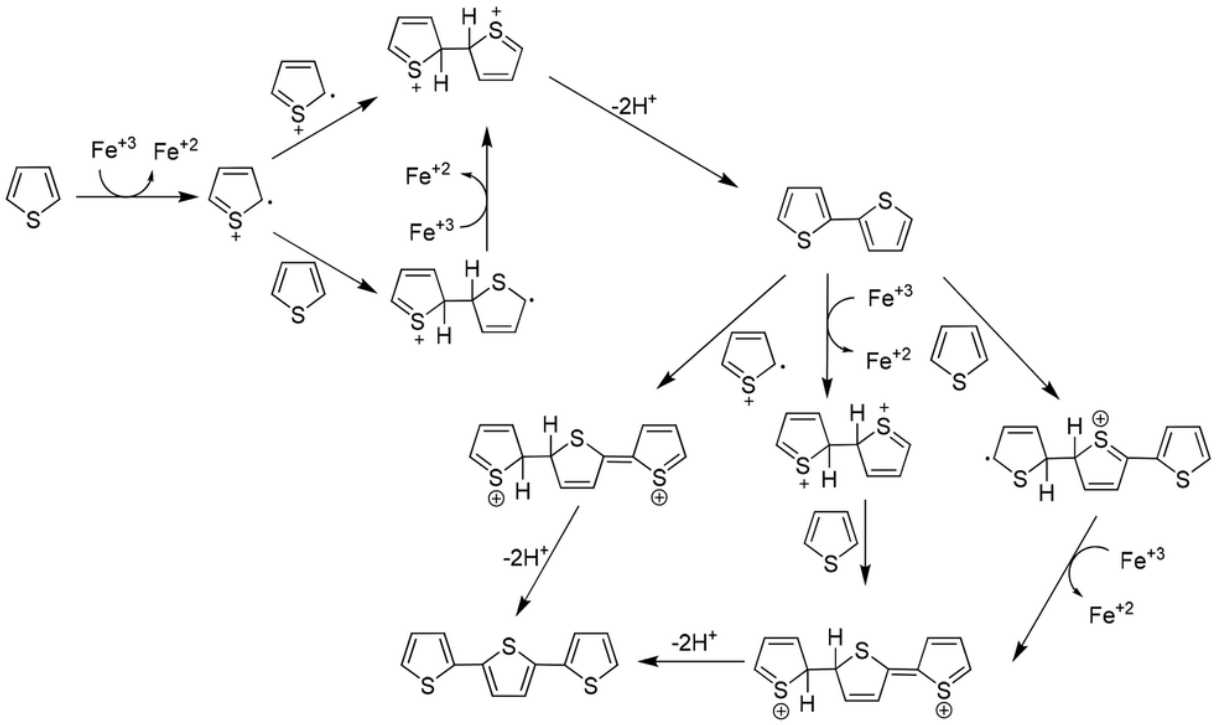


Figure 2.4 Example of chemical polymerisation route for thiophene-based monomers. Reproduced from Khalid et al.[79] with permission

Chemical polymerisation of CPs has the advantage of being substrate independent and easily scalable compared to electrochemical techniques, however chemically-polymerized CPs typically require post-synthesis modification to enable high electrochemical performance[80] and the conductivity of the synthesized polymers ranges from that of an insulator and a semiconductor.[81] An early example of post-processing chemically-polymerized CPs was demonstrated by Chiang et al.[82]. They were able to increase the conductivity of polyacetylene eleven orders of magnitude by introducing vaporized halogens into the system.

Other chemical-based polymerisation strategies have been developed, which have enabled novel fabrication techniques and strategies to tailor the physicochemical properties of CPs. For example, Grignard-metathesis polymerisation techniques can be used to tailor and control more specific polymerisation processes.[83] The use of Grignard reagents allows for the easy modification of functional end-groups with moieties such as vinyl, allyl or phenyl groups. In addition, the presence of these functional end groups allows for further chemical modification of the CP after synthesis.[84,85] Furthermore, by varying the metal in the Grignard complex, it is possible to control the head-to-tail ratio and molecular weight of the resulting polymer.[86] These properties are key factors that influence both the electrochemical performance, the thermal behaviour and thus, the processibility of CP systems.

Chemical and electrochemical fabrication methods exhibit inherent limitations with regard to the processibility of the resultant CPs. This is mainly because, in the absence of pre- or post-polymerisation modification and depending on the molecular weight, the resulting polymers are commonly

mechanically fragile, and unfit for the use in biomdecial applications.[87] In general, chemical polymerisation allows for simple scaling up, as it is not limited to the substrate surface. However, the cleaning and post-modification steps often increase the costs and complexity associated with the process. Although electrodeposition is largely restricted to the surface of electrodes, this constitutes a relatively simple strategy for the coating of functional interfaces used in electronic devices. Ultimately, the choice of synthesis route will depend on the desired properties of the final product and the required means of production for the specific application.

2.1.3 Properties of CP

Two major interactions are responsible for the physical and chemical properties in a polymeric system. First, intramolecular interactions refer to the chemical bonding between single chain links (i.e., atoms) that hold the polymer chain together. Second, intermolecular interactions correspond to adhesion forces such as Van-der-Waals forces, which are responsible for the cohesion between polymer chains and with the dopant counterion.[88] These adhesion forces are additive and, in general, their strength will increase as the length and the molecular weight of the polymer chain increase, while the overall chain mobility will decrease. The development of strategies that can enhance the processibility of CPs should take into account the role that the chemical and molecular structure plays in the establishment of these interactions, which in turn determine the chemical and physical properties of CPs.

2.1.4 Chemical stability and influence of dopant counterions

Chemical stability is key for the performance of CPs used in bioelectronic devices in order to maintain stable functional performance and prevent unwanted reactions with the surrounding tissues. CPs have the potential to exhibit lower chemical stabilities than conventional inert polymers due to the conjugated structure that gives rise to their electroactive nature.[89] For instance, the charged backbone of CPs has been shown to react with surrounding oxidants such as water or air.[90] Furthermore, CPs need to remain stable in their electrically active (i.e., reduced or oxidized) states in order to ensure consistent device performance. Furthermore, dopant counterions also play a significant role in determining the electrochemical stability of CPs. Size and type of dopants play a key role due to interaction with the backbone and hence influence on chemical stability. Small, mobile ions with low electronegativity have a much lower stability effect compared to larger, steric hindered and strongly electronegative dopants.[91] PANI exists in four different states.[92] While the leucomerladine (fully reduced), emeraldine base and pernigraniline (fully oxidized) are non-conductive, only the emeraldine salt is electrically conductive. PANI shows good chemical stability in water and under dry air conditions. In contrast, under acidic conditions (pH 1-2), a degradation of the polymer is observed. PPy is less stable in its reduced or de-doped state, but shows better stability under acidic conditions.[93] Due to H-N-bonding in the pyrrole-ring a pH of approximately 7 must be maintained during synthesis to ensure chemical stability.[94] If the pH is too high, electrodeposition is inhibited due to nitrogen deprotonation, while low pH would

promote the dimerization of pyrrole molecules and yield a non-conductive polymer. Overoxidation refers to the process of oxidative degradation that hinders the electrical performance of PPy, which can occur due to expelling of anions and carbonyl groups in β-position, as well as in aqueous solutions under anodic potentials.[95] To circumvent this limitation, previous works have reported the addition of organic anions and polar aromatic compounds to prevent overoxidation.[96]

Although PEDOT has a similar heterocyclic structure and low oxidation potential, it is considerably more stable than PPy in the oxidised state.[97] This is due to the fact that during synthesis of PPy a significant amount of alpha-beta coupling occurs, which induces structural disorder, limits the electrochemical response and could lead to overoxidation.[98] In addition, PPy is less stable in the oxidised state and is susceptible to reducing agents such as dithiothreitol or glutathione. In contrast, the beta-position in PEDOT is chemically blocked and the second electron pair on the sulphur atom is orthogonal to the ring plane, which prevents its interaction with electron delocalisation. It has been shown that PEDOT:PSS retains its electrical properties when heated to 100 °C or when exposed to air for over 1000 hours.[99] Analogous to the delocalisation of the electron pairs through the ring mentioned above, the electron density has been measured to be located at the sulphur atom in a thiophene molecule. This results in an unreactive sulphur atom compared to other sulphides. In contrast, carbon atoms in the alpha position are highly responsive to an electrophilic reaction. However, since the carbon in the alpha position forms part of the backbone after polymerisation, it is less reactive to electrophilic side reactions. Heywang et al[100] reported that the higher stability of PEDOT compared to other CPs is due to a stabilisation effect (i.e., delocalisation) of the positive charge that occurs because of the electronegativity of the heteroatom. Furthermore, they proposed that introducing steric hindrance by substituting in bulky side groups can chemically stabilize the positive charge of the polymer. However, the increase in steric hindrance was also associated with a negative impact on the electrical properties of PEDOT, which was due to the disruption of the packing and arrangement of the polymer chain. The authors demonstrated that the use of alkylenedioxythiophene derivates could stabilise the chemical structure of PEDOT with minimal impact on electrochemical performance. However, it should be mentioned that the overall conductivity was determined to be in the range of 10^{-2} to 1 S cm^{-1} compared to typical PEDOT conductivity of 1 to 15 S cm^{-1}.[100]

Similar stabilisation effects can be achieved through the selection of different dopant counterion molecules. Green et al.[101] studied the impact of dopants onto the stability of PEDOT coatings for medical electrodes. The researchers were able to demonstrate an improvement in stability under in-use conditions. Herein, PEDOT/*p*-toluenesulfonate (pTs) and PEDOT/ClO_4 showed a much better durability than PEDOT/PSS. Thiéblemont et al. [102] demonstrated that the stability of chemically synthesized PPy films in an inert atmosphere could be increased by changing the sulfonate dopant used for synthesis from classic *p*Ts to naphthalene sulfonates. It should also be noted that the conductivity of PPy films increased by exposing them to moisture in the first few days.[103] It is believed that a slight exchange of

the original dopant with ambient oxygen is the reason for this observed phenomena.[102] Kanwat et al.[104] demonstrated a similar effect of dopant counterions within a PEDOT:PSS system. The authors hypothesized that the stability of PEDOT could be compromised by exposing it to air or light. They demonstrated that the addition of a secondary WO_x dopant counterion led to a 95% reduction in the rate of degradation of the PEDOT:PSS system. Kim et al.[105] were able to increase the conductivity and the overall stability of PEDOT:PSS films through the use of a mild dopant counterion, such as perfluorooctane sulfonic acid. Their result demonstrated that the conductivity and stability of the CP under ambient conditions could be preserved for more than 25 days and the sheet resistance was stabilized at around 300 Ω sq^{-1}. Furthermore, the authors suggested that the hydrophobic/hydrophilic character of perfluorooctane sulfonic acid was key for the improvement observed in the properties of the materials.

Another consideration when choosing a dopant counterion molecule is the nature of its interaction with the CP matrix. Some dopant counterions show better incorporation into the polymer matrix than others. Spanninga et al.[106] investigated the effect of different dopants on PEDOT. They showed that especially bulky counterions such as PSS or poly (acrylic acid) (PAA) are maintained within the matrix more effectively compared to small anions such as tosylates, sulfonates or chlorates because of their polymeric nature. Furthermore, they determined that PEDOT affinity for counterions exhibits a general similarity to the Hofmeister series. This degree of anionic hydration plays a significant role for intermolecular interaction forces. Baek et al.[107] investigated the effect of dopant size and chemistry on the mechanical properties of PEDOT and showed that larger dopants resulted in stiffer PEDOT films with lower charge storage capacity and higher impedances. This demonstrates that ensuring the chemical stability of CPs requires careful consideration of the chemical structure of the CP, choice of dopant, intended function (voltammetry, stimulation or recording), as well as environmental factors such as exposure to oxidants, solvents, humidity, and temperature. As processing of polymers conventionally exposes the polymer pre-cursors or products to several of these factors, they are critical considerations for the successful development of processible CP materials.

2.1.5 Thermal properties of CPs

Thermal properties, encompassing both thermal tuneability and stability, are critical to the processibility of CPs. Elevated temperatures are used for many conventional polymer forming techniques, such as injection moulding and extrusion, but in the context of temperature mediated AM are fundamental to achieving a functional component. Due to the sp^2-hybridisation of the carbon atoms in a conjugated macromonomer, CPs are quite stiff and properties such as a theoretical melting point and glass transition temperature (T_g) are increased compared to non-conjugated systems.[108] Previous work has shown that the interparticular alignment of polymer and dopant within a CP can be increased by applying elevated temperatures, which results in increased intermolecular connections and higher conductivity.[109,110]

However, this is also associated with a decrease in thermal stability, which occurs due to molecular reorientations that make polymer side groups vulnerable to reactions with air or moisture.

In contrast to metals and other polymeric-based materials, electroactive polymers with a conjugated backbone without further modification such as aliphatic side-groups do not have a sharp melting phase. Consequently, this has critically hindered their use in temperature mediated fabrication. Non-conjugated polymers such as polycaprolactam[111,112] and polyethylene alcohols[112] exhibit a glass transition temperature (T_g) under 200 °C. T_g refers to the temperature at which a phase transition (second-order phase transition) between rubbery and vitreous structures occurs.[113] At this point, rotation of chain segments comprising several monomer units (crankshaft movement) is initiated, which promotes higher chain orientation within the matrix. Although the T_g of several CPs have been reported (Table 2.1), continuous heating results in thermal decomposition and not in a melting.[114] Moreover, it is important to note that T_g cannot be equated with the melting temperature T_M. From a macroscopic point of view, T_g is the temperature where a polymeric material changes from a flexible, elastic state to a hard, brittle one, while the T_M is the temperature where the ordered crystal structure collapses and an unordered liquid occurs. Due to the relatively small temperature gap between phase transition and the decomposition temperature, the melting phase of CPs cannot be observed. This in turn precludes the use of the majority of thermal processing technique, which also restricts potential applications. In addition, structural properties such as bulky side chains, polar substitutes or stiff backbones often lead to increases in T_g and T_M.[108] However, the higher T_g brings the CP closer to decomposition rather than transitioning to a mobile chain phase.

High energy is required to induce oscillation of the CP chains that results in scission of the C-C bonds and ultimately thermal decomposition. The energy introduced during a thermal treatment can initiate decomposition since the binding energy of carbon double bonds is around 600 kJ mol^{-1}.[115]As with the T_g, bulkier polymers such as PEDOT decompose at higher temperatures than more mobile CPs such as linear polyacetylenes. The initial stages of CP decomposition have been observed at relatively low temperatures. Decomposition is a multi-step process and usually starts with deprotonation or partial oxidation on the material outside and leads to a rougher surface. Figure 2.5 shows scanning electron microscope images of PANI, which has been treated using different temperatures. The first stages of degradation can be observed at 100 °C due to thermal deprotonation.[116,117] At 200 °C a complete deprotonation is observed, which can be observed as the evolution of surface roughness. Thermal degradation continues at around 200 °C and progresses until 350 °C.[118] Although it is possible to stabilize the thermal behaviour by adding SnO_2 nanoparticles (Figure 2.5c), this does not result in the evolution of a polymer melt phase and is not compatible with requirements for biocompatibility in bioelectronics applications.

Interestingly it has been shown that PPy is more adaptable to thermally tuning. PPy is more complex with a T_g that typically ranges between 65 and 95 °C.[119] This behaviour can be modified through the chemical modification of PPy side groups. The ability to use chemical modification to tailor the thermal properties of CPs is a promising strategy from a processibility standpoint. However, the lack of actual melt temperatures and the onset of thermal decomposition at 150 °C largely prevent the use of PPy in thermal processing. Unlike PPy, thiophene based CPs remain stable at temperatures of approximately 200 °C, which is expected to facilitate their use at higher operating temperatures.[120] CPs with a complex π-system structure can tolerate thermal treatments for longer periods of time compared to CPs with simple backbone structures.[121] Bulky polymers such as PEDOT require greater energy inputs (i.e. treatment temperature and time) to induce a glass transition owing to stereochemical hinderance.

CPs are largely incompatible with thermal processing due to the lack of a defined melt phase prior to decomposition, which is a critical factor in AM. This characteristic remains a significant challenge because it stems from the fundamental chemical structure of CPs, which is also inherent to their functionality. One approach to address this limitation is the development of CP complexes and composites, which enable thermal tuning through the introduction of a secondary polymer with a known melt phase. It is critical to ensure that the melt phase of the secondary polymer is below that of the decomposition temperature of the CP, and that the CP chains retain motility within the secondary polymer melt. This creates additional constraints as CPs then need to be incorporated as a dispersed particulate, such as PEDOT:PSS, or with an additional solvent carrier.[20,122,123]

Table 2.1 Glass transition temperature (T_g) of different conductive polymers.

Polymer	**Glass Transition Temperature**	**Decomposition Temperature**	**References**
PPy	65-95 °C	150 °C	Biswas,[119] Ennis[124]
PEDOT	60-70 °C	Up to 300°C (PEDOT:PSS)	Ju,[120] Ng[125]
Poly(aniline)	30-40 °C	100°C; 200°C	Bhadra,[126] Yang[117]
Polyacetylene	~200°C (estimated)	160 °C	Masuda[127,128]

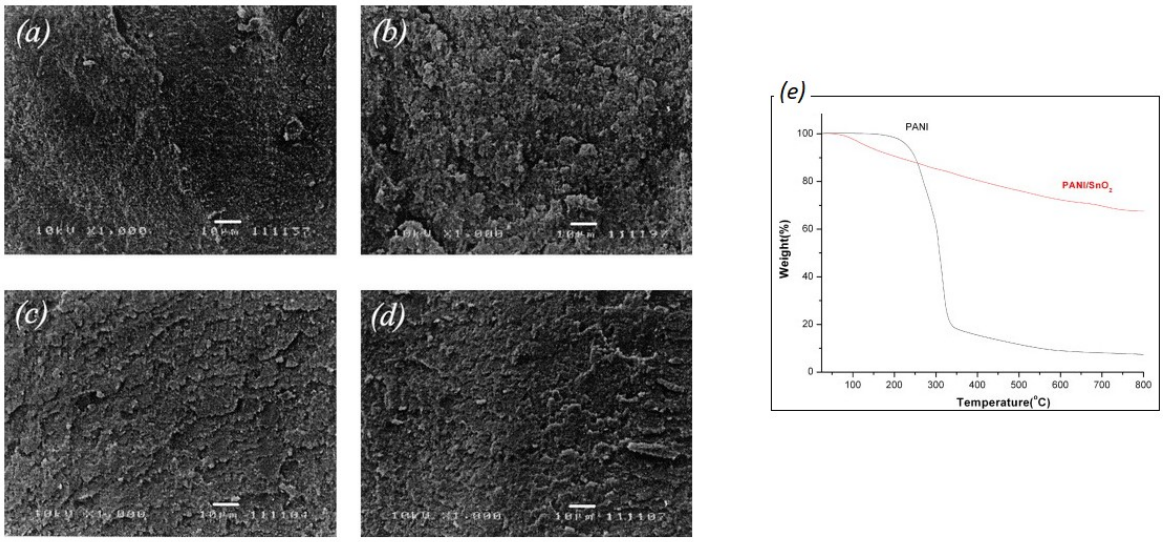


Figure 2.5 SEM image showing thermal annealing of PANI-base at Rt (a), 160°C(b), 180°C (c), 200 °C (d)). Reproduced from Lu et al.[116]*, with permission. (e)TGA graph of PANI. Reproduced from Alam* et al.,[118] *with permission.*

2.1.6 Solubility of CPs

The limited solubility of CPs is a considerable challenge that is critical for upscaling multiple fabrication processes, including AM. Although the monomers of most CP systems are readily soluble in several commonly used solvents, the chemical structure of their polymerized forms often leads to poor solubility with few exceptions such as poly(3-hexylthiophene) or modified PEDOT. Without substitutes, conjugated polymers are insoluble due to strong π-π-interactions between the single chains. A fundamental principle in chemistry states *similia similibus solvuntur* (like dissolves like).[129] This means, in order to dissolve a CP such as PEDOT, the molecules of the solvent must possess similar physicochemical properties. The polarity of most CPs is unique to their heterocyclic nature, making solvents that dissolve or even disperse these molecules quite difficult to identify. Two major classifications of solvents exist: polar and nonpolar. The molecules in polar solvents contain interactions between adjacent atoms with varying electronegativities leading to the evolution of dipole moments (for example water-molecule-interactions through hydrogen bonding). Polar solvents can be further categorized into protic and aprotic solvents. In contrast, nonpolar solvents lack this property and thus, they do not interact via charge mediated mechanisms such as dipoles. In addition to the degree of solubility, the choice of solvent can also affect reaction kinetics and chemical stability by causing unwanted reactions and degradation of the CP structure. Due to conjugated nature of CPs and varied localised charge state, neither of these solvent groups can fully dissolve most CPs.

Polymer solubilisation requires that the interaction forces between polymer and solvent molecules overcome the intermolecular forces between polymer chains. Increasing the length of molecular chains increases the intermolecular interactions, which reduces polymer solubility. CP chains are polymerised

to ensure long continuous conjugation of the backbone to preserve conductivity. As a result of this extensive chain length, Wessling et al.[130] proposed that CPs cannot be fully dissolved without further modification. Kaynak et al.[131] reported a strategy to solubilise PPy in chloroform through the addition of alkyl groups to the third or fourth ring position. It was determined that the solubility increased concomitantly with the length of the alkyl group, while the conductivity decreased. More recently, Lv et al.[132,133] investigated the influence of side groups on PPy oligomers. The insertion of a methacrylic ethyl-side group enhanced the solubility in commonly used aprotic solvents, which enabled a polymeric solution in chloroform with increased thermal stability and conductivity. John et al.[134] synthesised a doped PPy by chemical polymerisation, which enhanced the solubility in various organic solvents. The authors used a mixture of ammonium persulfate and sodium salts, which yielded an overall conductivity of 10^{-1} S cm^{-1}. In another study, a soluble polymer based on PEDOT was synthesised by Ponder et al.[135] The authors used alkoxy-functionalised 3,4-propylenedioxy-thiophene (ProDOT) and copolymerized it with unfunctionalized EDOT. The resultant polymer, which contained 67 % PEDOT and 33 % ProDOT, maintained the electrochemical performance of PEDOT, while also exhibiting a higher solubility due to the addition of ProDOT. This study suggested that the combination of CP monomers with different functionalities constitutes a viable strategy to tailor specific properties of CP systems. The problem here is that very toxic substances such as DMF and bromine were used during the synthesis and, in addition, the multi-step synthesis had an absolute yield of less than 50 %.

Previous groups have also demonstrated that certain CPs systems are able to be solubilised in water. Hussin et al.[136] recently reported the polymerisation of PANI in an aqueous solution of cellulose derivates. Although unmodified PANI is usually insoluble in water, the use of cellulose as a steric stabilizer and hydrogen chloride as an acidic dopant yielded a water-soluble PANI with a higher conductivity (~10 - 100 S cm^{-1}) than pristine PANI. Similarly, Gribkova et al.[137] developed water soluble PANI complexes by optimising the ratio of PANI to poly(sulfonic acid), which enabled its use in ink-jet printing. However, the compatibility of this system with biological systems was not demonstrated as it was applied as an anodic buffer layer for organic solar cells. Early research on PPy also showed that water solubility could be imparted through dopant ions. Jang et al.[138] synthesised PPY with limited water solubility (~4 %) and a conductivity of 0.5 S cm^{-1} by using sulfosuccinic acid sedum salt as a functional dopant. These results were in agreement with another study by Bae et al.,[139] which reported a similar behaviour using polystyrene sulfonic acid (PSSA) as a dopant. Alizadeh et al.[140] were able to synthesise another water soluble PPy-based CP through the addition of dicarboxylic acids, which acted both as a dopant and a stabilizer. Furthermore, they demonstrated that this material could be used as a highly fluorescent sensor for cell imaging.

It is important to note the distinction between the dissolution and the dispersion of CPs, which is often done. Dispersions such as PEDOT:PSS are made from small complexes of PEDOT wrapped in excess PSS. Wessling et al.[130] established the term “organic metals” for these dispersions of polymer

aggregates. While not considered a pure CP, these dispersions do enable solution-style processing and are discussed in greater detail in Section 2.1.9. Furthermore, the rapid adoption of commercial materials based on PEDOT:PSS and the rise in the number of publications related to this subject is a strong indicator of the demand for CPs that are water soluble. This is particularly pressing in the context of biomedical applications, where the use of toxic solvents is undesirable.

2.1.7 Mechanical properties of CPs

The mechanical properties of CPs have been largely studied in the context of thin films laminated to a substrate, as electrode coating or transistor technologies.[12] The interest in CPs as standalone materials, without a rigid substrate, has driven the investigation of AM to produce soft and flexible bioelectronics. However, CPs both as coatings and as standalone films, often exhibit poor mechanical robustness and are prone to cracking,[141,142] limiting the use of AM to create bespoke bioelectronics.[143] Figure 2.6 shows common failures modes of CPs coatings. CP mechanical properties are largely due to their high stiffness, which is reflected in having Young's Modulus in the MPa to GPa range and low fracture toughness.[144–146] These properties also make CPs generally unsuitable for conventional processing techniques that involve mechanical shaping through the use of shear forces.

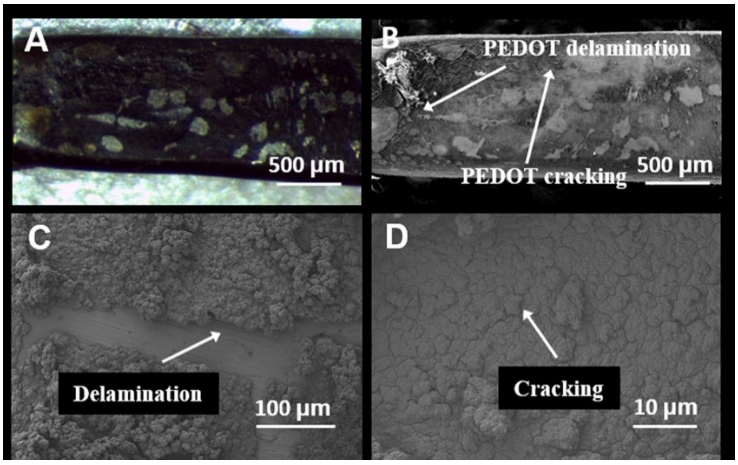


Figure 2.6 Delamination and cracking of PEDOT coating on stainless steel electrodes. Reproduced from Qu et al.,[143] *with permission.*

Attempts have been made to overcome these limitations, which are based on the use of additives such as plasticizers. While PSS acts as a plasticizing dopant, there are other additives that can be used to fine tune the mechanical properties of CPs. For instance, Sun et al.[147] described the effect of different additives, including diisobutyl phthalate (DIBP), diethyl phthalate (DEP), as well as solvents such as acetonitrile and propylene carbonate on the mechanical behaviour of PPy films. The authors demonstrated that all additives resulted in PPy films with improved mechanical properties. The best results were obtained by adding DIBP during the electrodeposition process. Furthermore, they demonstrated that using propylene carbonate instead of acetonitrile resulted in a 200% increase in strain at failure. Similarly, the plasticizer effect of PSS in PEDOT:PSS was investigated by Savagatrup et

al.[148] It was demonstrated that additives such as dimethylsulfoxide (DMSO) and Zonyl fluorosurfactant could reduce cracking under strain (Figure 2.7). Plasticizers provide a simple and relatively direct way to modify the mechanical properties of CPs without fundamentally altering their chemical structure. However the inclusion of these molecules is often associated with a reduction in electrical conductivity and increase in cytotoxicity.[149] As with other properties, the most promising approach to modifying the mechanical properties of CP materials is through the design of CP complexes and composite materials.

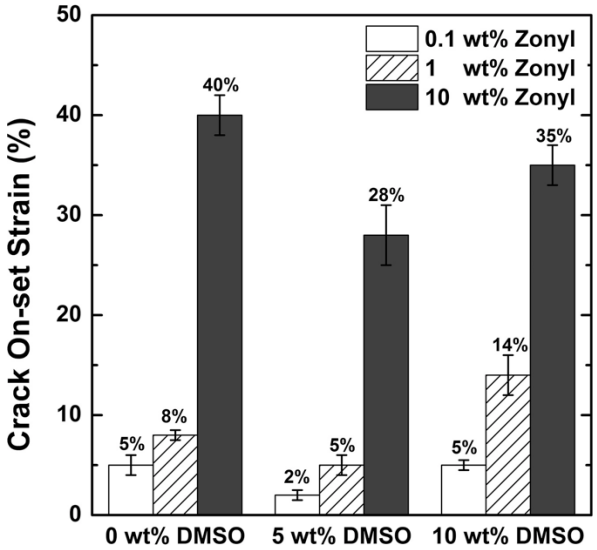


Figure 2.7 The effect of DMSO and Zonyl on the mechanical properties of PEDOT:PSS. Reproduced from Savagatrup et al.,[148] *with permission.*

2.1.8 Limitations of CPs

The limited ability to manufacture free-standing, three-dimensional components using CP-based materials is one of the major issues that prevent the widespread implementation CP technologies in bioelectronics. Significant efforts have been made towards incorporating CPs into conventional and emerging AM processes through the modification of CPs and use of complementary polymers to facilitate tailoring of the bulk properties. It has been shown that the processibility of CPs can be improved through the chemical modification of CP functional groups,[150] the formation of CP-based complexes (such as dispersible PEDOT:PSS),[151] or the synthesis of CP-based composite materials.[152]

Electrically conductive polymers can theoretically achieve the conductivity of metals, but processing is limited in comparison due to the lack of a melt phase. By using additives, which are mostly insulating, the processability can be improved, but this minimizes the electrical conductivity. Cuttaz et al.[153] synthesized a CE by creating a dispersion of PEDOT:PSS within a thermoplastic polyurethane solution, which could be solvent-cast into thin films. PEDOT:PSS loadings of 20 wt% were found to produce composites with a suitable balance between mechanical and electrochemical properties. In particular,

these composites exhibited a Young's modulus of 42 MPa and a conductivity of 6.6 S cm^{-1}. The thin CE films were fabricated into fully organic, soft and flexible electrode arrays using conventional laser machining processes (Figure 2.8). The performance of the CE electrodes was found to be comparable to traditional platinum electrodes, with CE electrodes having a biphasic charge injection limit of 0.020 mC cm^{-2} compared to 0.013 mC cm^{-2} for platinum electrodes. This approach relied on dispersible PEDOT:PSS complexes to enable solvent-based processing of a CP composite. In addition, owing to the use of a thermoplastic polymer matrix, these composites could be readily integrated into thermal processing techniques. The addition of more polyurethane would improve the physico-chemical properties, but it would minimise the electrical conductivity further.

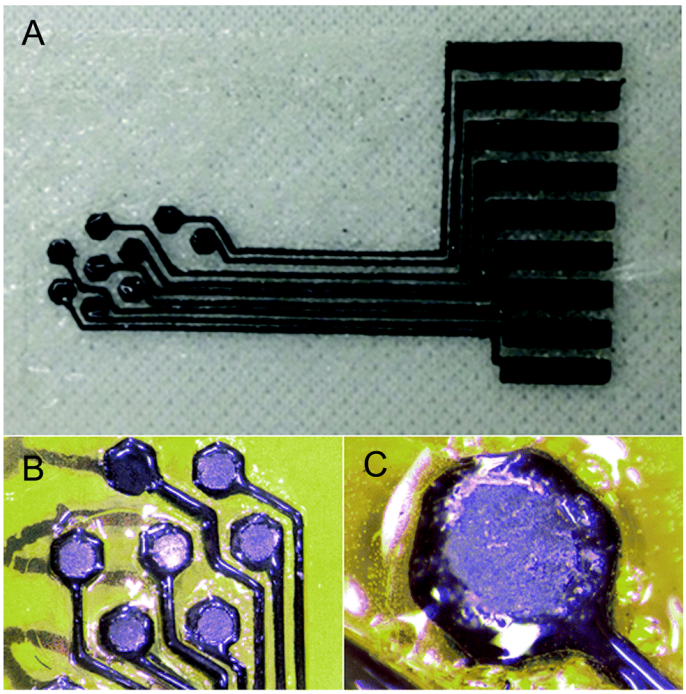


Figure 2.8 Polyurethane/PEDOT:PSS composite electrodes. Exposed electrode sites are 900 µm in diameter. Reproduced from Cuttaz et al.[153] *with permission.*

2.1.9 Processability via Chemical Modification

The processability of CPs for bioelectronics can be realised by changing the physiochemical material properties such as solubility, thermal behaviour, or flexibility due to chemical modification. Although this is mainly done to precursor monomers, the post-synthesis chemical modification of CP materials is also possible. Several efforts have been made to improve the practical applicability of CPs and introduce new functionality through their chemical modification.[154,155]

Doping of CPs is a well-known strategy to change their physicochemical properties.[156,157] One approach to control the impact of dopant on the structure and properties of CPs is to covalently incorporate it as a pendant functional group of the monomer unit. Patil et al.[158] developed a water-soluble CP in 1987 by first modifying thiophene monomers by adding alkane sulfonates at the third ring position. In a second

step, those monomers were polymerized to obtain sodium poly(3-thiophene-*beta*-alkanesulfonates). These types of polymers were characterised as self-doped, as their covalently attached sulfonate groups can lose a proton during oxidation. In 2012, Bu et al.[159] used the same technique to synthesise a solvent soluble PEDOT-based polymer. The researchers synthesised dihexyl- and azidomethyl-substituted EDOT monomers, which were then electrochemically copolymerized. The copolymer was soluble in common solvents such as DCM, THF and toluene with a concentration of up to 0.15 wt%, and remained electroactive even after solvent processing by spin-coating. In addition, this polymer could be post-functionalized by a "click"-cycloaddition with a terminal alkyne. These are both important examples of approaches used to fundamentally alter the processability of CP materials through minor functional group modifications.

The most direct approach to chemical modification of CPs is to directly modify the monomer. Mantione et al.[155,160] described different strategies to functionalise EDOT-monomers, which are easily accessible by chemical modification of chlormethyl-EDOT (Figure 2.9). Then, carboxy-EDOT was synthesized in a further two-step reaction. Carboxy-EDOT is of particular interest in bioelectronic applications, since its capacity to form peptide bonds with amine groups is a common approach for the biofunctionalization of materials. Thiole-EDOT is another important modification of EDOT monomers, which relies on the formation of covalent bonds between their free thiol groups and a substrate to improve coating stability, or to enable secondary, post-synthesis chemical modifications.

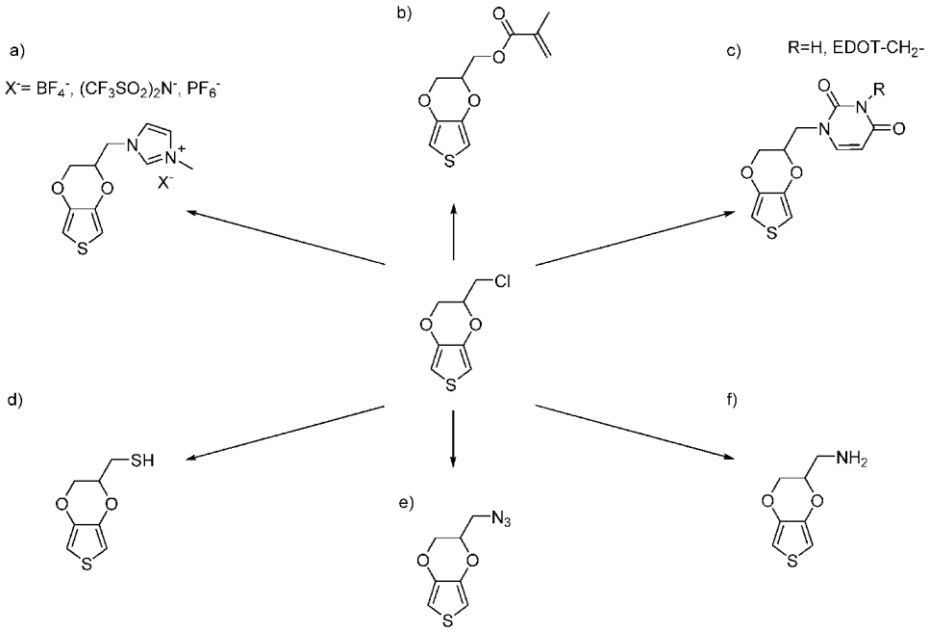


*Figure 2.9 Functionalisation of EDOT monomers with (**a**) imidazolium salts, (**b**) methacrylate (**c**) pyrimidine bases, (**d**) thiole, (**e**) azide, and (**f**) amino group. Reproduced from Mantione* et al.,[155] *with permission.*

It has been well documented that the properties of single homopolymers can be transferred and combined with other macromolecules to produce a multifunctional system. Particularly in the biochemical and biomedical fields, this approach is used to synthesise polymer micelles.[161–163] Blatz et

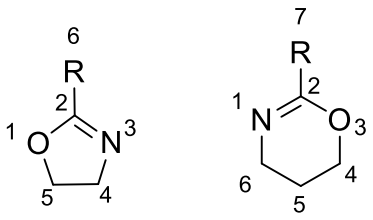
al.[164] synthesised a biofunctional self-assembly CP-peptide by covalently attaching tetra peptide sequences onto thiophene-based monomers. This macromolecule self-assembled to form nanofibrous gels with CP 'wires' encapsulated in the centre of insulating peptide tubes with a resulting conductivity of 10^{-4} S cm^{-1}. While advances still need to be made with regard to the conductivities of self-assembled systems such as CP-peptides, their ability to be used as injectable, in-situ forming materials is significant from a processing perspective. These systems hold the potential to be a useful tool in the development of tissue engineering approaches for repairing damaged nervous tissues.

Other end-group modifications of CPs can be used to introduce a range of functionalities. Yagci et al.[165] synthesised a CP-based block and grafted copolymer in a two-step synthesis process. First, they used a wide range of conventional polymerisation techniques to synthesise homopolymers of various common polymers, and end-functionalised them either with thiophene or pyrrole groups. Second, they electrically or chemically polymerised the functionalised homopolymers via formation of CP chains. A broad library of copolymers was created, a subset of which maintained their conductivity while exhibiting a wide range of thermal and mechanical properties.

Chemical modification of CPs and their monomers is a promising approach to improving their processibility. It provides an avenue to tailor the physicochemical properties of CPs, while also enabling post-fabrication modifications of CPs, such as biofunctionalization. Small changes in chemical structures can result in significant changes in the structure-property relationships of CP-based molecules, often in the form of reduced conductivity. However, for some applications this is a welcomed trade-off owing to the enhanced functionality it affords. Conjugated self-assembly systems, such as the CP-peptide systems are prime examples of careful macromolecular design enabling novel fabrication processes and creating new applications for CP-based materials.

2.2 Polyoxazoline and Polyoxazine

As a general notation in the scope of this thesis, analogous to the literature, 4,5-dihydrooxazole will be simplified and expressed as oxazoline (Ox) and the higher homologue 5,6-dihydro-4H-1,3-oxazine as oxazine (Ozi)



Chemical structure of substituted 4,5-dihydrooxazole (Ox) and substituted 5,6-dihydro-4H-1,3-oxazine (Ozi)

Polymers based on Ox or Ozi offer an alternative to conventional materials for improving the physicochemical properties of CPs. POx and POzi are already known to have broad synthetic flexibility in modification opportunities[23]. Both polymers have been demonstrated to be cytocompatible and have tailorable mechanical properties via modification of side-group chemistry [24]. For example, while short-chain POxs have a hydrophilic character, longer chains show a more hydrophobic character[166]. Besides solubility, thermal properties can also be controlled by the modification of side groups or the synthesis of copolymers. Thermoresponsive behaviour or inverse hydrogelation are further examples of the versatility of POx and POzi[25,26]. This unique character enables a high tunability of material properties and can be used as a useful tool to modify the physical properties of CPs.

High control and broad variation possibilities can also be observed during the synthesis process[167]. Ox have been known from the literature since the late 19th century.[168] Here, 2-methyl-2-oxazoline was the first molecule to be synthesised and chemically isolated. Ox played a crucial role in the synthesis of penicillin, especially during World War II, as it was assumed that ox form the basic structure. More recently, Ox are mainly used as ligands in asymmetric catalysis,[169] as antibacterial coating and as polymers[23] and for the analysis of fatty acids.[167] Ox are five-membered cyclic imino ethers. This means that the cyclic rings contains both a nitrogen and an oxygen atom. Cyclic imino ethers with six or seven atoms are also known but are currently of lesser scientific importance. A distinction is also made between endo- (nitrogen in the ring) and exo-imino ethers (nitrogen outside the ring structure). In the context of this work, only endo structures with five or six atoms are examined and developed. Although there are many different Ox monomers, the main focus of research is still on the use of the aliphatic Ox derivatives such as the above-mentioned 2-methyl-2oxazoline. Glassner et al.[24] summarised the current state of art; It can be stated here that different functional side groups can be introduced, but only furans or benzyl derivatives are known as aromatic and thus potentially electrically conductive structures. It was also found that no crystal structures are known from the literature. Usually synthesised via Ring-opening polymerisation, POx and POzi are initiated by Lewis acids and terminated by electron donors. A commonly used initiator is methyl trifluoromethanesulfonate (MeOtf), but other halides or tosylates can be used. Termination with functional groups allows for subsequent post-modification steps[170].

The chemical structure of POx based on an N-substituted glycine backbone is similar to the structure of polypeptides (Figure 2.10). The side chain of POx is in opposition to polypeptides attached to the nitrogen and not to the α-Carbon. Therefore, the group of POxs are exclusively hydrogen bond acceptors without donor properties. POzis, unlike polypeptides, do not have a hydrogen donor in the backbone, which prevents them from forming secondary structures. With a neutral charge, POx is soluble in the most polar organic solvents and water.[23] While POzi was developed at the same time, it has only recently been explored as an alternative to POx.[171] Unlike commonly used polymers such as PEG, POx and POzi show much better chemical versatility with the same or even better cytocompatibility due to

easy access of side-chain modification. This enables a high control of material properties such as solubility, thermal and other physio-mechanical properties.

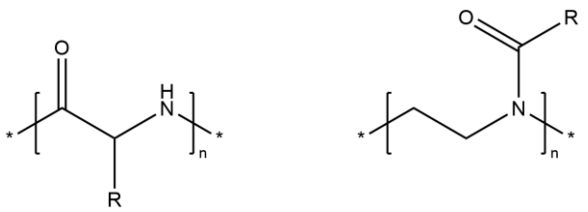


Figure 2.10 General structure of polypeptides (left) vs polyoxazoline (right)

In contrast to the polymerisation techniques that can be used for the polymerisation of conductive polymers, POx and POzi are obtained by ring-opening polymerisation. Since these polymer classes form the basis of this work, they are described in detail below. The synthesis options and finally the physio-chemical properties are discussed. Above all, the detailed synthesis is of great importance here, as this enables the possibilities of chemical modifications and impacts the viability of developing copolymer systems.

2.2.1 Synthesis of POx and POzi

As a historical recapitulation, the first successful synthesis of Ox was reported by Gabriel et al.[172] almost 150 years ago. Ox and the higher derivates of Ozi are cyclic-imino ethers (imidates) and can usually be polymerised via Living cationic Ring-opening polymerisation (LCROP). However, due to the nucleophilicity of several functional side groups, not every Ox and Ozi derivate can be polymerised. Alkyl-Ox/Ozi are the most common, but show limitations in their tunability and, therefore, in their physicochemical properties. Only through copolymerisation of different monomers can their properties be controllably tailored. Ox and Ozi are typically used as ligands in asymmetric catalysis or as protecting groups for carboxylic acids.

Aoi et al.[167] summarised the known synthesis strategies of Oxs and Ozis. Starting with nitriles or non-activated carboxylic acids, the monomers are generally received in good yields. In the scope of this thesis, only three common methods are briefly described here (Figure 2.21). While the Wenker method is useful for larger scales, the Witte and Seeliger methods enable a good alternative for laboratory scale work. To receive more complex monomers, α-deprotonation is another useful technique. The Wenker method uses non-activated carboxylic acids and amino alcohols catalysed with metals. This technique requires high temperatures. In contrast, the Witte-Seeliger method uses nitriles instead of carboxylic acids. Zinc acetate is used as a catalyst and this technique is usually performed at moderate temperatures in a one-pot reaction. α-deprotonation is usually performed with methyl-oxazolines (MeOxs) in a two-step reaction. Firstly, a strong base substitutes the methyl group and in a second step, functional groups are enabled using alkyl halogens. These approaches allow for a wide range of functional variants of Ox

and Ozi, thus enabling a high degree of control when tailoring the physicochemical properties of the resultant polymer systems.

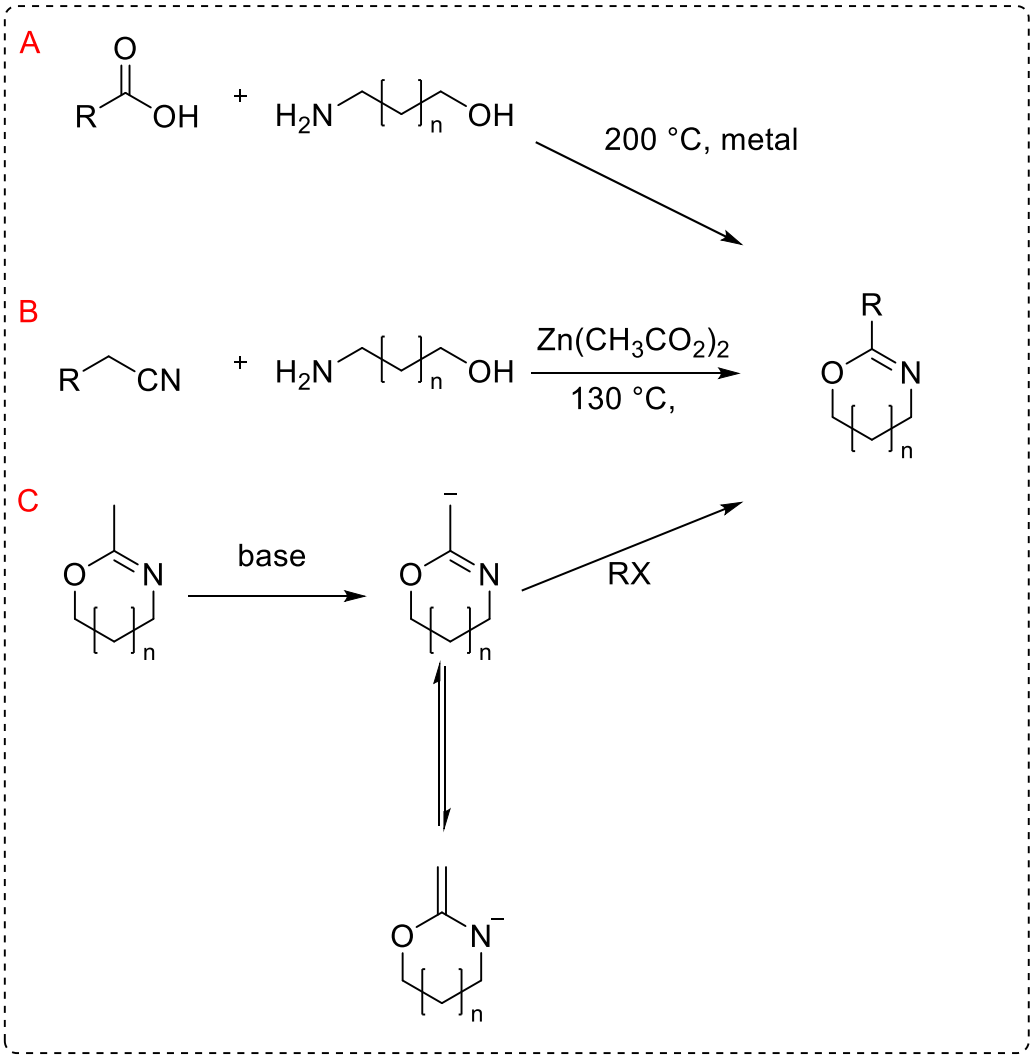


Figure 2.11 Synthesis of Ox and OZi monomers by a) Wenker using Carboxy acid, amino alcohols and a metal catalys, b) by Seeliger and Wittig using carbonitriles, amino alcohols and zinc acetate, c) by α-deprotonation of MeOx or MeOzi

Cationic ring polymerisation (CROP) is the traditional way of polymerising POx and POzi. The polymerisation is generally divided into initiation, propagation, and termination stages. Due to the high level of control during polymerisation, it can be described as a living polymerisation. This makes it possible to synthesise polymers with an exact molar mass distribution, thus allowing a direct influence on the material properties. It should be mentioned, as a disadvantage, that the starting materials must be of high purity during the synthesis since even the smallest impurities have a direct influence on the polymerisation.[173] Above all, water and other nucleophiles interfere considerably. While the polymerisation of Ox has been studied in-depth, the polymerisation of Ozi has received less attention. However, it is assumed that the polymerisation of Ozi takes place analogously.

CROP is initiated by nucleophiles such as Lewis acids, strong protic acids or esters, and alkyl halides.[174] MeOtf and methyl tosylate are the most widely used initiators.[167] The ring-opening is a highly exothermic reaction, whereby the initiation proceeds rather slowly at room temperature since an individual energy barrier has to be overcome first.[173] The above-mentioned reactive initiators can nevertheless also enable the polymerisation to take place at room temperature. The nucleophilic attack is shown graphically in Figure 2.12. The chemical modification of the initiators allows functional groups to be introduced into the polymer, which, however, has a direct influence on the reaction kinetics of the polymerisation and thus on the living character of the polymerisation.[167] The most important factor during polymerisation is the constant number of reactive species.[108] The initiation rate must therefore be significantly greater than the propagation rate since termination can only take place with a high purity of the starting materials when termination reagents are added. Another important property of the CROP initiation, which plays a subordinate role in the context of this work, is the possibility of producing so-called initiator salts. As shown in Figure 2.12, there is an equilibrium between the cyclic cationic and linear species. The balance is mainly determined by the choice of counterion. Solvent and monomer properties also have a direct influence.[23] The cyclic species is more reactive. In the case of initiator salts, this reactive factor is "frozen" and can be stored for a longer period of time.[175] On the one hand, this allows inert monomers to be used in a CROP. On the other hand, it allows the thermodynamically very reactive initiation of polymerisation to proceed more mildly as the reaction is almost "frozen". For safety reasons, this is very important for studies on a laboratory scale and for up-scaling attempts.

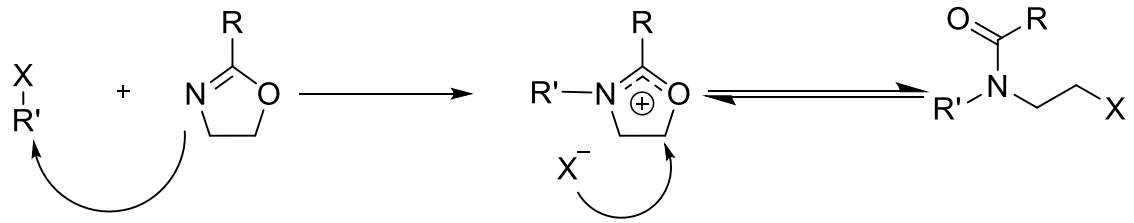


Figure 2.12 Initiation of polymerisation mechanism of POx

Both the cyclic cationic and the linear species, shown above, have an electrophilic character and can be attacked nucleophilically by further monomer units. This enables the propagation reaction (Figure 2.13).[167] The ring-opening is represented by a tertiary amide structure, the introduction of the first monomer unit being the rate-determining step since this takes place much more slowly than the introduction of further monomer units. The reason for this is that the carbonyl group of the previous group coordinates to the tertiary amide and thereby the electron density on the active group is electrophilically influenced. This cannot take place with the introduction of the first monomer. Further influencing factors for the speed of the propagation are the structure of the monomer and the sterics of the side group.[108] As an example, alkyl side groups can be considered in more detail. The + I effect reduces the reactivity of the cyclic imine but increases the nucleophile of the imine group. The nucleophile of the monomer is reduced by electron-withdrawing side groups. Furthermore, the rate of propagation is influenced by steric side groups. Short-chain alkyl groups are far more reactive than long-

chain ones. These properties, therefore, have a direct influence on the statistical distribution during the copolymerisation. While reactive monomer units are incorporated more quickly into the polymer chain, sterically and less reactive monomers are incorporated later. As a result, despite copolymerisation, statistically distributed copolymers are only synthesised if the reactivity of the monomers is approximately the same.[176] Otherwise, Ox tends to form homopolymers or block copolymers.

Block co-polymerisation of Ox and Ozi can also be produced by a controlled reaction procedure. Kobayashi et al.[177] was the first to synthesize amphiphilic block copolymers. Here, homopolymerisation is first initiated by a monomer species. After all the monomers have reacted completely, a second block can be produced when a new species is added. This allows copolymers with precisely defined areas with specific properties to be produced. Due to the wide variety of monomers, copolymerisation enables interesting properties that can also be used for biomedical applications.

The polymerisation of Ozi has been much less studied.[171] In general, it has been found that the polymerisation of Ozi takes place more slowly than analogous Oxi because the active Oxazolinium species is not planar and therefore steric hindrance is present.[167] The reduced ring strain in the six-membered ring further reduces the reactivity of Ozi. However, a more extensive investigation of the reaction kinetics of Ozi is not known from the literature and thus little can be said about a theoretical prediction of reaction products in the run-up to a polymerisation.

The polymerisation of Ox and Ozi is considered a living polymerisation. However, molecular chains with more than 200 units are difficult to produce because side reactions such as chain transfer or chain coupling occur.[178] This creates polymers with broad molecular weight distribution. These side reactions occur more frequently, especially as a result of longer reaction times. As such, it is difficult to produce POx and POzi with narrowly distributed molar masses when long reaction times are used. This is more notable with POzi because of side reactions occurring due to β-elimination and imine-enamine tautomerism. Contamination and solvents also can also have a significant effect on molecular weight distribution..[167]

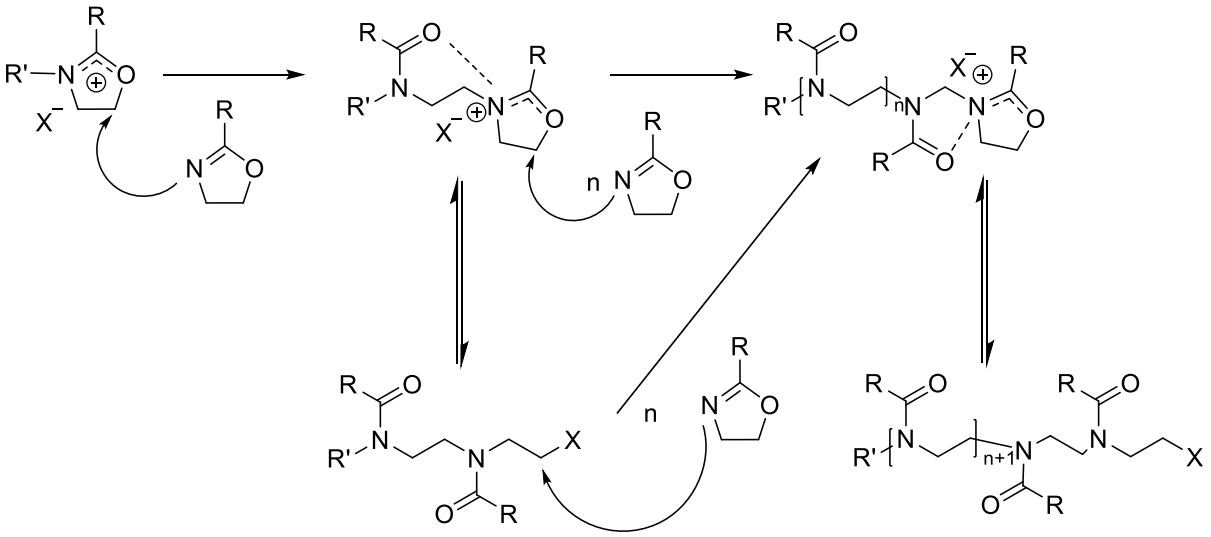


Figure 2.13 Propagation of polymerisation mechanism of POx

The termination of POx and POzi can be carried out by any nucleophile.[23] Analogous to the initiation, functional groups can also be inserted here. As mentioned above, the active species has two possible nucleophilic targets that can be used for termination (Figure 2.14).[167] The termination is based on the HSAB (hard and soft acids and bases) principle. Soft nucleophiles (water, alcohols or amines) terminate preferentially at the second position.[179,180] This initially creates an amide-like structure that is in equilibrium with the oxazolonium structure. A ring-opening of this transition structure can occur with water through the formation of an amino ester.[180] Alternatively, the termination at the fifth position involves a more direct ring-opening as shown in Figure 2.24.[167] Common terminating reagents are piperidine or basic methanol solution.[181]

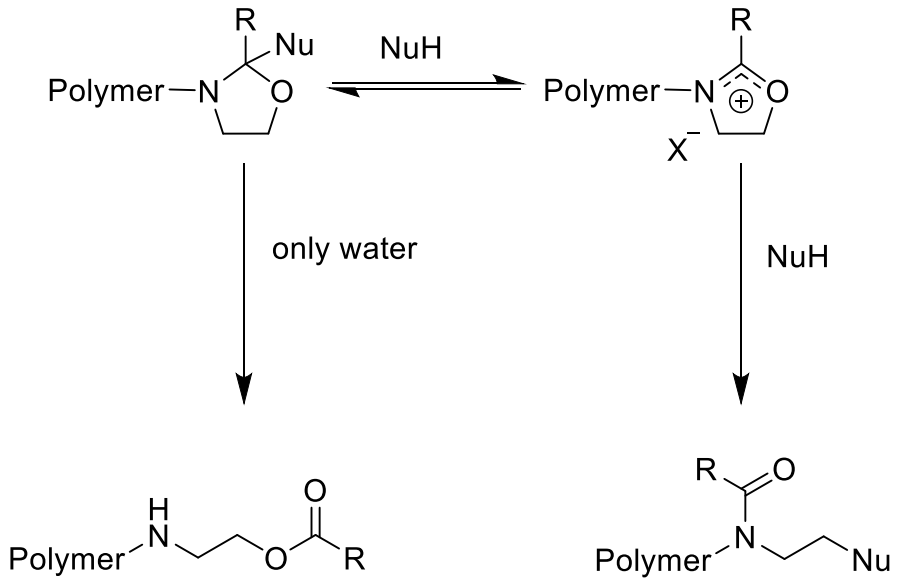


Figure 2.14 Termination propagation of polymerisation mechanism of POx by nucleophilic attack

2.2.2 Physicochemical Properties of POx and POzi

Because of the simple and easily controllable synthesis of POx and POzi, there is currently great interest in the possible use of these polymers for a wide variety of applications. Biomedical applications are also conceivable due to the non-toxic properties of POx and POz. In addition, the properties of the polymer can be adjusted through the use of suitable modified monomers. Above all, the thermal behaviour and the solubility can be changed individually. The limited chain length, on the other hand, has a negative influence on the mechanical properties of the polymer.

In general, the thermal decomposition of POx is 300 °C, with thermal aging already starting at lower temperatures.[182] This decomposition limit is thus comparable to the polythiophenes listed above and enables a wide temperature range for the simultaneous processing of both polymer classes. The thermal behaviour is significantly influenced by the side groups and POx can therefore be present either as an amorphous or semicrystalline polymer.[108] The melting temperature depends on the nature of the side group and not on its length. For example, semicrystalline polymers with alkyl side groups show a T_m of 160 ° C.[182] In the case of cyclic side groups, melting temperatures of over 300 ° C were found, whereby the decomposition is already beginning and, therefore, cyclic POx can only be used to a limited extent in thermal processing options. In contrast, the T_g of POx and POzi is significantly influenced by the number of carbons in the side chain.[108] Longer polymer chains lower the T_g. The simplest alkyl POx, poly(methyl-oxazoline) (PMeOx), has a T_g of 80 ° C.[182] In comparison, poly(hexyl-oxazoline) has a T_g below 0 ° C. One possible explanation here is the degree of crystallinity. The crystal structure is less disordered by smaller side groups such as methyl than by long-chain side groups. As a result, there is higher crystallinity and the T_g increases. Furthermore, the same trend is observed for cyclic side groups, with the molar mass having a lesser influence. For example, poly(2-phenyl-2-oxazoline) has a mass-independent T_g.[183] Knowing the individual temperature properties of homopolymers enables the T_g to be controlled by statistical copolymerisation.[23] With the combination of amorphous and semicrystalline polymers, on the other hand, the melting temperature usually rises. Furthermore, it should be said that the thermal behaviour of POzi has not yet been extensively investigated. However, initial investigations show that in general, the T_g of POzi is around 50 ° C lower than that of analogue POx derivatives.[171]

The solubility of POx and POzi is also significantly influenced by the type of side group.[184] Modifying side groups can shift the nature of POx systems from hydrophobic to hydrophilic. Short-chain P(alkyl-Ox) result in hydrophilic behaviour whereas long-chain groups result in hydrophobic behaviour.[184] [24] The lower critical solution temperature (LCST) can also be controlled, with longer side chains resulting in lower LCST.[185] In addition to the chain length, the degree of polymerisation and the end group chemistry of the polymer also have a decisive influence on the polymer solubility.[184] [186]

Statistical copolymerisation, mentioned above as a means to carefully control thermal behaviour, can again be used to carefully modify the solubility of POx copolymer systems[187] Combined behaviour is

also of great interest. Luebtow et al.[188] were able to produce micelles through a combination of hydrophobic and hydrophilic POxs.

2.2.3 Biological Properties of POx and POzi

In general, homopolymers of POx have been shown to have both good cytocompatibility and good hemocompatibility. Early investigations into the cytotoxicity of POx systems have demonstrated functional variants PMeOx and PEtOx to have excellent cytocompatibility and hemocompatibility. [189] While further studies are still needed to demonstrate biological safety of POx and POzi materials in biomedical applications, early indications are promising.

In order to investigate the full potential of POx, in vitro cytotoxicity and in vivo experiments were carried out as early as the 1980s. It was shown that POx was rapidly degraded in the bloodstream with no evidence of toxicity/nephrotoxicity. [190] A more recent study by Wyffels et al.[191] investigated the degradation of PEtOx more intensively. It was found that especially polymers with a molar mass of less than 20 kg/mol could be rapidly transported through the kidney. It is significant that larger polymer chains (> 20 kg/mol) remained in the body for a much longer time. In the context of drug delivery, a clinical study based on POx was carried out only recently.[192] POx was used as a drug delivery conjugate for the treatment of Parkinson's disease and was successfully tested on 20 volunteers. BioNTech Manufacturing GmbH is also investigating POx as a nanogel drug carrier for tumour targeting. Due to these good results in the field of drug delivery, POx has great potential for various applications such as coatings or matrix materials.

Biodegradation of POx can be initiated by hydrolysis.[193] The POx backbone is chemically very stable. However, the amide side group can be split off by strong bases or acids and degradation can take place. However, studies have shown that POx remains stable under physiological conditions.[189] Even in a strongly acidic milieu, such as in the stomach, no hydrolysis and thus biodegradation of the polymer could be observed. There are also indications that degradation by oxygen and/or enzymes can take place, but here as well, no significant evidence has been found on a biologically relevant level.[23] Thus, in general, it can be said that POx is stable under such conditions.

2.2.4 Limitations and Potential of POx and POzi

Even if a large number of different Ox and Ozi monomers can in principle be used for the synthesis of polymers, only a few are commercially available. Glassner et al.[24] compiled an overview of monomers known from the literature. There are almost no limitations with aliphatic monomers. Side chains of 15 carbon atoms are also possible. However, aromatic heteroatoms are not listed. As seen in the previous chapter, there is a wide range of ways to synthesize monomers, but these are usually complex and therefore only feasible on a laboratory scale and are not typically commercially available. This

limitation of the commercially available and the costly implementation ultimately leads to the restriction of large-scale technical applications. However, only heptadecadiene-2-oxazoline, i.e. functional Ox from Henkel, is currently used for commercial applications. The Ox serves as an activator for lactam polymerisation, as it is comparable to a soy-alkyl functional group. The other areas of application as ligands,[194] drug delivery components or as an antimicrobial coating of textiles has yet to be translated from research to commercial applications. However, as previously discussed, it is possible to produce POx in a comparatively simple manner. The end functionalisation through initiation or termination is of particular interest here. In this way, commercially available aliphatic polymers can be modified with groups and functionalisation can be introduced into the polymer as a result. Podevyn et al.[195] use a methyl bromoacetate as initiator for this. This made it possible to functionalise the polymer with various end groups in a further reaction (amidation). An analogous way of inserting functional groups into a polymer is to deprotonate PMeOx using LDA and reacting with bromoalkenes afterwards.[196] Ultimately, it is also possible via the Seeliger and Wittig reaction to introduce a large number of functional groups into the polymer during the monomer synthesis. The starting materials here are alcohol-amines and the respective functional nitrile. This is then implemented in an almost full conversion and enables easy access to a wide range of functional monomers.

The use of POx and POzi in 3D printing and thus a large-scale implementation is currently of great interest. The advantage here is that this class of polymers can be modified very easily and thus has good control over the physicochemical properties. Above all, it is possible to specifically influence the melting range of the polymer used. This enables a wide temperature range to be covered. Nahm et al.[29] produced a biomaterial based on PEtOx, which could be implemented in 3D printing via MEW. The authors had a great deal of control over the printing parameters and were able to influence them in a targeted manner. In addition, it was possible in a post-modification to chemically crosslink the printed structures and thus produce hydrogels. This made it possible to demonstrate the use of a functional polyoxazoline in a process that can be implemented on an industrial scale. Shubba et al.[197] investigated the use of polyoxazolines as a blend for polyvinylpyrrolidones (PVP) to influence the material properties. Using aliphatic PEtOx, the authors were able to vary the physiochemical properties of the blend in a targeted manner and determine an optimal ratio of PEtOx:PVP of 80:20 wt%. The disadvantage here is that PEtOx usually has non-conductive properties. Due to the hygroscopic properties of PEtOx, water-free processing is essential for the manufacturing of smooth surfaces and therefore in high accuracy. Therefore, PEtOx had to be modified with PVP to develop a robustness against water and thereby ensure better processing. It is therefore sensible to keep the proportion of additives that have no or only very poor conductivity as low as possible in order to continue to ensure an improvement in all material properties. Polymer blends have become increasingly important in recent years.[198] This means that different plastics can be mixed together, and no chemical bonds are formed. This means that materials with different properties can be mixed and new combined properties can be generated. The advantage is that no time-consuming synthesis has to take place. However, the problem is that due to the lack of

chemical bonds, phase separation can occur during processing. Therefore, the starting materials must usually have similar physico-chemical properties. This inevitably limits the possible combinations. As seen above, the physico-chemical properties of POxs are very variable and therefore the chemical modification is preferred and blending is not necessary.

2.3 Processability of CPs via Additive Manufacturing

Conventional fabrication processes for polymers, such as injection moulding, extrusion or stretch blowing are limited by the need of formative supporting materials, minimum number of units and the inherent processibility properties required of the stock material.[199–201] Traditionally, geometrically complex structures can only be realised with high effort and cost, especially at lower economies of scale. Furthermore, functional materials with poor physical fabrication properties such as CPs are difficult to produce at industrial scales. New fabrication approaches such as AM have created emergent possibilities in applications of CPs which were previously unfeasible due to their poor processability. Printing of CPs needs to include the simultaneous printing of dopant counterions or post-processing of components to improve conductivity. AM is a universal definition for layer-to-layer fabrication processes, which include stereolithography, laser sintering, melting, extrusion, jet-modelling and photopolymerisation. 3-dimensional, rapid prototyping and bespoked custom-made items can be realised with this technique. A key advantage of 3D printing is the lack of a stencil or other formative masks, and the potential to produce complex geometries. A summary of novel CP fabrication approaches is provided in Table 2.2.

Table 2.2 Conductive polymers in AM fabrication

Material	Process	Applications	Pros	Cons	Citation
PEDOT:PSS	Roll-to-roll printing	Flexible transparent electrodes	Low cost	substrate-dependant	Hu[202]
PEDOT:PSS	Roll-to-roll printing	Electrochromic devices	Surface functionalisation	Substrate-dependant	Santos[203]
PEDOT:PSS	Inkjet printing	OLEDs	Easy of handling	Solution based processing technique	Yoshioka[204]

PPy/polythiophene	Lithography	Stretchable transistor	Scalable fabrication technology	Substrate-dependant	Wang[205]

An early first step in the direction of AM of CPs was made by a process called roll-to-roll printing. This technique allows the fabrication of thin films of CPs on any kind of materials without the need for electroactive materials or expensive metals such as gold or platinum. The roll-to-toll method utilized by Hu et al.[202] and Santos et al.[203] enables the use of a broader range of viable substrate materials. Hu et al.[202] demonstrated a roll-to-roll method for printing nano-patterned CP coatings on flexible substrates (Figure 2.15). A flexible polyethylene terephthalate (PET) membrane is nanopatterned with a PEDOT:PSS:graphene oxide film using a slot-die printing head. The wet films were then passed through a hydroiodic acid bath, methanol washing and thermal annealing, which yielded a conductivity of 1949 S cm^{-1}. One advantage of this technique is that the resultant CP films are comprised of highly aligned PEDOT domains. In turn, these could be used for to manufacture highly conductive, flexible and transparent electrodes, which could potentially be used for bioelectronic devices. However, one limitation of the roll-to-roll method is that it is still dependent on a substrate material and cannot be used to fabricate 3D geometries without further processing.

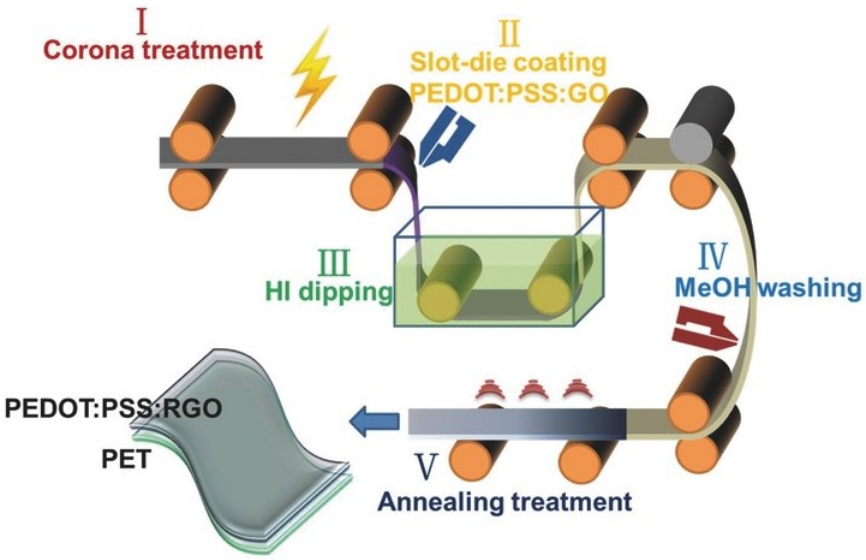


Figure 2.15 Roll-to-roll method for conductive polymer coating. Reproduced from Hu et al.*[199] with permission.*

Due to the lack of a melt phase, the use of CPs in AM fabrication remains challenging. A common approach is the use of additives or chemical modification to create a printable or transferable solution to form custom-made bioelectronics. Inkjet-printing is an AM technique in which a polymer ink is pushed through a printing nozzle using a piezoelectric element, which generates a constant stream of ink droplets (Figure 2.16). This method does not require an intermediate carrier, specific stencils, screens

or rollers, and is relatively cost-effective. However, the inks used in this technique require specific rheological and thermal properties. Yuk et al.[206] described the use of inkjet printing to fabricate CP meshes from inks with different concentrations (1 to 10 wt %) of PEDOT:PSS. The resulting scaffolds could be formed with resolutions in the range of 30 – 200 µm, with up to 20 print layers and a conductivity of 155 S cm^{-1} (Figure 2.16). The best results were achieved with 7 wt% PEDOT:PSS.

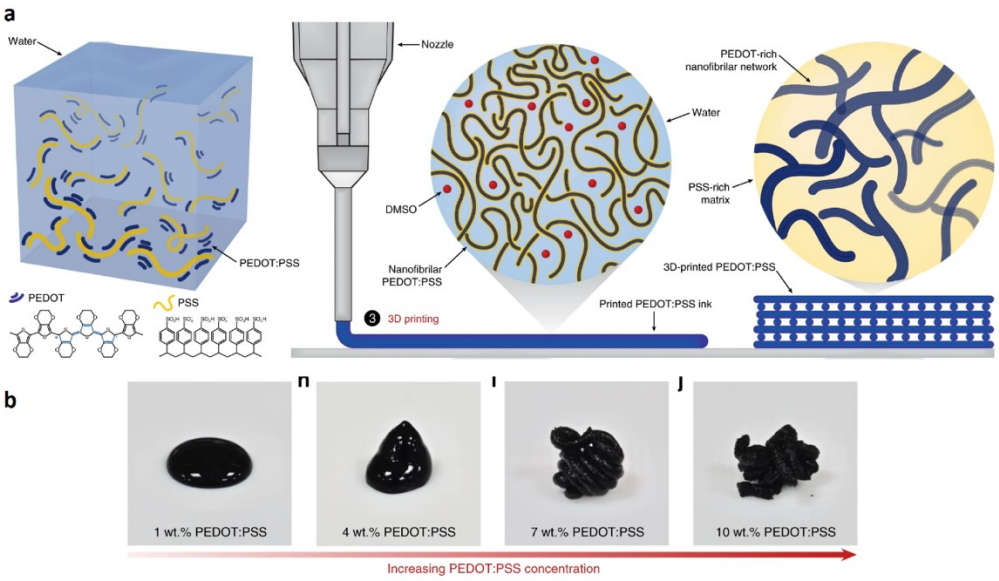


Figure 2.16 (a) Inkjet printing of PEDOT:PSS; (b) Printable inks made with different concentrations (1 to 10 wt %) of PEDOT:PSS. Reproduced from Yuk et al.*[202] with permission.*

CP composites have also been used in lithography-based AM processes. Stereolithography uses light-curing polymers, such as epoxides, acryl or vinyl resins to form a laser-initiated 2D matrix in a resin-filled bath. By moving the collector into the bath, it is possible to fabricate 3D objects using a layer-by-layer process. Scordo et al.[207] synthesised a CP composite by combining different concentrations of PEDOT:PSS with poly(ethylene glycol) acrylate (PEGDA) (Figure 2.17). The addition of a photoinitiated crosslinking agent resulted in a printing material that could be used for stereolithography. Their results showed that the ratio of 5:1 PEDOT:PSS to PEGDA exhibited the good mechanical performance as an accurate structure was manufactured and the overall conductivity was estimated to be 0.05 S cm^{-1}. A similar CP hydrogel was recently developed by Heo et al.[208], which was used to 3D print scaffolds for neural tissue engineering. In addition, dorsal root ganglion neuronal cell lines were encapsulated in gelatin methacryloyl (GelMA) hydrogels after printing, which were then integrated into the conductive structures. Figure 2.18 shows the different printing resolutions that could be achieved as well as primary neural cells encapsuled within the printed patterns.

It could be shown that there are many different approaches to addressing the limitations of processing CPs including the use of adjuncts such as dopants and plasticizers and the adoption of novel

manufacturing techniques. However, none of the techniques listed could process CPs without extensive pre-treatment or by using additives. Furthermore, the techniques could not achieve the desired high resolution. Therefore, it is of great interest that chemical modification enables techniques that depend only on one critical parameter such as melting temperature for MEW for example and that those techniques offer a high resolution of the printed structure.

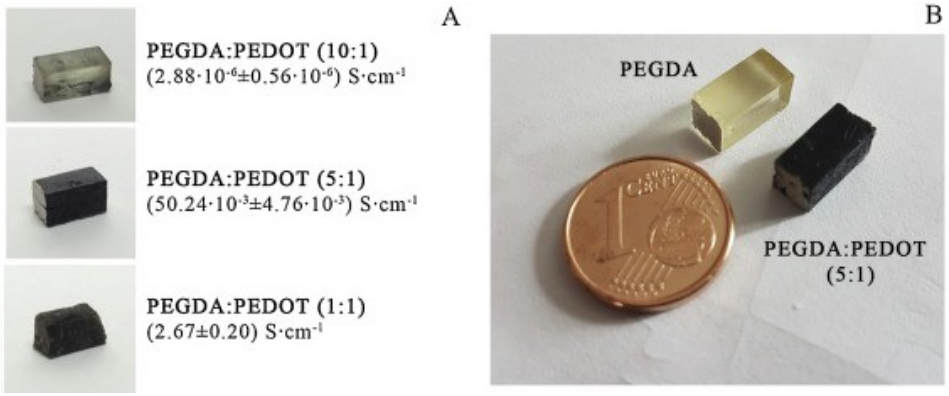


Figure 2.17 (a) Different ratios of PEDOT:PSS/PEGDA used for stereolithographic fabrication; (b) Pristine PEGDA and PEGDA:PEDOT (5:1) hydrogels. Reproduced from Scordo et al.*[208] with permission.*

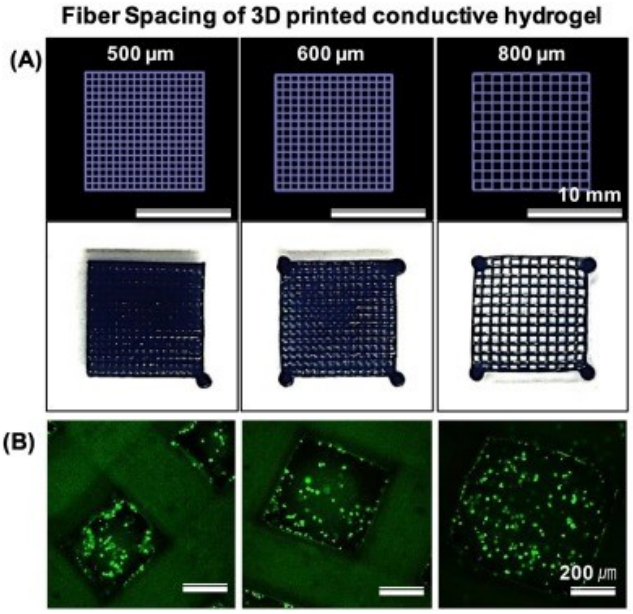


Figure 2.18 (a) Different patterns printed using photocurable PEDOT/PSS hydrogels. (b) Cells derived from dorsal root ganglia encapsulated in GelMA with 3D printed PEDOT/PSS hydrogels. Reproduced from Heo et al.*[209] with permission.*

2.3.1 Melt Electrospinning Writing (MEW)

Biofabrication is a relatively new term in research and summarises a multidisciplinary field including biofunction, biocompatibility, and the manufacture of constructs for TE and regenerative medicine. Often referred to as the next industrial revolution, AM plays a key role in TE and regenerative medicine.

With CAD technologies there is almost no limit to the design of 3D objects that can be realised via AM. The combination of AM and TE principles opens up the possibility of bespoke TE constructs for patient-specific therapies. AM is a useful tool as the fabrication allows for well-defined structures with high control of accuracy. From a technical view, most of the AM methods like stereolithography, selective laser sintering, fused deposition modelling (FDM), or 2-photon polymerisation are limited in TE applications due to their resolution limit of around 20—30 µm. In contrast, the recently developed technique, MEW achieves a low-micron level resolution with fibre diameters of approximately 5 µm. These fibres can be directly written and stacked on top of each other (Figure 2.19). This approach enables highly porous 3D scaffolds (87—98% void space) ideal for seeding with cellular cultures

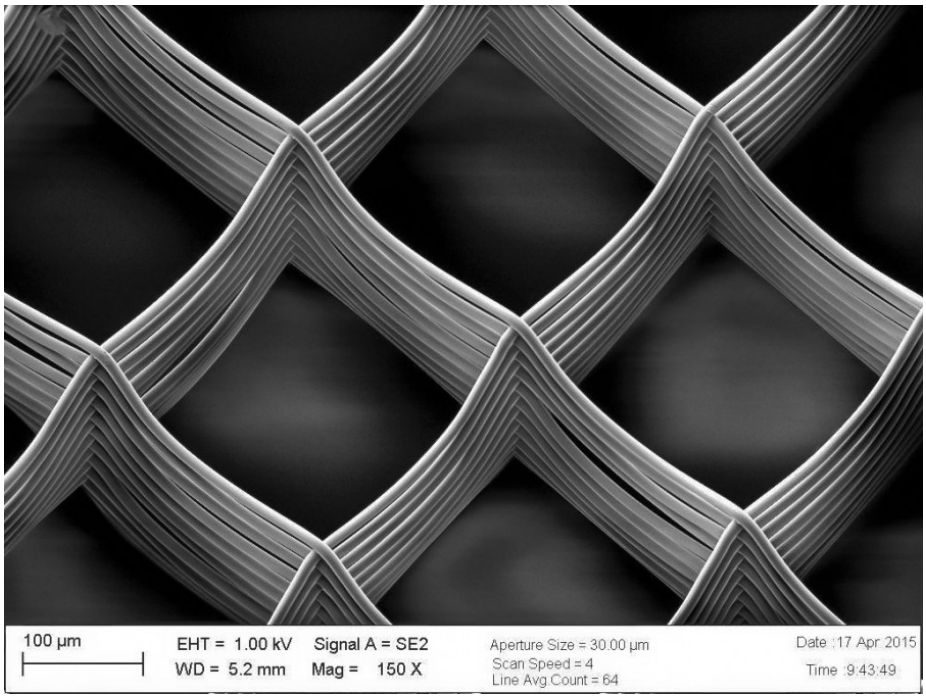


Figure 2.19 MEW printed scaffold of PCL with a resolution of 100 µm

Fibre diameter is typically limited by the 'die swell' or 'extrudate swell' effect. Also known as the Barus effect, it occurs when a polymer melt is pressed through an orifice. The external pressure used to pass the polymer through the die orifice force the polymer chains into thermodynamically critical alignments, leaving residual stress within the material. After extruding from the nozzle, the elastically stored energy is released, and a relaxing process occurs when the polymer fibre swells in aqueous environments. Minimising the orifice radius correlates strongly with an increase in pressure at the die orifice, thus increasing the swelling effect. Further increases in applied pressure can also result in unstable extrusion jets which negatively impact upon print fidelity.

To overcome this limitation, MEW is based on electrospinning processes which use the Taylor Cone phenomena (figure 2.20) to print at smaller resolutions than is possible with other AM techniques. Herein, a high electrical voltage is applied to a liquid droplet. Due to the charge, an electrical loading

occurs, and the droplet is stretched. At a critical point of stretching, the droplet breaks, and a fine jet (Electrospinning) is observed, which decomposes shortly after into a fine spray (Electrospraying). Using polymer melts instead of solutions, allow the jet to stabilise due to cooling processes and viscosity. MEW exploits this phenomenon to print micron-scale features without the use of solvents.

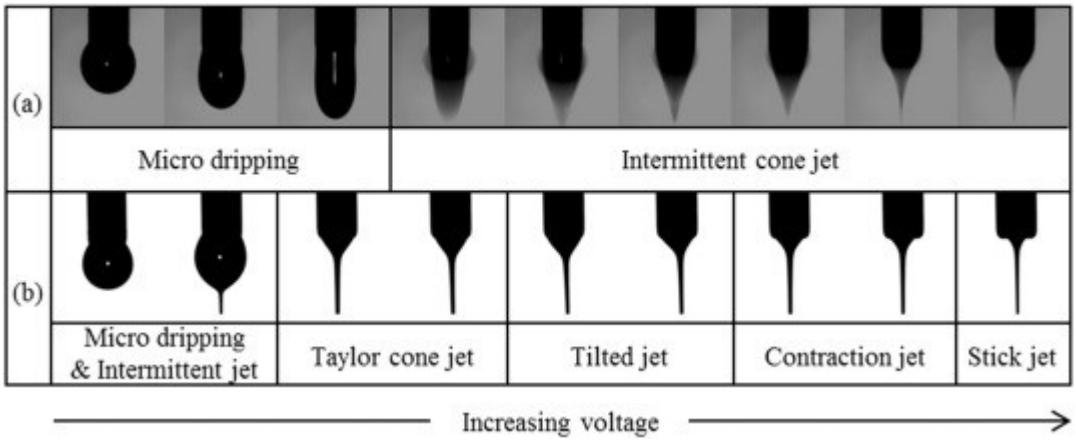


Figure 2.20 Formation of different cone jets[209]

In principle, MEW is quite simple: A meltable polymer material is heated in a reservoir until it forms a melted state (Figure 2.21). The polymer is then pushed through a small orifice by air pressure and a high electric potential difference between the print nozzle and collector. Inert gas like nitrogen allows printing at higher temperatures while prevent oxygen and moisture mediated decomposition of the printed polymer. Due to the electrical field between the nozzle and the collector, a Taylor cone is developed, and a fine jet can be formed. Layer-by-Layer structures can then be formed by moving the collector in all three dimensions. Another critical printing variable is therefore the speed of moving the collector (CS). Depending on CS, temperature, pressure, voltage and humidity, an optimal fibre with a resolution down to 5 µm can be generated.

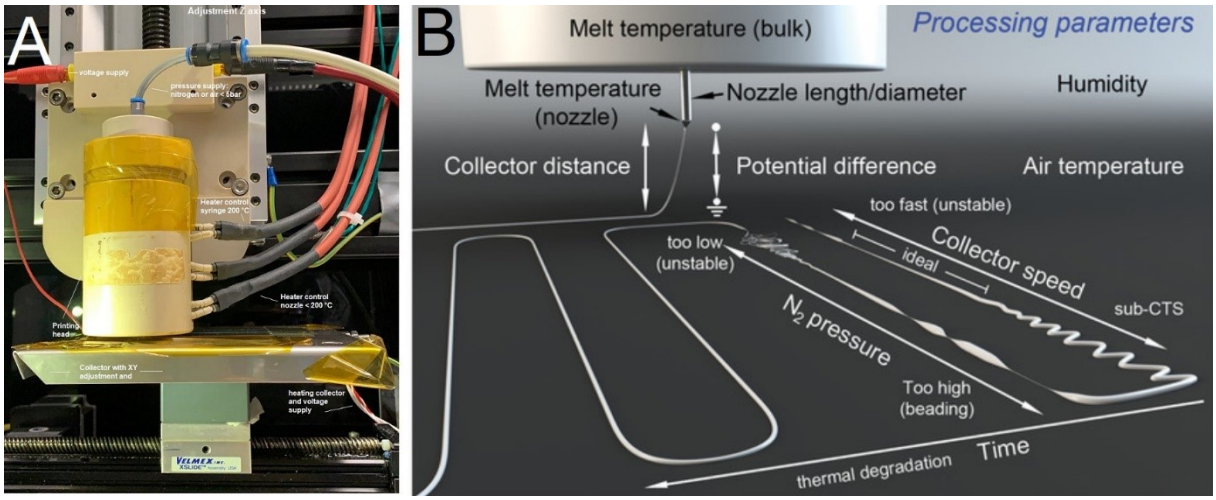


Figure 2.21 a) MEW printing setup with the printing head, collector and electrical connections b) processing parameters, which can occur during printing with different printing parameters

While an electrical field between nozzle and collector brings the advantage of forming low-resolution fibres, it also brings some restrictions with it. A voltage of around 3 kV/mm must be used to create a stable Taylor cone. The ionisation of surrounding gas molecules can either destroy the polymer jet, initiate side reactions or create an electrical spark between orifice and collector. Therefore, usually non-conductive polymers like PCL , with conductivities of around 10^{-6} – 10^{-8} S m^{-1}, are used for MEW printing. Incorporating conductive elements, such as CPs, within printed material presents a challenge since they have the potential of shorting the nozzle and the collector, thus destabilising the Taylor cone.

2.3.2 MEW Applications of CPs

As previously discussed, CPs are prone to thermal degradation and do not inherently possess melt phases. Therefore, in order to be compatible with MEW processes, CPs need to be modified to be meltable and thermally stable. Ma et al.[30] developed a 3D printing ink that met these criteria by dispersing PPy nanoparticles in a solution of poly-l-lactide (PLLA) dissolved in 1,4-dioaxane. A pneumatic extrusion-based 3D printer was used to fabricate conductive scaffolds at room temperatures. The solvent was subsequently removed via lyophilisation to produce cytocompatible PPy-PLLA scaffolds with low conductivities (up to $7x10^{-5}$ S cm^{-1}). The first actual MEW printed electroactive scaffold was demonstrated by Olvera et al.[210] The authors used a MEW printed PCL scaffold as a substrate for the subsequent in-situ chemical polymerisation of PPy. This strategy was used to fabricate conductive cardiac patches capable of elastic deformation up to 40 % strain with a conductivity between 2.0 and 2.5 S cm^{-1}. Furthermore, the cytocompatibility of the scaffold was demonstrated in culture with primary rat cardiac fibroblasts. This approach of post-printing modifications avoids the issue of directly printing a conductive polymer under an applied high voltage.

In addition, as already mentioned above, a short circuit can occur when printing Cps. This must be avoided at all costs, both for the functionality of the printer and for the safety of the personnel. Therefore, only material with a conductivity in the range of 10^{-6} S cm^{-1} or less should be printed. However, this would be in direct competition with the development of materials that are as conductive as possible. A possible solution would be to first print undoped CPs and then convert them in a chemical oxidative reaction. This approach would thus make it possible to print CPs.

By bringing together the approaches of CP monomer modification, complexing, and composites it is possible to develop techniques for using AM to create conductive 3D components from CPs. Ritzau-Reid et al.[211] recently reported an oligo-EDOT system that could be either crosslinked by 8-arm PEG to form hydrogels or co-polymerised with PCL to build ABA-block co-polymers (Figure 2.22). Electroactive fibrous mats of PEDOT:PSS and EDOT oligomers were fabricated and used Human episomal iPSC line. Their results showed that neurite length and branching of neural stem cells could be enhanced following electrical stimulation on the conductive spin coated mats. In addition, a high architectural control of the material could be achieved either through solution electrospinning or MEW.

These examples demonstrate that by understanding the behaviours of feed materials it is possible to work around their inherent limitations and create new and exciting possibilities in the fabrication of CP-based components.

A key to the implementation of CPs with AM could be the chemical modification of CPs. POx and POzi offer a very good platform for this, as the material properties can be precisely defined through targeted synthesis. This approach also offers the possibility of producing compatible polymers that can be converted via MEW. The main criterion here would be that the developed material is thermally stable at temperatures above 100 °C and also has a melting phase.

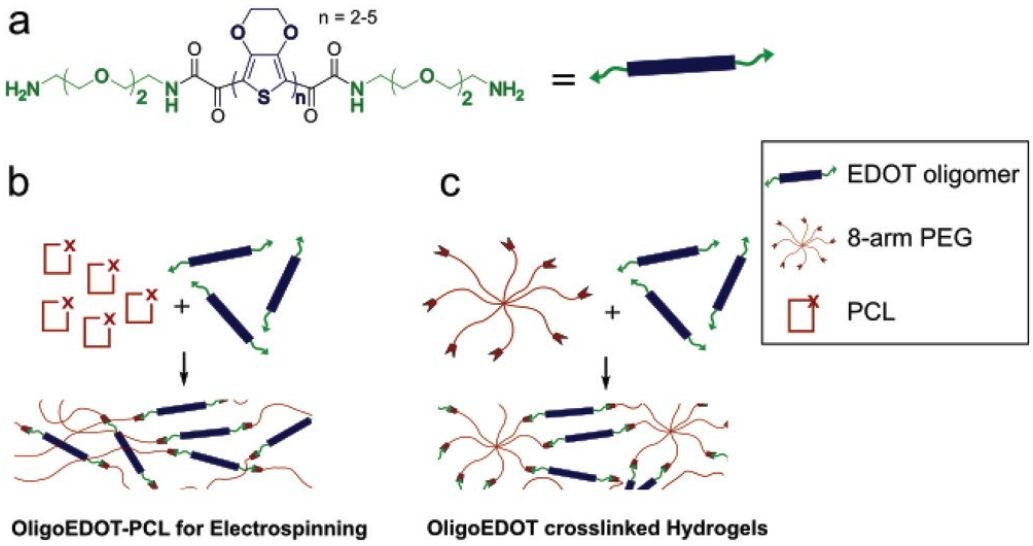


Figure 2.22 Structure of (a) oligo-EDOT (b) copolymerised with caprolactam, (c) crosslinked with 8-arm PEG. Reproduced from Ritzau-Reid et al.*[211] with permission*

2.4 Conclusion

CPs have gathered considerable attention over the past twenty years due to their unique combination of electrochemical properties. Despite significant research interest, CP-based technologies are yet to make significant impacts in terms of clinical translation. The reasons for this are multifaceted and cannot be pinned down to a specific contributing factor. It could be argued that, from current industry perspectives, the potential benefits of these technologies do not yet outweigh the potential risks and regulatory burdens associated with adopting new material technologies. Therefore, CP technologies need to offer more than incremental increases in electrochemical performance in order to unseat incumbent industry best practices.

The poor processibility of CPs largely contributes to the risk of adopting these technologies, while also limiting the potential benefits that they can offer. Therefore, overcoming this limitation may help to unlock the full potential of CP-based materials. Understanding the physicochemical properties of CPs and their structure-property relationships is critical to addressing key limitations such as poor solubility,

and chemical and thermal instability. Several novel approaches to addressing these limitations have been reported, including the use of adjuncts such as dopants and plasticizers, the development of novel CP-chemistries, the formation of CP-based complexes and composites, and the adoption of novel manufacturing techniques such as AM. The approaches discussed here permit new synthesis and processing routes, which will also enable the development of novel technologies based on these highly versatile materials. This higher degree of control over the physicochemical properties of CP systems will enable the development of tailored biomaterials with enhanced tissue integration and thus, higher clinical efficacy. In addition, the pairing of these approaches with emerging AM fabrication techniques will enable exciting new functionalities and applications for CPs within the field of bioelectronics.

Chapter 3 – Synthesis of Thiophene-based Ox and Ozi

3.1 Introduction

Mixing, co-polymerising, or the end-functionalising of CPs with other polymers is a common approach to mediating the physico-mechanical properties of CPs. Mixing CPs with elastomers such as polyurethanes to form conductive elastomers enables better mechanical properties but reduces the electrical conductivity[212]. More freedom is given by the copolymerisation or the end-functionalisation of CPs. Spicer et al.[213] developed an oligo-EDOT platform, which can be modified in a second step with either PCL or poly(ethylene oxide) to modify the physico-mechanical properties of the material and therefore enable better processability via electrospinning and MEW. Yagci et al.[165] copolymerised pyrrole and thiophenes with different non-conductive polymers such as polyacrylates, polystyrenes, PCL and POx. Most copolymers were synthesised by electrodeposition and showed almost similar conductivity as homopolymers of CPs, but with the benefit of better mechanical properties. Of interest is that the authors were able to synthesise end-functionalised Ox-based macromonomers with pyrrole but failed to either electropolymerise or chemically polymerise those macromonomers. The design of macromonomers incorporating CP components is critical to their ability to be subsequently polymerised. This chapter will focus on design of a library of macromonomers to facilitate investigation of novel co-polymers of CPs.

As an alternative for the end-functionalisation of POxs, this class of polymers also offers the possibility of functionalisation by changing the side group. Herein, the approach is mostly the same. Functional side-groups are introduced before polymerisation by the synthesis of the specific functionalised monomers. Glassner et al.[24] showed that there is almost no limitation to this approach. Besides the introduction of aliphatic side groups, phenyl, perfluoroalkyl or thiol side groups, among others, could also be developed with this synthetic route. Therefore, this approach is hypothesised to be transferable for the introduction of electrically active side groups such as thiophenyl or pyridinyl. It should be noted that the only aromatic and thus potentially electrically conductive structures that have been explored as POx side groups are furans and benzyl derivatives.[24] The introduction of side-groups has a direct impact on the material properties. For example, short-chain aliphatic side groups have a hydrophilic character and thus good solubility in aqueous solution. In contrast, longer-chain aliphatic side groups have a hydrophobic character and thus impart better solubility in non-polar solvents. This unique character enables a high tunability of material properties and can be used as a useful tool to modify the physical properties of CPs.

In this chapter, it was hypothesised that thiophene-molecules can be introduced directly into POx by changing the side group. To achieve this, it was proposed that thiophenecarbonitriles or thiopheneacetonitriles can be reacted with ethanolamine or propanolamine via a Seeliger and Wittig

reaction to obtain thiophene-based Ox or Ozi monomers (Fig 3.1). Since it is a new subclass of Ox and Ozi monomers, a systematic nomenclature of the proposed monomers was established. The monomers made from acetonitriles are abbreviated with "At", while the monomers made from thiophenecarbonitriles are abbreviated with "Th".

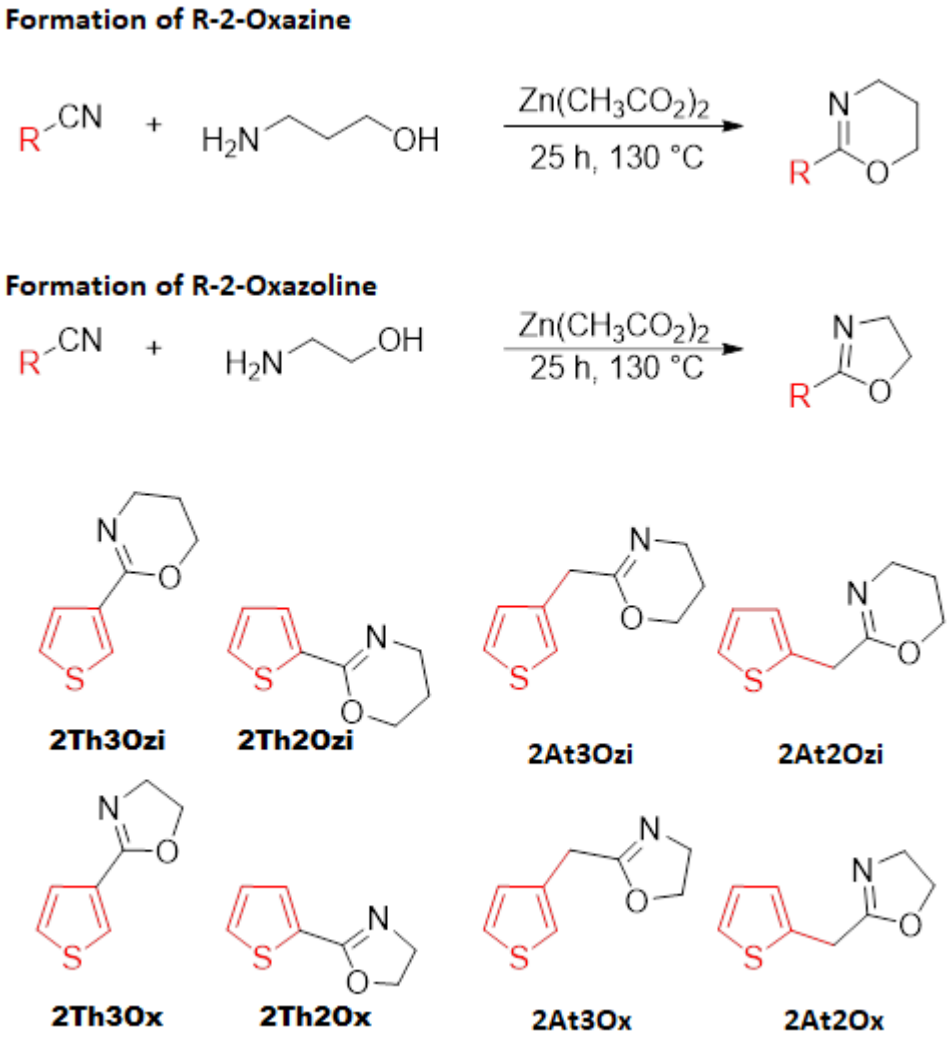


Figure 3.1 Synthesis of thiophene-based monomers

It was further hypothesised that, due to the sterically demanding side groups, some of the thiophene-based monomers may be present in the solid phase. This would have the advantage that characterisation via crystallography would be possible. Due to the mostly liquid phase of aliphatic Oxs, this was not known from the literature at the time this work was written. The analysis by means of crystallography enables a precise statement to be made about the structure of the individual molecule. The exact chemical composition, chemical bonding and properties of a material can be obtained. The parameters obtained in this way can be used for theoretical calculations in physical chemical research and enable predictions on reactions and synthesis pathways.

As detailed in the initial chapters, the motivation for this material design is the application of conductive scaffolds for TE. The most facile method of scaffold development is AM and in particular 3D printing.[214] As such, even at these initial stages, it was considered essential not only to have a simple synthesis route, but also to enable up-scaling of material synthesis and hence scaffold production. For this purpose, material in the gram range is required. Furthermore, simple purification is also of great importance. It is necessary to obtain the purest possible starting product for the subsequent polymerisation in order to prevent side reactions. To enable exploration of co-polymers of CPs and POx or POzi, a monomer platform was developed. This platform was specifically designed to have bi-polymerizable functionality, where Ox and Ozi rings were used as a core structure and were functionalised with thiophene-based side groups. Due to the different ways in which these monomers can be combined and then subsequently polymerised, there is a wide range of combinations to be explored.

At the time of this writing, no thiophene-based monomers or polymers from Ox or Ozi were known from the literature. A focus was initially placed on the synthesis of different monomers, which were then investigated for their ability to scale-up. The established method according to Seeliger and Wittig was chosen as the basis for the monomer synthesis, as shown in Figure 3.1.[167] The advantage here is that the synthesis can be carried out in a one-pot reaction and the yield is in the quantitative range. The starting materials are the monosubstituted cyano-derivatives of the thiophene basic structure and, depending on the ring size, either amino-ethanol (five-membered) or amino-propanol (six-membered). The reaction can be initiated catalytically by adding zinc acetate.

3.2 Aims and Hypotheses

The primary objective of this chapter was to synthesise novel monomers of thiophene and either Ox or Ozi. It was hypothesised that thiophene-structures could be introduced to Ox or Ozi by the reaction of either thiophenecarbonitriles or thiopheneacetonitriles with amino alcohols. To facilitate the proposed reaction where thiophene-nitriles were not commercially available, they were obtained by Kolbe-nitrile synthesis or analogous reactions such as Feuerstein variation. A general exclusion criterion for all developed monomer synthesis strategies was the need for up-scaling with appropriate yields in the gram range.

The specific aims of this chapter were to:

1. Design and synthesise a library of novel monomers based on thiophenes and Ox or Ozi;
2. Identify the most likely candidate monomers for polymerisation and 3D printing; and
3. Optimize the synthesis parameters for up-scaling.

3.3 Results and Discussion

Due to the generally better electrical conductivity of PEDOT compared to other polythiophenes in the literature[215], this monomer was attempted first. The synthesis of 2-EDOT-oxazoline was different to that of other thiophenes as a carbonitrile group was required. As such, chloromethyl EDOT was converted to a nitrile in a first-synthesis step via Kolbe nitrile synthesis. In principle, both, the substitution product and the elimination product can be obtained during synthesis (Figure 3.2), the reaction conditions were varied to find the ideal conditions and summarized in Table 3.1.

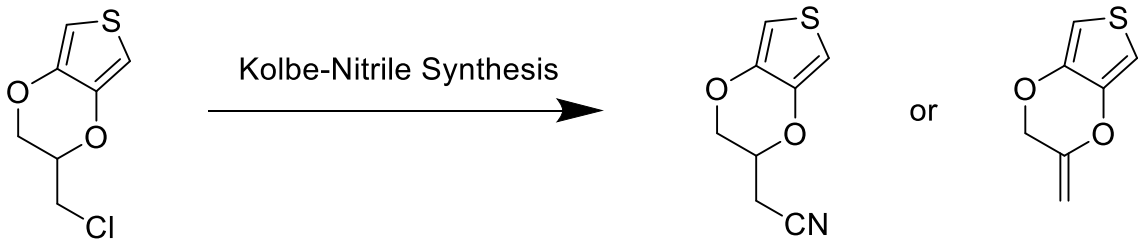


Figure 3.2 Synthesis of EDOT-acetontrile via Kolbe-Ntrile synthesis

Parameters including temperature, nucleophiles, solvents, additives, and time were examined. The reaction time was between 4 and 72 hours. A general trend could be found here that a longer reaction time had a negative influence on the reaction as more side reactions occurred. It can also be stated that the product of the following conditions could only be detected in an aprotic-polar solvent. Isolation of the product was not possible due to the physically similar properties to the elimination product. No conversion could be found at low temperatures, and side reactions occurred at higher temperatures. As such, a modified approach using the Finkelstein variant of the Kolbe nitrile synthesis[216] was also investigated. The chlorine was substituted with iodine to subsequently enable a better leaving group for the nucleophilic attack of the cyanide ion.[216] Again, this reaction did not promote the desired product as the major product was the elimination product instead of the substitution product.

Table 3.1 Conditions (temperature, solvent and nucleophil) of Kolbe nitrile synthesis strategies of EDOT-oxazine

		Nucleophile	**Temperature**			
			40 °C	80°C	100°C	120°C
Solvent	Acetone	NaCN	NP	–	–	–
		KCN/NaI	NP	–	–	–
	Ethanol	NaCN	NP	E + S	–	–
		KCN/NaI	NP	NP	–	–
	Ethylene glycol	NaCN	NP	NP	NP	NP
		KCN/NaI	NP	NP	NP	SP
	DMSO	NaCN	NP	EP + SNP	EP + SNP	SNP + EP + SP
		KCN/NaI	NP	EP	NP	EP +SP
	DMF	NaCN	–	–	NP	SP
		KCN/NaI	–	–	NP	SP

NP = no product, EP = elimination product, SNP = substitution product, SP = side reaction

In an attempt to achieve an EDOT based monomer, another reaction route was proposed. Based on the synthesis by Taubmann et al.[196], a direct reaction of the chloromethyl EDOT with MeOx using BuLi and tetramethylethylenediamine in THF was implemented at - 80 ° C (Figure 3.3).

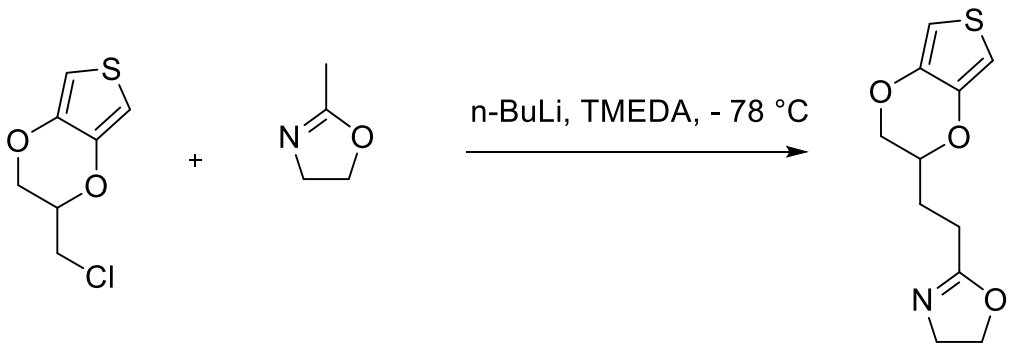


Figure 3.3 Synthesis of 2-EDOT-2-ethyl-oxazoline with n-BuLi and TMEDA analogous to Taubmann et al.[196]

The successful conversion was checked by the H,H-COZY-NMR-Spectroscopy (Figure 3.4). A coupling between the protons of the ethoxy-bridge of Chlormethyl-EDOT (~4.3 ppm) and the methyl-group of Ox (~2.3 ppm) was found, which can be seen in a "square" formation. However, the yield here was only qualitative and better purification via column chromatography was not successful. Therefore, no further investigation on this material was carried out within the scope of this work.

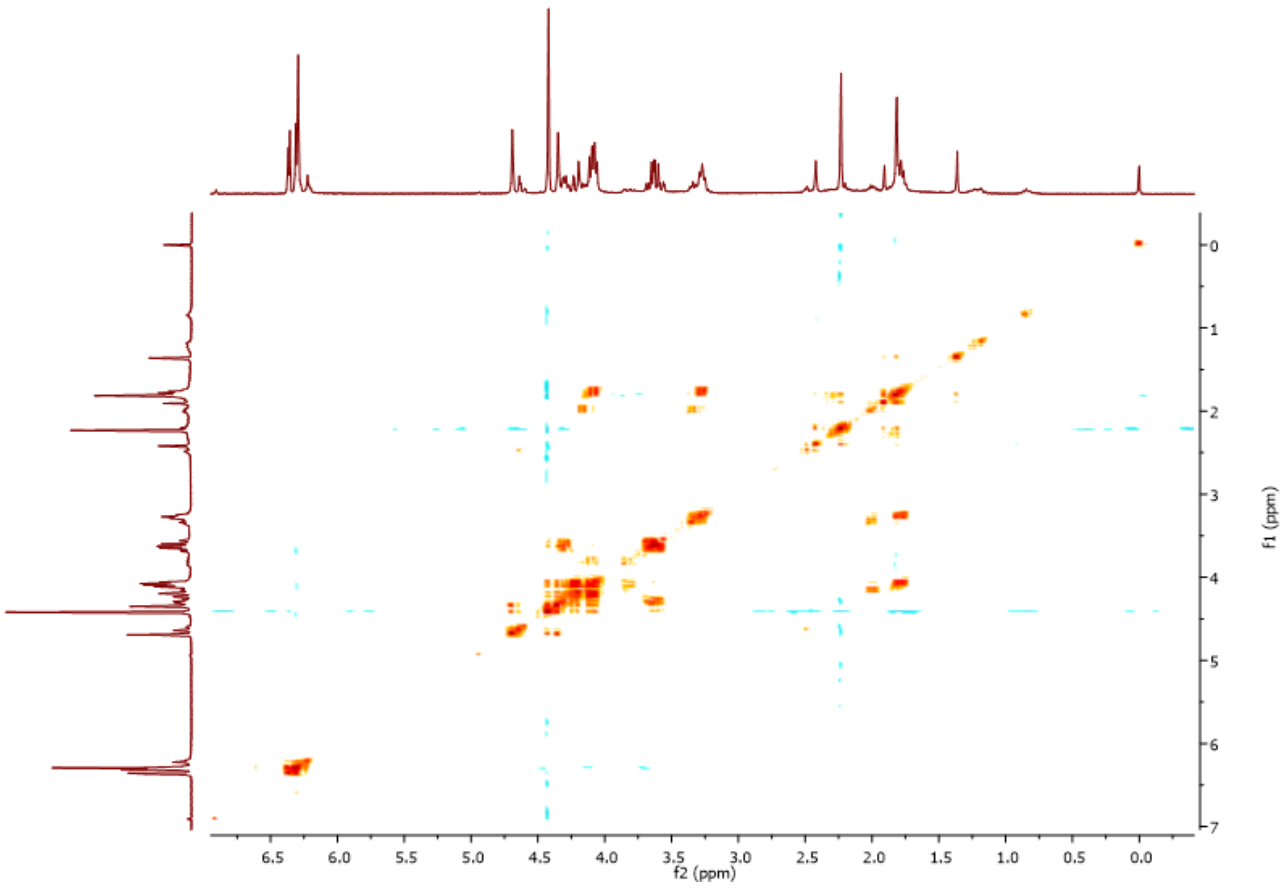


Figure 3.4 H,H-COSY-NMR spectrum of EDOT-6-ethyl-2-oxazoline. A succesful synthesis can be seen by cross peak's („square" formation), which identfies a coupling oft wo nucleis. Here, the coupling of methyl-group in the fourth position of the Chlormethyl-EDOT (~4.3 ppm) and the methyl-group of Ox (~1.9 ppm) was detected

As an alternative approach, it was investigated whether a functionalisation of the side group can be achieved by monosubstituted thiophene-nitriles. The average reaction time was approx. 25 hours at a

reaction temperature of 130 °C. While shorter reaction times did not show a full conversion, longer reaction times led to side reactions and deteriorated the overall yield.

Since all molecules are substances not known from the literature, IR spectroscopy, mass spectrometry, ^{1}H-NMR spectroscopy, and ^{13}C-NMR spectroscopy were carried out for complete characterisation. The monomers which were solid at room temperature were also analysed through crystal structure analysis. The crystals listed here are the first crystals in the family of Ox and Ozi known from the literature.

Figure 3.5 shows a representative IR spectrum of 2-thiophene-3-oxazine (2Th3Ozi). Characteristic transmittance bands for the thiophene ring are at 857 and 835 cm^{-1} (C-H deformation vibration), 724 and 699 cm^{-1} (α-position C-H deformation vibration), and at 608 cm^{-1}, which corresponds to the C-S-C-stretching vibrations.[217] The characteristic bands for the Ozi rings are at 1640 cm^{-1} (C=N-valence vibration), 1336 cm^{-1} (C-N-valence vibration), and 1255 and 1131 cm^{-1} (C-O-C-valence vibrations). Bands for =C-H- and -C-H- valence vibrations are at 3100 cm^{-1} and around 2900 cm^{-1}. Furthermore, in the characteristic region of around 1500 cm^{-1} for aromatic vibrations, several bands can be observed, but are not highlighted in Figure 3.6.

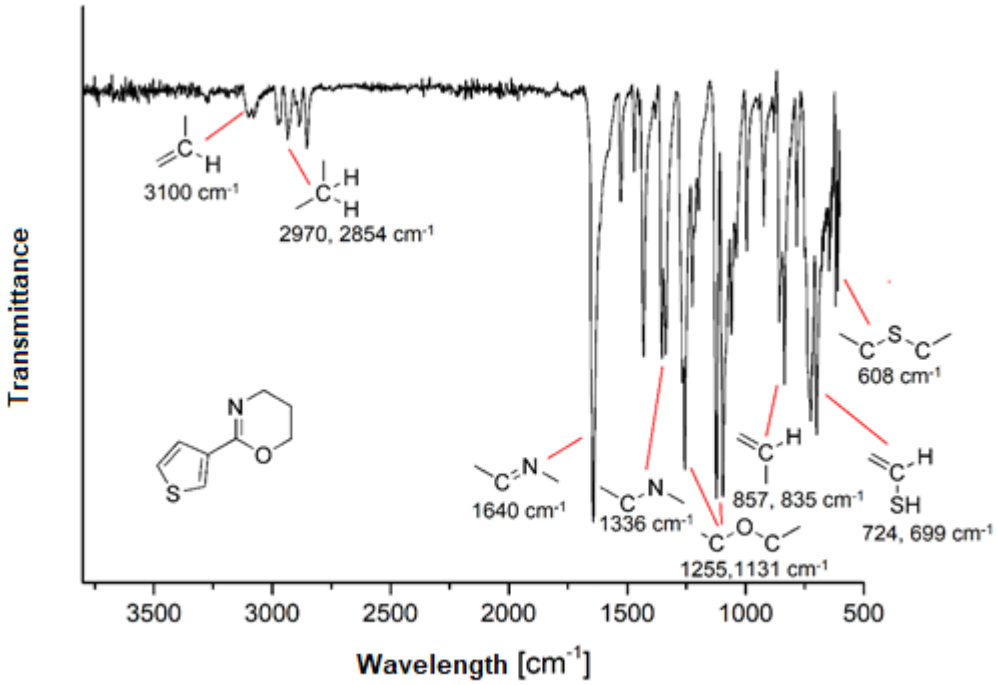


Figure 3.5 IR spectrum of 3-thiophene-2-oxazine. Identification of functional groups are presented as red lines

ThOx were synthesised from thiophenecarbonitriles and aminoethanol according to the general synthesis method listed above.[167] Four different ThOx could be produced. The yield of the individual ThOx was between 55 – 93%. Figure 3.6 shows representatively the ^{1}H-NMR spectrum of 2-thiophenes-3-oxazoline (2Th3Ox). All signals in the spectrum could be assigned. The signals for the thiophene ring

were in the range of 7.30 – 7.90 ppm and the triplets for the Ox ring were in the range of 4.00 ppm and 4.40 ppm.

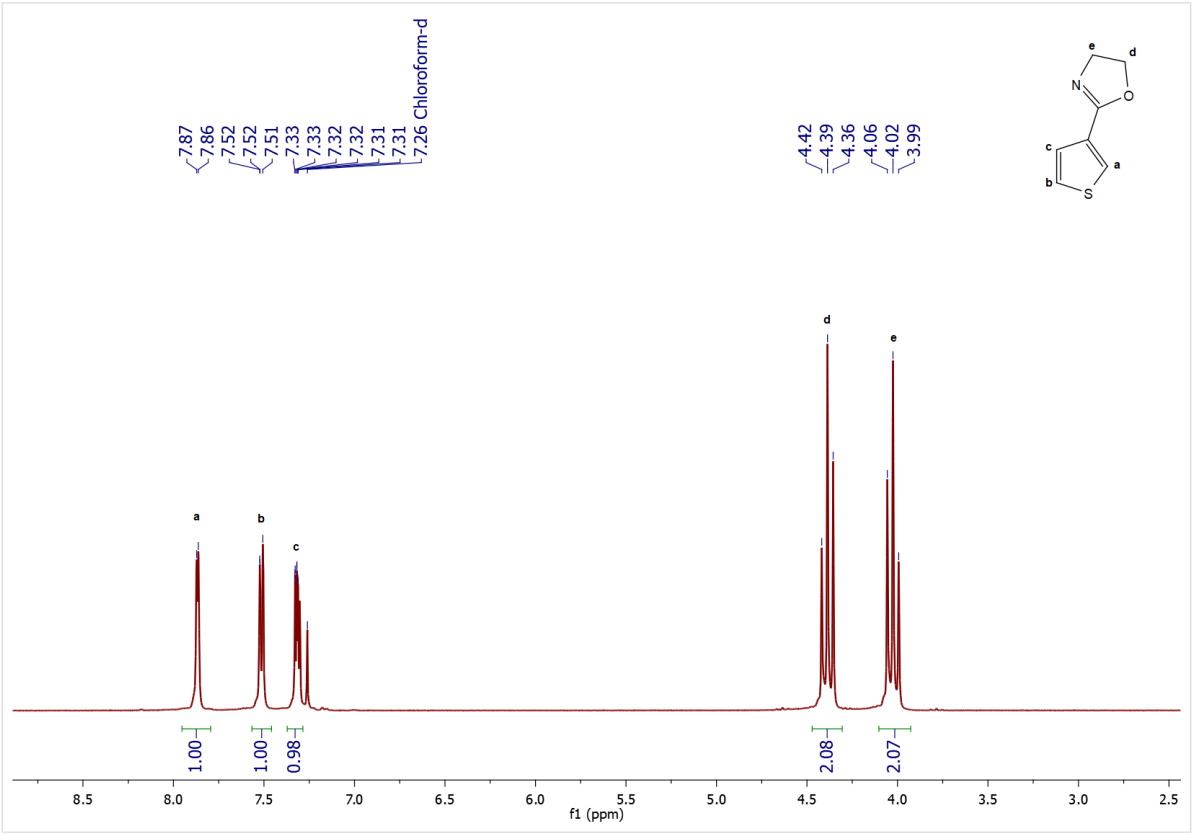


Figure 3.6 1H-NMR-Spektrum (CdCl3, 7.26 ppm) of 3-thiophene-2-oxazoline

2-thiophenes-2-oxazolines (2Th2Ox) and 2-thiophenes-3-oxazolines (2Th3Ox) form a colourless solid at room temperature and were further characterised through crystal structure analysis (Figure 3.8). In contrast, 2-acetothiophene-2-oxazoline (2At2Ox) and 2-acetothiophene-3-oxazine (2At3Ozi) formed colourless liquids at room temperature. With standard storage at room temperature and under an inert atmosphere, a discolouration from colourless to orange to brown could be perceived within 48 hours of synthesis, which indicates a oxidation or aging process of the polymer.[218]

Analogous to ThOx, four different oxazines could also be produced according to the general synthesis procedure. Another carbon was built into the oxazine ring through the use of 1-propanolamine. The yield here was analogous to the synthesis of Ox and was between 50 – 90% as described in Table 3.3. The ^{1}H-NMR spectrum of 2-thiophenes-3-oxazine (2Th3Ozi) is shown in Figure 3.7 as representative. The signals are in similar ranges as already observed for ThOx. The signals of the thiophene ring are between 7.00 – 7.50 ppm. Due to the deshielding of the heteroatoms in the Ox ring, the protons in the alpha position have a downfield shift to 4.32 ppm and 3.56 ppm. The protons in the beta position, on the other hand, experience greater shielding and are consequently shifted further upfield to 1.96 ppm.

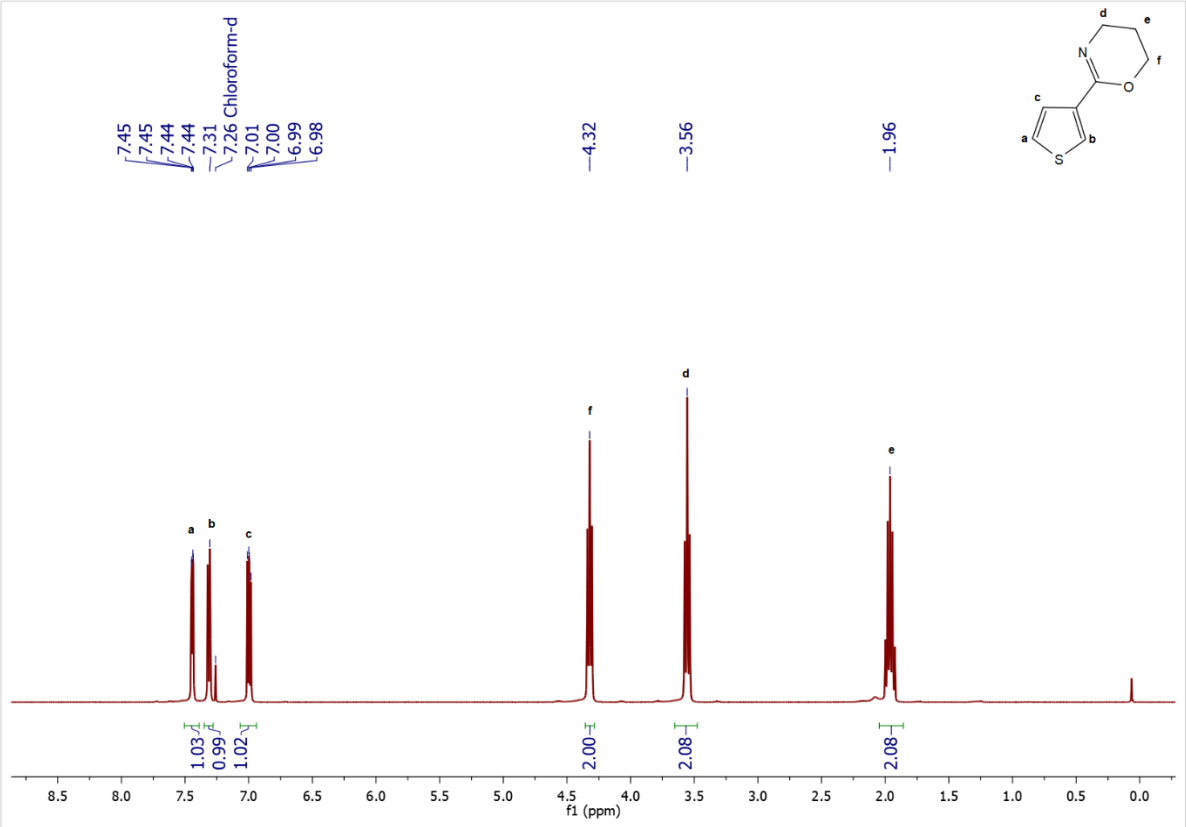


Figure 3.7 1H-NMR-Spektrum (CdCl3, 7.26 ppm) of 3-thiophene-2-oxazine

The monosubstituted Oxs. 2-thiophenes-2-oxazines (2Th2Ozi) and 2Th3Ozi also formed colourless solids at Rt and could be further characterised using crystal structure analysis (Figure 3.8). In contrast, the aceto-substituted AtOzi formed colourless liquids at Rt and with standard storage, undergo a colour change after 24 h.

Dissolution in toluene and slowly evaporating the solvent yielded single crystals. Therefore, and to our knowledge, we were able to demonstrate the first crystal structures of single Ox and Ozi (Figure 3.8). The five-membered (for Ox) or six-membered (for Ozi) ring was confirmed by crystallography. For all crystals, a disorder of 180° along the bonding axis of the thiophene-ring was observed. The ratio was between 0.7 – 0.8 and 0.2 – 0.3. Table 3.2 summarised the details of the crystal structures.

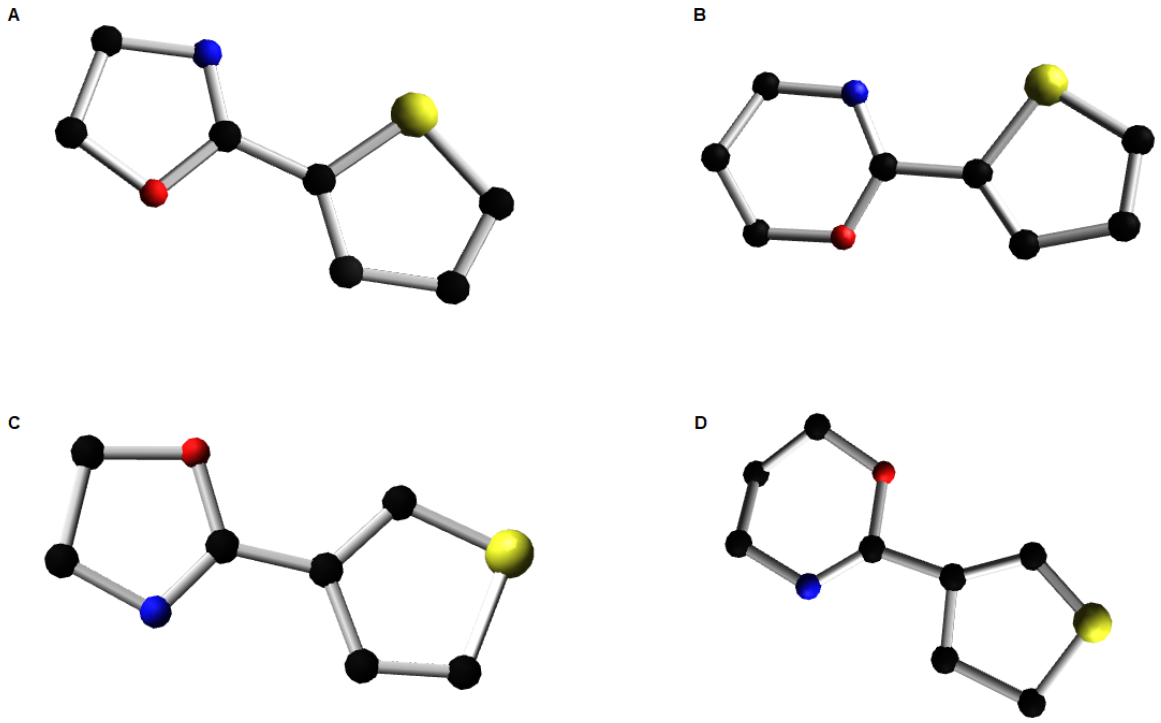


Figure 3.8 crystal structures of A) 2-thiophene-2-oxazoline, B) 2-thiophene-2-oxazine, C) 2-thiophene-3-oxazoline, D) 2-thiophene-3-oxazine

For 2Th3Ozi, Sulfur, nitrogen, and oxygen were disposed of with an orientation of S–C, O–C and N=C distances of 1,68 (4) Å – 1,71(10) Å, 1,36 (3) Å, and 1,27 (3) Å, respectively. The C–S–C and N=C–O angles were 91,9 (3)° Å and 128,1 (2)°. For 2Th3Ox, The orientation distances were for S–C, O–C and N=C 1,67 (2) – 1,76(7) Å, 1,33 (3) Å, and 1,29 (3) Å with angles of 93,4 (3)° for C–S–C and 118,2 (19)° for N=C–O. 2Th2Ozi, Distances were measured for S–C, O–C and N=C 1,71 (7) – 1,74(4) Å, 1,32 (3) Å, and 1,27 (8) Å. The angles for C–S–C and N=C–O angles were 90,7 (3)° Å and 128,1 (8)°. For 2Th2Ox, S–C, O–C and N=C were 1,66 (2) – 1,67(3) Å, 1,36 (4) Å, and 1,27 (2) Å and the angles were measured to be 94,5 (10)° Å for C–S–C and 119,6 (5)° N=C–O.

Table 3.2 Selected crystallographic data for 2Th2Ox, 2Th2Ozi, 2Th3Ox and 2Th3Ozi

	2Th2Ox	**2Th2Ozi**	**2Th3Ox**	**2Th3Ozi**
Formula	C_7H_7NOS	C_8H_9NOS	C_7H_7NOS	C_8H_9NOS
Formula weight	153.2 g/mol	167.22 g/mol	153.2 g/mol	167.22 g/mol
Crystal System	Orthorhombic	monoclinic	monoclinic	monoclinic
Space group	Pnma	P 2_1/n	P 2_1/c	P 2_1/c

a (Å)	10.7303(13)	7.8486(8)	10.7476(12)	9.5031(3)
b (Å)	10.1694(14)	10.8107(9)	6.5050(5)	8.0553(2)
c (Å)	6.6720(8)	9.6253(10)	11.1934(12)	20.8308(6)
α (°)	90	90	90	90
β (°)	90	100.190(8)	114.329(8)	91.427(3)
γ (°)	90	90	90	90
V (Å3)	728.06(16)	803.81(14)	713.07(13)	1594.11(8)
Crystal size (mm^3)	0.422 x 0.278 x 0.187	0.09 x 0.47 x 0.75	0.04 x 0.37 x 0.88	0.397 x 0.320 x 0.230
Z	4	4	4	8
Temp. (K)	173	193	193	173
dcalc (gcm-1)	1.398	1.382	1.427	1.394
Abs. coeff. μ (mm-1)	3.341	0.339	0.375	3.097
Reflections Collected	1932	4251	4072	5296

The basic properties of the monomers are summarised again in Table 3.3. In general, the following trends can be recognised:

- The yield of the ThOxs and ThOzis are comparably higher than of AtOx and AtOzi.
- AtOx and AtOzis form a colourless liquid at Rt, which has a high potential for oxidation over time.
- Due to the phase state at Rt, the ThOx or ThOzi are obtained through sublimation, while the AtOx and AtOzi can be obtained via classic distillation.

Table 3.3 Summary of monomer properties (Yield, MP, Phase and BP)

Monomer	Yield (%)	MP (°C)	Phase at Rt	BP (°C at 0.01mbar)
2-thiophene-3-oxazoline	92,4	27–29	solid	105–115
2-thiophene-3-oxazine	89,5	24–28	solid	110–120
2-thiophene-2-oxazoline	74,8	23–30	solid	102-107
2-thiophene-2-oxazine	77,3	19–25	solid	110–120
2-acetothiophene-3-oxazoline	64,0	–	liquid	80-85
2-acetothiophene-3-oxazine	60,2	–	liquid	85–95
2-acetothiophene-2-oxazoline	56,4	–	liquid	80–90
2-acetothiophene-2-oxazine	53,2	–	liquid	85–95

While aliphatic Ox and Ozi form a liquid phase at room temperature, some representatives of the thiophene-based Ox and Ozi showed a solid phase at room temperature. This has the advantage that both, storage and further use are improved, since contamination of water can be more easily identified due to subsequent phase separation. Since the polymerisation was intended to be performed under inert conditions, a further advantage of a solid phase is that fewer consumables such as syringes and cannulas have to be used, which makes the polymerisation easier. A disadvantage compared to aliphatic Ox and Ozi is the purification of the synthesis via sublimation, since the deposited product has to be collected in the sublimation tube, which is more complex. Rinsing out or dissolving the product with toluene was suggested as a possible solution. This had the advantage that when the solvent was subsequently removed, residual traces of water were simultaneously removed by azeotropic distillation.[216] The yield is generally comparable to that of aliphatic Ox and Ozi. [219,220]

It could be shown that the yield of ThOx and ThOzi compared to the AtOx and AtOzi monomers was up to 30% higher. The reason for this could be the steric effect of the thiophene ring, which is restricted

in its rotation due to the missing carbon atom in the bond between the two ring systems. A similar behaviour has been observed in frustrated Lewis pairs.[221] In this way, an ionic charge separation can be stabilized and isolated by steric hinderance. In addition, a solid crystalline phase could be observed for some monomers. Again, this could be due to the steric effect of the system. Koßmehl et al.[222] investigated liquid-crystalline phases of thiophene systems. It was found that planar thiophene systems in particular form a crystalline phase. Something similar could be found in the crystal structures of the novel monomers. An almost planar structure was found here. The disorder of the thiophene ring is due to a 180 ° rotation. This is possible because the sulphur atom has approximately the same size as the opposite CH group.

Above all, 2Th3Ox and 2TH3Ozi showed a very good yield of approx. 90%. Compared to other thiophene-based Ox and Ozi, 2Th3Ozi showed also the best handling during synthesis and clean up procedure. Forming a solid at room temperature has also the advantage, compared to other Ox or Ozi monomers known from the literature, that anhydrous storage is much easier, which is essential due to the fact that water contamination would initiate side reaction and a pure product could not be obtained. Consequently, the liquid thiophene based Ox and Ozi, namely AtOx and AtOzi, were excluded due to the instability over time. Compared to 2Th2Ozi, 2Th3Ox and 2Th3Ozi had the advantage of two free alpha positions, which are necessary for the bi-polymerisation functionality and gives more freedom in further synthesis and polymerisation approaches. Furthermore, a hypothesis was also stated that the flexibility of the resulting polymer can be increased due to an additional carbon atom in the backbone of 2Th3Ozi compared to 2Th3Ox and thus better processing can be achieved. This was further investigated in the following chapter.

3.4 Conclusion

A novel class of thiophene-based Ox and Ozi monomers were successfully produced using the Seeliger-Wittig reaction. Most notably, monosubstituted Ox and Ozi monomers were prepared. While EDOT derivatives via Kolbe nitrile synthesis were detectable, the yield was low and did not meet the minimum requirements for a polymerisable quantity. This library of monomers also reports the first Ox and Ozi monomers that form a solid at room temperature. As a result, the first crystal structure of Ox and Ozi could be confirmed and thus a direct detection of the ring structure and orientation.

Across the monomers designed and synthesised, 2Th3Ox and 2Th3Ozi were obtained in quantitatively appropriate yields. Furthermore, these two monomers showed the easiest handling during the synthesis and purification. Long-term storage under normal conditions was also possible and showed no oxidative degradation reactions.

The following chapter explores these monomers and their ability to produce polymers. This includes the polymerisation approach and the resulting physicochemical properties of these materials.

3.5 Experimental section

3.5.1 Materials and Equipment

For inert conditions during synthesis, all reactions and workup were performed using either a standard Schlenk System or a glovebox (LabMaster 130, Mbrazn, Garching, Germany) under inert atmosphere of dry, oxygen-free argon. The water impurity of the glovebox was detected and had an average of less than 5 ppm. All commercially available chemicals were purchased by Sigma Aldrich or Acros Organics and used without further purification unless otherwise described. Toluene was dried for 72 hours over molecular sieves (4 Å). 2-Ethyl-2-oxazoline, benzonitrile, Methyl-2-2oxazoline were dried by refluxing over CaH_2 and distilled afterwards prior use. $FeCl_3$ was dried under vacuum at 50 °C for 24 h prior use. If not stated different, all reactions and work-up procedures were performed under inert conditions (water-free Argon atmosphere using a $CaCl_2$ filter).

3.5.2 Characterisation and Analysis of Material

Nuclear Magnetic Resonance (NMR) Spectroscopy

NMR spectroscopy was used for the initial identification of chemical compounds. Above all, the carbon-hydrogen frame of organic compounds can be described, and a structure elucidation can thus take place. Furthermore, NMR spectroscopy allows information about ratios of functional groups, a quantitative statement and tacticity of polymer chains.

If a chemical substance is placed in a magnetic field, certain atomic nuclei with an odd number of protons and neutrons (^{1}H (hydrogen), ^{13}C (carbon)) align themselves along the electromagnetic field.[223] It can either be in a lower energy or higher energy spin state. The energy difference between the two levels is linearly dependent on the applied magnetic field strength. If an electromagnetic voltage with the exact energy for the transition is applied, it is excited in the higher energy level and thus absorption. Due to relaxation processes, there is a return to the energetically more favorable energy state. This emits energy that can be detected by NMR spectroscopy. The frequency is plotted against the intensity in an NMR spectrum. Due to the shielding of nearby atomic nuclei, the applied magnetic field and nucleus type, there is a shift (in ppm) of the theoretically expected energy levels. As a result, protons that are not chemically equivalent are separated from one another and generate different signals in the NMR spectrum and structure elucidation can occur.

NMR spectroscopy was performed on a Bruker Fourier 300 (^{1}H 300.12 MHz; ^{13}C: 75.47 MHz) and a Bruker Fourier 400 equipped with a Bruker BioSpin (Rheionstettet, Germany) at 298 K. The spectra were calibrated to the signals of residual protonated solvent signals ($CDCl_3$ 7.26, HDO 4.67, D_6-DMS 2.50). The analysed product was dissolved in the appropriate solvent at a concentration of 15 mg/mL. The successful reaction was determined by comparing the integral of peaks corresponding to the

theoretical expected values of protons and the chemical shift. Multiplicities of signals are depicted as following: s, singlet; d, dublet; t, triplet; q, quartet, quin, quintet; dt, dublet of triplets; m, multiplet; b, broad, ps, pseudo. Coupling Constants were automatically calculated by the Software Mestrenova (version 6.0.2-5475). NMR assignments are supported by additional 2D experiments.

Infrared (IR) Spectroscopy

IR spectroscopy is used to identify functional groups in a compound. Due to molecular vibrations, chemical bonds can either be stretched or deformed.[224] An exact energy and thus a characteristic frequency is required for each oscillation. Basically, more energy is used to stretch a molecule instead of deforming it. If a chemical compound is treated with an external radiation, then this molecule absorbs in exactly the wave range that is necessary for the excitation of the oscillation. Functional groups are therefore detected in the range of 4000 - 1400 cm^{-1}, while the characteristic vibrations of the chemical compound are detected in the fingerprint area (1400 - 600 cm^{-1}). The excitation energy is between 4 to 40 Kj/mol.

The IR spectroscopy was performed on a Jasco (Gross-Umstadt, Germany) FT/IR-4100. The spectrum had an ATR-unit. The scan rate was 64 with a resolution of 4 cm^{-1}. A baseline correction was performed using the Spektra Manager Version 2. Therefore, prior to every series of measurements a Background was measured using an empty probehead togenerate a background noise and subtracted afterwards. IR spectroscopy was used for general characterisation of molecular vibration such as fundamental oscillation, natural oscillation and normal mode. The signals were differenced in w = weak, m = medium, s = strong, vs =very strong, b = broad.

X-Ray diffraction (XRD)

XRD is used to determine the structure of crystalline substances.[224] For this purpose, diffraction on the crystal lattice is caused in the atomic range with the use of suitable radiation. The distance between the individual crystal lattices is in the same order of magnitude as the wavelength of X-rays. In general, X-rays belong to high-energy radiation and therefore have a short wavelength. In contrast to other spectroscopic methods such as IR spectroscopy, diffraction takes place on the electrons. Therefore, hydrogen atoms can only be localized with great difficulty. The radiation is a monochromatic X-ray radiation that is generated by an X-ray tube. A molybdenum (MO) core is usually used, as this is ideally suited for diffraction due to the wavelength at the C-C bond. The best results are achieved with single crystals, since the diffraction is not disturbed by the superimpositions. Less accurate information can be obtained from crystalline powders. The crystal structure is determined by computer based on the diffraction pattern using *Bragg's equation* ($n*\lambda = 2*d*\sin(\theta)$). The diffraction maxima provide information on the geometry of the unit cell.

The XRD spectroscopy was collected on a Bruker D8 Advance and a Stoe IPDS. The voltage and current was at 30 kV and 53.3 mA. A Cu-K or Mo-X alpha radiation source was used. 0.015° angle steps with a 0.7 s dwell time and a rotation of 15 rpm was chosen. The 2θ angle range was between 10° and 80°. A zero-background sample holder, a silicon single crystal was used. Measurements of the background were done by using a beam knife and DIFFRAC:EVA. SHELXL-2018 and SIR-2004 were used to determine the heavy atoms positions and remaining non-hydrogen atoms were located from successive difference Fourier map calculations.

Mass spectrometry studies

Mass spectroscopy allows the molar mass and the empirical formula of a compound to be determined.[223] Therefore, the substance was evaporated in a high vacuum and ionized in an ion source. This leads to the formation of radical cations, which can further disintegrate. This usually results in the breaking of the weakest bonding or which gives the most stable secondary product. In a magnetic field, the ions are on circular paths deflected, the radius of which depends on their mass/charge ratio, and thereby separated. A mass spectrum then records these parts on the basis of their relative frequency as a function of the mass to the charge. The base peak is the signal peak with the greatest intensity.

The Mass spectrometry was performed with an Agilent Technologies 6200 series TOF/6500 series Q-TOF B.08.00. The ionization took place here by means of electron spray ionization (ESI) and peaks were recorded as mass-to-charge vs. counts.

3.5.3 Synthesis of thiophene-based Ox and Ozi monomers

One monomer was explored using commercially available CP monomer Hydroxy-EDOT, but all other monomer designs were based on unsubstituted thiophenes (Th) as the starting material were easily accessible and were not known from literature before. As such the first approach (2-EDOT-2-ethyl-oxazoline) is detailed below, and then subsequently, the library of unsubstituted thiophene monomers are described more generally due to the same synthesis procedure.

2-EDOT-2-ethyl-oxazoline[196]

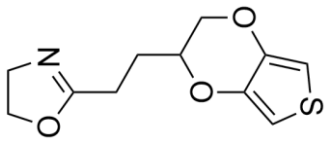


Figure 3.9 2-EDOT-2-ethyl-oxazoline

The synthesis of the new Ox-monomer, 2-EDOT-2-Ethyl-oxazoline was synthesized analogous to a synthesis route described by Taubman et al.[196] previously. Briefly, in a 250 mL round Schlenk flask, chlormethyl EDOT (1 g, 0.005 mol, 1 eq), tetramethylethylendiamine (TMEDA,0.61 g, 0.005 mol, 1eq),

n-BuLi (3.28 g, 0.005 mol, 1 eq) and MeOx (0.52 g, 0.005 mol, 1 eq) were mixed in 25 mL of THF at – 78 °C. The solution was stirred for 5 hours at -78 °C and then stirred overnight while warming up to Rt. The mixture was terminated with an excess of methanol and then concentrated under vacuum. The mixture was then shaken out three times with 50 mL of water each time. The aqueous phase was then extracted three times with THF (50 ml each). The combined organic extractions were dried above magnesium sulfate. After removing the solvent, the product was obtained.

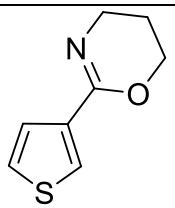
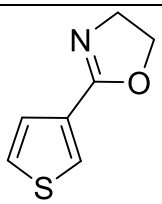
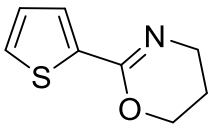
Yield: <5 % (colourless solid)

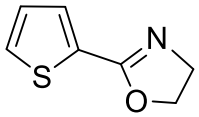
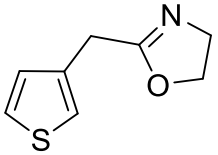
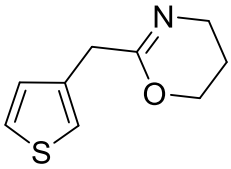
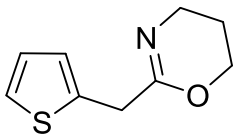
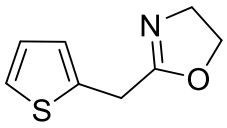
^{1}H-NMR (300 MHz, $CDCl_3$, δ ppm): 6.43 (d, *J* = 3.6 Hz, 1H), 6.37 (d, *J* = 3.6 Hz, 1H), 4.43 – 4.15 (m, 3H), 3.79 – 3.58 (m, 2H), 3.36 (m, 2H), 2.28 (m, 2H), 1.95 – 1.77 (m, 2H).

General monomer procedure

The monomer synthesis of all monomers were carried out analougously to the synthesis route as described by Seeliger and Wittig previously[225], but with a different cleaning procedure as all monomers are fully new and not known from literature before. Briefly, 1 eq of monomer was mixed with 1 eq of alkanoamine and 0.25 eq zinc acetate dihydrate in a 100 ml round flask with refluxing condenser and stirred at 130 °C under argon atmosphere for 25 h. The mixture was cooled down and approx. 100 mL of water was added. The mixture was extracted three times by using ethyl ether (3x50 mL). The organic phases were collected and washed two times with water and dried over $MgSO_4$. After removing the organic solvent, a raw product was obtained. For further purification either sublimation distillation or distillation was performed.

Table 3.4 Overview of synthesised monomers

Name	Structure	composition of synthesis
2-thiophene-3-oxazine		3-amino-1-propanol (17.2 g, 0.23 mol, 1eq) 3-thiophenecarbonitrile (25.0 g, 0.23 mol, 1eq) zinc acetate dihydrate (1.26 g, 5.73 mmol, 0.025 eq)
2-thiophene-3-oxazoline		ethanolamine (5.60 g, 0.09 mol, 1eq) 3-thiophencarbonitrile (10.0 g, 0.09 mol, 1eq) zinc acetate dihydrate (0.50 g, 2.29 mmol, 0.025 eq)
2-thiophene-2-oxazine		3-amino-1-propanol (2.75 g. 0.04 mol. 1eq) 2-thiophencarbonitrile (4.00 g. 0.04 mol. 1eq) zinc acetate dihydrate (0.20 g. 0.91 mmol. 0.025 eq)

2-thiophene-2-oxazoline		ethanolamine (2.80 g. 0.05 mol. 1eq) 2-thiophencarbonitrile (5.00 g. 0.05 mol. 1eq) zinc acetate dihydrate (0.25 g. 1.15 mmol. 0.025 eq)
2-acetothiophene-3-oxazoline		ethanolamine (4.96 g. 0.08 mol. 1eq) 3-thiophenacetonitrile (10.0 g. 0.08 mol. 1eq) zinc acetate dihydrate (0.44 g. 2.03 mmol. 0.025 eq)
2-acetothiophene-3-oxazine		3-amino-1-propanol (6.10 g. 0.08 mol. 1eq) 3-thiophenacetonitrile (10.0 g. 0.08 mol. 1eq) zinc acetate dihydrate (0.44 g. 2.03 mmol. 0.025 eq)
2-acetothiophene-2-oxazine		3-amino-1-propanol (3.05 g. 0.04 mol. 1eq) 2-thiophenacetonitrile (5.00 g. 0.04 mol. 1eq) zinc acetate dihydrate (0.22 g. 1.02 mmol. 0.025 eq)
2-acetothiophene-2-oxazoline		ethanolamine (2.48 g. 0.04 mol. 1eq) 2-thiophenacetonitrile (5.00 g. 0.04 mol. 1eq) zinc acetate dihydrate (0.22 g. 1.15 mmol. 0.025 eq)

3.6 Summary of thiophene-based Ox and Ozi monomer properties

2-thiophene-3-oxazine

Yield: 35.3 g, 0.21 mol, 92.4 % (colourless solid)

^{1}H-NMR (300 MHz, $CDCl_3$, δ ppm): 7.45–7.44 (d, *J* = 3.0 Hz, 1H), 7.32–7.30 (d, *J* = 5.1 Hz 1H), 7.01–7.98 (m, 1H), 4.32 (t, *J* = 5.3 Hz 2H), 3.56 (t, *J* = 5.9 Hz 2H), 1.96 (m, 2H)

^{13}C-NMR (75 MHz, $CDCl_3$, δ ppm): 153.12 (N=**C**–O), 137.06 (N/O–C–β**C**–thiophene) 126.61(α**C**–thiophene), 126.27 (α**C**–thiophene), 125.35 (β**C**–thiophene), 65.12 (O–**C**–CH_2), 42.41 (N–**C**–CH_2), 21.95 (H_2C–**C**–CH_2),

MS (ESI) m/Z: $[M]^+$ 168.04, bp: 110 – 120 °C (0,01mbar)

2-thiophene-3-oxazoline

Yield: 12.5 g 0.08 mol, 89.5 % (colourless solid)

^{1}H-NMR (300 MHz, $CDCl_3$, δ ppm): 7.80 (d, *J* = 2.6 Hz, 1H), 7.45 (d, *J* = 5.1 Hz, 1H), 7.25 (dd, *J* = 4.9, 3.0 Hz, 1H), 4.33 (t, *J* = 9.4 Hz, 3H), 3.96 (t, *J* = 9.4 Hz, 3H)

^{13}C-NMR (75 MHz, $CDCl_3$, δ ppm): 163.43 (N=**C**–O), 131.47 (β**C**–thiophene) 128.59(α**C**–thiophene), 127.32(α**C**–thiophene), 126.99 (β**C**–thiophene), 69.09 (O–**C**–CH_2), 59.28 (N–**C**–CH_2)

MS (ESI) m/Z: $[M]^+$ 154.05, bp: 105 – 115 °C (0,01mbar)

2-thiophene-2-oxazine

Yield: 5.16 g, 0.03 mol, 77.3 % (colourless solid)

^{1}H-NMR (300 MHz, $CDCl_3$, δ ppm): 7.48–7.47 (d, *J* = 2.5 Hz, 1H), 7.35–7.32 (m, 1H), 7.04–7.00 (m, 1H), 4.36–4.34 (dd, *J* = 8.9, 5.3 Hz, 2H), 3.59–3.57 (dd, *J* = 9.1, 5.8 Hz, 2H), 2.00–1.98 (m, 2H)

^{13}C-NMR (75 MHz, $CDCl_3$, δ ppm): 152.64 (N=**C**–O), 138.38 (N/O–C–α**C**–thiophene) 128.13(α**C**–thiophene), 127.24(β**C**–thiophene), 128.01 (β**C**–thiophene), 65.41 (O–**C**–CH_2), 42.50 (N–**C**–CH_2), 21.95 (H_2C–**C**–CH_2),

MS (ESI) m/Z: $[M]^+$ 168.05, bp: 110 – 120 °C (0,01mbar)

2-thiophene-2-oxazoline

Yield: 5.24 g, 0.03 mol, 74.8 % (colourless solid)

^{1}H-NMR (300 MHz, $CDCl_3$, δ ppm): 7.59–7.58 (d, *J* = 3.5 Hz, 1H), 7.45–7.43 d, *J* = 5.0 Hz, 1H), 7.09–7.05 (m, 1H), 4.46–4.39 (t, *J* = 9.5 Hz, 2H), 4.07–4.01 (t, *J* = 9.3 Hz, 2H)

^{13}C-NMR (75 MHz, $CDCl_3$, δ ppm): 160.40 (N=**C**–O), 130.40 (N/O–C–α**C**–thiophene) 130.14(α**C**–thiophene), 129.71(β**C**–thiophene), 127.57 (β**C**–thiophene), 68.05 (O–**C**–CH_2), 55.02 (N–**C**–CH_2)

MS (ESI) m/Z: $[M]^+$ 154.07, bp: 102 – 107 °C (0,01 mbar)

2-acetothiophene-3-oxazoline

Yield: 8.68 g, 0.05 mol, 64.0 % (colourless liquid)

^{1}H-NMR (300 MHz, $CDCl_3$, δ ppm): 7.29–7.26 (dd, *J* = 7.7, 2.9 Hz, 1H), 7.16–7.15 (m, 1H), 7.06–7.05 (d, *J* = 4.9 Hz, 1H), 4.30–4.23 (t, *J* = 9.5 Hz, 1H), 3.89–3.82 (t, *J* = 9.4 Hz, 1H), 3.65 (s, 2H),

^{13}C-NMR (75 MHz, $CDCl_3$, δ ppm): 166.56 (N=**C**–O), 134.87 (α**C**–thiophene), 128.42 (α**C**–thiophene) 125.75(β**C**–C–oxazoline), 122.35(β**C**–thiophene), 67.67 (O–**C**–CH_2), 54.52 (N–**C**–CH_2), 29.36 (thiophene–**C**–oxazoline)

MS (ESI) m/Z: $[M]^+$ 168.06 , bp: 80 – 90 °C (0,01 mbar)

2-acetothiophene-3-oxazine

Yield: 8.85 g, 0.05 mol, 60.2 % (colourless liquid)

^{1}H-NMR (300 MHz, $CDCl_3$, δ ppm): 7.18–7.16 (dd, *J* = 4.9, 3.0 Hz, 1H), 6.95–6.91 (m, 2H), 4.18–4.15 (t, *J* = 5.5 Hz, 2H), 3.64 (s, 2H), 3.41–3.37 (t, *J* = 5.8 Hz, 2H), 1.89–1.82 (m, 2H)

^{13}C-NMR (75 MHz, $CDCl_3$, δ ppm): 162.33 (N=**C**–O), 142.70 (α**C**–thiophene), 138.38 (α**C**–thiophene) 126.03(β**C**–C–oxazine), 124.42(β**C**–thiophene), 66.77 (O–**C**–CH_2), 44.44 (N–**C**–CH_2), 38.79 (thiophene–**C**–oxazine), 19.65 (NC–**C**–CO)

MS (ESI) m/Z: $[M]^+$ 182.08, bp: 85 – 95 °C (0,01 mbar)

2-acetothiophene-2-oxazine

Yield: 3.91 g, 0.02 mol, 53.2 % (yellow-orange liquid)

^{1}H-NMR (300 MHz, $CDCl_3$, δ ppm): 7.18–7.16 (dd, *J* = 5.0, 1.4 Hz, 1H), 6.95–6.90 (m, 2H), 4.19–4.16 (t, *J* = 5.5 Hz, 2H), 3.65 (s, 2H), 3.42–3.38 (t, *J* = 5.9 Hz, 2H), 1.90–1.83 (m, 2H)

^{13}C-NMR (75 MHz, $CDCl_3$, δ ppm): 158.14 (N=**C**–O), 138.50 (α**C**–C–oxazine), 126.69 (α**C**–thiophene) 125.94(β**C**–thiophene), 124.35(β**C**–thiophene), 65.21 (O–**C**–CH_2), 42.36 (N–**C**–CH_2), 36.81 (thiophene–**C**–oxazine), 21.62 (NC–**C**–CO)

MS (ESI) m/Z: $[M]^+$ 182.06, bp: 85 – 95 °C (0,01mbar)

2-acetothiophene-2-oxazoline

Yield: 8.85 g, 0.05 mol, 60.2% (light yellow liquid)

^{1}H-NMR (300 MHz, $CDCl_3$, δ ppm): 7.13 (m, 1H), 6.96–6.94 (m, 2H), 4.31–4.24 (t, *J* = 9.5 Hz, 2H), 3.89–3.83 (m, 4H)

^{13}C-NMR (75 MHz, $CDCl_3$, δ ppm): 166.03 (N=**C**–O), 159.40 (α**C**–C–oxazoline), 126.86 (α**C**–thiophene) 126.57(β**C**–thiophene), 124.80(β**C**–thiophene), 67.87 (O–**C**–CH_2), 54.54 (N–**C**–CH_2), 29.00 (thiophene–**C**–oxazoline)

MS (ESI) m/Z: $[M]^+$: 168.04, bp: 80 – 85 °C (0,01 mbar)

Chapter 4 – Exploring the Polymer behaviour of thiophene-based Ox and Ozi

4.1 Introduction

In view of the growing interest in electrically conductive polymers for a wide variety of applications, such as sensors or energy storage devices, improving the physicochemical properties and processability of CPs is of great interest. CPs are often characterised as insoluble and lack a definable melt phase, as such they are limited in fabrication routes and often used as coatings rather than freestanding polymer components. Improving the processibility of CPs through creating new co-polymers will enable the use of these materials across a wider range of research and commercial applications.

The fundamental question of this chapter was whether it is possible to successfully polymerise the monomers produced in the previous chapter. Basically, Ox and Ozi are converted in a CROP reaction and Lewis acids such as methyl tosylate are used as initiators, which initiate the ring opening of the Ox and Ozi ring.[167] An anhydrous reaction condition must be observed, as the nucleophilicity of water can lead to side reactions. These circumstances raise further questions in addition to the synthesis route as side reactions can occur and the polymerisation can therefore be inhibited. On the one hand, it is important that the synthesis can proceed in a controlled manner and, on the other, that it offers the possibility of obtaining a high-quality product in a yield of almost 100 %. From the monomers of the previous chapter, 2Th3Ozi showed the best properties in terms of availability of the starting materials, synthesis and upscaling. In general, these monomers have a bi-functional polymerisation possibility. Firstly, the Ox and Ozi ring can be opened and polymerized, or alternately the thiophene rings can be polymerised. For the latter polymerisation, however, Lewis acids such as iron chloride are usually necessary, which can attack the Ox and Ozi ring at the same time. This can lead to side reactions and controlled polymerisation is no longer possible. During the synthesis of thiophene-based Ox and Ozi, it was observed that the reactivity of the Ox or Ozi ring is higher than the reactivity of the thiophene ring, since a nearly quantitative yield of the products was possible, and side-reactions initiated from the thiophene-ring were not observed. Furthermore, the reactivity of thiophene systems are lower than analogue amine-based systems.[226] It is to be expected that the opening reaction of the Ox and Ozi is preferred, since a further charge shift in the ring system is to be expected due to the oxygen.[227] It is therefore important that the polymerisation of the Ox or Ozi chain takes place first and that the thiophene rings are polymerized in a subsequent reaction. A simple way to avoid side reactions is to keep the concentration of the initiator as low as possible and thus also to minimise the concentration of the reactive polymerisation chains.[23] A diluted reaction solution is also very useful here. This would have the consequence that a pure product can be realised in good yield. In principle, the yield of the synthesis of POx and POzi is approx. 90 % and more. The purity of the products is ensured by various purification

steps such as dialysis, precipitation or phase separation. In the polymerisation of thiophene-based Ox and Ozi, the aim was to achieve a similar yield and also a pure product.

There are many ways to optimise the properties of the produced material based on the chemical structure of the polymer. A functional group can be introduced by end-functionalization, as demonstrated by Mathias et al.[228] who functionalized poly(4,4‘-dimethyl-triphenylamine) (poly(TPA)) with an anchor group. A catechol group was used to enable surface bonding to inorganic nanoparticles. Due to the conductivity of poly (TPA), a conductive surface coating of inorganic particles could be produced. The end functionalization of POx and POzi is also possible. Podevyn et al.[195] have investigated the addition of multiple functionalities to aliphatic POx. An ester end-group was used to implement azido, amines or alkene groups into the system. With this approach, the authors were able to show that a further modification is possible, since, for example, end-functionalisation with alkenes enabled radical polymerisation. POx offers a good platform here, since functional groups can be introduced through initiation and termination. Due to the simple availability and synthesis of sulfonates or sulphate esters, which can serve as initiators, a large number of molecules can be produced and therefore used as functionalization end-groups. POx and POzi also offer a good way of inserting functional groups into a polymer via the side group via two established approaches. The functionality of the side group can be changed as required in a post-polymerisation modification by deprotonating PMeOx and using bromoalkenes.[196] Alternately, the functional group can be inserted as a monomer and then polymerized in a conventional ring-opening reaction. Through the synthesis of initiators or termination reagents based on EDOT, a chemical functionalisation of aliphatic POx or POzi could take place by this approach. This approach would have the advantage that commercially available monomers can be used and modified for further reactions via end group functionalisation. Through this approach, the material properties such as mechanical flexibility or solubility can be specifically changed by end-functionalisation, side group modification or copolymerisation.

CPs belong to the class of conjugated polymers and, without modification, are considered electrical insulators ($<10^{-7}$ S cm^{-1}). However, chemical or physical treatment with heat, light or additives can improve the conductivity by several orders of magnitude to form electrically conductive materials in the range from semiconductors ($10^{-7} – 10^{2}$ S cm^{-1}) to electrical conductors ($> 10^{2}$ S cm^{-1}). A basic distinction is made here between intermolecular and intramolecular conductivity. A continuous sp^2-conjugated system must be present for intermolecular conductivity. This can be observed, for example, with the naturally occurring carotenes. With this approach, nature can cover and process different energy ranges depending on the chain length of the conjugated system. Technically, however, this perfectly coordinated system is difficult to implement, as infinitely long chain lengths cannot be implemented due to secondary- and termination-reactions. In the case of intramolecular conductivity, the individual chains must be in close proximity to each other in order to enable electron hopping between the chain lengths. The maximum distance here is approx. 20 nm.[229] One commonly used approach to imparting high

conductivity is the use of dopants. In the 1960s, Shirakawa, MacDiarmid and Heeger[156] were able to improve the electrical conductivity of poly(acetylene) by a factor of 10^9 through suitable doping with halides and achieved a conductivity similar to copper. Mendez et al. was able to increase the conductivity of PEDOT through targeted cross-linking with conjugated linkers. Here, an addition of 0.5-2% of the crosslinker based on thiophene molecules could increase the conductivity by up to 36%. Similar behaviour should be observed when adding EDOT monomers to a system. The conductivity can also be increased with other additives such as solvents or anionic surfactants. By using anionic salts, Shi et al.[230] were able to increase the conductivity of PEDOT:PSS by a factor of 500. Here sodium dodecyl sulfonate achieved the best results. Lingstedt et al.[231] chose a different approach. PEDOT:PSS was treated with DMSO. This also made it possible to increase the conductivity significantly by a factor of 500. It is assumed that the PEDOT chain is stretched due to hydrogen bonds and thus a better intramolecular interaction can take place, which improves electron transport. The heat treatment of PEDOT is based on a similar principle. The electrical conductivity is dependent on the morphology of the system due to the intramolecular interactions and therefore charge transport. It could be shown here that heating PEDOT:PSS leads to an increase in the surface roughness and thus the conductivity can be increased. Treatment with light, on the other hand, has a different approach. Alishah et al.[232] examined the treatment with light from ITO/PEDOT:PSS solar cells and was able to determine an improvement of approx. 9% compared to untreated solar cells. Targeted exposure to light can introduce imperfections in the system, which can serve as placeholders for electrical charge. When electrons are transported, these defects can then be filled and the conductivity of the electrical charge increased. In summary, it can be said that the electrical conductivity of CPs can be improved by several orders of magnitude through post-modification treatments.

Figure 4.1 gives an overview of the synthesis approaches in the following chapter. The nomenclature for the polymers was chosen in the same manner as in the previous chapter for the thiophene-based monomers.

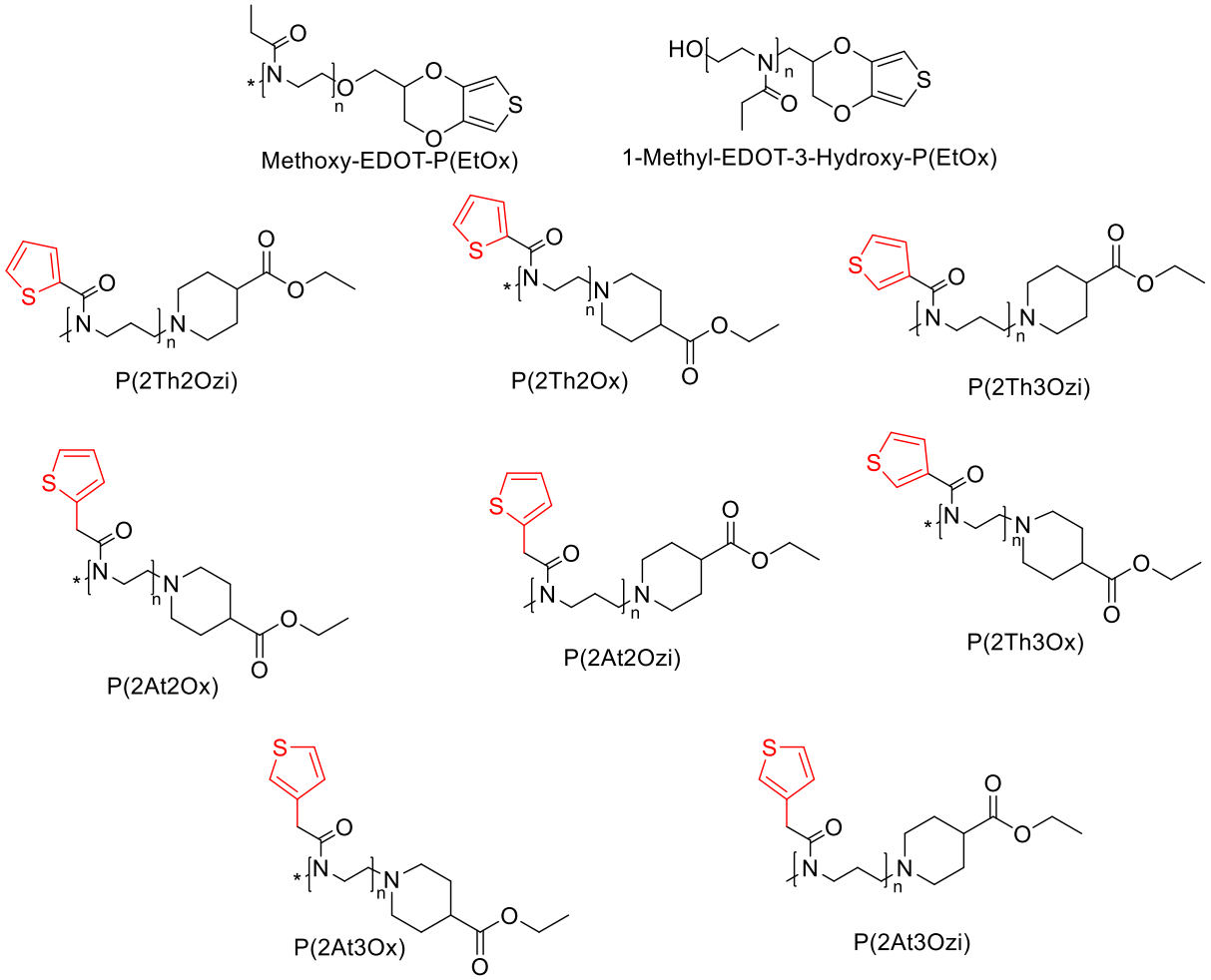


Figure 4.1 Overview of polymer synthesis approaches

4.2 Aims and Hypotheses

The primary objective of this chapter was to investigate the polymerisation behaviour of the previously introduced thiophene-based Ox and Ozi monomers. Up-scaling is also an important consideration for obtaining adequate product. Therefore, due to the availability of the starting materials and the multiple synthesis possibilities, the use of 2Th3Ozi is the focus of this study. It was hypothesised that the properties of the resultant polymer would be aligned with those of the component polymers with materials exhibiting a thermal melt property, some conductivity and cytocompatibility. It was also proposed that the electrical conductivity could be improved through the introduction of additional CP units into the polymer system through post-fabrication modifications.

The specific aims of this chapter were to:

1. Establish the polymerisation routes of thiophene-based Ox and Ozi based on fundamental analysis methods;

2. Identify and optimise the synthesis parameters for up-scaling strategies; and,
3. Investigate the introduction of improved electrical conductivity through post-modification;

4.3 Results and Discussion

4.3.1 Synthesis of novel polymer platform

First, the termination of POx with EDOT derivatives was investigated (figure 4.2). This approach was chosen to produce an electrically conductive polymer by chemical functionalisation of aliphatic POx as previously described. For this purpose, PEtOx was polymerized with MeOtf as an initiator in benzonitrile (BCN) at 70 ° C under inert conditions. The initiator-monomer ratio was verified between 1:15 and 1:40. Termination was carried out with methoxy-EDOT due to its nucleophilic character. When the terminating reagent was added, a direct precipitation of the polymer could be observed. In the case of longer chain lengths, no solubility of the final product could be observed either. The polymer was not soluble in any solvent and therefore, unable to analysed further.

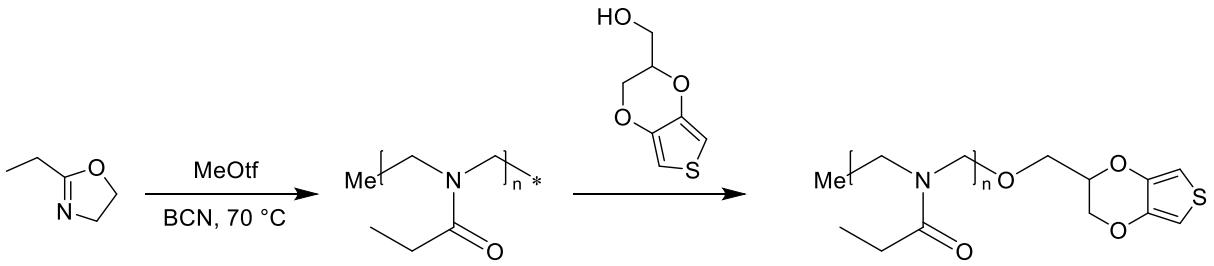


Figure 4.2 Termination of PEtOx with Methoxy-EDOT

The strategy for developing a copolymer based on aliphatic POx and PEDOT was also carried out by initiating the polymerisation of ethyl oxazoline (EtOx) with 3,4-ethylenedioxythiopene tosylate (OTs-EDOT, Figure 4.3).

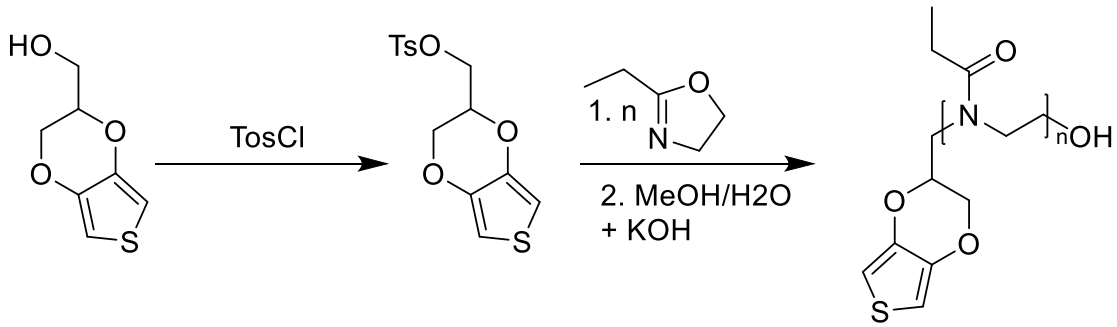


Figure 4.3 Initiation with of MeOc with Tosyl EDOT and termination with methanol and KOH

For the synthesis of the initiator, 3,4-ethylenedioxythiopehene methanol (EDOT-Met) according to Lima et al.[233] was produced and in a second step, according to Skompska, et al.[234] converted into the OTS-EDOT as described in details in the methods section. The yield of the five-step reaction was 15 % for EDOT-Met, comparable to the literature. The conversion into the OTS-EDOT could be carried out

with a 75 % yield. After the OTS-EDOT had been purified, the EtOx was polymerized in dry benzonitrile at 130 °C. An initiator/monomer ratio of 1:40 was chosen. Due to the high proportion of PEtOx compared to the end group, the physical properties of the polymer should in theory be adopted to obtain as much flexibility as possible for the subsequent copolymerisation of the PEDOT. The starting materials and products were analysed using ^{1}H-NMR spectroscopy (Figure 4.4, a). In addition, the polymer obtained was further characterised via GPC (Figure 4.4, b).

The introduction of the tosylate group was initially be observed in the representative NMRs (~ 7–8 ppm). During the subsequent polymerisation, a bond break occurs between the oxygen and the methyl group of the EDOT. As a result, the tosylate group is cleaved and can no longer be detected in NMR if the conversion is successful. In addition, the polymerisation leads to a broadening of the PEtOx signals (~ 3.5, 2.4 and 2.0 ppm). Furthermore, all signals could be assigned. A monodisperse distribution was detected in the representative GPC spectrum (Mw = 4.791 g/mol, Mn = 3.488 g/mol, D = 1.38).

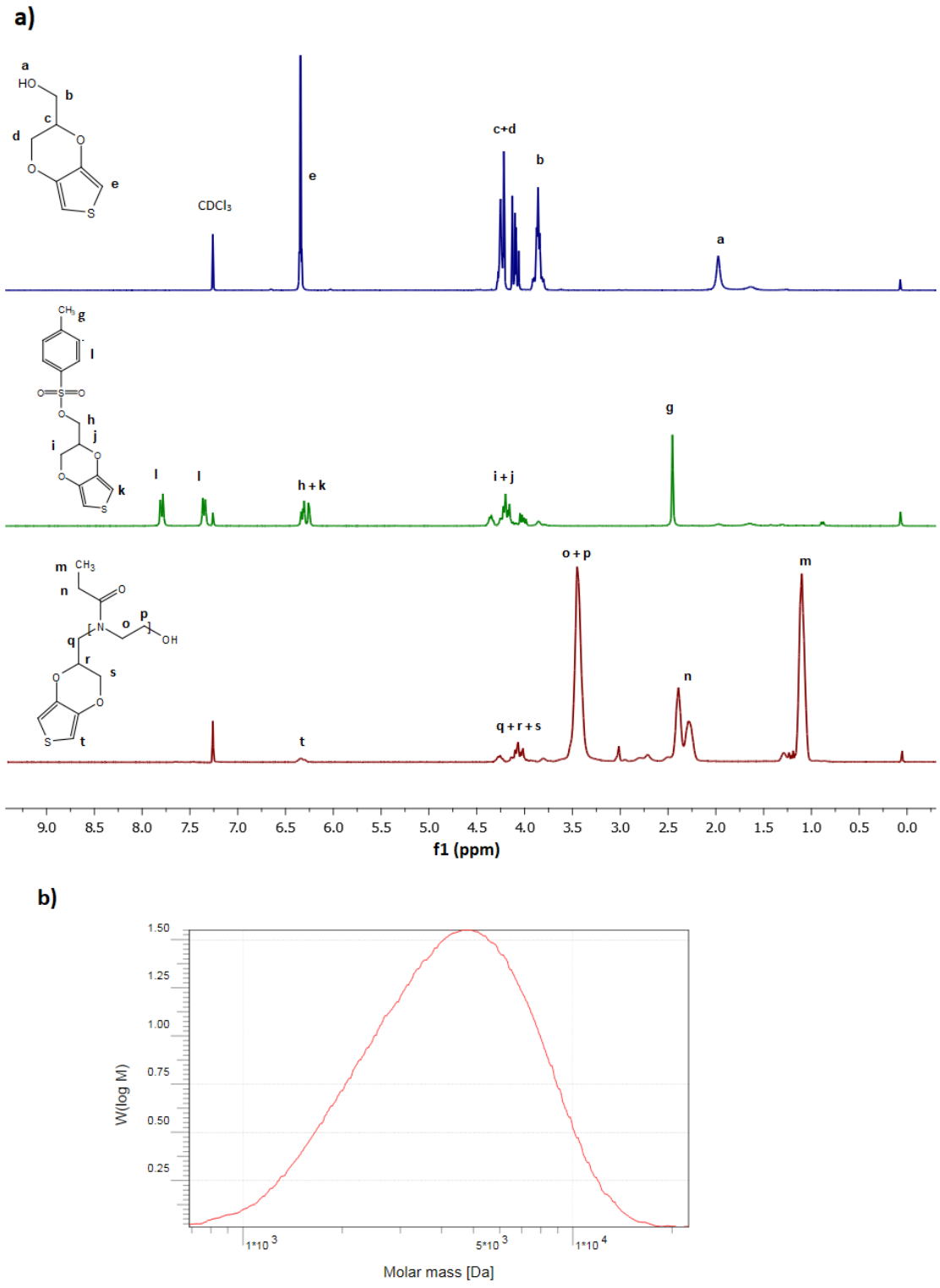


Figure 4.4 a) [1]NMR spectrum of PEtOx initiated with EDOT-tosylate for the synthesis of EDOT-P(EtOx)-OH, b) GPC of EDOT-P(EtOx)$_{30}$-OH show monodispers distriution

As initially described, the EDOT-PEtOx polymer obtained should be polymerised oxidatively by either chemical or electrochemical methods in a second reaction. This allows an electrically active segment based on PEDOT or other thiophene derivatives to be introduced into the polymer. By separating the polymerisation into two independent reactions, more freedom is given due to a better control of polymer properties as the chain length can be individually verified.

Analogous to Sugimoto and Yoshino et al.[83], the chemical oxidative polymerisation of EDOT-PEtOx was carried out in chloroform with iron chloride as initiator at ambient temperature. The initiator-to-EDOT ratio was estimated to be 1:3 and the reaction time was 24 hours. Inert conditions were chosen. Analogous to the termination of PEtOx, a direct precipitation of the polymer could be observed. The insoluble product could not be dissolved in any solvents either and therefore further analysis of the polymer could not take place.

The polymerisation of the EDOT via the end group could only be carried out through electrochemical polymerisation in the presence of additional free EDOT monomer. In the case of chemical oxidative polymerisation, an insoluble solid precipitated immediately after initiation, which could not be further chemically characterized. Similar behaviour could also be found in electrochemical polymerisation. Yagci et al.[165] observed the same behaviour when synthesising electroactive macromers based on pyrrole or thiophene and Ox. Limited analysis of the electrochemical behaviour of the produced PMeOx-PEDOT systems was carried out but will not be presented in detail (data can be found in appendix). The focus of this work was on resource-saving and, above all, sustainable research. To achieve this, it is essential that both an almost 100 % conversion and yield are achieved. As a result, yields in the gram range would enable further application in the 3D printing area. The poor overall yield of the starting materials is, therefore, a limiting factor. Methoxy-EDOT is commercially available, but the cost is very high and the purity of the material is insufficient for a successful ROP. Furthermore, this approach has a limiting polymerisation potential as it is only achievable through electro polymerisation and the overall yield is only around 10% and thus the cost-benefit factor is not given here and was therefore not considered any longer in the further course of this work. The main focus of this work was therefore on the further investigation of the thiophene-based Ox and Ozi monomers presented in the previous chapter.

The ability to polymerise monomers developed in Chapter 3 were investigated and characterised. Two polymerisation approaches were used, homopolymerisation and copolymerisation of ThOx and ThOzi with selected aliphatic Ox or Ozi.

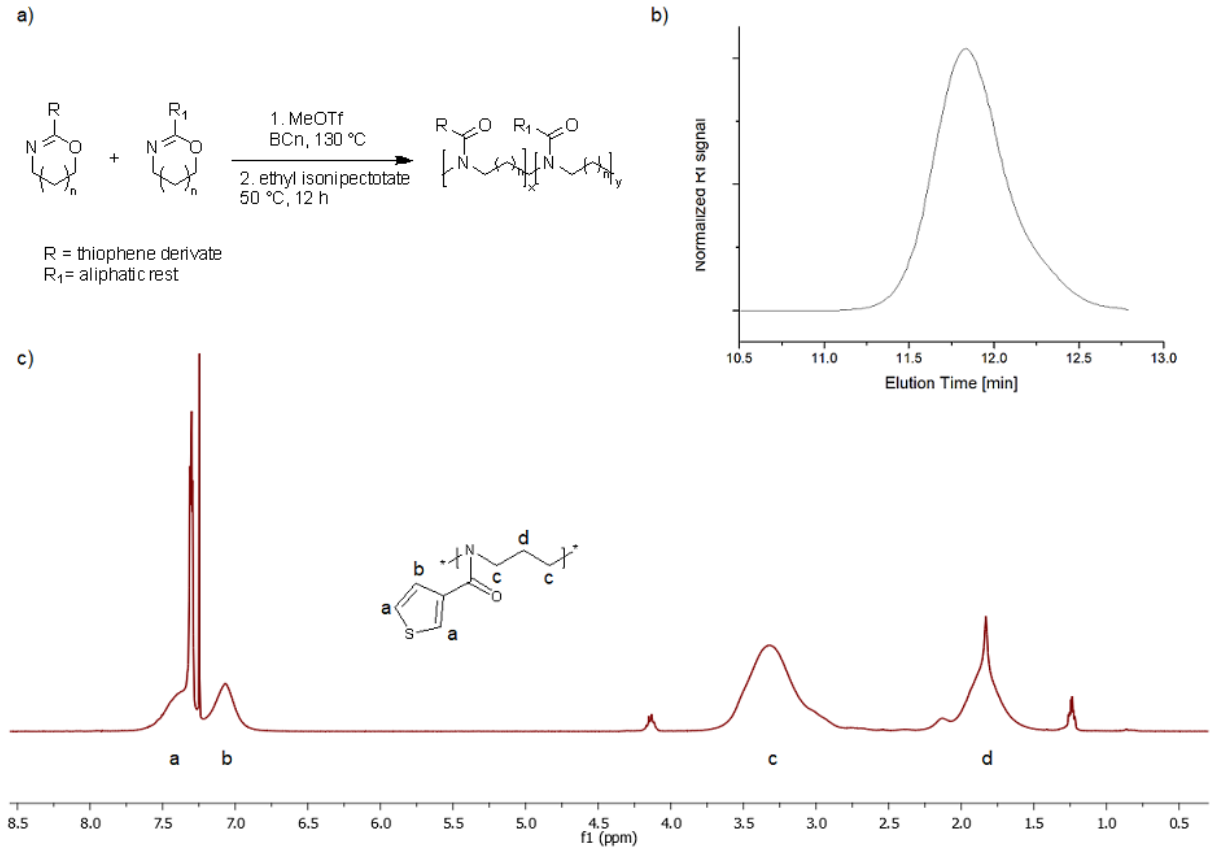


Figure 4.5 a) general polymerisation and copolymerisation of poly(thiopheneoxazoline/oxazines) via CROP and initiated with MeOTF in BCN, b) Representative GPC of poly(2-thiophene-3-oxazine) (P2t3Ozi) shows monodisperse distribution, c) ^{1}H-NMR spectrum of P(2t3Ozi)$_{25}$

The CROP and copolymerisation of PThOx and PThOzi were carried out in benzonitrile at 130 °C (Figure 4.5a). Acetonitrile was initially investigated a solvent for polymerisation but found to be limiting as the polymer precipitated too quickly. As such benzonitrile was chosen and found to provide more stable conditions for polymerisation. MeOtf was used as cationic initiator acceptor. Ethyl isonipectotate was used for a functional termination of the polymer chain and as an alternative termination reagent, a methanolic KOH solution was established. The monomer-to-initiator was verified between 25:1 and 50:1. The polymerisation time was around 5 hours for long-chain polymers (n = 50). The initiator concentration was kept low (1/40 eq.) due to potential oxidative side reactions between the initiator and thiophene ring. Polymers were characterized via NMR-spectroscopy and GPC. An example of GPC and NMR spectrum for P2Th3Ozi is shown in Figure 4.5 (b,c). Furthermore, a ^{13}C-NMR of P2Th3Ozi is shown in the Appendix. Characteristics of synthesised polymers are illustrated in Table 4.1. While the monomers of P2Th2Ox and P2Th3Ox were soluble in benzonitrile, the polymers became insoluble as the reaction time continued and only showed solubility in HFIP. Therefore, the analysis of those polymers was limited. The polydispersity index (PDI) showed a monodisperse distribution and was in the range of 1.13 – 1.19 and the glass transition temperature (T_g) was between 95 – 100 °C. The corresponding PThOzi showed a much better overall solubility. The PDI of these polymers was in the range of 1.09 – 1.27 and were obtained as colourless powders. However, in solution, the colour changed

to light yellow. T_g was between 55 – 62 °C. P2At3Ox and P2At2Ox also showed good solubility during polymerisation and were obtained as light-yellow powders with a PDI between 1.12 – 1.39. P2At3Ox_{50} had the highest dispersity with a PDI of 1.67. The T_g of PAtOx materials were between 59 – 65 °C. The polymerisation of P2At2Ozi and P2At3Ozi was much more difficult due to the instability of the monomers as described in chapter 3. The overall yield was approximately 50 – 60 %. The PDI was between 1.15 – 1.47. This sub-class showed the lowest T_g of 40 – 48 °C. Due to the cheap price of starting materials, the ease of synthesis, overall yield and high control during polymerisation, further work was focused on P2Th3Ozi.

Since the polymerisation of P2Th3Ozi was generally most efficient, a systematic copolymerisation study with the use of this monomer was investigated further. This is also essential for further use of the polymer class in 3D printing to ensure the most precise control possible of the thermal behaviour of the polymer. For this purpose, a simple copolymerisation analysis with different monomer ratios was performed (listed in Table 4.1). The use of aliphatic Oxs enabled the T_g of the copolymer to be influenced and controlled. The theoretical calculation of the T_g was comparable to the values found experimentally and followed that of the Flory-Fox equation (eq. 4.1).[108] Here, n-propyl Ox was found to be particularly suitable as an aliphatic monomer, since the corresponding homopolymer has a known T_g of 9 ° C[166,235] and is thus below the T_g of P2Th3Ozi measured experimentally (Table 4.1).

$$\frac{1}{T_{g,mix}} = \frac{w_1}{T_{g,1}} + \frac{w_2}{T_{g,2}} \qquad \text{(eq. 4.1)}$$

A ratio between 1:1 and 4:1 was chosen. Furthermore, no phase separation between the two monomers could be observed during the polymerisation. The polymerisation of ThOzi with MeOx or MeOzi, on the other hand, was not possible due to phase separation. An investigation of the block copolymerisation was not carried out since the main application should be in 3D printing and therefore a block-co-polymer with different physicochemical properties along the polymer chain would not be likely to meet the required material properties.

Table 4.1 Number average of Molar Mass, polydispersity, T_g, yield of synthesized polymers

polymer	M_n[a] [kg/mol]	M_n[b] [kg/mol]	M_n[c] [kg/mol]	Đ[d]	T_g [°C] **	yield [%]
P2t3Ox_{25}*	4.00	–	1.50	1.14	101	–
P2t3Ox_{50}*	7.80	–	1.40	1.13	105	–
P2t3Ozi_{25}	4.30	4.00	2.90	1.09	59	84
P2t3Ozi_{50}	8.50	8.30	6.70	1.11	62	82
P2t2Ox_{25}*	4.00	–	1.10	1.19	95	–

P2t2Ox$_{50}$*	7.80	–	1.70	1.18	102	–
P2t2Ozi$_{25}$	4.30	2.80	7.50	1.27	55	77
P2t2Ozi$_{50}$	8.50	6.20	9.70	1.21	58	73
P2At3Ox$_{25}$	4.30	3.00	3.10	1.12	59	63
P2At3Ox$_{50}$	8.50	7.20	3.30	1.21	65	60
P2At3Ozi$_{25}$	4.70	2.10	5.90	1.36	42	44
P2At3Ozi$_{50}$	9.30	4.60	8.60	1.15	44	65
P2At2Ox$_{25}$	4.30	3.20	1.20	1.39	59	40
P2At2Ox$_{50}$	8.50	6.30	3.90	1.67	61	45
P2At2Ozi$_{25}$	4.70	2.70	5.80	1.47	40	42
P2At2Ozi$_{50}$	9.30	3.80	7.40	1.45	42	48
P2t3Ozi$_{20}$-*ran*-PnrPOzi$_5$	3.98	–[e]	3.50	1.28	50.5	83
P2t3Ozi$_{20}$-*ran*-PnrPOzi$_{10}$	4.61	–[e]	5.6	1.34	44.6	86
P2t3Ozi$_{20}$-*ran*-PnrPOzi$_{20}$	5.88	–[e]	7.8	1.29	37.9	75

[a] theoretical value, [b] calculated by ^{1}H-NMR, [c] obtained from GPC (T=40°C,the flow rate was set to 0.7 mL/min (HFIP) and calibrated using poly(ethylene glycol) standards), [d] Obtained from GPC (Mw/Mn), [*] became insoluble during polymerisation, [e] NMR value was not calculated as no reference signal could be identified, [**]manually calculated by NETZSCH Proteus©

The polymers P2Th3Ox and P2Th2Ox were analysed using MALDI TOF because of their insolubility (Figure 4.6). The molar mass agrees with the theoretical value and corresponds to an expected Poisson distribution, which is to be expected for a living polymerisation.[236] Due to the undefined spectra, a more precise molar mass distribution analysis was not demonstrated.

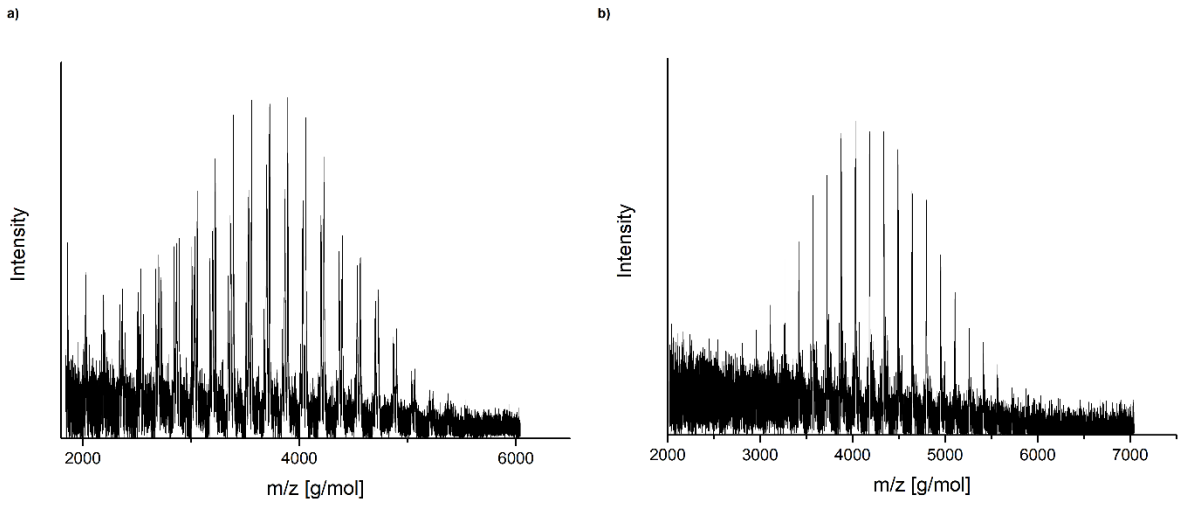


Figure 4.6 MALDI-TOF spectrum of a) P2t2Ox$_{25}$ and b) P2t3Ox$_{25}$. As seen in both graphs, the polymers follow a poison distribution

The thermal properties were analysed by thermogravimetric analysis (TGA) and differential scanning calorimetry (DSC) (Figure 4.7). The DSC graph shows the measurement data for the homopolymers with a chain length of 30 repeating units for all polymers. The DSC analysis is carried out in three cycles in a temperature range of -50 – 250 °C. The thermal analysis was carried out with P2Th3Ozi with different chain lengths and under a nitrogen atmosphere. A high thermal stability up to approx. 300 °C could be determined for all polymers. It should be mentioned that the first mass loss at approx. 100 °C in two series of measurements is probably due to residual moisture and is therefore defined as a thermal artifact. The mass loss began at around 350 °C, which is in line with the general trend for POx and POzi. This resulted in a wt % loss of approximately 80 %. A further weight loss was observed at approximately 500 °C. This could indicate a thermally initiated superstructure or the splitting of the thiophene rings. Similar behaviour was found for PEDOT-based hydrogel by Amella et al.[237]

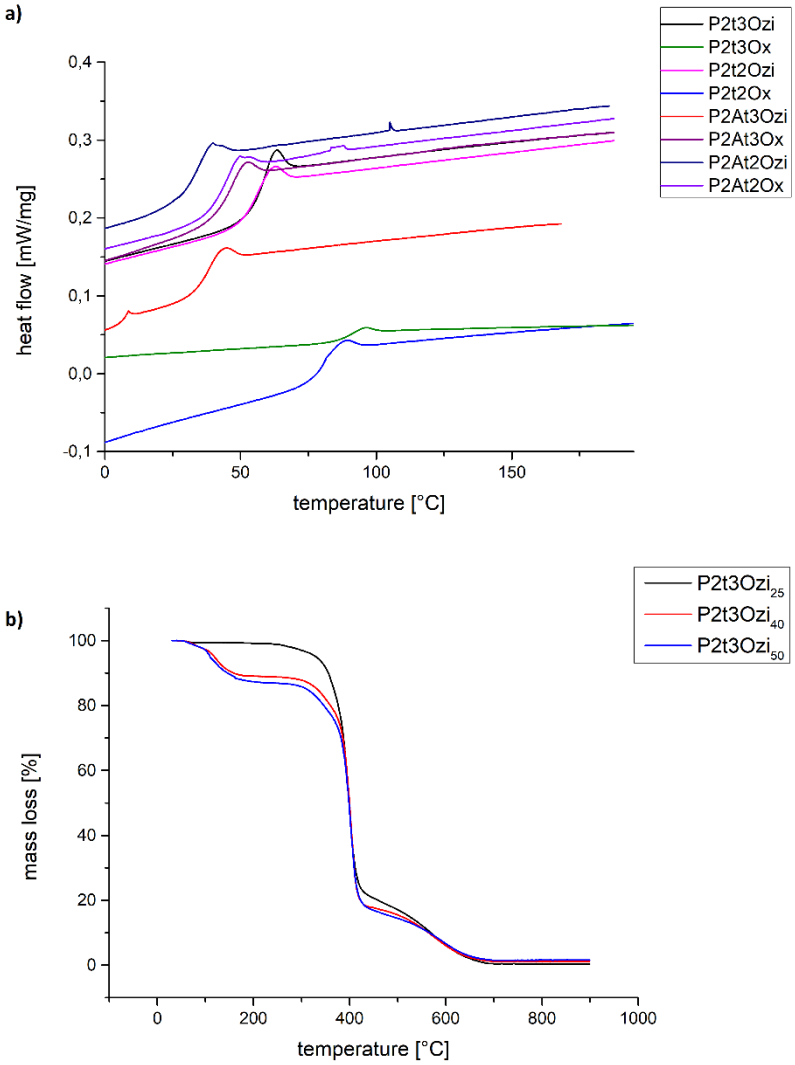


Figure 4.7 a) DSC analysis of various PtOx and PtOzi show peaks at glass transition b) TGA of P2t3Ozi with different chain length. A thermal stability till approx. 350 °C can be seen

Further investigations focused on the chemical stability of the polymer class. To examine the chemical stability, the polymer material was subjected to a treatment corresponding to the thermal stress, similar

to that experienced during the 3D MEW printing. For this purpose, the polymer was stored for 48 hours at 120 °C under an ambient atmosphere. Afterwards, the polymer was then placed in water for a further 48 hours. Using IR spectroscopy (Figure 4.8), no significant difference could be observed before and after the treatment. Furthermore, the signals in the fingerprint area of the IR spectrum are almost identical. It should be noted that the conditions of 120 °C for 48 hours is longer than typical expected melt times for 3D printing and hence a good indicator of the thermal stability required for compatibility with 3D printing processes.

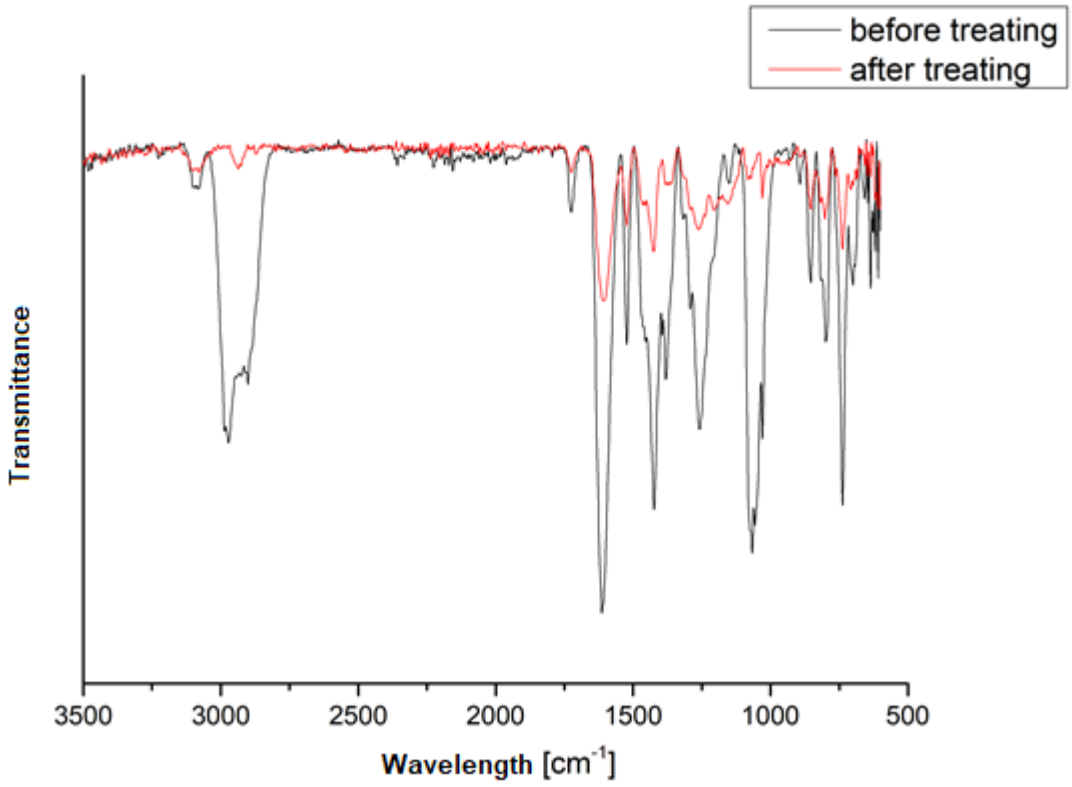


Figure 4.8 IR spectrums of P2Th3Ozi before and after treating show almost identical peaks

The polymer material was also examined for its chemical stability by NMR spectroscopy and X-ray structure analysis (XRD). As the NMR spectroscopy showed no significant differences, the spectrums were not presented in detail. Results from XRD analysis are shown below in figure 4.9. No significant change of the diffraction intensity and angle could be observed before and after treatment.

For many 3D printing processes, such as MEW, the thermal stability of the polymer is essential, since many production steps take place at temperatures above 100 °C. It could be shown that P2Th3Ozi did not show any significant thermal decomposition even after prolonged heat treatment above this temperature. In comparison, many CPs in particular show the first decomposition reactions above 100 °C. PANI in particular has been shown to undergo thermally induced degradation. The polymer goes through several stages of decomposition and the first stage starts at 100 °C. At 200 °C,[238] PANI then decomposes completely. Thiophene-based CPs are thermally more stable because of the larger

heteroatom. PEDOT in particular shows interesting properties. While the initial thermal treatment and therefore reaction occurs at temperatures similar to PANI, this does not lead to decomposition but to a superstructure that can improve electrical conductivity. The thermal decomposition takes place at approx. 300 °C.[239] In contrast, polyoxazolines have higher thermal stability. Cyclic alkyl-POx show melting temperatures above 300 °C.[182] This is due to the high crystallinity of the basic structure. In the case of cubane-POx, on the other hand, no melting temperature has been calorimetrically determined, since the polymer decomposes at 250 °C with no melting temperature identified below this level. Thermally induced structural changes have been detected in POx. For example, PiPrOx showed an irreversible structural transformation to coagulated particles at just 60 °C, which can be attributed to hierarchical self-organisation.[240] A reason for the thermal stability of P2Th3Ozi could be due to the steric interference of the crystal order by the organic rest combined with the size of the heteroatom, analogous to the theory of POx and CPs.

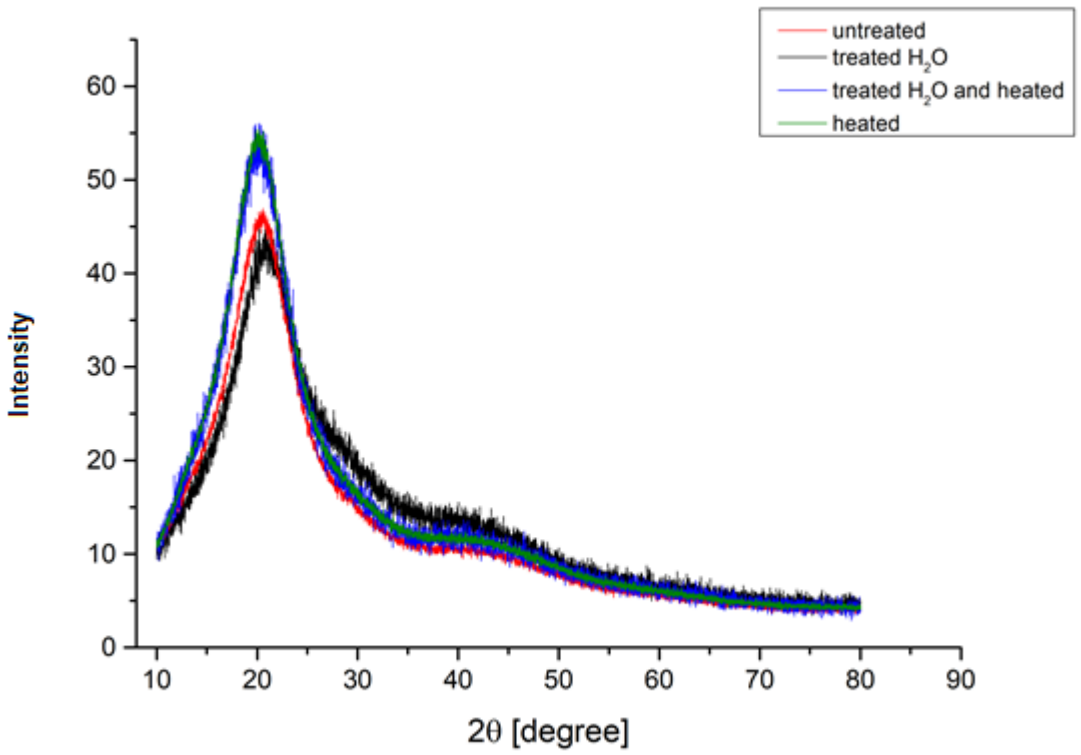


Figure 4.9 XRD analysis of P2Th3Ozi before (red) and after treatment with water (black), with water while heated (blue) and only heated (green) show no significant varieties

The relationship between crystallinity and an amorphous phase of P2Th3Ozi could also be determined by XRD analysis. Since polymers are generally always partially crystalline materials, the two phases can be differentiated based on their scatter and thus the ratio can be calculated. The following applies to the weight fraction w_c with $A_{c;a}$ for the area of the individual scatter area[108]s:

$$w_c = \frac{A_c}{A_a + A_c} \qquad \text{(eq. 4.2)}$$

Figure 4.10 shows the graphic evaluation of the weight fraction. For this purpose, the areas were calculated using OriginLab and equation 4.2 results in an approximate ratio between the crystalline and amorphous phase of 27.1 ± 1.4 % for untreated, 28.3 ± 1.4 % for heated, 25.6 ± 1.3 % for treated in H_2O and 29.3 ± 1.5 % for treated H_2O and heated.

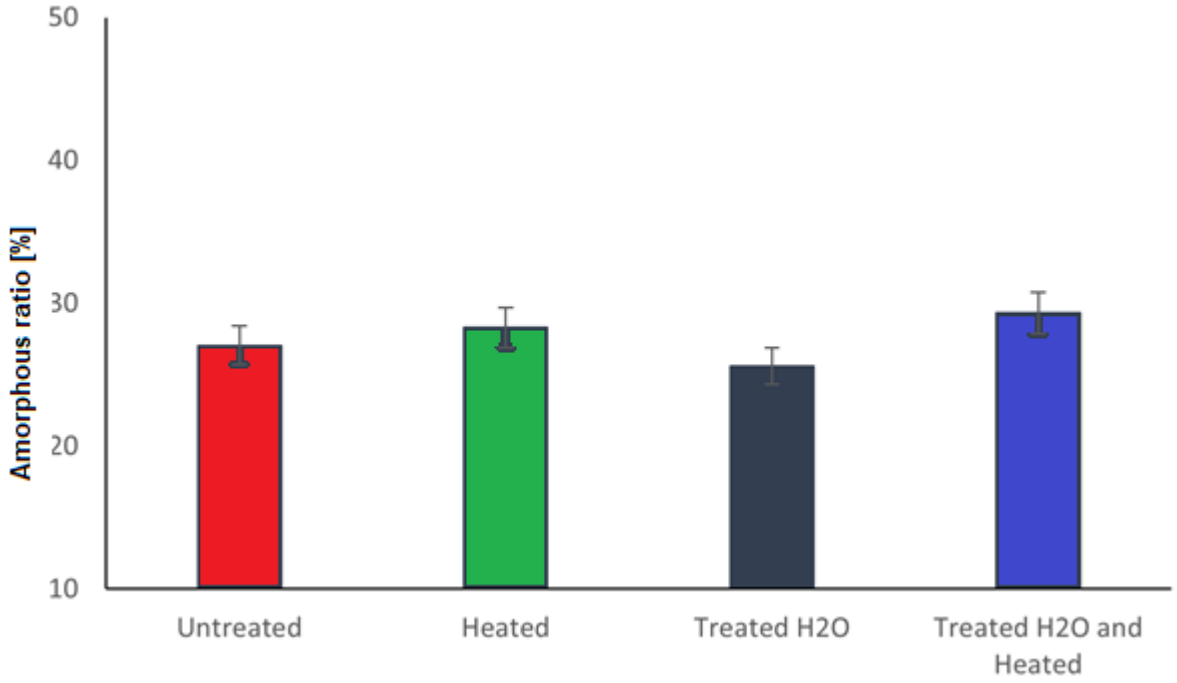


Figure 4.10 XRD analysis of crystallinity of untreated (red) and treated P2Th3Ozi with water (black), with water while heated (blue) and only heated (green)

The proportion of crystallinity has a direct influence on the chemical stability and on the mechanical properties of the polymer. Below their glass transition temperature, amorphous polymer areas have brittle, hard-elastic properties. This is due to the immobility of the frozen chains.[108] If the glass transition temperature is increased, the molecular chains move against one another, and typical rubber-elastic properties occur. With increasing temperature, the mobility of the chains increase and the material becomes softer. The modulus of elasticity decreases significantly. With constant force acting on the component, a viscoelastic deformation occurs. Amorphous polymers therefore only have heat resistance below the glass transition temperature. In contrast, crystalline polymers have an opposite behaviour. Intermolecular forces act between the chains of the crystalline areas, which prevent softening. The modulus of elasticity is still relatively high above the glass transition temperature. The crystallites only melt at a significantly higher melting temperature with the addition of significant amounts of energy, which are necessary to overcome the regular arrangement of the chains (melting enthalpy). It is only at

this transition to the viscous melt that there is a sharp drop in the modulus of elasticity. Partly crystalline polymers can therefore be used at significantly higher temperatures without the corresponding component changing its dimensions or shape. The mechanical properties of any polymer are made up of the properties of the crystalline and amorphous areas, and largely determined by the ratio between these areas. The higher the proportion of densely packed crystallites, the harder, but also more brittle, the component becomes. A certain crystallinity is therefore desirable for flexible applications and devices, since this is responsible for the stability of the plastic. The amorphous areas, on the other hand, are necessary to give the macromolecular materials a certain elasticity and impact strength. While nylon, as an example of a flexible polymer, has a crystallinity of between 30 – 50%, PTFE can have a crystallinity of up to 80 %.[108] Shen et al.[241] investigated the crystallinity of poly(3-hexylthiophenes). For regioregular poly(3-hexylthiophenes), a crystallinity between 47 – 56% was found. In general, the crystallinity can be up to 80%. Torbus et al.[242] investigated the crystallinity of POx on the basis of poly(2-isopropyl-2-oxazoline). A maximum crystallinity of 60% could be achieved. The crystallinity of around 70 % for P2Th3Ozi is thus in the range between the two component polymer classes and showed an increased crystallinity when compared to aliphatic POx. In comparison to polythiophenes a slight reduction was observed.

A simple kinetic analysis was carried out by the measurement of monomer concentration during polymerisation by ^{1}H-NMR spectroscopy. Due to the onset of insolubility with continued polymerisation of P2Th3Ox and P2Th2Ox, measurements could only be made for 60 and 30 minutes respectively. Figure 4.11 also shows that the PAtOx derivatives show a deviation in the linear course with increasing polymerisation time.

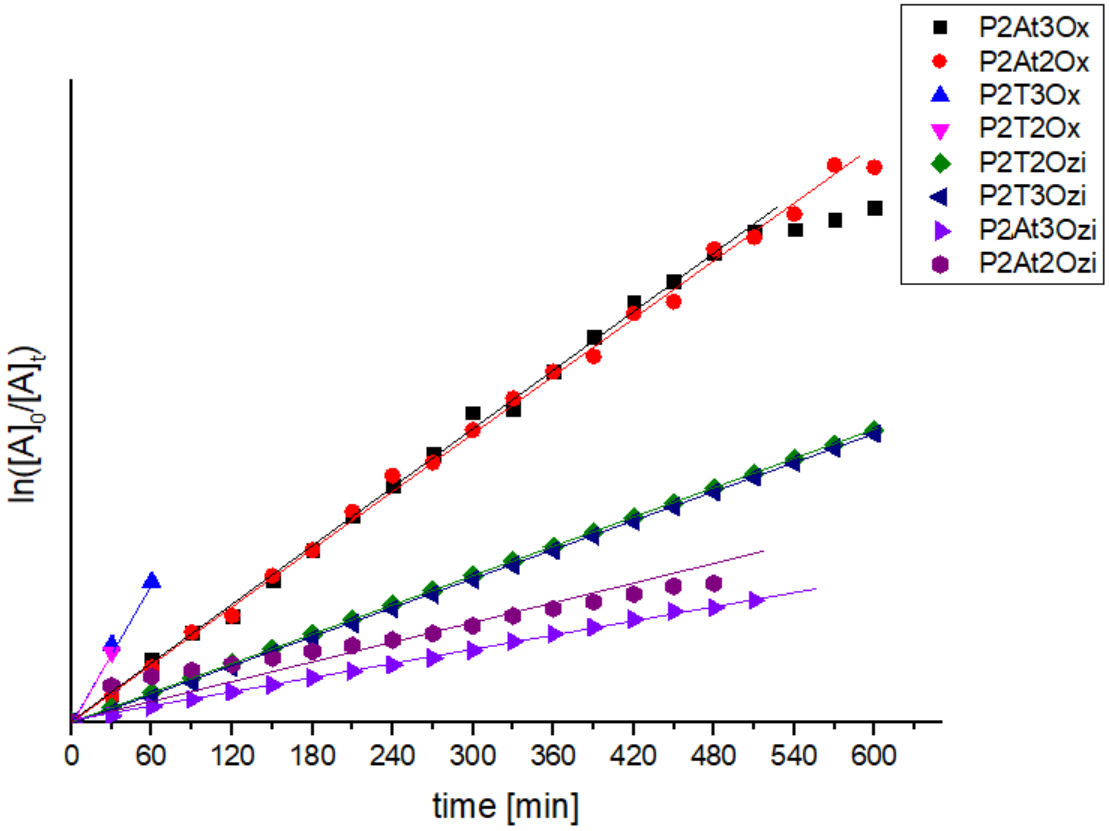


Figure 4.11 First order kinetics of polymerisation of tOx and tOzi. All polymers show a linearity for the first 6 hours of polymerisation

The yield of thiophene-based POx and POzi is comparable to the yield of around 90 % for alipahatic POx and POzi.[24] Above all, the monosubstituted polymers showed an almost 100 % conversion. The acetothiophenes showed a deviation from the linear course, especially after prolonged polymerisation, and therefore polymers with a comparatively low polymer mass are to be preferred. Due to the slight nucleophilicity of the thiophene ring compared to aliphatic side groups, this could be the reason for side reactions of PAtOx and PAtOzi. Due to the lack of a carbon atom and thus the restriction of the freedom of rotation, this cannot be observed with monosubstituted thiophene-based POx and POzi. Another advantage of P2Th3Ozi over aliphatic POx and POzi is the possibility of having the monomers in solid phase during material preparation, thus facilitating anhydrous processing. This was confirmed by the good agreement between the theoretical polymer chain length and the measured values. Furthermore, the thiophene-based POx and POzi cover a wide range of the Tg. This, too, is only known from the literature for aliphatic POx and POzi. It should be noted here that the T_g of thiophene-based POX and POzi are approx. 40 ° C higher than the T_g of aliphatic POx and POzi. The disadvantage here is that the polymer melt range is generally above 100 °C. As a result, the temperature range up to the onset of decomposition is minimized. However, compared to other POx, the thiophene-based POx and POzi showed good stability at elevated temperatures.

4.3.2 Solubility of thiophene-based POx and POzi

The stability and the physiochemical properties of this new polymer class are of critical importance. As such, preliminary experiments on solubility, stability and crystallization were performed. The solubility of polythiophenes is a much-cited problem in the literature.[243–245] This limits a large-scale application since many processes are based on the solubility of plastics. At the beginning of this work, a focus was made on the solubility during the synthesis and development of the monomers and polymers. As already described in the Literature Review (Chapter 2), similia similibus solvuntur applies in general. A semi-empirical description of this fact for practice work was suggested by Hildebrand et al.[108,246]. The method describes the connection that intramolecular forces between two polymer chains have to be broken up by solvent molecules. Here Hildebrand et al. defined a solubility parameter δ. This is made up of the interaction energy ε and the unit volume.

$$\delta_1^2 \sim \frac{\varepsilon_{1;1}}{V_1} \qquad \text{(eq. 4.3)}$$

From the thermodynamic point of view, the total enthalpy of the system ΔG_m must be negative during the dissolving process. This is only possible if the entropy of mixing ΔH_M is only slightly positive since the entropy ΔS_M is always negative during the solution process.

$$\Delta G_M = \Delta H_M - T\Delta S_M < 0 \qquad \text{(eq. 4.4)}$$

$$\Delta H_M \sim (\delta_1 - \delta_2)^2 \qquad \text{(eq. 4.5)}$$

ΔH_M can only be slightly positive if the solubility parameters δ, and thus the properties of the solvent and the polymer, are similar. One problem with this method is the empirical determination of the solubility parameter and that no intermolecular interactions are included.[108] Due to this assumption, polymers are considered to be in low concentrations in various solvents.

As part of this work, the solubility was assessed using a simple laboratory test and was repeated three times as a standard for each sample. The standard solvents were used as testing solvents. For the sake of clarity, the solubilities have been grouped into three groups in Table 4.2:

- Soluble: when 1 mg per mg is dissolvable
- Insoluble: when < 0.1 mg per mL is dissolvable
- Swelling: when gelation is observed

Table 4.2 Solubility overview of monomers and polymers

Solvent	Monomers	POx-EDOT	PtOx	PtOzi	PAtOx	PAtOzi
H_2O	X	X	X	S	-	S
Acetone	X	X	X	S*	X	-
Ether	L	X	X	X	X	X
Chloroform	L*	X	X	L	L	L
Dichloromethane	L*	X	X	L	-	-
Acetonitrile	L	L*	X	L	L*	L
Toluene	L	X	X	L*	-	-
Benzonitrile	L	L*	X	L	L	L
Hexafluoro isopropanol	L	L	L	L	L	L
EtOH/MeOH	X	X	X	S*	-	-
DMSO	-	L	X	L	L	L

X = not soluble, L = highly soluble, S = swelling, S* = the swelling is temperature relevant, L* = poor solubility

While the monomers showed good solubility in most common solvents, the solubility of the polymer was structure dependent. End-group-functionalized POx-EDOT showed insolubility after prolonged polymerisation although it was dispersed in nitrile solvents. Among the homopolymers, the

monosubstituted PThOzi showed the best solubility and, therefore, the best handling. Furthermore, PThOzi also showed swelling properties in water. A temperature-relevant solubility behaviour was observed in alcohols. PThOzi was virtually insoluble in cold alcohols but showed a solubility/swelling property at elevated temperatures. The same could be observed for acetone. All polymers showed good solubility in HFIP, but due to the high toxicity of this solvent, this was only used for analysis (GPC, Maldi-TOF).

In the case of aliphatic POx and POzi, the solubility depends on the length of the side chain.[23] Short-chain side groups show a hydrophilic character while long-chain groups have a hydrophobic character. A temperature dependency is also known for these polymers. This makes it possible to produce hydrogels[247] or micelles[240] in a targeted manner by copolymerisation. A certain solubility in water is particularly advantageous during purification, since dialysis can thus be carried out in the aqueous phase. This is not possible with the thiophene-based polymers. Here, purification must take place either via precipitation or dialysis in organic solvents. For thiophene-based POx and POzi, no general trend could be determined. Only the number of carbon atoms was found to have an influence on the solubility, but without following a rule. The behavior in water and alcohols of the thiophene-based POx and POzi is of great interest. This would make it possible to develop hydrogels easily and without the use of additives or through copolymerisation. In contrast, hydrogels can be developed from aliphatic POx and POzi only via copolymerisation.[248]

4.3.3 Swelling properties of P2Th3Ozi

Since aqueous swelling can occur in biological environments, this initially anecdotal behaviour seen in thiophene-based POx and POzi was investigated further using P2Th3Ozi. The results are shown in Figure 4.12. It can be seen that the swelling increases faster at higher temperatures (37 °C). Especially in the first few hours of swelling, a sharp increase can be observed. A maximum weight increase of approximately 11.5 ± 0.96 % was measured after 48 hours. A similar total increase in weight could be measured at room temperature after 48 hours. Swelling at 4 °C limited the degree of swelling over 48 hours to 6.75 ± 0.55 %. It can be seen that the swelling capacity was reduced by approximately 40% in a cold environment. Due to the lower temperatures, the system has less energy according to the law of free enthalpy and consequently the freedom of rotation is restricted.

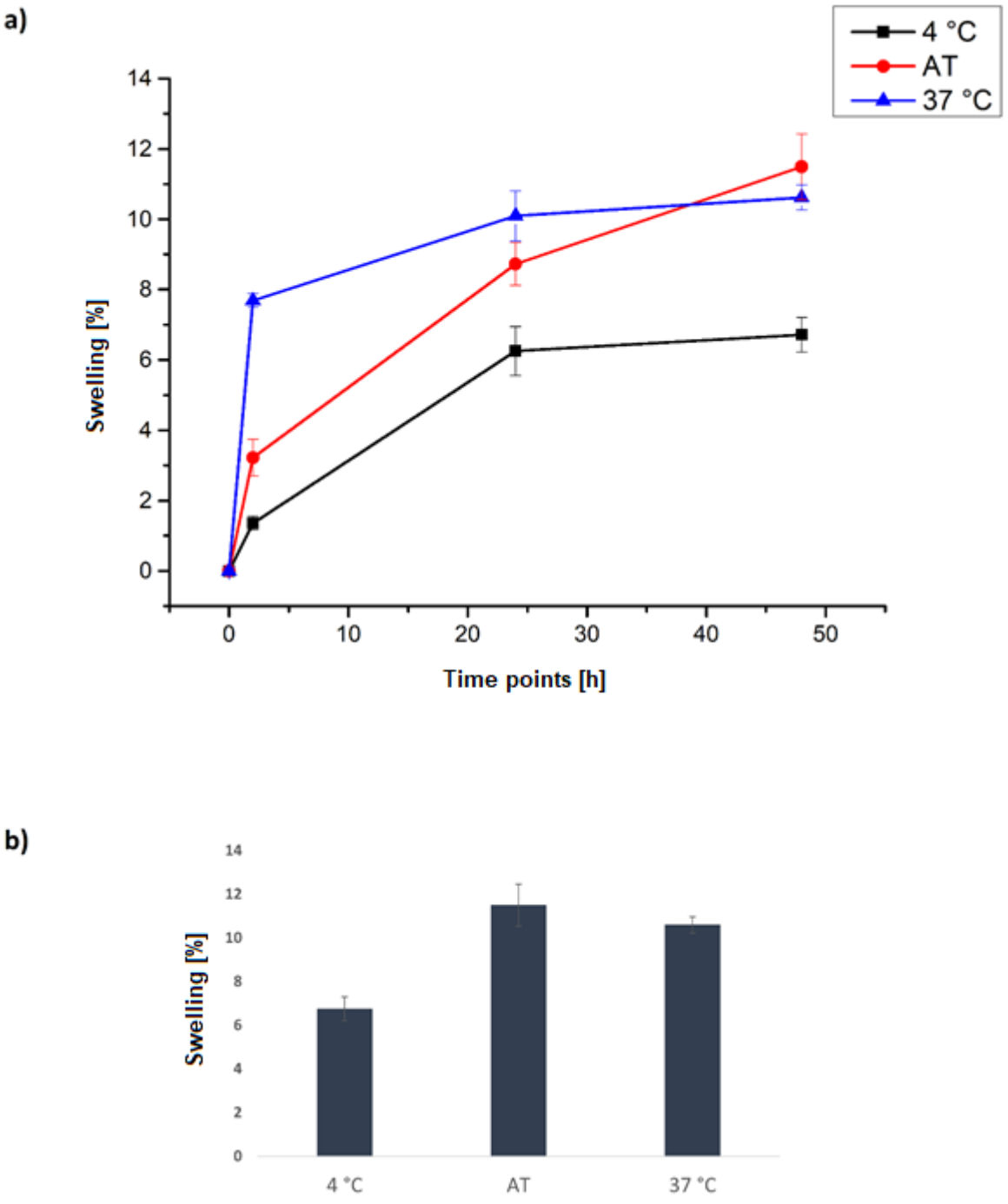


Figure 4.12 Swelling properties of P2Th3Ozi a) swelling vs time, b) swelling vs temperature. The swelling of P2Th3Ozi depends on the temperature of water and most of the swelling was done in the first 10 hours

Biological tissue is soft and has a water content of more than 70%.[249] In contrast, conventional electrically conductive materials such as metals or CPs are generally very hard. The use of hydrogels can fill this gap and hence are of interest for tissue engineering applications. Lu et al.[249] were able to produce hydrogels based on PEDOT:PSS. The authors treated PEDOT:PSS with DMSO. This made it possible to reduce the Young's modulus to 2 MPa while maintaining an electrical conductivity of 20-30 S/cm due to intermolecular connections. This treatment allowed a swelling of up to 20 wt % of the pure PEDOT:PSS. Hydrogels based on POx are currently of great interest.[247] Segiet et al.[250] investigated

the hydrogel behavior of simple aliphatic POx and found swelling of up to 15 wt % under suitable conditions. P2Th3Ozi showed more than 10 % wt. This is comparable to other hydrogels based on POx.[248] The percentage water content of PEDOT:PSS hydrogel systems could not be reached. However, hydrogels based on P2Th3Ozi do not require any additives and production is relatively easy compared to PEDOT:PSS and POx hydrogels.

4.3.4 Mechanical properties of P2Th3Ozi

Even if conductive polymers achieve high electrical conductivity, they are usually stiff and fragile. The average modulus is between 20 and 100 MPa. However, its use as an electroactive material for wider biomedical applications requires softer and, at the same time, more flexible properties. Tensile testing was performed with P2Th3Ozi bulk samples.

From a macroscopic point of view, the material showed a high degree of brittleness when dry and under normal handling. However, the mechanical properties could be significantly changed by treatment with water and a plastic behaviour could be observed (Figure 4.13). Strain vs. stress curves obtained from tensile tests were used to calculate a Young's modulus of 54.6 ± 6.7 MPa and elongation at failure of 112 % for dry and untreated P2Th3Ozi polymer. This is in alignment with the Young's modulus of PetOx (50.5 ± 16.9 MPa).[251] For P2Th3Ozi treated with water, a Young's modulus of 26.3 ± 3.8 MPa and an elongation at failure of 121 % was found. While the Young's modulus could be almost halved, the elongation at failure only increased by about 10% when treating with water. The Young's modulus of treated P2Th3Ozi is in the range of PU/PEDOT:PSS 15-20 wt% produced by Cuttaz et al.[153] However, the elongation at failure of 200-300% of PU/PEDOT: PSS could not be achieved. Furthermore, Lu et al.[249] achieved a Young's modulus between 2-10 MPa for PEDOT: PSS hydrogels with the treatment of DMSO, which is almost 3-fold lower than treated P2Th3Ozi. However, the advantage of P2Th3Ozi is that no additives were required in the manufacture of the hydrogel and values of the same order of magnitude could be achieved.

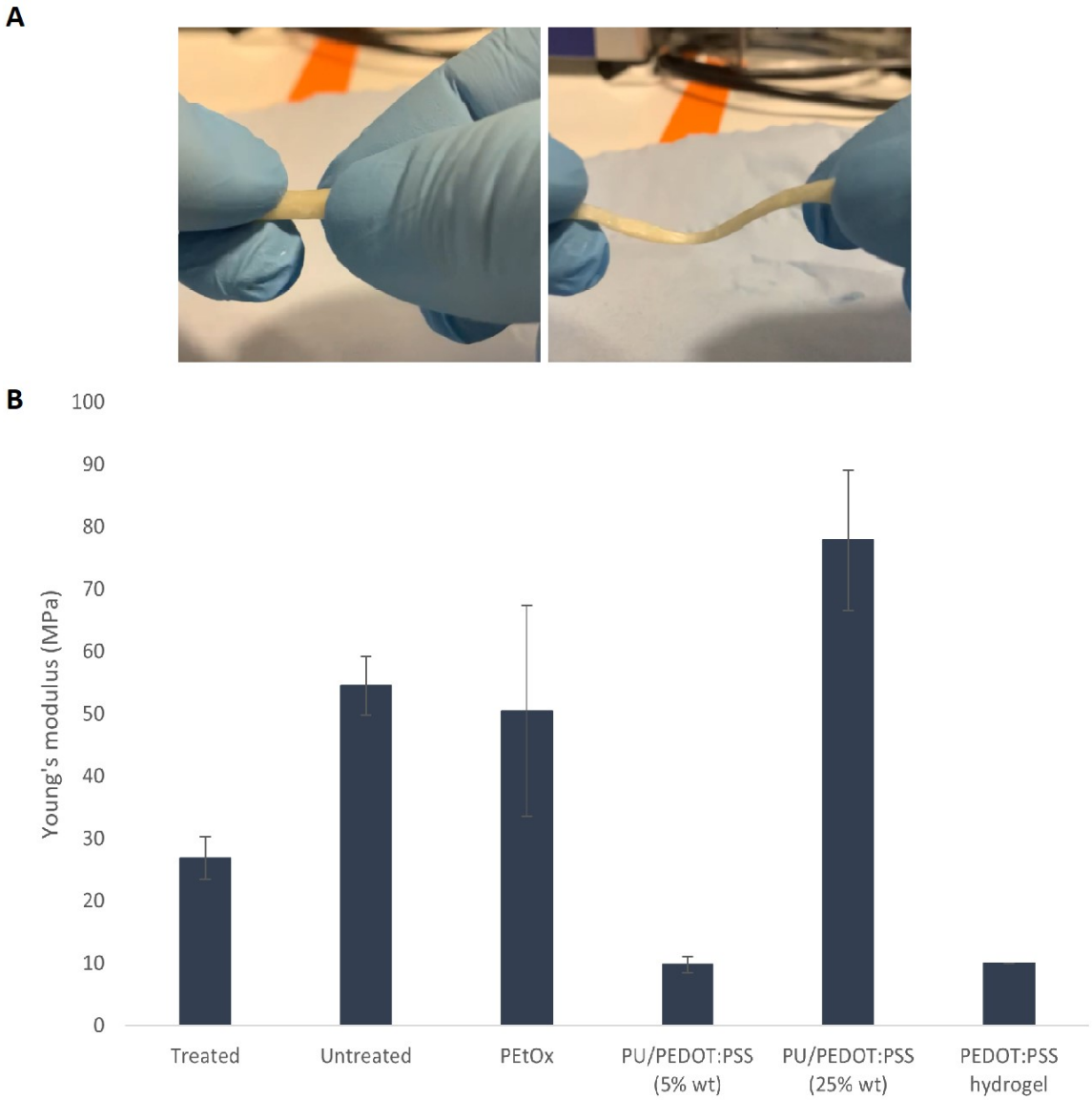


Figure 4.13: Mechanical properties of P2Th3Ozi. a) macroscopic view of mechanical properties of treated (H_2O) P2Th3Ozi, b) Youngs modulus of (un)treated P2Th3Ozi (n≥6). Literature values are used for PEtOx, PEDOT:PSS hydrogel produced by Lu et al. *and PU/PEDOT:SS produced by Cuttaz* et al.

4.3.5 Electrical properties of P2Th3Ozi

Several CPs have been investigated for applications in the biomedical field. Due to their chemical and electrochemical stability, polythiophenes and PPy are preferred. Due to the well-varied physical properties of thiophene-based POx and POzi described above, these polymers are a possible alternative to conventional CP systems. For this purpose, the basic electrochemical properties of P2Th3Ozi were examined.

It was proposed that the electrical conductivity of P2Th3Ozi can be realised by adding a dopant, since the thiophene rings of the side group are in close proximity to each other and thus electron hopping may theoretically be possible. It is known that electrical conductivity for CPs occurs when there is a continuous conjugated backbone present. As shown in Figure 4.14, there are two options for conjugated chain development in these polymers. Independent polymer chains can be connected through

intermolecular crosslinking (Figure 4.14 (1)), or alternately individual thiophene side groups of a single polymer chain can be linked to create intramolecular linking (Figure 4.14 (2)). The introduction of EDOT monomers in a time-separated reaction, was also investigated to determine whether additional conjugated units were required to impart conductivity to the P2Th3Ozi.

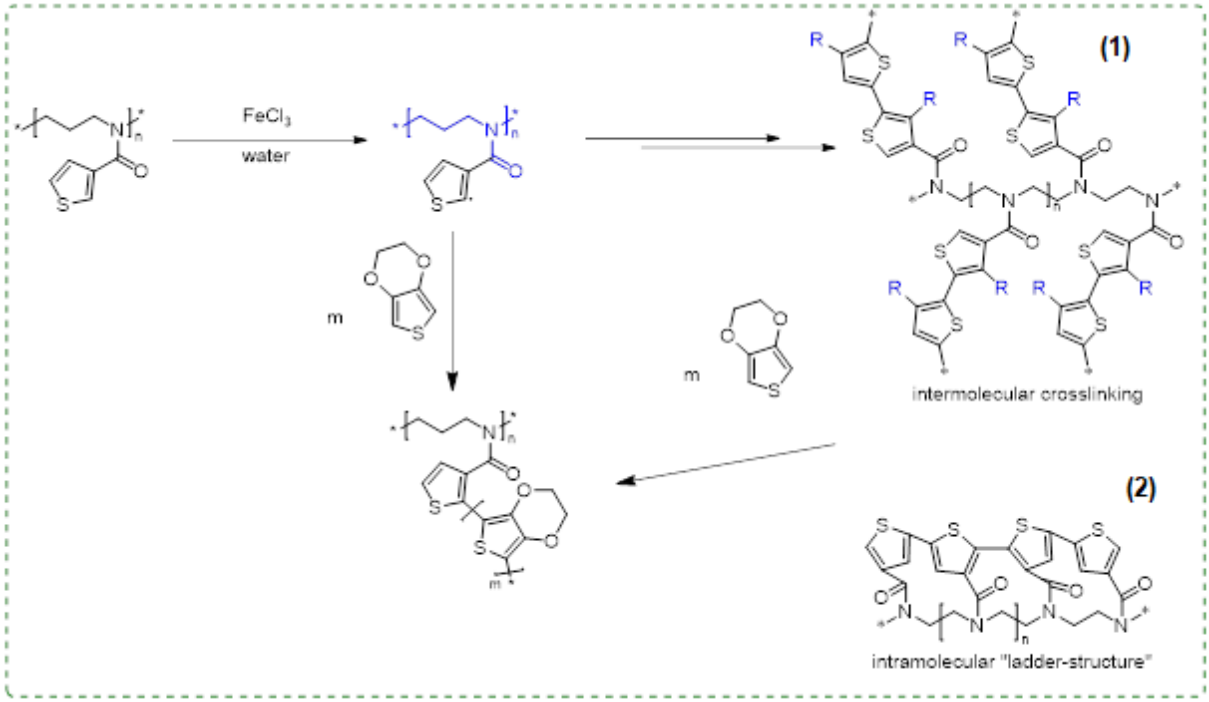


Figure 4.14 Post-modification of polythiophene oxazines can lead to two different transition structures (1. intermolecular crosslinking, 2. Intramolecular crosslinking)

Polymer chains must be arranged at the smallest possible distance from one another to enable electrical conductivity. To initially investigate chain packing, the starting polymers were analysed using dynamic light scattering (DLS). Figure 4.15 summarises the measurement data. Polymers with a theoretical chain length of approx. 25 repeating units were used for the measurement. Because of their insolubility, P2Th3Ox and P2Th2Ox could not be investigated using DLS. P2At2Ozi also absorbed the laser light instead of scattering and was not able to be analysed. None of the polymers showed an angle dependence. The values of Figure 4.15 are the average of all angles. The hydrodynamic radius is generally below 3 nm for all thiophene-based POx and POzi. The smallest radius was measured for P2Th2Ozi to be 1.79 ± 0.03 nm. A similar radius could be measured for P2Th3Ozi (1.94 ± 0.07 nm) and P2At3Ozi (2.00 ± 0.08 nm). P2At2Ox had a slightly larger Stokes radius of 2.11 ± 0.27 nm. With 2.93 ± 0.26 nm, P2At3Ox had a radius 1.5 times that of the analogous POzi. Therefore, intramolecular hopping should be possible because the dynamic radii of neighbouring thiophene rings are only separated by only a few nanometres (approximately 2-5nm). Some trends can also be identified, which follows the knot-building theory. P2Th2Ozi and P2Th3Ozi show a smaller radius than P2At2Ox and P2At3Ox. This could be explained by the larger number of carbon atoms in the side chain. A carbon atom in the backbone improves the freedom of rotation and thus better knot formation. In addition, the β-substituted thiophene rings show

a larger radius than the α-substituted due to the orientation of the sulphur atom and therefore a better packing of the chain is achieved. A reverse analogue trend was observed for the mass diffusivity. While P2Th2Ozi showed the highest mass diffusivity of (2.28 ± 0.03)*10^{-6} m²/s, P2At3Ox showed almost a 2-fold decline of (1.40 ± 0.11)*10^{-6} m²/s. It should be mentioned again that these are hydrodynamic radius in solution. Thus, this series of measurements only serves as an estimate for theoretical conductivity as they will differ from the solids that can be produced in a melt.

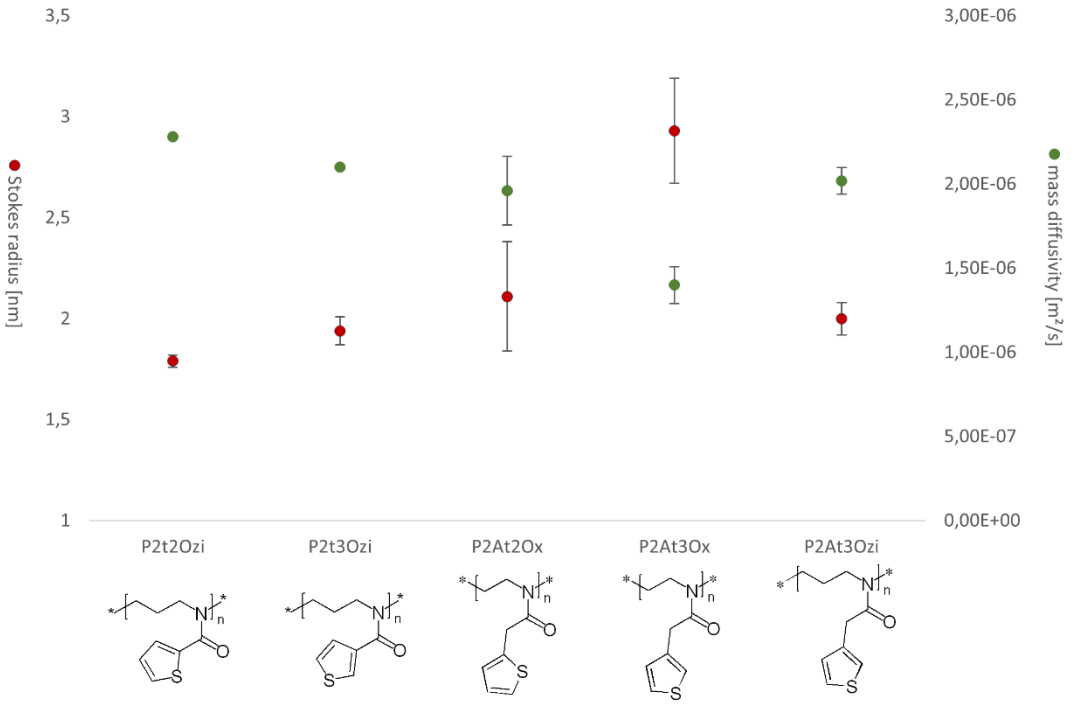


*Figure 4.15: DLS measurment of Stokes radius and mass diffusion of thiophene-based POx and POzi (n=8) show a stokes radius between 1,5 and 2 nm and mass diffusivity of ~2*10^{-6}m²/s*

Conductivity was measured via a 4-point probe (Figure 4.16 a). For this purpose, P2Th3Ozi polymers with a chain length of 25 and 50 were synthesized and further chemically oxidised as described above. Ferric chloride was used as dopant. While no electrical conductivity could be measured with undoped P2Th3Ozi, a maximum electrical conductivity of 1.05 ± 0.8*10^{-5} S cm^{-1} was measured for doped P2Th3Ozi, the conductivity increased by more than 2-fold by adding EDOT 2.61 ± 0.8*10^{-4} S cm^{-1}. The successful reaction could be detected by UV-VIS spectroscopy (Figure 4.16 b). For this purpose, the polymers were dissolved in chloroform and measured at a concentration of 3 mg/mL. The verification was based on visualization of the characteristic blue coloration of the sample. The chemical oxidation shifts the absorption in the longer-wave range (297 nm → 318 nm) due to a longer conjugated system and thus minimized the excitation energy (π-π*). Khan et al.[252] observed similar behaviour for other thiophene-based systems, when polymerising thiophene[2]rotaxane with nitrosium hexafluorophosphate as oxidant. Due to the more complex system, the absorption is at longer

wavelengths. However, the authors were able to observe an analogous shift in the absorption maximum of approx. 60 nm.

Due to the many washing steps, it can be assumed that a chemical or mechanical bond has formed between P2Th3Ozi and PEDOT. A more precise analysis is not possible due to the chemical similarity. Future research can investigate the type of bond more precisely through polarity experiments. While optimized PEDOT/PSS systems can now achieve an electrical conductivity of several hundred S/cm,[253] Gonzales et al. showed conductivity of polythiophene-derivate cellulose composites with a conductivity between 10^{-4} to 10^{-7} S cm^{-1}. Chemically modified PEDOT from Person et al.[254] are in the range of 0.03 - 0.12 S cm^{-1}. Other chemical polythiophenes also showed similar conductivity with $FeCl_3$ as dopant.[255] As chloride is not an optimal dopant, future work will focus on the introduction of other dopants. It should be noted that the electrical conductivity of tissue is in the range of 0.03 and 0.6 S cm^{-1} and therefore a conductivity in the same range will be considered acceptable.[256]

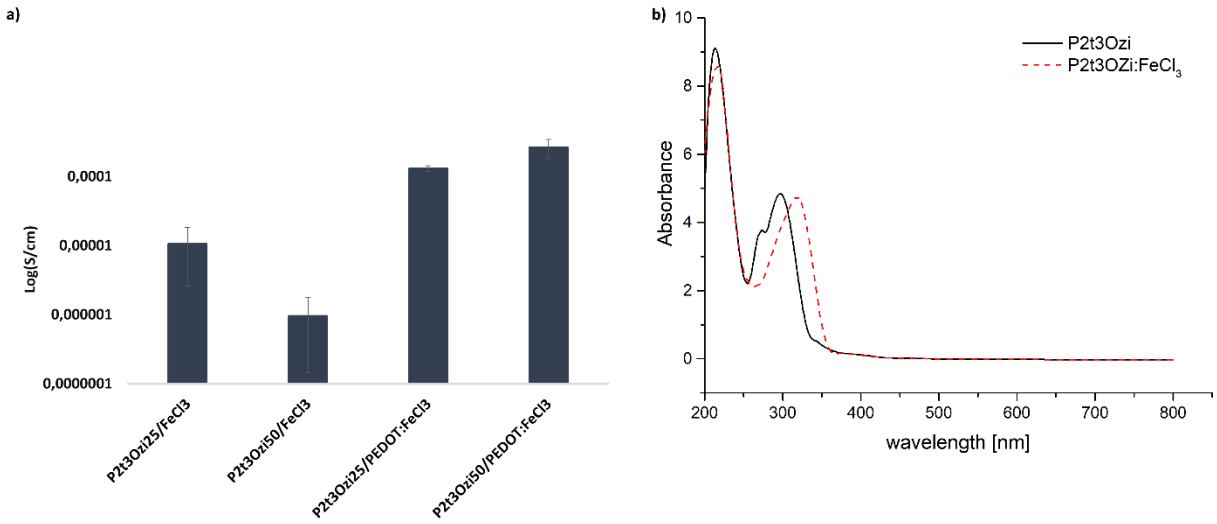


Figure 4.16 a) Conductivity values of P2Th3Ozi + FeCl3, b) UV-VIS spectrum of P2Th3Ozi + FeCl3 shows a shift between pure polymer and polymer/$FeCl_3$

In summary, it can be said that the side group and the backbone have a direct influence on the polymerisability of the individual monomers. It was found that the polymerisation by an additional carbon atom in the backbone (Ozi vs Ox) caused a fundamental improvement of the polymerisation. This is due to the hydrophilic vs hydrophobic character of the individual polymer parts (backbone vs side-group). However, no improvement could be observed by adding another carbon atom between the thiophene ring and the backbone, which enables a degree of freedom, but leads to a different macroscopic formation, and has a direct influence on the material properties such as conductivity, solubility or mechanical flexibility. However, this could be useful for the further polymerisation of the thiophene group to enable an improvement in the macroscopic network (intramolecular network vs intermolecular network). With a larger macroscopic network, the system would increase conductivity, but the solubility would be directly affected and possibly worsened. In summary, it can be said that

certain properties are influenced by modifying the individual molecular parts, but solubility is usually in contrast to electrical conductivity.

4.4 Conclusion

This chapter investigated the ability for novel ThOx and ThOz monomers to be polymerised, and their subsequent material properties. While the introduction of a functional thiophene-based group was successfully implemented, the yield and further processing was only possible to a limited extent. All monomers could be polymerized and, the monosubstituted thiophene-based Ox and Ozi monomers produced a quantitative yield and could also be stored for a long time under ambient conditions. The acetopthiophene-based monomers, however, could not be stabilized over a longer period of time. In summary, it could be shown that the polymerisation follows the generally good polymerisation properties of POx and POzi.

Furthermore, the physiochemical properties of the polymer class could be examined in detail in order to offer a broad platform for further processing options. PThOzi showed the best solubility of this class of novel polymers and was dissolved in a variety of solvents. The solubility in chloroform is an advantage here, as this ensures good further processing. The glass transition temperature was also investigated. In contrast to standard conductive polymers in the biomedical field, those polymers have a T_g below 60 °C. This demonstrates the potential usage of those materials in fabrication processes based on material melting. In addition, a specific control of the glass temperature could be demonstrated by copolymerisation and the use of the Fox equation. The polymers are also thermally stable and thus form a good platform for MEW 3D printing.

4.5 Experimental Section

Two different approaches were chosen to realise electrically active polymers based on POx and POzi. Firstly, it was investigated whether end group-functionalisation of aliphatic POx is possible. For this purpose, initiators or termination reagents were synthesised on the basis of EDOT and in a second reaction it was investigated whether a polymerisation of aliphatic POx is possible using these reagents. As a second approach, the monomers introduced in the previous chapter were examined for their polymerisation ability. These were to be oxidatively polymerised in a second reaction with further EDOT using ferric chloride.

4.5.1 Materials

For inert conditions during synthesis, all reactions and cleaning procedures were performed using either a standard Schlenk System or a glovebox (LabMaster 130, Mbrazn, Garching, Germany) under inert atmosphere of dry, oxygen-free argon. The water impurity of the glovebox was detected and had an average of less than 5 ppm. All commercially available chemicals were purchased by Sigma Aldrich or Acros Organics and used without further purification unless otherwise described. Toluene was dried for 72 hours over molecular sieves (4 Å). 2-Ethyl-2-oxazoline, benzonitrile, Methyl-2-2oxazoline were dried by refluxing over CaH_2 and distilled afterwards prior use. $FeCl_3$ was dried under vacuum at 50 °C for 24 h prior use. If not stated different, all reactions and work-up procedures were performed under inert conditions (water-free argon atmosphere using a $CaCl_2$ filter).

4.5.2 Polymer synthesis and end-group functionalisation

Synthesis of EDOT-tosylate as an initiator for CROP polymerisation of POx or POzi[234]

The synthesis was performed following the general synthesis procedure by Skompska et al.[234]. Paratoluensulfonyl chloride (442.3 mg, 2.32 mmol, 2 eq) was added to a solution of hydroxymethyl-EDOT (200 mg, 1.16 mmol, 1 eq) in 3 mL pyridine in a round flask at 0 °C. The mixture was stirred at 0 °C for 24 hours. By dilution with 10 mL of water, the resulting solution was extracted three times with 20 mL of ether. The combined organic extractions were dried above $NaHCo_3$ and the organic solvent was evaporated.

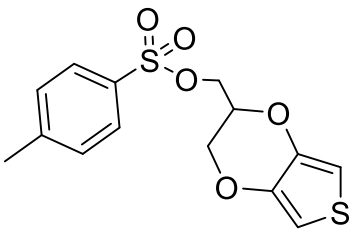


Figure 4.17 EDOT-tosylate

Polymerisation of PEtOx initiated with EDOT-TOs

EtOx (1 g, 111.8 mmol, 30 eq) dissolved in 2.5 ml dry benzonitrile in a Schlenk flask under dry and inert conditions. EDOT-TOS (127.8 mg, 0.39 mmol, 1 eq) was added and stirred for 7 hours at 130 °C. The mixture was allowed to cool down (50 °C) and the termination was carried out by adding a methanolic saturated NaOH-solution and stirring was continued at 50 °C for another 12 hours. After cooling down to room temperature, the mixture was precipitated in cold diethyl ether (volume was 15 times of polymer solution). The polymer was resolved in chloroform and the precipitation procedure was repeated at least 3 times. Afterwards, the organic solvent was removed, and the polymer was dried under vacuum for approx. 24 hours.

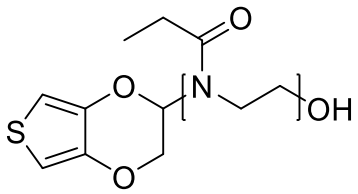


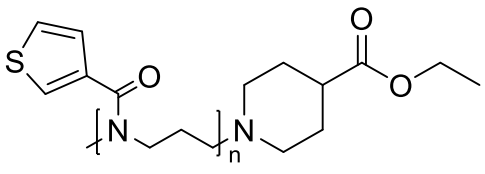
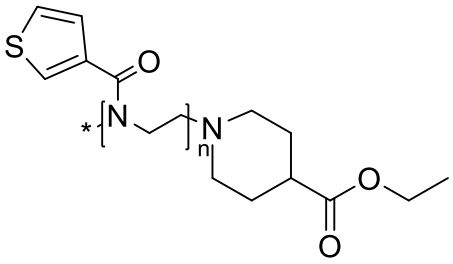
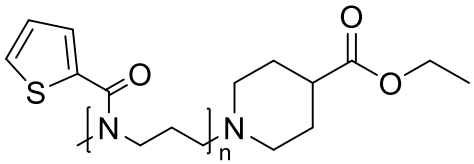
Figure 4.18 EDOT-P(EtOx)-OH

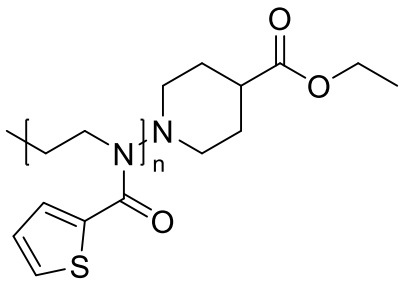
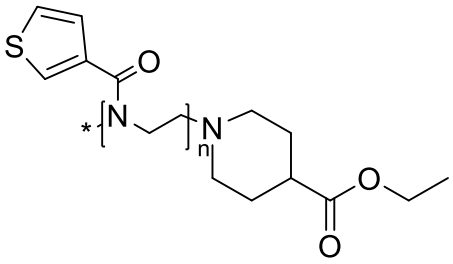
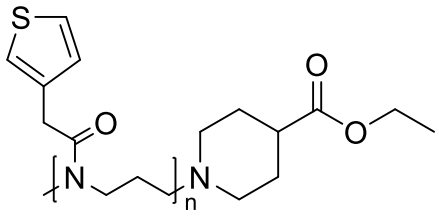
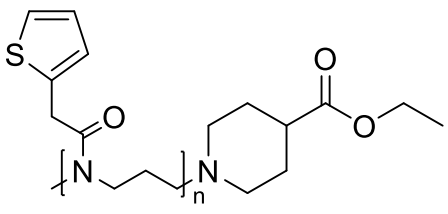
Polymerisation of thiophene-based monomers

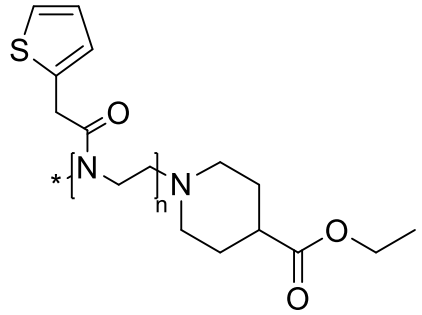
The polymerisation of the thiophene-based monomers, which were prepared in the previous chapter, was carried out according to the following general polymerisation procedure. In a two-neck flask, the respective polymer was dissolved in dry benzontrile under inert conditions. Then methyl triflate was added as initiator and stirred at 130 °C for 3-5 hours. After the reaction mixture was cooled to 50 °C, ethyl isonipecotate was added for termination and stirring continued at room temperature for at least 12 h. The exact quantities for the individual polymerisations are given in Table 4.3. For purification, the cooled reaction mixture was precipitated in at least four times the amount of cold diethyl ether and then centrifuged. The solvent was decanted and the precipitated polymer was dissolved in a maximum of 25 mL chloroform. The reaction mixture was then precipitated again in four times the amount of ice-cold ether. This purification step was repeated at least four times. As a final step, the polymer obtained was dried for at least 72 h under vacuum at room temperature. Synthesis presented within was confirmed using at least 5 replicates for each synthesis strategy and a minimum of 10 repetitions for the key products.

Table 4.3 Polymerisation quantities of thiophene-based monomers

Name	**Structure**	**composition of synthesis**

poly(2-thiophene-3-oxazine)		2-thiophene-3-oxazine (15.0 g, 0.09 mol, 25 eq) 3-Methyl triflate (0.59 g, 3.59 mmol, 1 eq) ethyl isonipecotate (1.69 g, 10.8 mmol, 3 eq) 45 mL benzontrile
poly(2-thiophene-3-oxazoline)		2-thiophene-3-oxazoline (10.0 g, 0.06 mol, 25 eq) 3-Methyl triflate (0.43 g, 2.61 mmol, 1 eq) ethyl isonipecotate (1.23 g, 7.84 mmol, 3 eq) 30 mL benzontrile
poly(2-thiophene-2-oxazine)		2-thiophene-2-oxazine (15.0 g, 0.09 mol, 25 eq) 3-Methyl triflate (0.59 g, 3.59 mmol, 1 eq) ethyl isonipecotate (1.69 g, 10.8 mmol, 3 eq) 45 mL benzontrile

poly(2-thiophene-2-oxazoline)		2-thiophene-2-oxazoline (10.0 g, 0.06 mol, 25 eq) 3-Methyl triflate (0.43 g, 2.61 mmol, 1 eq) ethyl isonipecotate (1.23 g, 7.84 mmol, 3 eq) 30 mL benzontrile
poly(2-acetothiophene-3-oxazoline)		2-thiophene-3-oxazoline (10.0 g, 0.06 mol, 25 eq) 3-Methyl triflate (0.39 g, 2.39 mmol, 1 eq) ethyl isonipecotate (1.13 g, 7.18 mmol, 3 eq) 30 mL benzontrile
poly(2-acetothiophene-3-oxazine)		2-thiophene-3-oxazine (10.0 g, 0.06 mol, 25 eq) 3-Methyl triflate (0.36 g, 2.21 mmol, 1 eq) ethyl isonipecotate (1.04 g, 6.63 mmol, 3 eq) 30 mL benzontrile
poly(2-acetothiophene-2-oxazine)		2-thiophene-2-oxazine (10.0 g, 0.06 mol, 25 eq) 3-Methyl triflate (0.36 g, 2.21 mmol, 1 eq)

		ethyl isonipecotate (1.04 g, 6.63 mmol, 3 eq) 30 mL benzontrile
poly(2-acetothiophene-2-oxazoline)		2-thiophene-2-oxazoline (10.0 g, 0.06 mol, 25 eq) 3-Methyl triflate (0.39 g, 2.39 mmol, 1 eq) ethyl isonipecotate (1.13 g, 7.18 mmol, 3 eq) 30 mL benzontrile

Oxidative polymerisation to improve conductivity of P2t3Ozi$_{15}$ and additional EDOT using iron chloride

P2Th3Ozi$_{15}$ (M = 2.5 kg/mol, 3.00 g, 1.19*10^{-3} g/mol, 1 eq) was placed in a beaker with a stirrer. 30 mL of water was added. $FeCl_3$ (0.58 g, 3.57*10^{-3} g/mol, 3 eq) was added. The solution was stirred at least 24 hours. The water was removed by filtration. The filtrate was washed several times with water and hexane. After purification, the filtrate was tried under vacuum for 48 hours. Afterwards, 3 – 5 droplets of pure EDOT were added and allowed to react for 15 – 30 minutes. The purification steps were repeated at least three times. A darkish blue product was obtained. After drying, the polymers were cast as round plates with a thickness of 1 mm.

4.5.3 Characterisation and Analysis

Nuclear Magnetic Resonance (NMR) Spectroscopy

For detailed description, see Chapter 3.5.

In order to make an initial statement on the kinetics during polymerisation, the monomer concentration was measured over time using NMR spectroscopy. For this purpose, the respective monomer was placed in benzonitrile in a Schlenk flask and MeOTf was used as the initiator. A first sample was taken at t = 0 min and was used as the starting concentration (A_0) of the monomer. The reaction was heated to 130 °C with measurements taken every 30 minutes and evaluated directly with NMR spectroscopy. With the assumption of a living polymerisation, the concentration of the active species A* can be set equal to the initiator concentration. As a result, the reaction order can be viewed as a pseudo-first-order and equation

4.6 applies to the change in the monomer concentration over time.[95] If this equation is integrated (Eq. 4.7), a linear dependence is obtained under ideal conditions, with the slope of the straight line being the rate constant of the polymer k_p.

$$-\frac{d[A_0]}{dt} = k_p[I_o][A_t] \quad \text{(eq. 4.6)}$$

$$ln\frac{[A_0]}{[A_t]} = k_p[I_o]t \quad \text{(eq. 4.7)}$$

Infrared (IR) Spectroscopy

For detailed description, see Chapter 3.5

Matrix-Assisted Laser Desorption/Ionization Time-of-Flight Mass spectrometry (MALDI-TOF)

Matrix assisted laser desorption ionization (MALDI) is a variant of mass spectrometry. The sample is first fixed in a carrier matrix and then bombarded with a pulsed laser. Here, molecules are released from the sample as gases (desorption) and ions are formed with the release of protons. These are then determined based on the flight time (TOF). The acceleration voltages are between 10 - 30 kV. The Maldi-TOF was performed on a Autoflex II LRF (Bruker, Mannheim, Germany). The matrix was DCTB. The polymers were dissolved in acetonitrile or HFPIP with a concentration of 1g/L. The matrix solution was 20 g/L.

Small Angle Neutron/X-Ray Scattering (SANS/SAXS)

Analogous to the crystal structure analysis in the previous chapter, the polymer were examined by X-Ray analysis. Therefore, the following applies:

$$q = \frac{4\pi}{\lambda}\sin\frac{\theta}{2} \quad \text{(eq. 4.8)}$$

The light used has a wavelength in the Angstrom range, which has the same order of magnitude as intermolecular bonds. If a small angle is used at the same time, the scatter vector q obtained is also very small and this enables larger structures to be examined.

Dynamic Light Scattering (DLS)

The term light scattering means the scattering of irradiated light by a scatter center, e.g. by a dissolved particle, molecule or polymer.[257] The irradiated electromagnetic wave hits the electron shell of the scattering center and shifts this, thereby polarizing the scattering center and changing its dipole moment. the electromagnetic wave induces a Hertz dipole, which in turn is a source of electromagnetic radiation

(scattered radiation or secondary radiation). This radiation is detected and allows conclusions to be drawn about thermodynamic parameters such as the second Virial coefficients, the hydrodynamic radius, the diffusion coefficient, and the radius of gyration of the diffuser and the molecular weight of the diffuser.

A distinction is made between static and dynamic light scattering. In the case of dissolved particles, the Brownian molecular motion to a temporal change in the locations of the Scattering centers. As a result, there is a temporal dependence of the interparticle Interference and thus also the measured scattering intensity at a given angle (Figure 4.19). In the static light scattering, these fluctuations for each measurement angle over the Averaged observation period. However, this is only possible with very dilute solutions low interparticle interactions, since only statistical effects here appear. With dynamic light scattering, the measured scattering intensities are in dependent on the observation period considered.

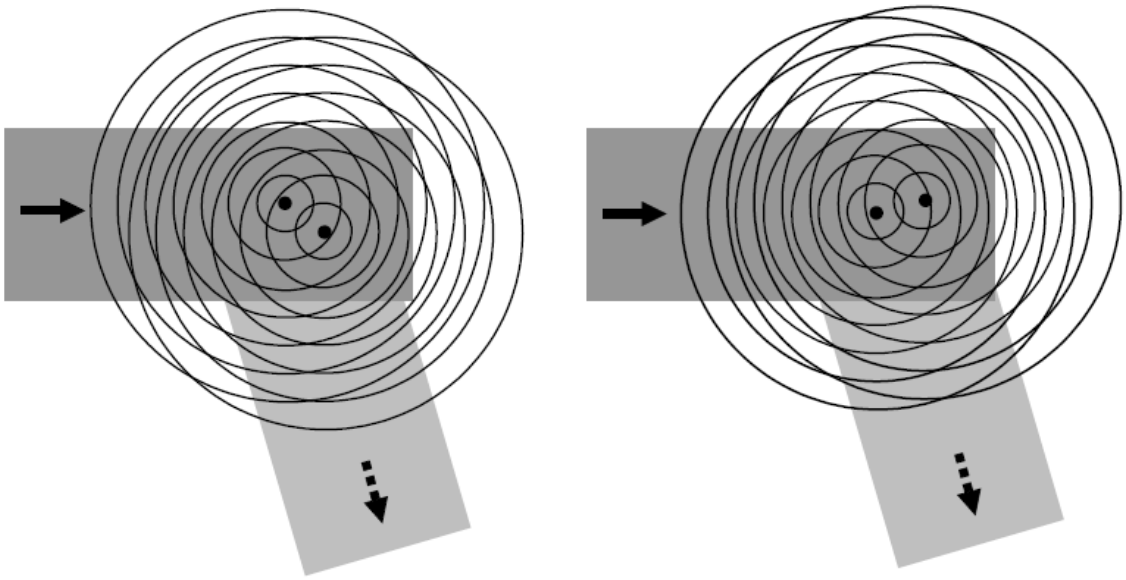


Figure 4.19 Temporal dependence of the interparticle Interference

DLS was performed with a HeNe laser (22 mW, wavelength = 632.8 nm and a ALV-CGS-3 goniometer equipped with eight simultaneously working APD Avalanche photodiode fiber optical detectors. All samples were measured at a temperature of 25 °C and a concentration of 0.02 g/L. Before measurements, the samples were filtered by using a PTFE filter with a pore size of 0.2 µm. The MilliQ water was used for sample preparation. The standard solvent was toluene. Data was analysed by using HDRC – V6.3.1 software developed by O. Nirschl and kindly provided by Prof. Schmidt from Johannes-Guttenberg-University Mainz. A set of eight angles were measured (26 °, 42 °, 58 °, 74 °, 90 °, 106 °, 122 °, 138 °).

Gel Permeation Chromatography (GPC)

A polymer sample is fractionated using GPC based on the different sizes of the polymer chains and the molecular weight distribution can therefore be determined.[108] The main element here is the chromatography column. It was filled with spherical, highly cross-linked polystyrene and has a pore size of 10-10^5 nm. The polystyrene is referred to as the stationary phase and the continuously flowing solvent as the liquid phase.

An alternative name for GPC is size exclusive chromatography (SEC), because the polymer chains stay longer or shorter in the stationary phase due to their size (figure 4.20). Small molecules stay longer on the column due to the cross-linking and interaction and larger molecules are detected first. The detection takes place here by measuring the refractive index or UV absorption of the eluate. Therefore, GPC is not an absolute method and requires calibration with polymers with a narrow molecular weight distribution.

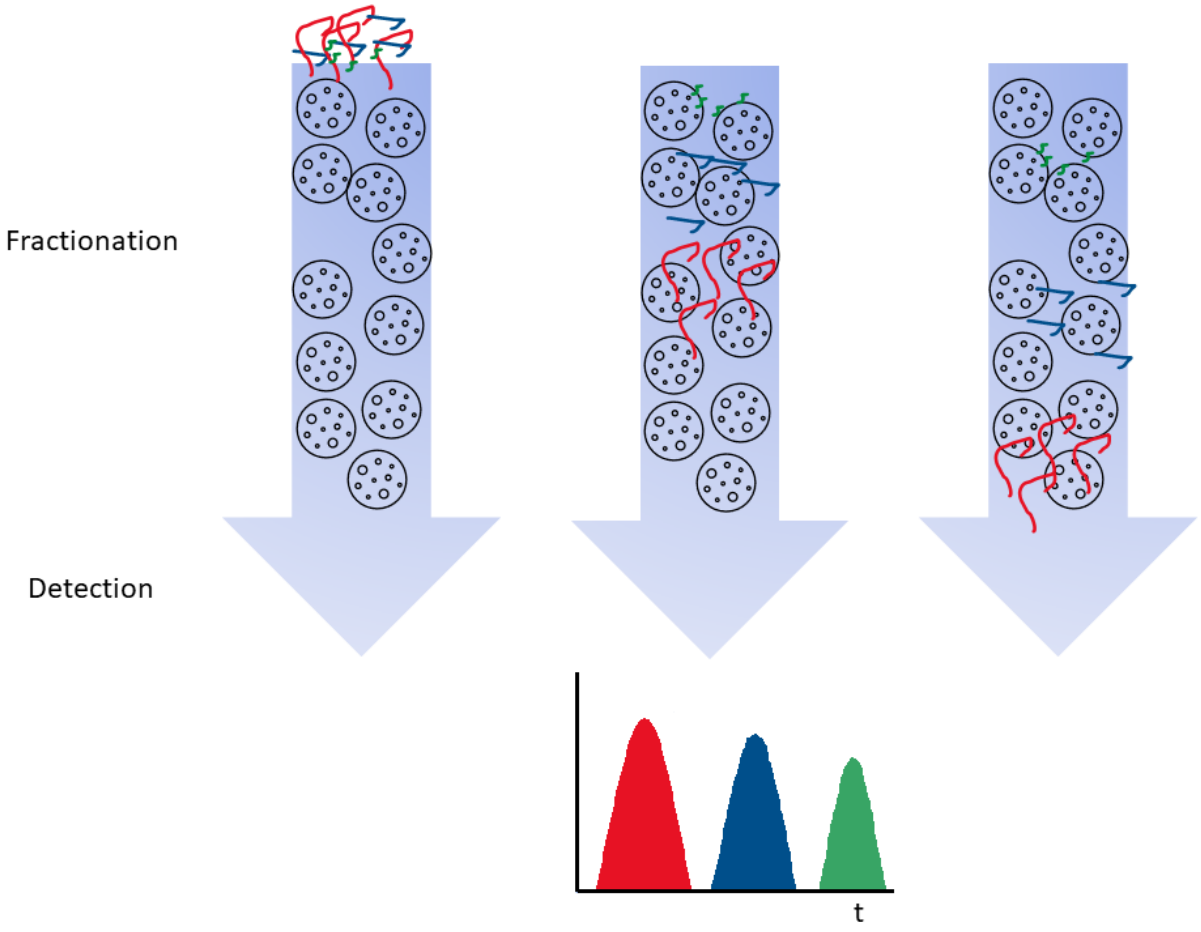


Figure 4.20 Seperation function of GPC measurement against time. Small polymer have a longer retention time than bigger polymers

The relative molar mass can be determined from the measured elution volume using an internal calibration curve. For this purpose, the log M is plotted against the retention time and elution volume

using a calibration curve . The individual molecular averages, such as number averages, weight average and Z-average can be determined- The ratio between the number average and the weight average gives the dispersity index.

GPC measurements were performed using different setups. DMF GPC was conducted on a Polymer Standard Service Security (PSS, Mainz, Germany) system (pump mod. 1260 infinity, MDS RI detector mod. 1260 infinity (Agilent Technologies, Santa Clara, California, USA), precolumn PSS GRAM 10 µm (50 x 8 mm), PSS GRAM 30 Å 10 µm (300 x 8 mm) and PSS GRAM 1000 Å 10 µm (300 x 8 mm)) at 313 K. DMF was supplemented with 1 g/L lithium bromide and the flow rate was adjusted to 1 mL/min. Prior to each measurement, the samples were filtered through a 0.2 µm Teflon filter (Thermo Scientific, Schwerte, Germany) to remove particles. The system was calibrated against PEG standards with molar masses ranging from 106 g/mol to 100 kg/mol. Data were processed using WinGPC Unichrom V.8.20 Build 5350 software.

HFIP GPC was performed on the same Polymer Standard Service Security (PSS, Mainz, Germany) system (pump mod. 1260 infinity, MDS RI detector mod. 1260 infinity (Agilent Technologies, Santa Clara, California, USA), precolumn PSS PFG linear M 7 µm (50 x 8 mm), PSS PFG linear M; 2 columns: 7 µm (300 x 8 mm)) at 313 K. HFIP was supplemented with 3 g/L potassium triflate and the flow rate was adjusted to 0.7 mL/min. Calibration was performed using PEG standards with molar masses ranging from 200 g/mol to 100 kg/mol. Sample preparation and evaluation was performed as described for the DMF GPC.

Thermogravimetric Analysis (TGA)

TGA is an analytical method for the thermal analysis of a sample.[108] The sample is placed in an aluminium oxide or platinum crucible and heated in a temperature-controlled oven. The sample holder is also a microbalance and can therefore detect the change in mass during heating. The heating can be divided into different phases. Here you can control the start and end temperature, heating rate, gas flow and intermediate temperatures. The aim of the TGA is to measure the decomposition temperatures or the detection of volatile components. In TGA, the change in mass is plotted against the temperature.

Thermogravimetric analysis of the polymers was performed on a *TG 209F1 IRIS* (*NETZSCH*, Selb, Germany). The samples (5 – 10 mg) were added to aluminium oxide crucibles (*NETZSCH*, Selb, Germany) and heated under synthetic air from 50 °C to 850 °C with a heating rate of 10 K/min while detecting the mass loss. The corresponding *NETZSCH Proteus – Thermal Analysis – V.5.2.1* software was used to evaluate the obtained spectra and OriginLab 9.0 was used for graphical illustration of the data.

Dynamic Scanning Calorimetry (DSC)

The DSC analysis is a thermal analysis to determine the amount of heat absorbed or emitted by a sample during a thermal process.[108] For this purpose, a sample with a sample amount between 5-20 mg is measured in an encapsulated aluminium oxide crucible against an equivalent empty crucible. Due to the heat capacity of a sample, thermodynamic processes lead to temperature differences between sample and reference and the different heat flows are measured. The parameters (temperature, heating rate, inert conditions) of the measurement can be set and controlled in the same way as the TGA. By integrating the $\Delta T\text{-}T_{ref}$ curve, the enthalpy change of the sample can be determined and the melting or glass transition temperature, degree of crystallisation, heat capacity or the decomposition point can be measured.

Differential scanning calorimetry (DSC) was performed on a DSC 204F1 Phoenix (NETZSCH, Selb, Germany) under N2-atmosphere (20.0 mL/min). The samples were placed in aluminium pans with crimped-on lids, cooled to -50 °C (10 K/min) and subsequently heated 200 °C (10 K/min). The samples were heated/cooled two additional times from -50 °C to 200 °C (10 K/min). Three cycles were performed. The second cycle was used for the evaluation, as possible fluctuations due to solvent contaminations or air humidity were minimized. Sample evaluation was performed as described for the TGA.

Conductivity studies

Previous work by Cuttaz et al.[153] was used as a guideline for the test specifications. Briefly, electrochemical characterisation was conducted using cyclic voltammetry (CV), electrochemical impedance spectroscopy (EIS) and probe based direct conductivity measurements. EIS and CV were performed under ambient atmospheric conditions using a conventional three-electrode cell construction. The counter electrode was made of platinum. The isolated reference electrode was a Ag/AgC electrode. Phosphate-buffered saline (PBS) was used as the electrolyte. EIS was examined with a sinusoidal voltage (amplitude 0.03 V_{RMS}) and a frequency range of 0.1 Hz – 10 kHz. CV was examined in a voltage range of -0.6 to 0.8 V and a scan rate of 0.15 V/s. 11 cycles were performed, with the last being used for numerical analysis. The charge storage capacity (CSC) was calculated by integrating the area under the current response with respect to time. The measurements were carried out on an AUTOLAB potentiostat-galvanostat (Multi Autolab/M101, Eco Chemie, Netherlands) and the associated software Nova 2.0. Area calculation of the CV was carried out using OriginLab 9.0.

Conductivity was assessed by either using a Jandel 4-point probe device (RM3000, Jandel Engineering Limited, Leighton Buzzard). Round testing plates were used. For the Jandel 4-point probe measurement, the probe spacing was 1 mm. The current was verified between 10 nA — 100 nA. According to Lu et al.[258] ,the conductivity was calculated using the following formula:

$$p = \frac{RA}{L} = \frac{1}{\sigma} \qquad \text{(eq. 4.9)}$$

p = Resistivity, L = probe spacing, A = cross-sectional area, R =two-point resistance, σ = conductivity

For two probe set-up, impedance output from EIS was extracted at 1 KHz while the slope of the resulting CV measurement was computed to derive the resistance and the resulting data were only used as confirmation of the obtained Janel 4-point measurements. Calculation was done by using the provided Formula of Jandel and using OrignLab 9.0 software. Results are reported as means over 4—6 series with 3 samples each and a minimum of five different locations as stated by Jandel and Bridge technology.

Swelling studies

The swelling studies were performed according to Begam et al.[259]. Briefly, the dynamic sweeling measurements were made by gravimetric measurements. The prepared samples (approx. weight of ~100 mg) were placed in petri dishes (100x20 mm) and suspended in 15 mL Milli-Q water at 4 °C, ambient temperature and 37 °C. The samples were removed at specific time intervals (2h, 24h, 48h) and residual surface water was removed using KIMTECH tissue. The samples were weighed on an VWR® LA 214 classic balances (accuracy ±0.0001 g). Swelling tests were conducted with 3 samples and minimum of 3 repeats each.

Fabrication of testing plates for Conductivity and swelling studies

The samples were prepared by melting the polymer material P2Th3Ozi into small plates (1 mm height, 5 mm diameter) using a silicone casting mould at an average temperature of 100 — 120 °C. To remove trapped air bottles, the plates were placed in a vacuum chamber in the melted state with a pressure of 10^{-3} mbar.

Mechanical behaviour

Mechanical behaviour was conducted by tensile testing using two independent Instron Universal test machines. The mechanical properties were tested for untreated P2Th3Ozi and treated by soaking in Milli-Q water at 4°C for 24h. The polymer strips were prepared according to ASTMD638. Using a casting mould, the test strips were prepared analogous to the fabrication of testing plates for conductivity and swelling studies. The dimensions were examined to have a length L_0 of 19 mm with a width of 5 mm and a thickness of 1 mm. This results in a tensile area of 95 mm². Tensile tests were conducted with a crosshead speed of 1 mm/min for untreated strips and 1-3 mm/min for treated strips. For each independent experiment, a minimum of five samples for each treatment were prepared according to the number of test specimens stated in ISO 527-1:2012.

UV-Vis-Spectroscopy

Ultraviolet and visual spectroscopy provide information about chemical compounds with conjugated systems.[216] The UV radiation is more energetic than visible light (the shorter the wavelength, the more energetic the radiation). Irradiation of the sample leads to excitation and thus to electron transitions. Excited electron transitions can be n $\rightarrow \pi^*$ and $\pi \rightarrow \pi^*$ (Fig 4.21). The Lambert-Beer law describes the quantitative relationship between the extinction of a sample, the concentration and the length of the light path. The following applies here, the longer a conjugate system is, the less energy (shift to longer wavelengths) it needs for excitation. In the UV-Vis spectrum, the absorption is plotted against the wavelength.

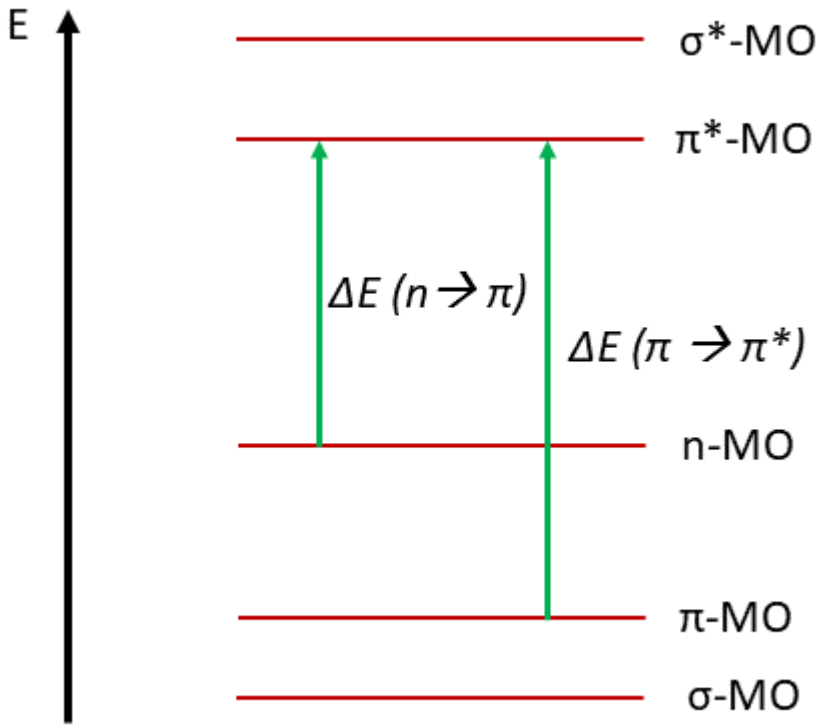


Figure 4.21 Energy level of MO and the excited states. Irradiation of the sample leads to excitation and thus to electron transitions. Excited electron transitions can be n $\rightarrow \pi^*$ and $\pi \rightarrow \pi^*$

Uv/Vis-Spectroscopy was measured at room temperature on Agilent Cary 500 UV-Vis-NIR spectrophotometer. The scan version was 6.2.1588 and instrument version 3.0. The range was between 200 and 800 nm. The measurement was performed in chloroform. Therefore, 300 to 350 mg of polymer was dissolved in 3 mL solvent to receive a concentration of around 1 mg/mL. For graphical illustration, the data were evaluated using OriginLab V9.0 and Microsoft Excel.

4.6 Summary of POx and POzi properties

Poly(2-thiophene-3-oxazine)

M: 4.3 kg/mol

GPC (HFIP): M_n = 2.9 kg/mol, Đ = 1.09

^{1}H-NMR (300 MHz, $CDCl_3$, δ ppm): 7.31 (2H), 7.06 (1H), 3.33 (4H), 1.83 (2H)

Poly(2-thiophene-3-oxazoline)

M: 4.0 kg/mol

GPC (HFIP): M_n = 1.5 kg/mol, Đ = 1.14

^{1}H-NMR (300 MHz, $CDCl_3$, δ ppm): 7.33 (2H), 7.07 (1H), 3.60 (4H)

Poly(2-thiophene-2-oxazine)

M: 4.0 kg/mol

GPC (HFIP): M_n = 7.5 kg/mol, Đ = 1.27

^{1}H-NMR (300 MHz, $CDCl_3$, δ ppm): 7.40 (1H), 7.27 (1H), 7.00 (1H), 3.49 (4H), 1.99 (2H)

Poly(2-thiophene-2-oxazoline)

M: 4.0 kg/mol

GPC (HFIP): M_n = 1.1 kg/mol, Đ = 1.19

^{1}H-NMR (300 MHz, $CDCl_3$, δ ppm): 7.40 (1H), 7.27 (1H), 7.00 (1H), 3.49 (4H), 1.99 (2H)

Poly(2-acetothiophene-3-oxazine)

M: 4.7 kg/mol

GPC (HFIP): M_n = 5.9 kg/mol, Đ = 1.36

^{1}H-NMR (300 MHz, $CDCl_3$, δ ppm): 7.27 (1H), 7.04 (1H), 6.97 (1H), 3.64 (2H), 3.23 (4H), 1,65 (2H)

Poly(2-acetothiophene-3-oxazoline)

GPC (HFIP): M_n = 3.1 kg/mol, Đ = 1.12

^{1}H-NMR (300 MHz, $CDCl_3$, δ ppm): 7.27 (1H), 7.23 (1H), 7.05 (1H), 3.71 (2H), 3.35 (4H)

Poly(2-acetothiophene-2-oxazine)

GPC (HFIP): M_n = 3.1 kg/mol, Đ = 1.39

^{1}H-NMR (300 MHz, $CDCl_3$, δ ppm): 7.16 (1H), 6.91–6.86 (2H), 3.81 (2H), 3.28 (4H), 1.73 (2H)

Poly(2-acetothiophene-2-oxazoline)

M: 4.7 kg/mol

GPC (HFIP): M_n = 5.8 kg/mol, Đ = 1.47

^{1}H-NMR (300 MHz, $CDCl_3$, δ ppm): 7.14 (1H), 6.89 (2H), 3.91 (2H) 3.41 (4H)

EDOT-tosylate

Yield: -

^{1}H-NMR (300 MHz, $CDCl_3$, δ ppm): 2.39 (s, CH3, 3H), 3.41 (m, 1H), 3.98–4.16 (m, 4H), 6.24 (m, , SC4H2, 2H), 7.27 (d, Ph, 2H), 7.71 (d, Ph, 2H).

EDOT-PEtOx-OH

M: 3.1 kg/mol

GPC (HFIP): 4.8 kg/mol, Đ = 1.38

^{1}H-NMR (300 MHz, $CDCl_3$, δ ppm): 4.22 – 4.13 (b, H2), 3.85 – 3.74 (b, H1)

Chapter 5 – Exploring the polymer platform of P2Th3Ozi

5.1 Introduction

MEW printing is currently of great interest and can be a promising method for the production of ultra-fine scaffolds,[259–261] however there are very few polymers that have been used for this process. Most commonly, neat PCL is used but other polymers represented in the MEW literature include PVDF, polypropylene, PLA or POx.[262] Much of the prior research in MEW has focused on optimising parameters for control of fibre thickness. MEW is able to achieve a low-micron level resolution (0.5 - 10 µm) in printing by optimising the printing properties. While this range of fibres can be produced with excellent repeatability and high precision, the possible areas of application are limited due to very few materials compatible with the melt parameters and in the absence of solvents. MEW printing could gain widespread uptake through the development of new melt compatible materials with a range of functional properties, facilitating application to bioelectronics, tissue engineering and sensors.

As such the focus of this chapter is whether the thiophene-based polyoxazolines, developed in Chapter 3 and 4, which have demonstrated appropriate melt characteristics, can be processed using MEW 3D printing. PCL has been shown to have appropriate properties for MEW printing, including melt temperature, stability and flexibility, but this material does not have any chemical functionality. More recently, POx have been explored in conjunction with MEW since the melting temperature of the polymer class can be varied in a targeted manner over a wide temperature range and can remain stable even at temperatures above 200 °C.[27] Nahm et al.[29] have shown that a hydrogel based on aliphatic POx can be processed via MEW printing. This biomaterial could also be crosslinked due to a Diels-Alder functionality and thus processed thermoreversibly. This approach made it possible to have a great deal of control over the mechanical properties of the polymer and to draw up the printed scaffold into a syringe without damaging it. Electrically active or electrically conductive materials are difficult to implement with this technology due to the applied voltage during the process. However, Kade et al.[260] showed that poly(vinylidene fluoride-co-trifluoroethylene), a piezoelectric polymer can be processed via MEW to form mesh type scaffolds. They also demonstrated that the piezoelectric properties of the material were retained.

The most important physical parameter for 3D printing is the melting temperature. Ideally, this should be between 100 and 200 °C, since most polymers are processed in this range, the printers are therefore pre-set to this temperature range and to facilitate dual or co-linear printing.[261,262] As seen in Chapter 4, copolymers based on P2Th3Ozi follow the Flory-Fox equation and the glass transition temperature can thus be specifically influenced by copolymerisation with aliphatic POx or POzi. It was found that copolymerisation with 20 % aliphatic Ox, such as n-propyl-Ox, significantly affects the T_g of the polymer and a lower melting temperature can be observed. Nahm et al.[29] was able to show that the

copolymerisation of different aliphatic POx and POzi could lower the melting temperature by up to 50 °C. As such, in this chapter, copolymerisation has been considered as a method for enabling control of the polymer properties for MEW by mediating the melting temperature. Additional components such as solvents, including water, have a further influence on the melting temperature of a material,[261] typically lowering the required print temperature. However, the presence of solvents can impact on the dimensional and chemical stability of the material and printed objects. Two effects can occur upon contact of a print feed with water. Extractable leachants can be generated, which can lead to toxicity; and the structure can be deformed, reducing the accuracy of the print and any targeted topographical features.

To realise new functional materials for 3D printing, the P2Th3Ozi produced in Chapter 4 was investigated across a range of properties critical for MEW. The essential property for MEW printing is the presence of a melt phase. In addition, the material used must be stable over a long period of time during thermal treatment, since the printing time can be several hours due to the individual process steps such as preparation, melting and printing. P2Th3Ozi meets these proposed criteria for printable material properties, with a tuneable melting temperature that can be controlled within the defined range. For MEW printing it is also important that the material is available in the gram range. P2Th3Ozi has been shown to possess capacity for simple scale up in production and the polymer is soluble in a large number of solvents. Due to the applied voltage (kV range) and the pressure (> 0.7 bar or 70 kPa) used during printing, it is important that the print material is stable under these conditions and retains adequate flow through uniform viscosity to enable a print jet. Investigations in the previous chapter suggest P2Th3Ozi meets these prerequisites for use in MEW printing. Scaffolds should be printed with high precision. In general, MEW printing has been shown to produce fibres ranging from 0.8 nm to 50 µm and in layers from single fibres to stacks of 50.[261] It has been shown that layers of 80 µm thick create scaffolds that are ideal for soft tissue cell interactions and therefore, are ideal TE regeneration.[263] As such the printing criteria targeted in these experiments will be within these same ranges targeting around 10 µm and 20 stacked layers. A successful MEW print of P2Th3Ozi would meet these conventional printing characteristics.

Improving the electroactive functionality of the printed scaffolds is challenging and would be beneficial for the restoration of excitable biological tissues.[211] An electrical impulse can be used to stimulate the tissue in a targeted manner and thus stimulate growth. For better cell communication, it is of great interest that the contact area between the surrounding biological tissue and the printed scaffold is as large as possible. At the time of this writing, no electrically conductive polymers could be used directly in 3D printing. However, it has been shown that post-polymerisation or post-print modification can result in surface functionalisation of scaffolds. Zhang et al.[264] has proposed that post-print modification can close the gap between 3D printing technology and biomedical functionality.

P2Th3Ozi was found to be minimally electrically conductive without further modification. Therefore, scaffolds made of this material require chemical modification to become sufficiently electrically conductive. There are several approaches that can be considered for imparting electroactivity, such as introducing additional electroactive elements, for example PEDOT:PSS or graphene particles, through a coating or polymerisation on the surface of the scaffold. The addition of conductive particles has been explored for 3D printing. Guo et al.[265] have shown that in addition to graphene, other particles such as molybdenum sulphide or boron nitride can also be used in 3D printing such as direct ink writing or fused deposition modelling. The problem here is that the use of a composite strongly influences the printing parameters and controlled printing cannot be guaranteed. Of note, the printing-head for MEW is in a vertical position and when heated for a long time, the additives in the melt can sink and clump, obstructing the print-head. A homogeneous distribution is therefore difficult to achieve with particulate composite systems. It must also be considered that the voltage between the print-head and the collector can lead to a short circuit if there is a direct connection through electrically conductive material, and this could impact on the maintenance of an effective linear print. Therefore, coating or surface functionalization of the printed scaffold may provide a good way to improve the scaffold conductivity. Similar to the coating of medical electrodes with PEDOT that is common in the literature, the scaffold surface can be coated with a thin layer of polymer.[266] A distinction is made here between coating by adhesion or by chemical bonding to the surface. While the first has been used to refine materials for thousands of years, the second has only gained attention in recent years. For example, Löblein et al. chemically functionalized the surface of a MEW scaffold with poly(2-hydroxymethyl methacrylate) by light-induced radical polymerisation.[267] It was possible to functionalise the surface with acrylate-groups, which can be used for further modification reactions. The chemical-oxidative surface functionalization with an electrically conductive polymer is already known from literature[268] and transferring this approach to P2Th3Ozi would therefore broaden up the possibility of surface functionalization.

5.2 Aims and Hypotheses

The aim of this chapter was to investigate the processability of the polymer class using MEW 3D printing. Due to the appropriate base properties of P2Th3Ozi, it was hypothesised that this polymer could be used for precise and reproducible printing of scaffolds with dimensions comparable to that of other fibre scaffolds in the literature. Additionally, it was proposed that the post-polymerisation modification through the introduction of PEDOT demonstrated for the bulk polymer, could be applied to printed scaffold fibers.

The specific aims of this chapter were to:

1. Examine the ability to MEW print fine fibers (target 10-50 µm) of P2T3Ozi with high accuracy (target > 10 layers) by optimizing printing parameters such as speed, pressure, temperature and voltage;
2. Investigate the ability of thiophene groups to impart increased conductivity to the scaffold through polymerisation with additional CP monomers; and,
3. Understand the dynamic scaffold properties and impact on cell growth in a biological environment.

5.3 Experimental Section

5.3.1 Materials

P2T3Ozi was synthesized as described in the previous chapter and was used without further preparation if not stated otherwise. The chain lengths were varied between 15 – 40 repeating units as specified below. To investigate the hypothesis of the Flory-Fox equation further, the copolymer of 2Th3Ozi and n-propylOx presented in Chapter 4 was prepared in a ratio of 20:5 and tested in a 3D printing process as well. $FeCl_3$ was dried under vacuum at 50 °C for 24 h prior use. Unless otherwise stated, all reactions and work-up procedures were performed under inert conditions (water-free Argon atmosphere using a $CaCl_2$ filter).

5.3.2 Characterisation and Analysis

Melt Electrowriting

The MEW printing was performed on a custom-built device[269] (Figure 5.1). It operated with either nitrogen or argon pressure. The nozzle material was stainless-steel of different diameters (22-25G was mostly used) and attached to a 3 mL glass syringe (Firtuna Optima 3 mL Luer Lock). The nozzle was hand-cut and ground to a total length of ~7 ± 0.2 mm. The distance between the nozzle and collector was between 3.3 and 4.4 mm. The heated collector was also custom-made. Printing was performed on glass microscope slide (VWR, ground edge). The syringe was loaded with 1 – 2 g per print run. The pre-heating was between 30 minutes and 1 hour. A systematic adjustment of the instrumental parameters was conducted and is described in the results section. The printing parameters (temperature nozzle and syringe, pressure, inert gas flow) were recorded during printing.

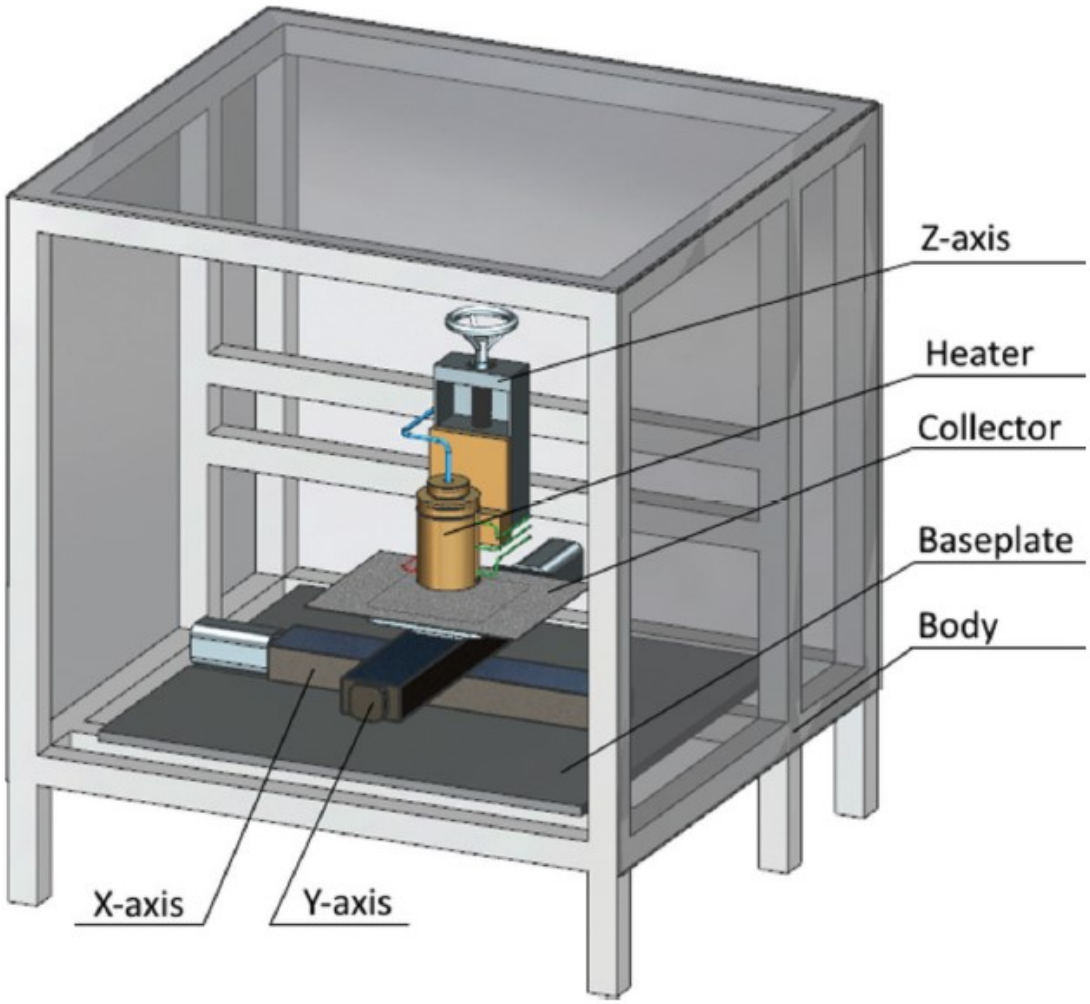


Figure 5.1 Setup of a MEW printing device[270]

To evaluate the processability of the polymer class, the materials were loaded into the printer head and the needle temperature (NT) and syringe temperature (ST) were gradually increased starting at 90 °C and increasing the temperature by 5 °C per 15 minutes while the other printing parameters, pressure (p), voltage (V) and PS were kept at base values of 0.8 bar, 2.6 kV and 600 mm/min according to the general procedure developed by Nahm et al.[180]. Due to the increased chain length of P2Th3Ozi, it was necessary to adjust the NT and ST separately. Once a stable polymer jet was established, the printing was optimised at constant NT and ST by tuning p, V and PS. Fine-tuning of the printing temperatures was performed afterwards

G-Code programming

Printing was performed using G-code Programming. Therefore, commonly used square grid scaffolds were printed with an edge length of 15x15 mm (Figure 5.2). The number of layers were varied between 5-20 layers for both directions of the mesh. The mesh size was defined to be 500 µm.

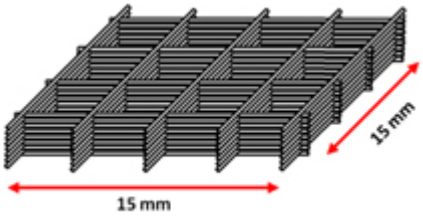


Figure 5.2 Design of printed scaffolds[271]

The speed of printing was varied to achieve a steady flow. The turning loop speed was kept constant as an optimizing of the fibre deposition was not necessary. For MEW processing, the CTS (critical translation speed) can be used as a sensitive measure to describe the processing of a polymer. Printing above this critical value results in the deposition of a straight fiber. Below the CTS, the deposited fiber is not straight but shows a loop or sinusoidal-like pattern.[261] To determine the CTS, a minimum of five straight lines were printed with the same CTS at three different speed points (TS) of 300, 700 and 1000 mm/min.

Scanning electron microscopy (SEM)

SEM was used for visualization and fiber diameter calculation.[216,223] The measurement takes place in a vacuum and must therefore be anhydrous (except for cryo-SEM). In the SEM, the sample surface is scanned in lines with a very thin electron beam (0.01 µm). The impact of the primary electrons of the electron beam releases secondary electrons from the metal-coated sample, which are then captured by an electron detector. The distribution of these secondary electrons over the sample surface is shown on a screen as light and dark zones. Protruding parts emit many secondary electrons and thus appear bright, while deeper areas remain dark. The oblique incidence of the electron beam creates a shadow that gives a three-dimensional image of the surface.

The SEM was performed using a Crossbeam 340 field emission SEM (Carl Zeiss Microscopy, Oberkochen, Germany). The acceleration voltage was set at 2 kV or 8 kV, depending on the resolution of the SEM image. The voltage has a direct influence on the resolution. While lower kV reduces artifacts such as charging or edge effects and do not destroy the sample by the laser beam, higher kV results in better resolution, but the sample can be damaged. Therefore, depending on the resolution of the image, the lower kV of 2 kV was used in general if not otherwise stated. The secondary electron was an Everhart-Thornley detector. The grid samples were coated using platinum sputtering with a thickness up to 5 nm to minimise charging artefacts.

During cryo-preparation, samples are frozen at - 185 °C. The advantage of cryo-SEM is the gentle stabilisation of hydrated structure by cryofreezing. By doing this, drying effects are minimised during the SEM measurements. For the preparation of the samples, initially, the scaffolds were placed in water

for 24 hours. Afterwards, the scaffolds were frozen in liquid nitrogen. By using a cryo-cold transfer unit, the sample was placed inside the cooled SEM device. This preparation keeps the scaffolds in a frozen state. The Cryo-SEM preparation was done by using two aluminium caps (d =3 mm). The sample was enclosed between. The inner diameter was 4 mm. The samples were frozen in slush nitrogen at – 210 °C. Samples were transferred into the sputter coater by a Leica EM VCT100 cryo-shuttle at -140 °C. The caps were split in the sputter coater and a platinum coating was applied under a vacuum of 10^-3 mbar. EDX measurements were performed on the same device, a Crossbeam 340 field emission SEM (Carl Zeiss Microscopy, Oberkochen, Germany).

Optical Imaging

Different optical methods were used for visualizing and measurement of the fibre diameters.

Stereomicroscopic images were taken with a Discovery V20 (Carl Zeiss Microscopy GmbH, Germany). The device was equipped with a Zeiss icc 5 colour camera (5MP, 12 bit), two lenses (0.63x and 1.5x Plan Apo) and a zoom range up to 20:1. All pictures were processed with the Zen2012 pro software. The scaffolds were imaged by a Nikon Z6 digital camera with a Nikon ED 200 mm lens (Nikon Corp., Japan). Videos of the printing process were taken at 50 frames per second and with a resolution of 1080 pixel. DaVinci Resolve 16.2.7.01 and ImageJ were used to analyse the images and videos to measure scaffold parameters such as distances of the mesh and diameter of single fibers. If not otherwise stated, the filaments for analysis were measured in the middle of a scaffold.

Swelling studies

The swelling studies were performed according to Begam et al.[259]. Briefly, the dynamic swelling measurements were made by gravimetric measurements. The scaffolds were placed in petri dishes (100x20 mm) and suspended in approx. 15 mL Milli-Q water or PBS at 4 °C, ambient temperature and 37 °C. The samples were removed a different time intervals (2h, 24h, 48h) and residual water was removed using KIMTECH tissue. The samples were weighed on an VWR® LA 214 classic balances (accuracy ±0.0001 g) and recorded and analysed with Davinci Resolve 16.2.7.01.

The dimensional stability of the scaffolds was investigated under the influence of temperature and water. Two tests were carried out for this purpose under atmospheric conditions. Scaffolds with 10 layers and a mesh size of 0.25 mm were used as testing material. For the first study, the scaffolds were placed in petri dishes and completely covered with PBS solution. Two temperature ranges were chosen (AT and 37 °C). A visual inspection was performed after 0 h, 1 h, 24 h and 96 h. For the second study, a dynamic measurement was chosen. For this purpose, the scaffolds were placed in a water bath at 37 °C for 30 minutes and the dynamic deformation of the scaffolds was recorded with an optical microscope. Afterwards, the water was removed and dried under a light flow of nitrogen for another 30 minutes. The

weight was measured before and after the study with a VWR® LA 214 classic balances (accuracy ±0.0001 g).

Cytotoxicity

C2C12 myoblasts cells were purchased from Merck, UK and cultured in high glucose (4,500 mg/l) Dulbecco's modified Eagle's medium (DMEM)(10% Foetal Bovine Serum + 1% Pen/Strep). Cells were cultured in 75 cm^2 tissue culture flasks at 37 °C in a 5% CO_2 humidified incubator prior to use. Cultures were not allowed to become confluent as this depletes the myoblastic population due to myotube formation.[272] Passages used were P5-10. The cells used were seeded at a density of 5 x 10^3 per cm^2.

The assays were performed as an extract of the test samples according to DIN-ISO 10993-5:2009. The extraction was conducted in inert glass vials, which were sterilised by autoclave at 121 °C for a minimum of 30 minutes. The extraction was performed with a ratio of 100 mg/mL at 37±1 °C for 24±2 hours.

Due to impurities of the bulk polymer detected via NMR, various additional purification steps were carried out and tested for their efficacy as part of the biological investigations. Table 5.1 gives an overview of the seven purification options.

Table 5.1 Table of different purification treatments

Treatment 1	Heated at 130 °C under vacuum for 24 h
Treatment 2	24 h treated with water, vacuum for 24 h afterwards
Treatment 3	Methanol washing
Treatment 4	Polymer of initial MTS assay
Treatment 5	Chloroform Dialysis
Treatment 6	Untreated polymer
Treatment 7	Cold water Dialysis

MTS assay was used to assess the enzymatic activity of C2C12 myoblasts as an indication of biocompatibility. The conversion is thought to be carried out by NADPH-dependent dehydrogenase enzymes in metabolically active cells and the formazan dye produced can be quantified by measuring the absorbance at 490 – 500 nm.[273]

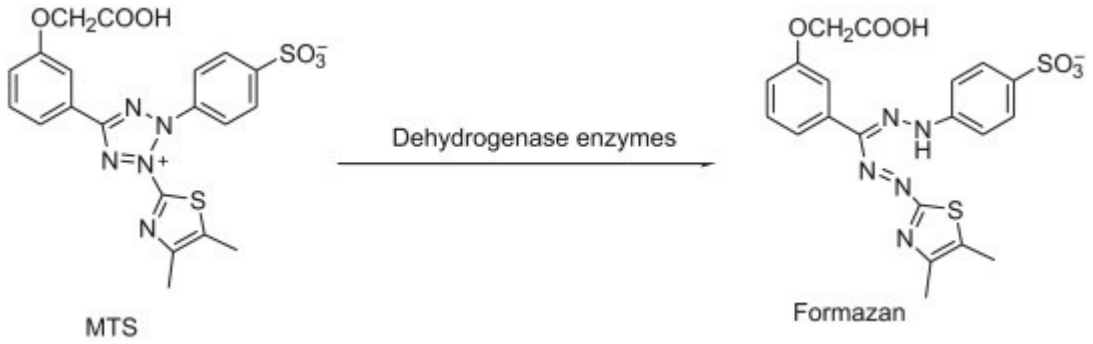


Figure 5.3 Reduction of MTS to form formazan

Measurements were made according to manufacturer's instruction and previously reported.[274] Briefly, myoblasts were seed in 96-well plates with a density of 5 x 10^3 per cm^2. The cells were allowed to attach to the well plate for 3 hours before application of the eluent. The cells were incubated for 24 hours at 37 °C and 5 % CO_2 using 0.1 mL of extraction medium from the different treatments. After 24 hours, the medium was aspirated from the cells and replaced with one part of the MTS solution in six parts of medium, which includes the MTS (3-(4,5-dimethylthiazol-2-yl-5-(3-carboxymethoxyphenyl-2-(4-sulfonphenyl)-2H-tetrazolium, inner salt) reagent. The microplate was then incubated for another 3 hours at 37 °C and 5 % CO_2 until a colour change was observed. The absorbance was measured at 490 - 500 nm.

A Live-Dead Viability/Cytotoxicity Kit by Thermo-Fisher consisting of calcein AM (live) and ethidium homodimer-1 (dead) was used to assess the impact of scaffold materials on cell survival. The cells were plated in 24 well plates at a density of 5 x 10^3 per cm^2 and the eluent was applied as detailed above. The samples were analysed after 24 hours. The medium was removed, and the cells were washed 3 times with PBS. Both dyes were combined into a single staining solution with the concentrations based on calibration using this cell type. The cells were covered with the staining solution and the incubated for 30 minutes at room temperature. The cells were then gently washed 2 times using PBS. The cells were then covered with a small quantity of PBS to prevent drying. The wells were imaged at 10x using light microscope and analysed using ImageJ.

Cell alignment study

To investigate the morphology of cells in contact with the printed scaffold, a fluorescence study was performed. C2C12 myoblasts cells were prepared as previously described. The cells were seeded onto the scaffolds at a density of 5 x 10^3 cells per cm^2 and samples were incubated at 37 °C and 5% CO_2.

Scaffolds with a mesh of 15X15 mm² and 10 layers were left on the glass slides on which they were printed and used without further sterilisation. The scaffolds were placed in 48-well plates and cells were seeded for 24 hours, after which unattached cells were removed by washing with cold PBS solution. 2',6-diamidino-2-phenylindole (DAPI) was used for staining the cell nuclei. CellMask™ Deep Red Plasma membrane stain was used for staining the filaments.

Cell orientation was observed under the fluorescence microscope and analysed with ImageJ. The orientation of the C2C12 cells was determined quantitatively according to Cha et al.[275] The angle between the long axis of the cells and the orientation of the scaffold of the DAPI images were measured and an alignment histogram was generated. The nuclei are oriented along the Z-axis and can thus reach angles between -90 ° and 90 ° (Figure 5.4). The histograms obtained can be distinguished between random, pependicular and parallel.

For the analysis of the scaffold samples, hyperstacked (2C x 10Z) images of each scaffold were taken at random locations (total n=120). Due to the contrast staining of scaffold and C2C12 cells, a qualitative analysis with ImageJ could be performed. The plane along the scaffold direction (xy-plane) was defined as 0 °. Through the stacked layers, the perpendicular (90 °) orientation of the cells along the Z-axis could then be analysed using the "local gradient orientation" plugin of ImageJ. The collected data were

transferred, and the statistical evaluation was done by combining the individual sets.

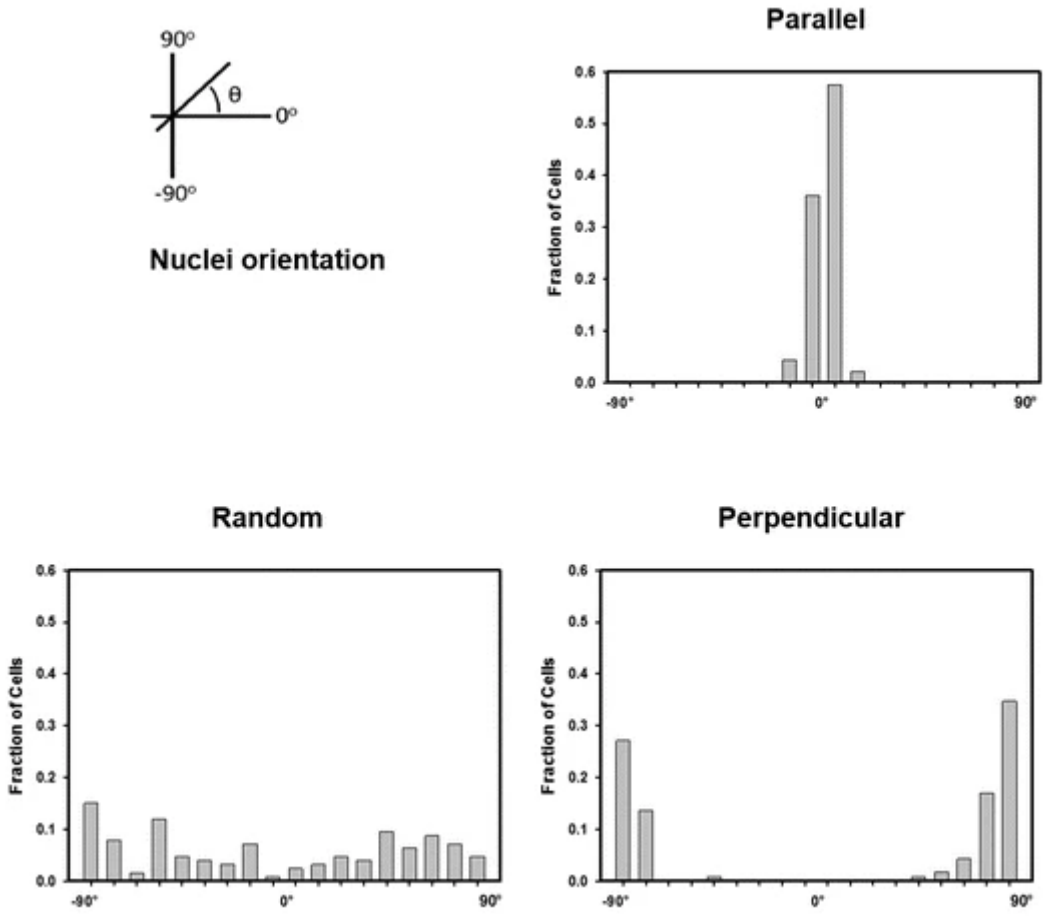


Figure 5.4 Cell alignment and orientation of nuclei[275]

Image Analysis and Statistical analysis for cell studies

Image analysis was performed with ImageJ software. 4 random images were taken for each well. Z-stacks images were deconvolved with ImageJ plugin. Cell counting was performed with imageJ plugin. Data was analysed using Excel 2021 software.

For statistical analysis, all experiments were conducted at least three times with three replicates. Experimental data are expressed as mean standard deviation (SD), unless otherwise stated. One way ANOVA (analysis of variance among groups) followed by t-tests to determine the statistical significance ($p > 0.05$), unless otherwise stated.

Post-Print Modification

The scaffolds were placed in a petri dish with 30 mL of water. $FeCl_3$ (0.58 g, $3.57*10^{-3}$ g/mol, 3 eq) was added and stored under ambient conditions for at least 24 hours. The scaffold was washed several times with water and hexane, then dried under vacuum for 48 hours. 1 droplet (~ 0.05 µL)of pure EDOT was

placed on the scaffold and allowed to react for 15 – 30 minutes. The washing steps were repeated again at least three times.

5.4 Results and Discussion

5.4.1 MEW 3D printing of P2Th3Ozi

The printability of P2Th3Ozi was examined by varying chain lengths (n = 15, 25, 40) of the homopolymer and a copolymer of P2Th3Ozi with P(n-Propyl-Ox) at a ratio of 20:5. Using general processibility procedure described in the methods section, parameter sets for the processing of all four polymer variants were found (Table 5.2). It was found that all polymers were able to be MEW printed. The printing temperature was between 115 and 145 °C. Pressure was in the range of 0.7 to 0.8 bar, while the voltage was between 2.8 – 3.2 kV. A slightly lower NT compared to the ST made it possible to improve the print appearance through more consistent fibre stacking and higher fibre accuracy (Figure 5.5).

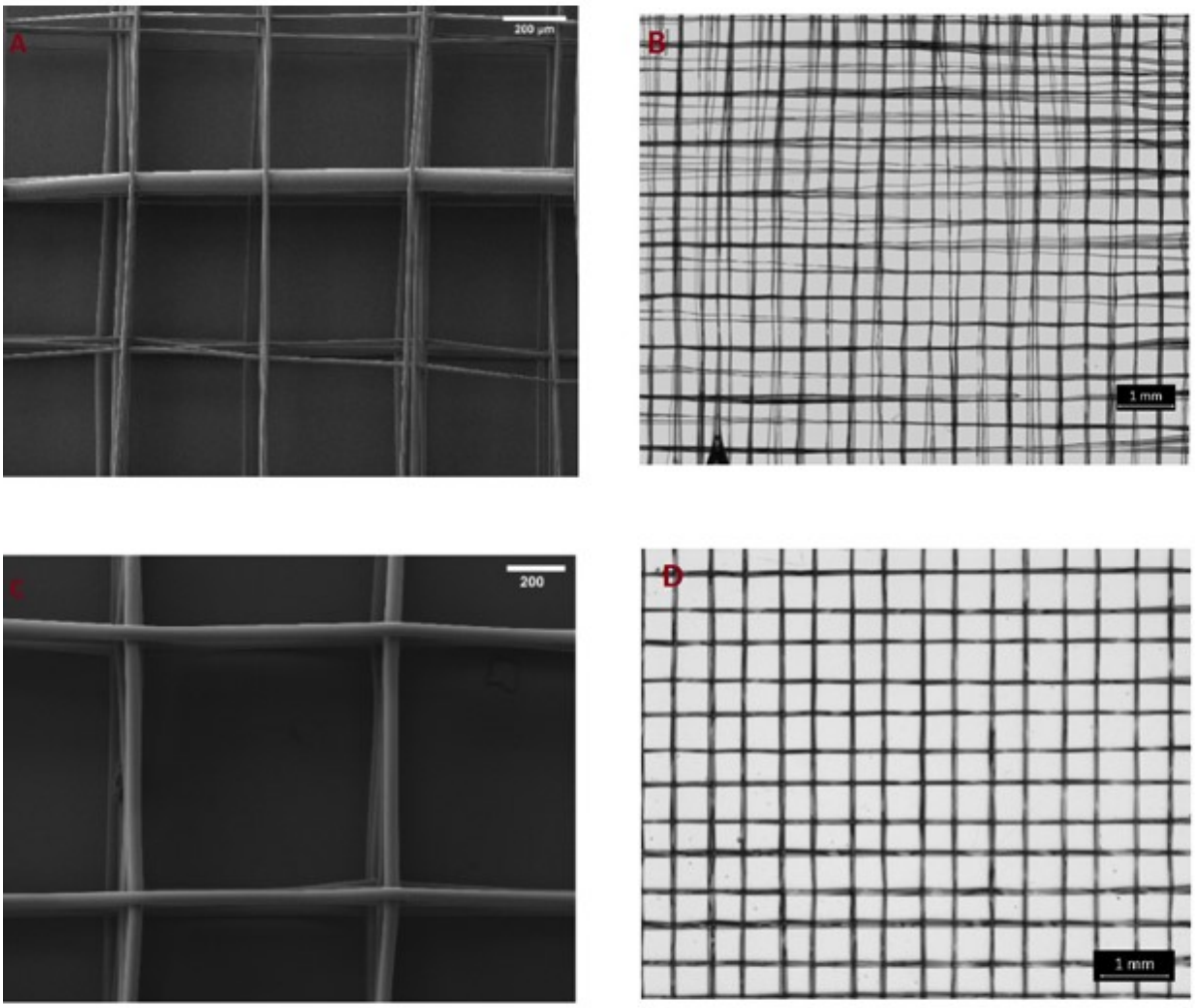


Figure 5.5 Images demonstrating the stacking and fibre accuracy of P(3Th3Ozi)25 a) SEM before adjustment, b) light microscope before adjustment. c) SEM before adjustment, d) Light microscope after adjustment. The adjusement was

carried out by changing the printing parameters like speed, pressure or voltage. Before adjustment, single fibers can be identified, and agglutination is observed. After adjustment, a clean scaffold with rectangular structure was obtained.

It could also be shown that the use of a copolymer could lower the printing temperature by approx. 30 ° C (table 5.2). In the case of the other parameters, such a strong influence on the printing properties could not be determined. The fibre morphology and fibre placement was dependent on the T_g. The optimal printing speed varied between 500 to 1100 mm/min. The highest molar mass polymer $P2t3Ozi_{40}$ was printed at moderate temperatures of around 150 °C. The shorter polymer chains were respectively printed at lower temperatures. For polymers $P2t3Ozi_{15}$ and $P2t3Ozi_{40}$ accurate placement was found and the morphology was also preserved after printing, but for $P2t3Ozi_{40}$, the fibre diameter could not be kept constant (Figure 5.6) and the fibre diameter varied between 2 – 60 ± 0.5 µm. All polymers showed accurate fibre placement capabilities up to 20 layers or more. Despite only small differences in molar mass between the tested polymers, there was an observable effect on the printing parameters. A direct correlation between the Tg and the MEW processing temperature was observed. As discussed in the previous section, the T_g of the polymer class follows the Fox equation.

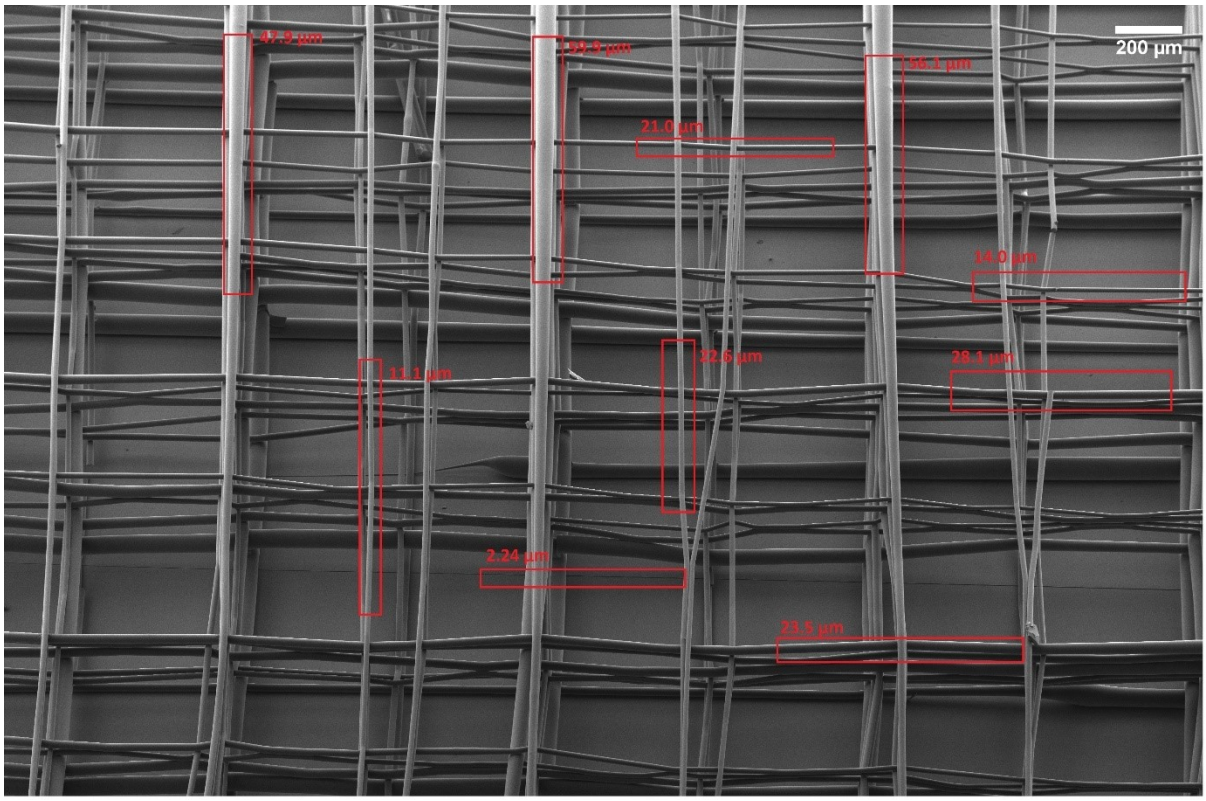


Figure 5.6 Fiber diamater fluctuation of P2Th3Ozi40. Before optimising the printing parameters, the printed fibers verified between 10 – 60 µm.

Table 5.2 Printing properties of P2t3Ozi15;25;40 and P(3t2Ozi)20-ran-P(n-propyl-2-Ox)5

Polymer	NT [°C]	ST [°C]	CT [°C]	p [bar]	V [kV]	PS [mm/min]
P2T3Ozi$_{15}$	120 ± 2	125 ± 2	40 ± 2	0,7 ± 0.05	3,1 ± 0.1	1100
P2T3Ozi$_{25}$	140 ± 2	140 ± 2	45 ± 2	0,8 ± 0.05	2,6 ± 0.1	900
P2T3Ozi$_{40}$	148 ± 2	154 ± 2	45 ± 2	0,8 ± 0.05	3,2 ± 0.1	700
P(3t2Ozi)$_{20}$-ran-P(n-propyl-2-Ox)$_5$	115 ± 2	120 ± 2	RT	0,7 ± 0.05	2,8 ± 0.1	500

Due to the rapid cooling of the printing jet, continuous printing could not be achieved without heating the collector. At temperatures above 50 °C, clumping of the individual fibres was observed over time (Figure 5.7). By heating the collector, an improvement in pressure could be observed without adjusting the pressure parameters. It was found that the CT is strongly related to the polymer chain length and had to be lower than 50 °C to minimise the clumping of printed fibres. An optimal CT of 45 ± 3 °C was determined.

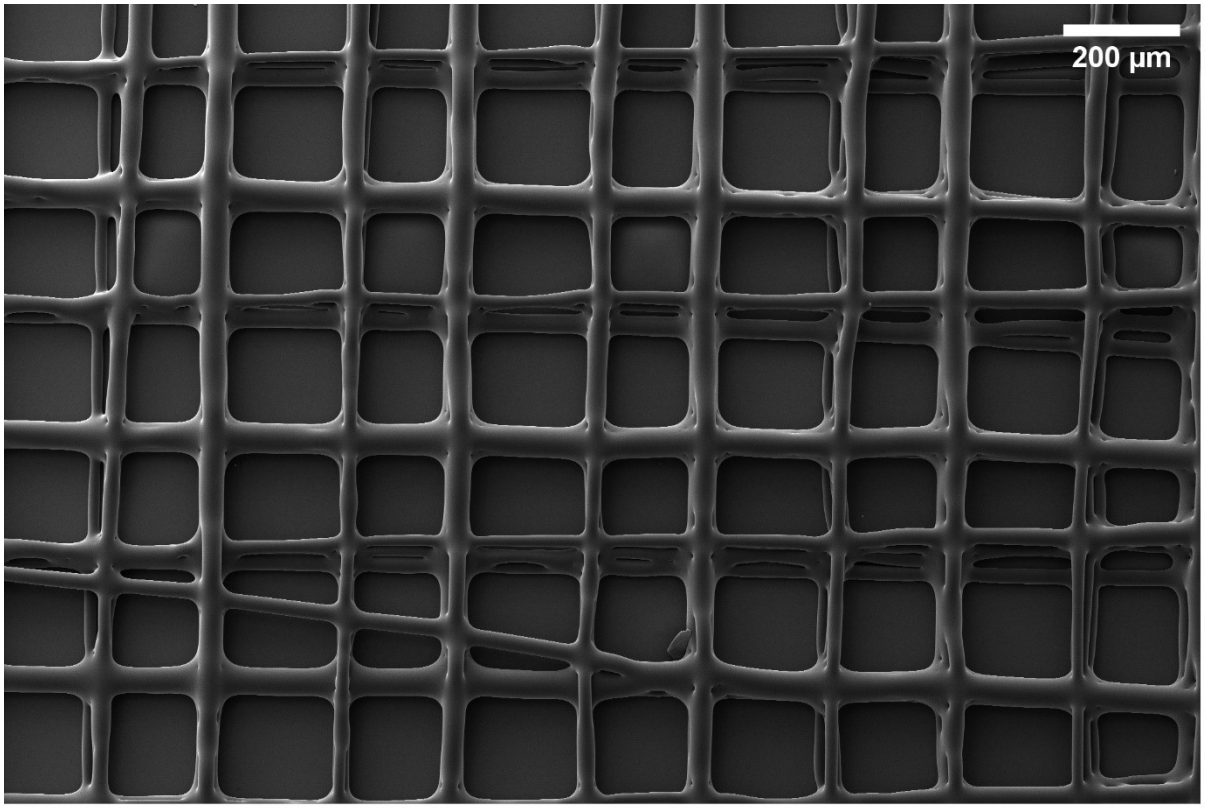


Figure 5.7: Scaffold clumping effect at collector plate temperature > 50°C

For all polymers, when the printed structures were left at RT overnight, the fibres stayed in a well-defined structure and no post-print clumping was observed. Furthermore, even after half a year, the fibre accuracy was still of high quality by storing them at Rt or lower under ambient conditions. The hydrophilic nature of the polymers allows them to absorb moisture from the environment. The moisture acts as a plasticizer and lowers the T_g of the polymer and facilitates material flow.[261] In general, the fibres produced from the homopolymer were very brittle and sometimes broke during or after printing (Figure 5.8). Detachment of the scaffold without pre-treatment with water was almost impossible. Therefore, for further investigation, all printed structures were kept on the glass plates.

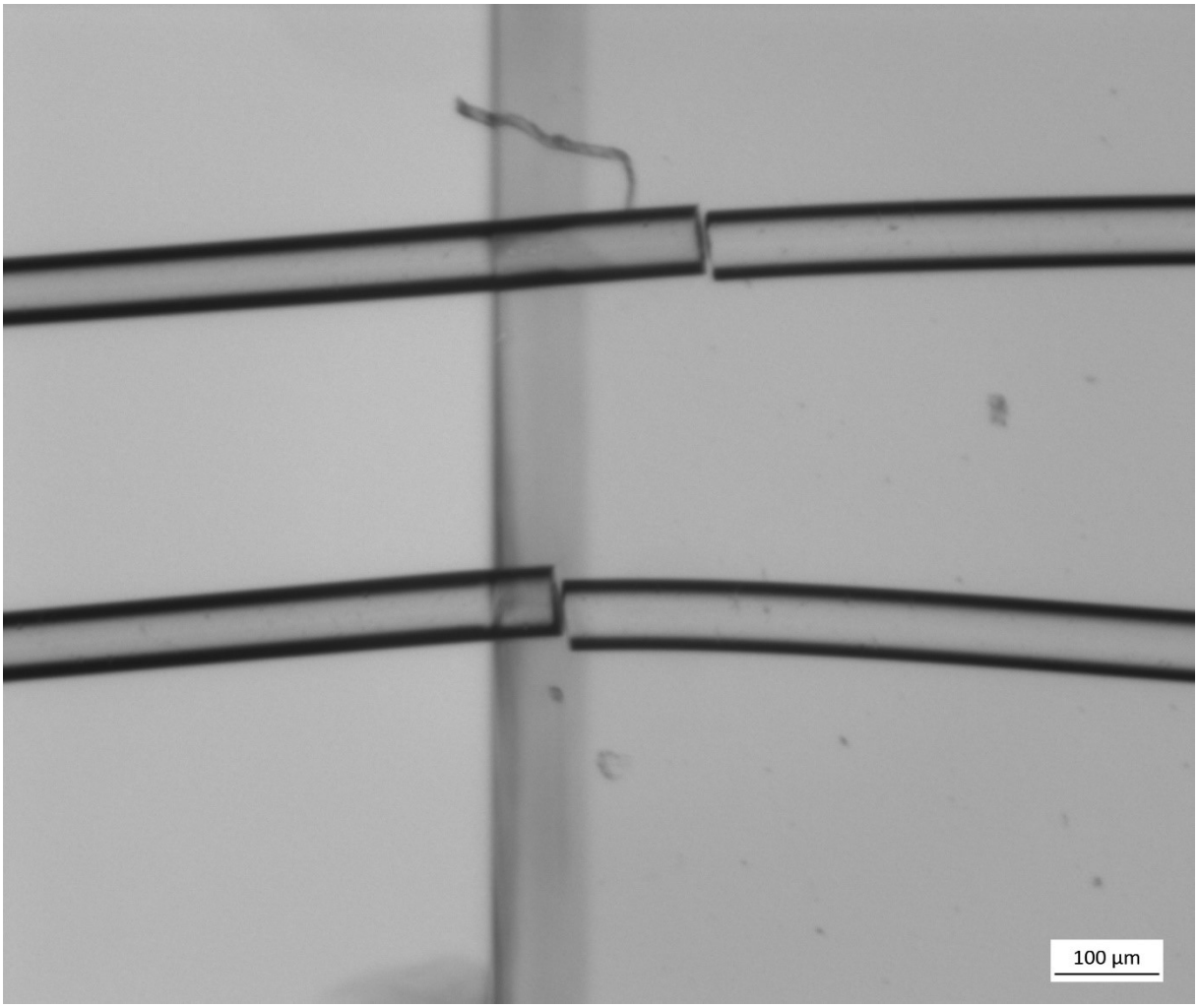


Figure 5.8 Broken fibers of P2Th3Ozi after printing. Due to the limited mechanical properties of the material and the thin fiber diameter (~35 µm), little forces applied to the fibers can damage them.

Furthermore, it should be noted that occasional arching of the print jet was observed. It was proposed that this was due to the electroactive property of the polymer as it was more prominent at higher voltages, however parameters were adjusted to avoid this behaviour and the phenomenon was not investigated further.

The most commonly used polymer in MEW 3D printing is PCl, which is processed at approx. 80 °C.[263] Ritzau-Reid et al.[211] developed a material based on PEG, PCL and EDOT. This produced a printable oligomer that could be processed via electrospinning. The researchers were able to create a network of fibres, but control over the fibre direction using this technique was not possible. The material was processed using MEW printing and a 10 x 10 cm scaffold was produced. However, the printing could only be achieved by adding purer PCL. Nahm et al.[29] produced hydrophilic POx and POzi based on poly(ethyl-2-oxazine) and were able to process them via MEW. This was the first example of a chemically functional material that could be processed by MEW. A dynamic Diels-Alder click chemistry was introduced to enable cross-linking of the material. This made it possible to stabilize the printed structure, which was then swollen in water to become a hydrogel with a water content of up to 84%.

While a significant achievement, this material could only be processed with great difficulty due to its hygroscopic properties and, in order to fill the pressure syringe, first had to be frozen in liquid nitrogen and then transferred in the frozen state. There was also substantial variability in the printing properties across different batches.[29] In contrast to this, P2Th3Ozi and the corresponding copolymers can be used comparatively easily as a powder directly without time-consuming preparation. In addition, no change in the printing parameters could be determined with different batches (number of batches n = 10) of the same material.

To further investigate the processability of P2Th3Ozi as a representative of the PThOx and PThOzi class, CTS studies were performed. Figure 5.9 presents the evaluated data. Within the TS of around 300 – 700 mm/min, a change from irregular to regular printing fibres can be observed. Even after 5 hours of printing, no progression CTS was observed. It was even possible to refill the syringe during process, and no difference in printing patterns was observed. To determine the optimum print speed, the CTS was determined at the point where the fibres were laid down straight and no more errors occurred. Using this method, the example shown in Figure 5.9 resulted in a CTS of 900 – 1000 mm/min. It is important to note that the printing parameters like *V*, NT, and ST were kept constant throughout the whole experiment. The speed of printing and thus the accuracy of the printingjet depends on several factors such as molar mass, viscosity, charge density and impurities. Since no difference in CTS could be detected even over longer pressure times (5 h), it can be assumed that no thermal degradation of the polymer takes place. This could be explained by the high thermal stability of more than 350 °C. However, Hochleitner et al.[28] reported thermal degradation during prolonged processing of PEtOx with high molar mass, even if the processing temperature was far below the degradation temperature of the polymer. In this case, sudden changes in the pressure jet occurred. Low molecular weight impurities can also be ruled out as they affect the printing jet and constant printing would not be possible.[180] The polymers were generally terminated with ethyl isonipecotate, an active amine. Since the work-up procedure was carried out in pH-neutral organic solvents and MilliQ water (neutral to slightly acidic conditions), some of these amines could be protonated and thus charged. Such charged molecules can drastically affect the MEW process[29].

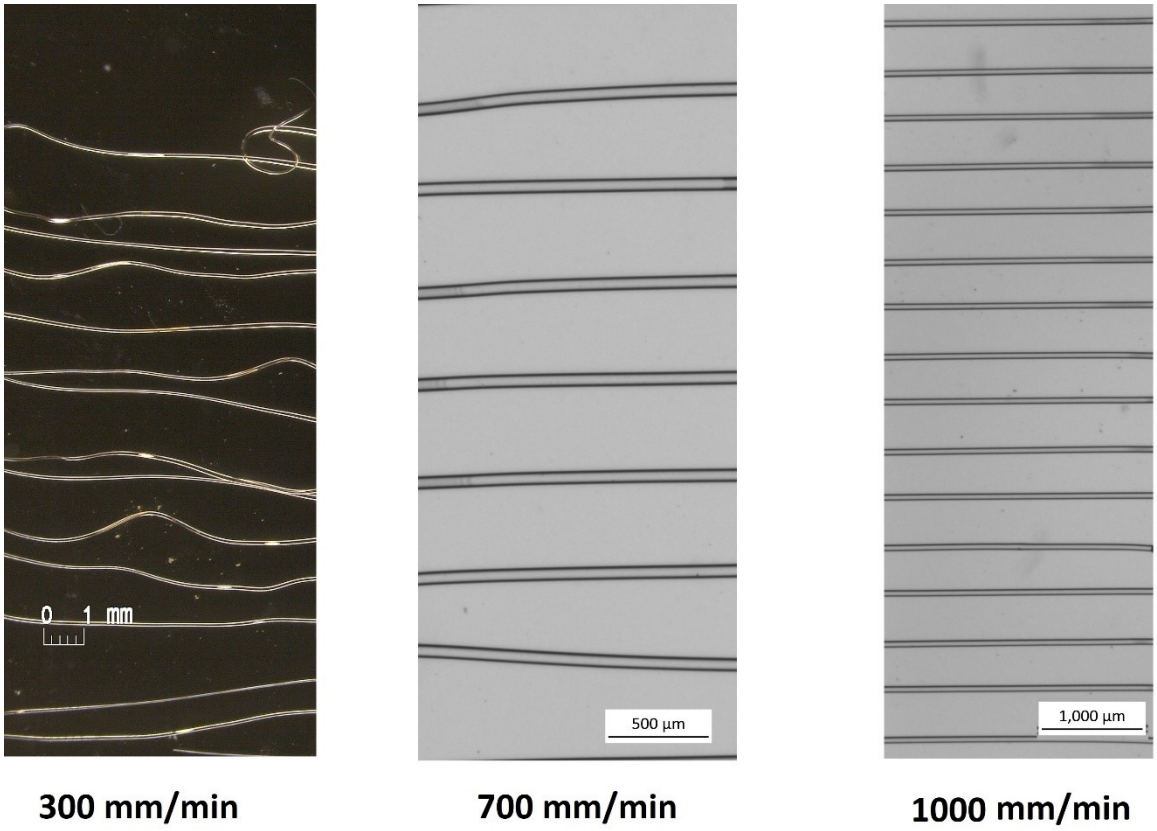


Figure 5.9 different printing speed and analysis of CTS for P2Th3Ozi. The figure shows printed fibers at 300, 700 and 1000 mm/min. At lower speed, printed fibers were not obtained, while printing and higher speed, straight lines were possible

It was possible to stack up to 20 layers with high accuracy. The fibre diameter has an average of around 35 µm (Figure 5.10). Furthermore, it was possible to print above a gap of around 1.5 mm. This is important because it was able to show that the static charge for MEW printing can be maintained, thus enabling a continuous jet. Furthermore, no difference in the fibre diameter was observed before or after printing through the gap.

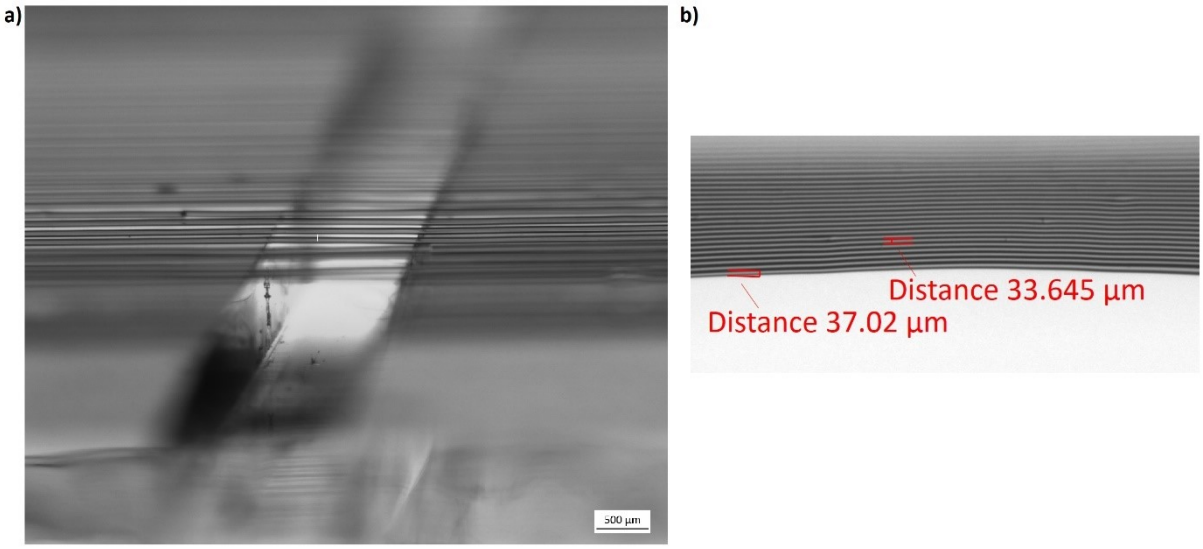


Figure 5.10 a) Printing of P2Th3Ozi through a gap (~ 2mm) was possible (loose of the homogeneous electrical field) and b) fibre stacking properties and diameter of P(2Th3Ozi)25

The printing speed of P2Th3Ozi was 6 times faster compared to reports on MEW printing of PCL.[261] This has the advantage that the production times can be drastically reduced. It could also be shown that the fiber thickness of approx. 35 µm is in the same order of magnitude and the accuracy of the printing reported for PCL.[28,261] It was possible to interrupt the constant electric field necessary for printing for a short time by printing over a gap. This has not been demonstrated for PCL, but can enable uneven surfaces to be used for 3D printing and permits greater freedom in the selection of carrier materials used. The voltage is of great importance when printing via MEW, as this allows the diameter of the printing jet to be kept constant. A fluctuation in voltage is thus a disadvantage. Since the voltage depends on the distance between the printing head and the collector, it changes with each new printing layer. This negative effect could not be detected when printing P2Th3Ozi, at least for a short time, since the fibre thickness remained constant even when a gap was printed. An improvement could also be observed compared to PEtOx and its derivatives.[29,261] While the fibre thickness and the printing speed were of the same order of magnitude, the handling and ease of use were a significant improvement since P2Th3Ozi can be used as received. In comparison PEtOx needs to be frozen in liquid nitrogen, ground and filled into the printing head to avoid coagulation behaviour typical of PEtOx particulates at RT. The stacking of P2Th3Ozi was significantly improved compared to PEtOx and print height of 20 layers could be achieved more easily with higher accuracy. The disadvantage of P2T3Ozi compared to PCL and PEtOx is that the material could only be removed from the glass substrate with great difficulty. PCL can be removed entirely from a glass slide without further preparation. In the case of PEtOx and its derivatives, treatment with water enables detachment from the glass substrate and the shape is retained. This approach could also be successfully used with P2Th3Ozi; however, the scaffold was fragile and prone to cracking during removal.

5.4.2 Swelling studies of printed scaffolds

PThOx and PThOzi form hydrogels in water. With a controlled increase in weight of approx. 10% of the homopolymer, a porous polymer structure can be obtained when the water is removed. For this purpose, in an analogous procedure, first, the printed scaffolds were placed in water at various temperatures for 24 hours. The temperatures chosen were 4 °C, ambient room temperature, and 37 °C. Three samples were prepared for each source study. Due to the low weight of the scaffolds (~ 10 – 100 mg), no further analysis of the swelling behaviour was carried out. After 24 h the scaffolds were dried in a vacuum and analysed by SEM. Figure 5.11 shows the results in summary. It could be shown that the swelling behaviour was influenced macroscopically with time and temperature. It was also observed that the pore size increased with higher temperatures.

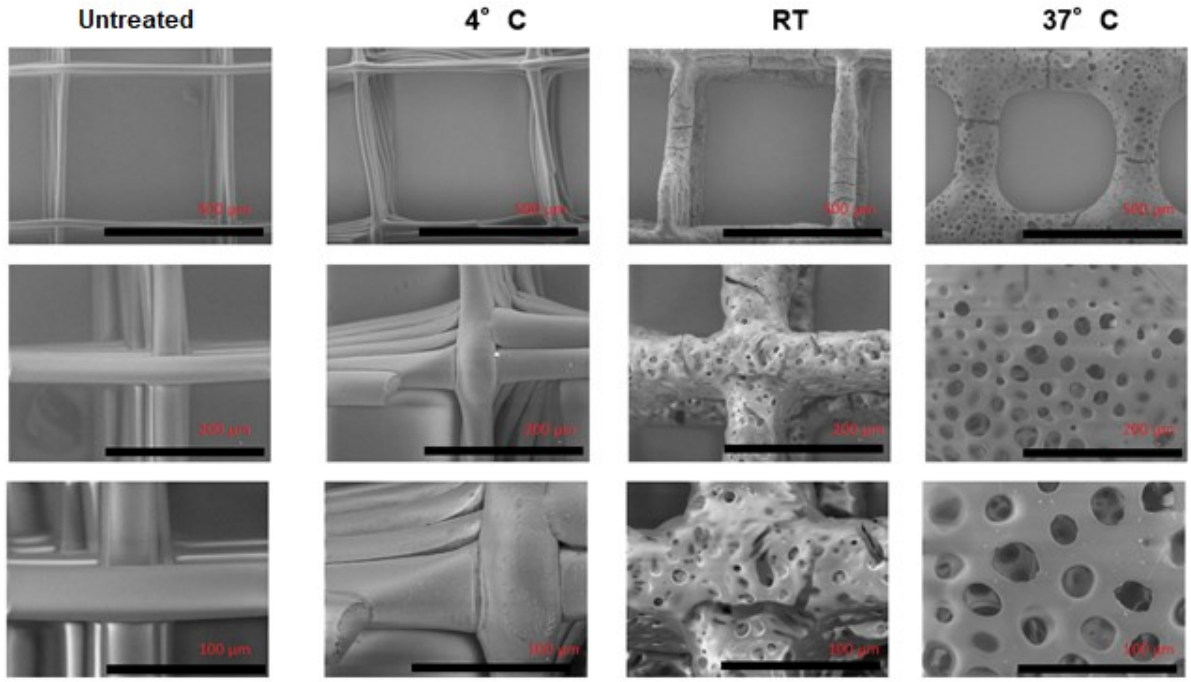


Figure 5.11 Swelling behaviour of printed scaffolds at different temperatures. Untreated scaffolds were swelled in water at different temperatures (4 °C, Rt & 37 °C)

High-resolution SEM images were made of the fibres (figure 5.12). Here it can be seen that the swelling takes place from the outside to the inside. The pores in cold water are significantly smaller than those produced at higher temperatures. The reason for this could be an interaction between water molecules and the carboxy-group of the sidechain.[276] These interactions decrease the T_g of the polymer and, therefore, allow more freedom in motion of polymer chains.[108] Prolongo et al.[277] was able to show a decrease of the T_g of an epoxy polymer of up to 10 °C by adding water to the polymer. Therefore, water can be used as a plasticizer for polymers with polar groups such as hydroxy or carboxy groups. As a result, increased temperature has a higher potential to deform the printed structure. Furthermore, the printed structure can be kept stable in cold water. At Rt and 37 °C the printing structure collapsed, and the polymer deformed into clumps. This deformation was able to be inhibited as shown by pre-treatment

in cold water and confirmed by immersion in warm water afterwards. It should be noted that degradation of the polymer was not observed even when deformation was present.

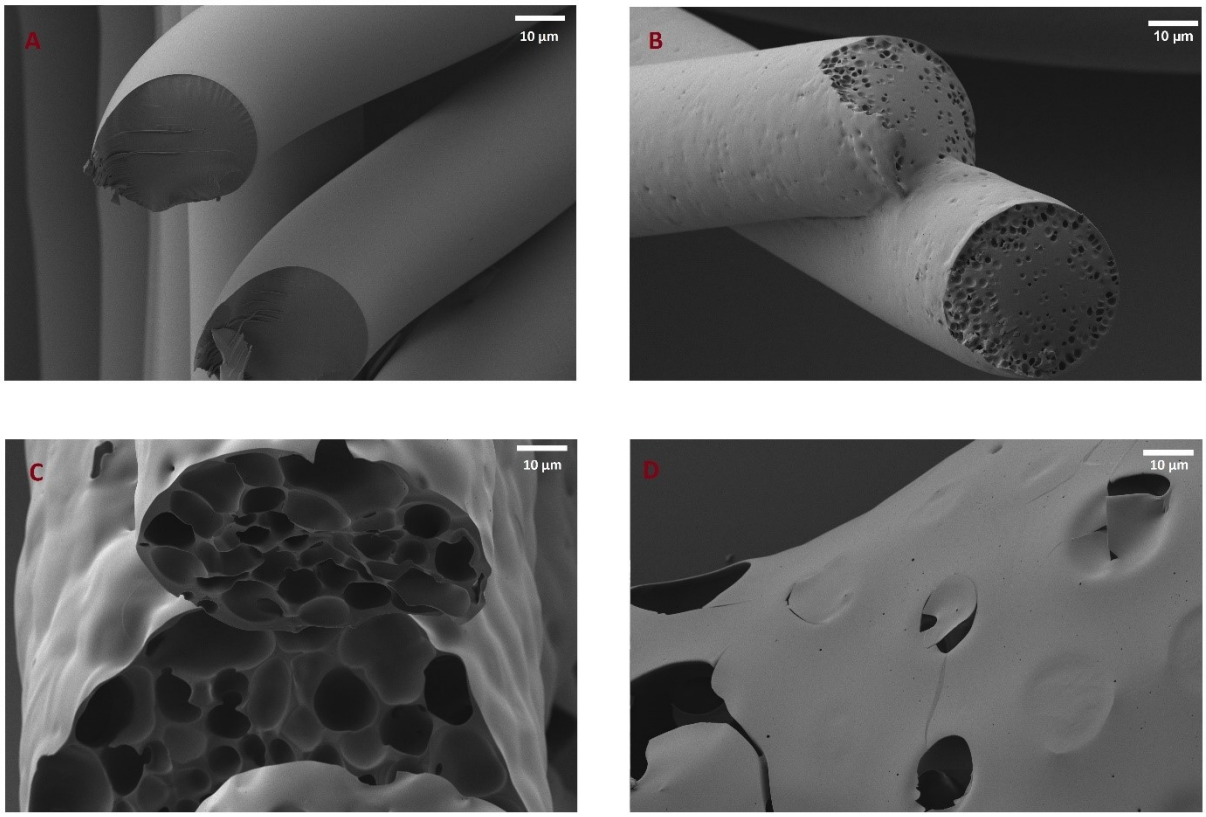


Figure 5.12 SEM images of printed fibre a) without treatment with water and at different temperatures b) 4 °C, c) Rt, d) 37 °C

No change of the material chemistry was observed via NMR, IR, or XRD analysis. Due to the swelling and deformation of the fibres, the average fibre size at 37 °C was much larger than the fibre size of untreated (dry) scaffolds, or those treated with water at 4 °C and Rt. To determine the presence of water inside the pores, a cryo-SEM study was performed. The cryo-preparation allows the analysis of wet samples with SEM. Figure 5.13 shows a longitudinal and orthogonal cross-section of the frozen fibres. The characteristic frozen water structure (white strands) can be observed inside the circles.[278] Some water droplets can also be observed, which is a result of the cryo-SEM samples being sectioned. These droplets are usually not visible and are rare observations. Table 5.3 shows the average pore size of the fibres treated with water at different temperatures. The range is between 1.4 ± 0.2 to 22.5 ± 1.2 µm.

Table 5.3 Fibre size analysis via SEM images and ImageJ (n ≥ 50)

Temperature [°C]	4 ± 0.5	At	37± 0.5
Fiber size [µm]	31.5 ± 1.6	56.2 ± 3.2	142.6 ± 4.4

Pore size [µm]	1.36 ± 0.2	4.37 ± 0.5	22.4 ± 1.2

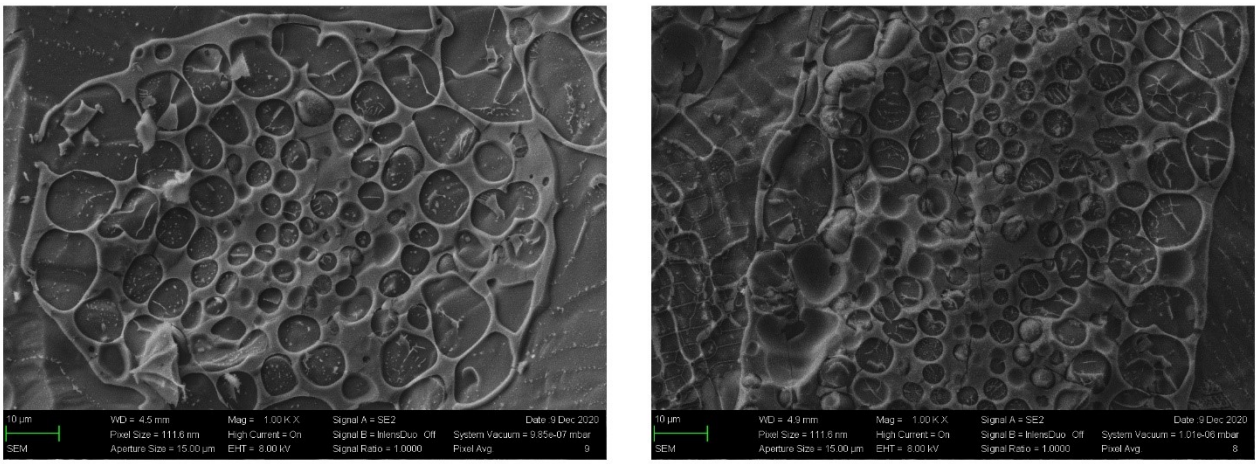


Figure 5.13 Cryo-SEM image of water treated fibres. As seen in the figure, water is encapsuled inside the porous structure

In addition to the physical properties, Aston et al.[279] postulated that the structure of hydrogels is also significantly influenced by water. Furthermore, water can exist in different crystalline structures and thus have different effects on the structure of the material. This effect is temperature dependent. The authors investigated the general possibility of analysing hydrogels with cryo-SEM. To do this, they produced hydrogels based on aliginate. Analogous porous structures of the materials could be shown in the core. In addition, the surface showed a rather smooth structure in comparison. Similar structures were found by Guerzoni et al.[280] The researchers examined hydrogels based on PEG and were able to determine a highly porous structure as well. In addition, it was found that, due to the freezing artifacts, the pores in the cryo-SEM appear larger compared to normal SEM images. Similar observations were found by cryo-SEM of P2Th3Ozi.

Both the P2Th3Ozi bulk material and the scaffolds did not change significantly during prolonged storage (up to one year) under dry, atmospheric conditions and at ambient temperatures. Furthermore, no deformation of the individual fibres of the scaffolds could be observed. However, when stored above 50 °C a clumping of the fibres was observed. For biomedical applications, it is important to understand the dimensional stability of the scaffolds under changing environmental conditions such as increased temperatures (37 °C) and humidity. To understand the deformation of the scaffolds during warm water treatment, additional studies were undertaken. In general, a turbidity of the scaffolds was observed (Fig. 5.14). This colour change was assumed to be a result of the presence of water in the swollen scaffold fibres and therefore, a refraction of light.[281] It can be seen that the scaffold structure collapses between 1 hour and 24 hours. After 96 hours, no clear structure is observed anymore. This can be explained in terms of surface tension.[223] Due to the increased temperature and the lowering of the T_g by water, the

particle movement in the material is increased. Since the horizontal and vertical fibres overlap at the nodes, the layer thickness is twice as high here. This increases the mass at these points and the surrounding particles are attracted due to cohesive forces. Droplets are formed at the nodes.

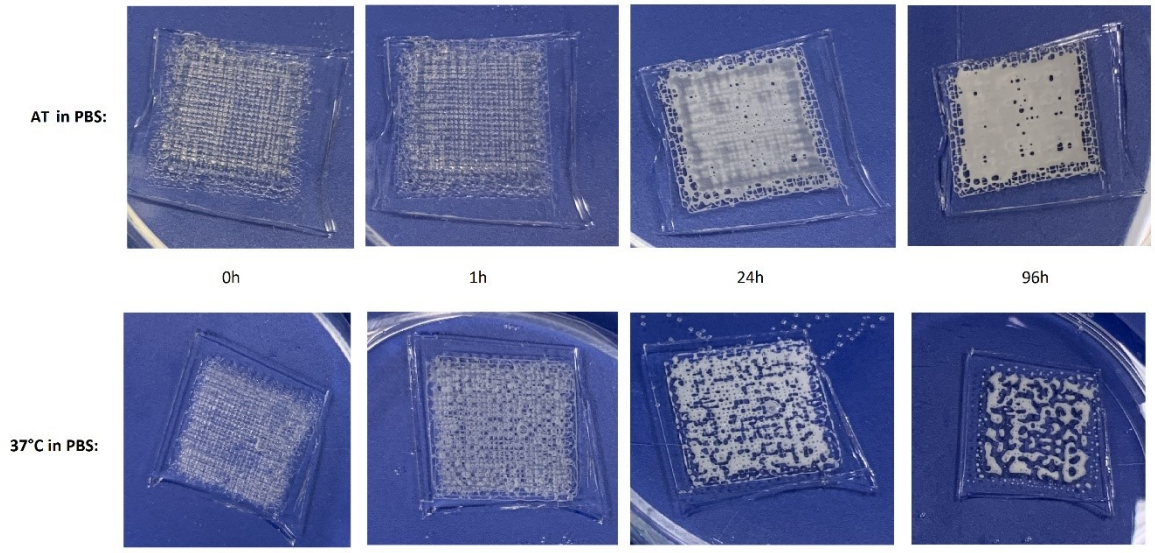


Figure 5.14 PBS treated P2Th3Ozi scaffolds over time at At and 37 °C. Over time, a loose of the grid structure can be observed. Higher temperature reinforce this observation

The influence of water on the scaffolds was also observed dynamically with an optical microscope (Figure 5.15) as well. It was observed that the individual fibres became cloudy after only 15 minutes. After 30 minutes, it was also observed that the lattice structure collapsed, and the scaffold thickened towards the nodes. During the drying process, a reversible clouding could be observed. While the structural change remained irreversible. A weight loss was not detected.

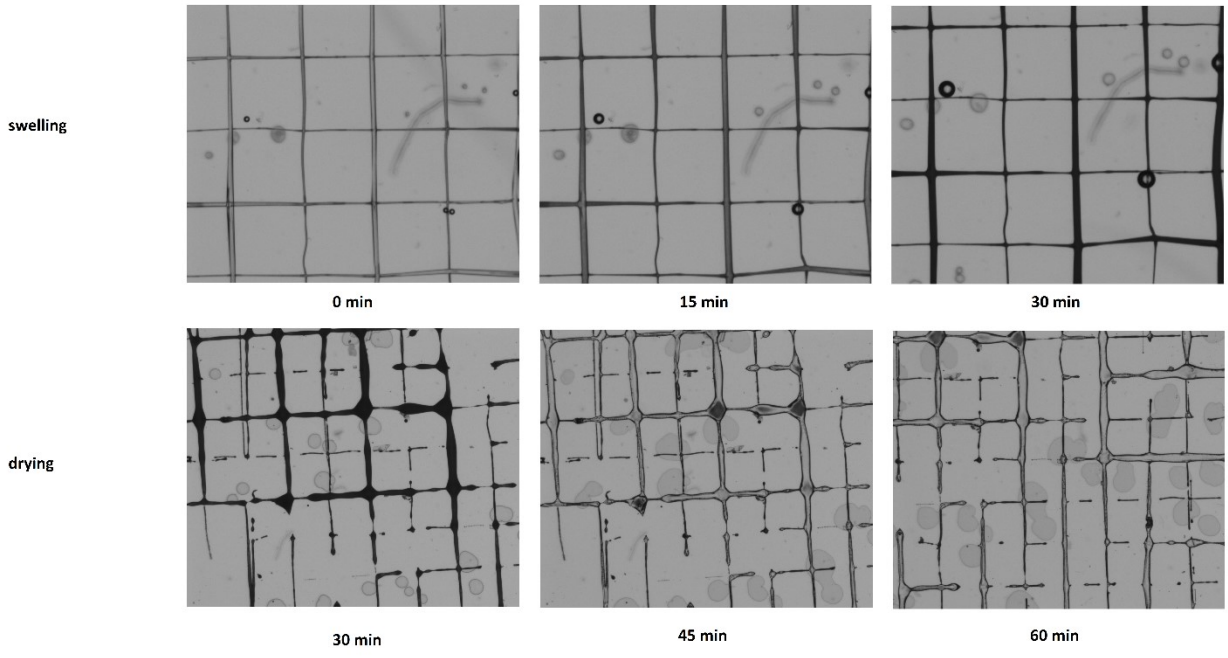


Figure 5.15 dynamic analysis of printed P2Th3Ozi scaffolds treated in water by light microscopy at At. The grid structure is dissolved and "material clumping centres" were formed

The defined structure and dimensional stability of the scaffolds at ambient temperatures and in a dry environment could not be guaranteed at elevated temperatures and under the influence of moisture. However, it could be determined with NMR and IR analysis that the treatment with water did not lead to any side reactions or degradation reactions. It was assumed that the deformation was due interaction between water and polymer, which leads to a decrease of T_g. A possible solution for the dimensional stability could therefore be the use of a polymer with a higher melting temperature such as P2Th3Ox. However, this would significantly impact the printing temperatures.

5.4.3 Biological properties of P2Th3Ozi

A basic cytotoxicity study is essential to demonstrate the potential of these scaffolds for tissue engineering. Prior literature demonstrates good cytocompatibility of POx.[282] However, as the PThOx and PThOzi are a novel class of polymers, a cytotoxic study was performed. Despite the component monomers having acceptable cytocompatibility, the first attempt at an MTS assay showed poor cell viability after 24 hours and a characteristic smell of benzonitrile was detected. NMR analysis revealed traces of benzonitrile in the sample (Figure 5.16). Here the significant signals of the benzene ring of benzonitrile come between 7.4 and 7.7 ppm. It was estimated that the cell death was due to contamination during synthesis. Therefore, additionally cleaning procedures were carried out. Several cleaning steps were tested, and the NMR spectrums are shown in Figure 5.16. The individual cleaning procedures are summarized in Table 4.9. A decrease in the contaminant signals could be observed following all cleaning procedures. Dialysis in chloroform and heating to 130 ° C for 24 h, in particular, showed a good purification.

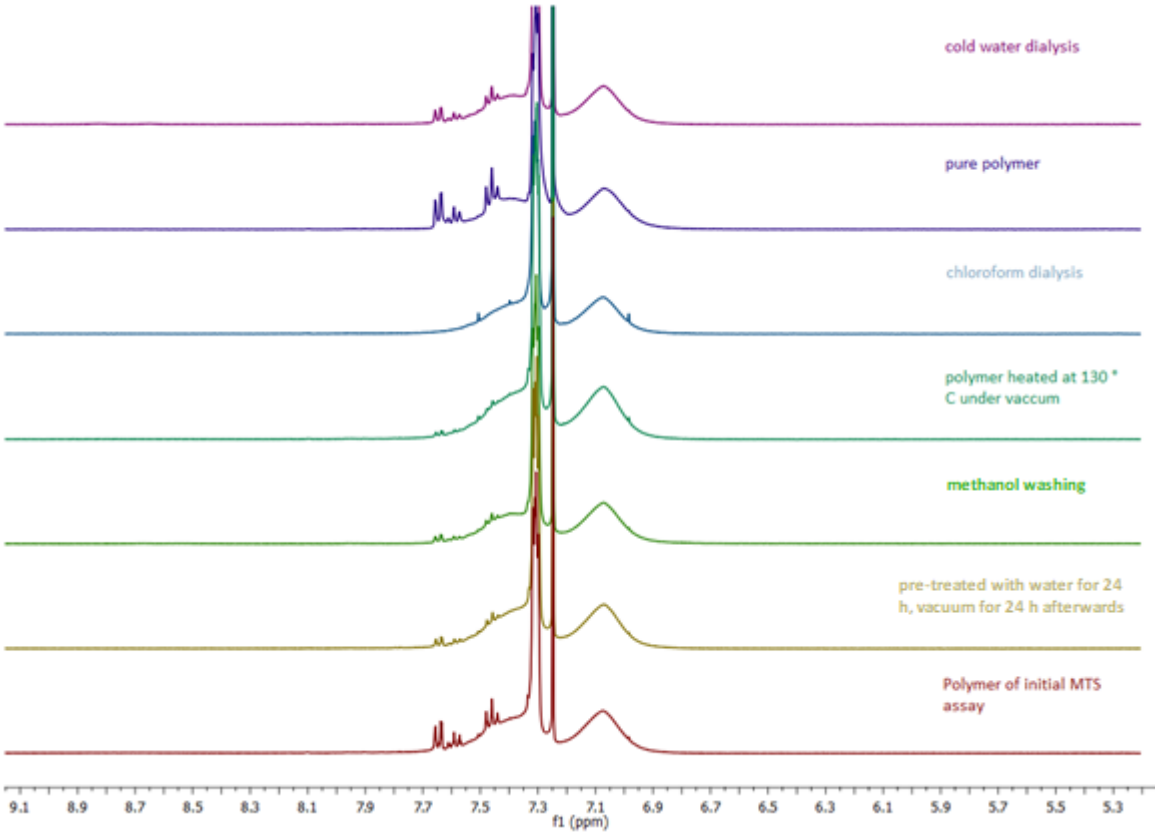


Figure 5.16 ^{1}H-NMR-spectrum of different purifications methods

Additional MTS assays were subsequently performed on the bulk polymer following individual cleaning procedures. Figure 5.17 summarizes the cell growth inhibition data. Aligning with the results from the NMR spectroscopy analysis, the same trend was observed during the MTS assay, confirming that the best cleaning and most pure product was obtained by heating the polymer powder at 130 °C under vacuum for 24 hours (Treatment 1) and cleaning via chloroform (Treatment 5). Due to the toxicity of chloroform, additional contamination with this solvent could have occurred and had an impact on the overall cell survival. Poor cell compatibility was expected from the untreated polymer powder (Treatment 6) and the polymer used for the first trial (Treatment 4). Washing with methanol and water also failed to show any improvement.

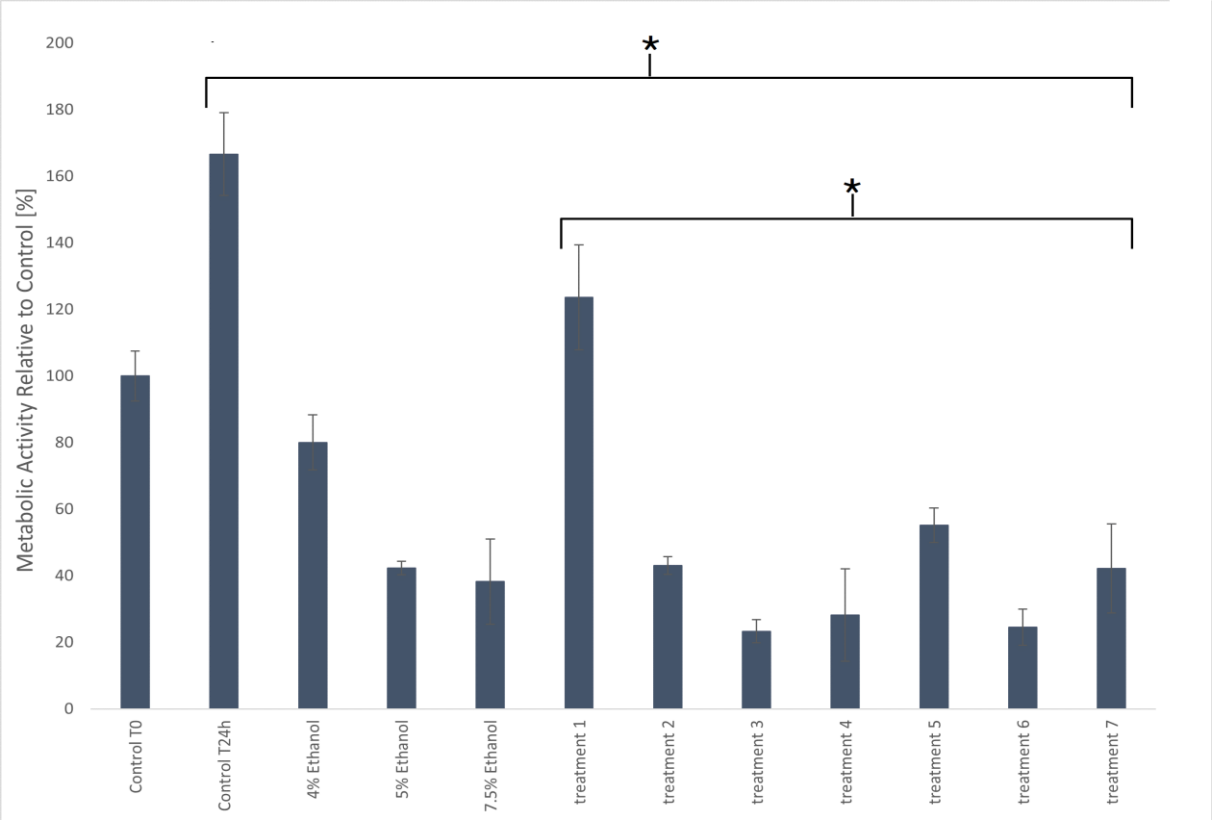


*Figure 5.17 Projected cell numbers of different purification treatments. Error is represented as SE, (N=3, n=3 with a minimum of 15 images analysed for each condition), * ANOVA p < 0.05*

Verifying the viability of cells exposed to leachants, an additional live/dead cell assessment was performed. Similar to the MTS assay, experimental control samples of different ethanol concentrations were performed along with null and cell culture only controls. Figure 5.18 summarizes the analysed live/dead ratios. A similar result was observed for the Live/dead assay compared to the MTS assay. While the metabolic activity for the individual treatments increased or decreased, the live/dead ratio and cell density showed analogous observations.

Sample micrographs that were considered typical of the cell response for representative treatments are shown in Figure 5.18 (a-d). The images indicate that especially treatment 1, heating to 130 °C for 24 h, achieved very good results. Furthermore, the results of the MTS assay were confirmed. Figure 5.18 E shows that most of the purification steps generally improved the viability to untreated polymer. In contrast, untreated polymer had a toxic effect on the cells. The cell density was determined analogously to Sun et al.[283]. Here, too, it was found that, analogous to the MTS assay, untreated polymer (treatment 6) is toxic. In summary, the already obtained results of the MTS assay could be confirmed.

To conclude, it was possible to remove most of the contaminations, which occurred during synthesis and the polymer was able to demonstrate a non-toxic leachable behaviour. It should be mentioned that the scaffolds were not used in the MTS assay or in the live/dead assay, these were bulk polymer samples. However, the purification step by heating the polymer to 130 °C for 24 hours should mimic the preparation for 3D printing. During the MEW process, the polymer is heated for at least 4-5 hours in the

printing head at these temperatures. The low level of cytotoxicity supports the continued exploration of this material in tissue engineering scaffolds, although it is noted that these are acute investigations and longer assays are required to understand chronic biological performance. Additionally, these leachant studies were not direct contact studies, which was to ensure that topographical contributions were decoupled from chemical effects on the cells. As such cells were subsequently cultured on the printed scaffolds.

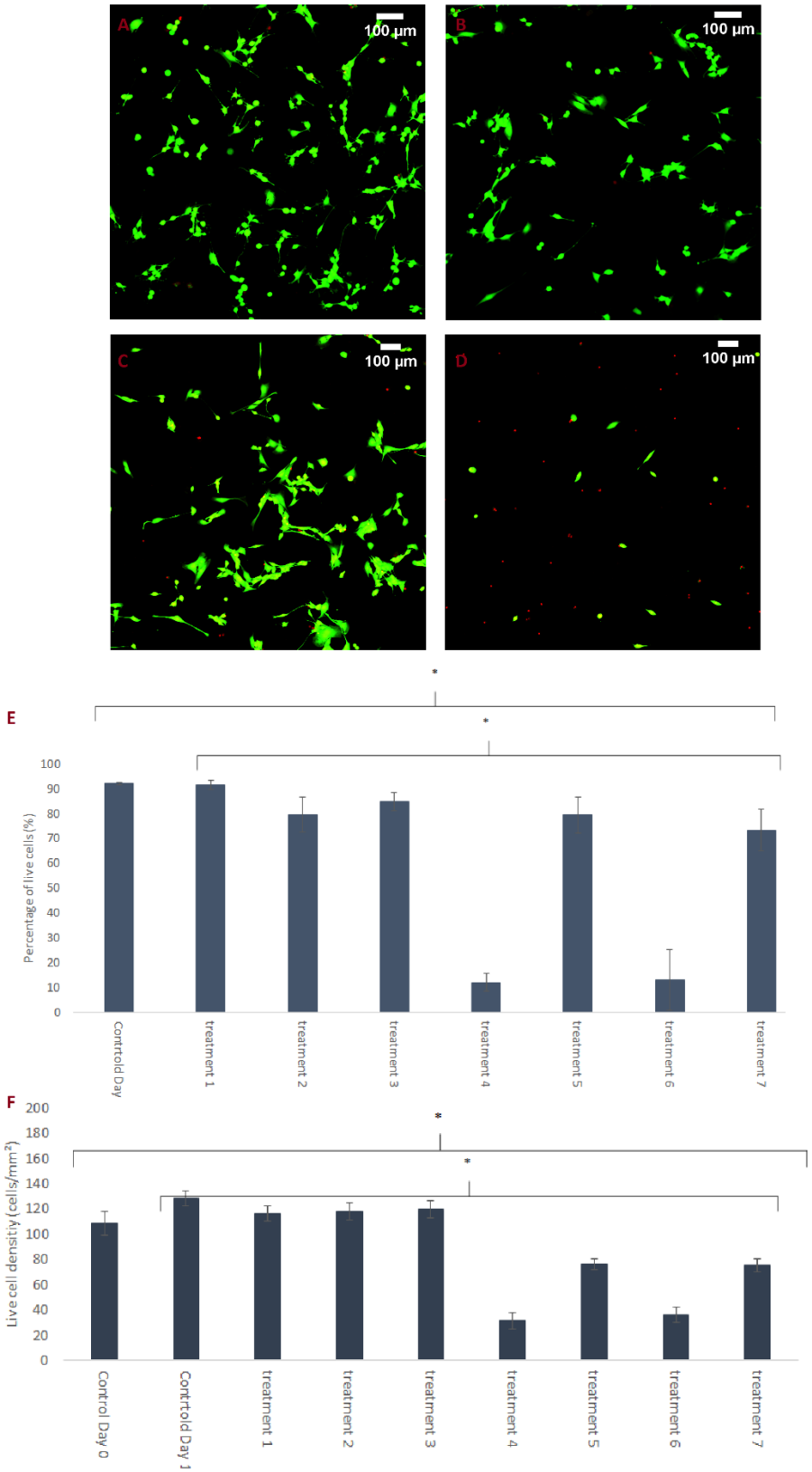


*Figure 5.18 Live/dead assay of C2C12 cells on different treated P2Th3Ozi. a-d) Repreentative confocal images of cells for specific treatments: a) Control 24h, b) Treatment 1, c) Treatment 5, d) Treatment 6. e) Perecentage of live cells. Error is represented es SE (N=3, n=3), *p<0.05 f) Live cell density (number of cells per mm²), Error is represented es SE (N=3, n=3), *p<0.05*

Because the sub-microscopic fibres could not be easily removed from the glass plates without damaging them, the fibres were left on these plates during the cell adhesion study. During the study, a deformation

of the scaffold structure due to the effects of water and heat could be observed. This deformation could not be inhibited. It could be determined that cell viability was not disturbed by the scaffolds. As seen in the previous chapter, P2Th3Ozi is auto-fluorescent. It is therefore difficult to distinguish between the cells and the scaffold. Figure 5.19 shows representative images of the study. Here it can be seen that the cells come into direct contact with the scaffolds. However, due to the formation of droplets, no specific alignment could be determined. Furthermore, it was found that cell adhesion occurred to both the glass plates and the fibres and that neither material was preferred. A pronounced orientation cannot be observed due to the short study period, but interconnected structures could be determined. The mesh of the scaffold and its fibres served as walls that separated the individual cell islands from one another. Nevertheless, a quantification of cell adhesion was carried out.

Figure 5.20 shows a representative image of the angular dependence of the cells. There was no significant difference between perpendicular and parallel orientation. Cells close to the scaffolds showed a more vertical orientation, while cells further away showed a horizontal orientation. This is also evident in the histogram (Figure 5.21). There are maximas at -90°, 0° and 90°. Due to the non-existing shape stability and the short study time, a more quantitative analysis was not possible. Nevertheless, it can be summarised that the scaffold had no negative effects on cell growth.

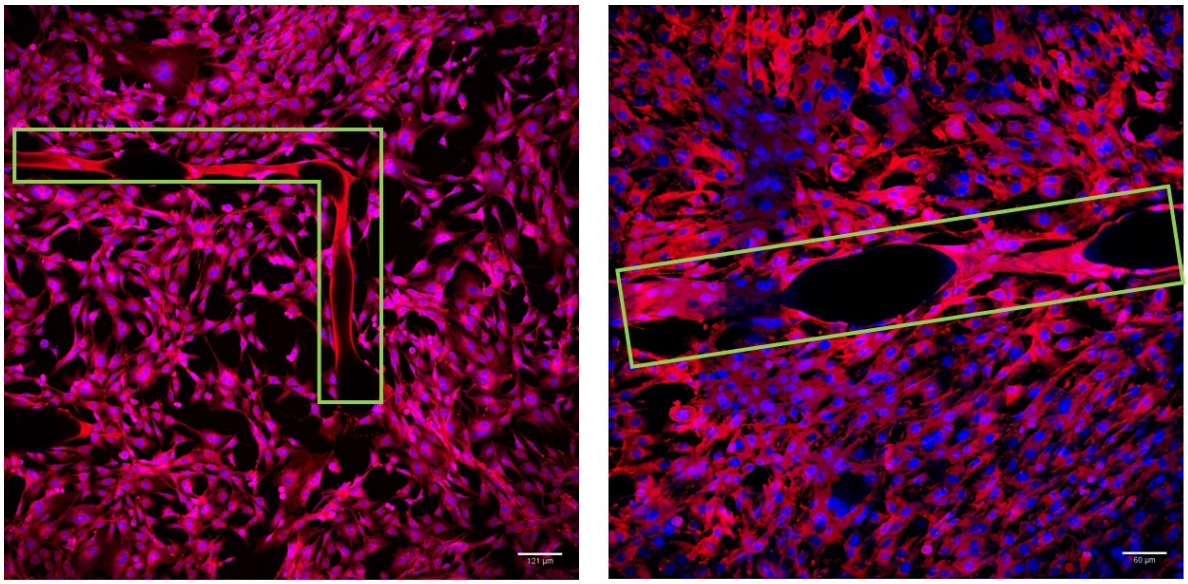


Figure 5.19 Representative images of cell alignment on P2Th3Ozi scaffolds

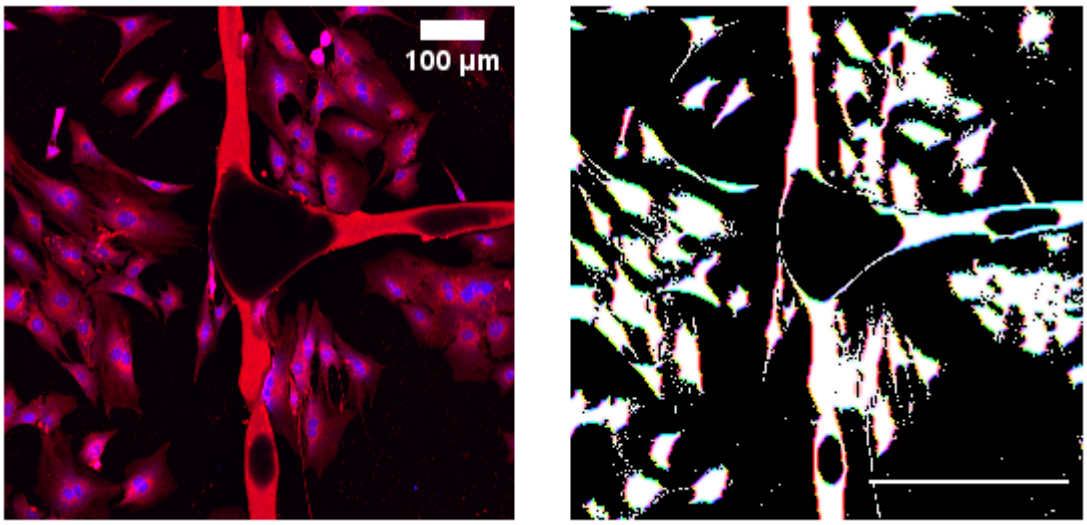


Figure 5.20 Representative image of elongination analysis of P2Th3Ozi scaffolds

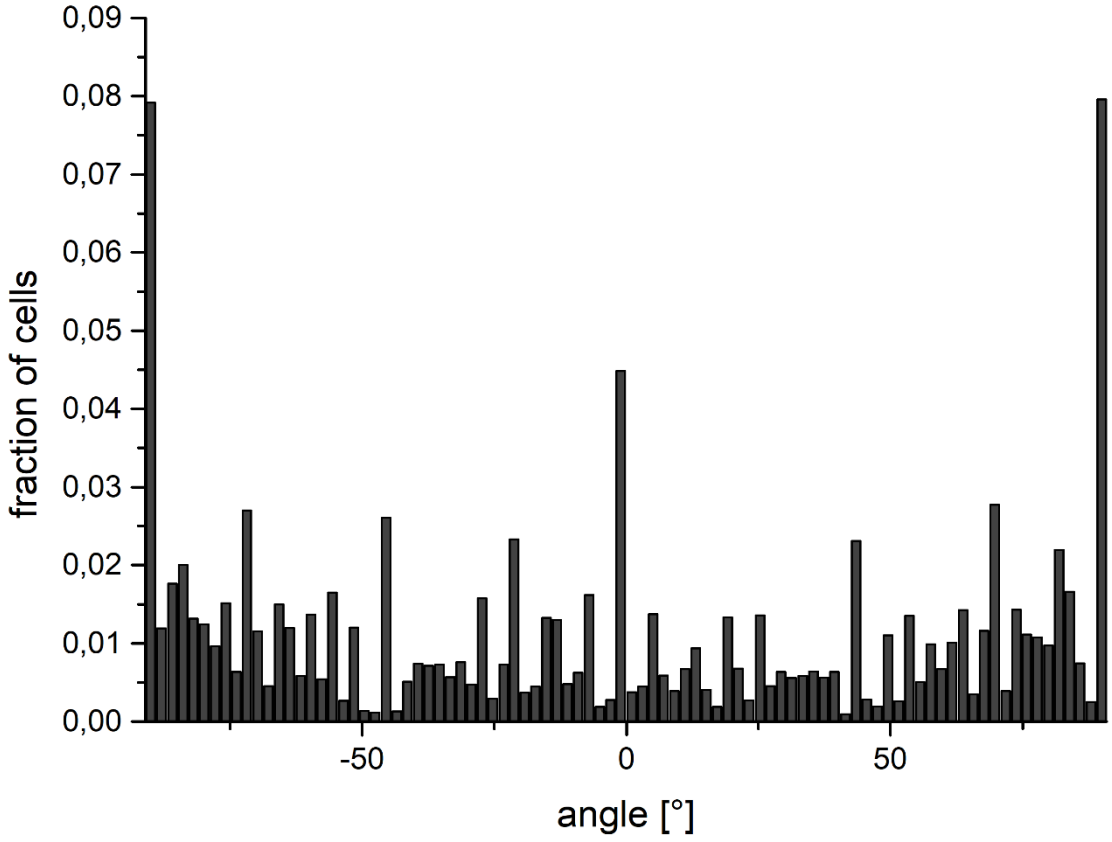


Figure 5.21 Histogram of the relative Cell elongiation measurment

5.4.4 Post-modification of P2Th3Ozi printed scaffolds

In the context of this work, the approach of the post-print modification of PThOzi, which was presented in Chapter 4, was attempted to improve the electrical function of the printed scaffolds. For this purpose,

10-layer structures of a P2Th3Ozi$_{15}$ were placed in a saturated $FeCl_3$ solution. The aim of this approach was to functionally coat the scaffolds with a thin layer of an electroconductive CP without losing the accurate structure of the scaffold. After 24 hours, the scaffolds were washed several times with distilled water and hexane. This was necessary to remove the excess of unbound $FeCl_3$. As shown in Figure 5.22, the cleaning was only partially successful with residual $FeCl_3$ being observed with EDX analysis. This was most prominent in the corners of the scaffolds. Following drying protocols, a colour change to reddish-brown was observed. This colour change could indicate an incorrect ratio between the dopant and the polymer of the scaffold,[284] which was likely due to the saturated iron chloride solution used.[285] In a second step, a drop of EDOT monomer was then placed on the scaffolds. The point of contact turned dark blue immediately. Furthermore, a continuous colour change of the entire scaffold could be perceived for 48 hours. The scaffolds were then washed again with water and hexane to remove unconverted EDOT monomers and again dried in a vacuum (Figure 5.22, b, c). Electrochemical analysis was not able to be carried out due to the fragility of the scaffolds. A comparable analysis was presented in Chapter 4.

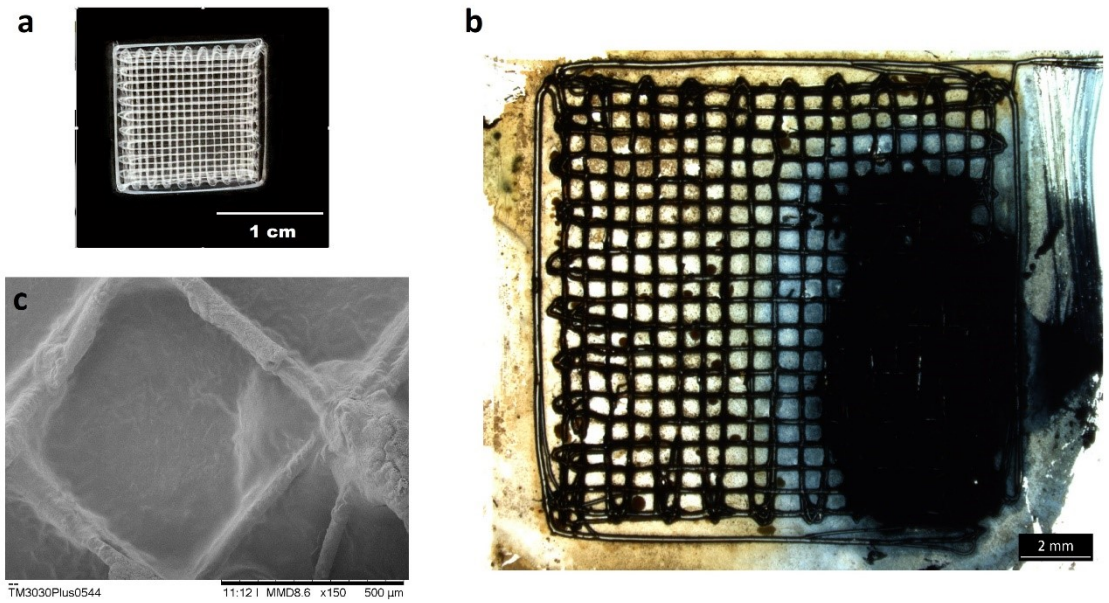


Figure 5.22 a) macroscopic image of printed scaffold untreated, b) light microscopy image of post-modification synthesis, c) SEM image of post-modification scaffolds

As such EDX analysis was performed via SEM to determine the chemical composition of the material formed at the scaffold surface. For this purpose, the scaffolds were analysed without a metallic coating (Figure 5.23). Nevertheless, high resolution SEM of the scaffold was possible, indicating that the blue polymeric material, at least qualitatively resulted in electrical conductivity. It could also be shown that an accurate deposition of iron and chloride on the individual fibres took place. Furthermore, a high sulphur content resulting from the presence of PEDOT in the fibres was visualized. It was found that the original mass ratio of 34:66 in FeCl3 could no longer be detected after addition of EDOT. This can

be explained by the redox reaction of FeCl3, which initiates the polymerisation of the thiophene systems and therefore changes the ratio of iron to chloride (Figure 5.24).

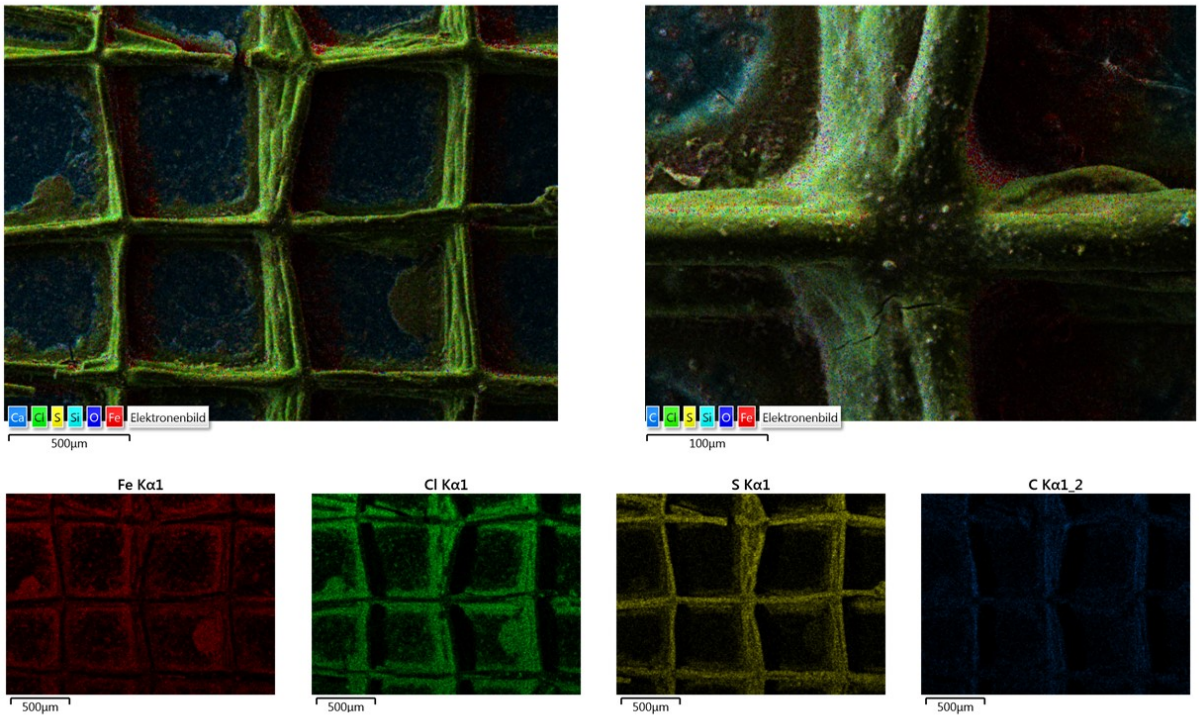


Figure 5.23 EDX SEM analysis of post-modification scaffolds

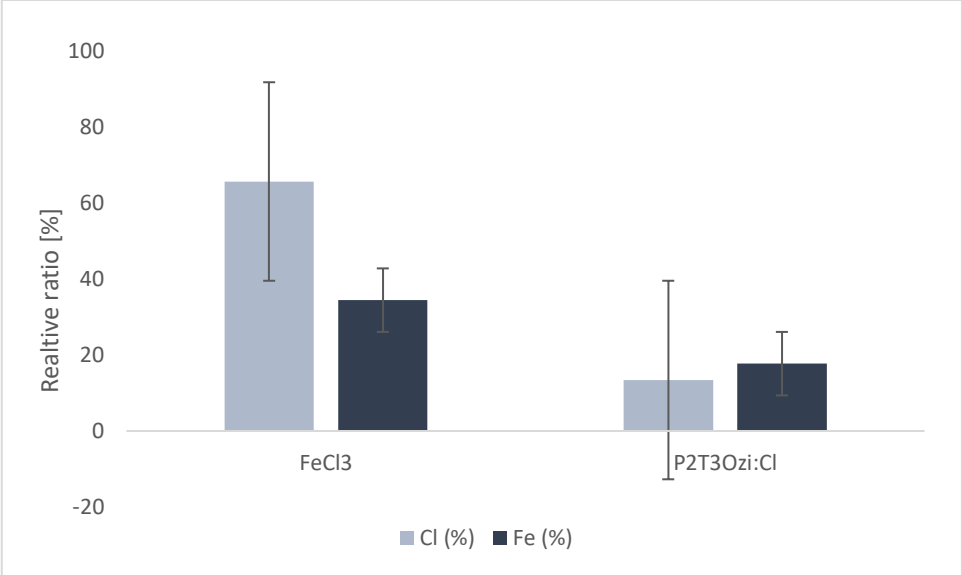


Figure 5.24: Initial ratio of Ironcloride vs P2Th3Ozi:Cl ratio measured by EDX analysis after post-modification

Shanmugapriya et al.[286] investigated the polymerisation of PPy by means of chemical oxidation with potassium chromate and copper nanoparticles. The authors were able to provide quantitative evidence

of copper via EDX analysis. Due to the chemical reaction of the post-print modification and the subsequent washing of the scaffold it is proposed that a coating in the micro to nano range was achieved, with the individual fibres still able to be distinguished from one another.

In a further experiment, it was checked whether the post-print modification can also be used during the printing process. For this purpose, polymer and doping agent $FeCl_3$ was added in a ratio of 3:1 to a pressure syringe and heated to 130 °C for 2 hours. In Figure 5.25 (a) the syringe is shown before and during the printing process. It can be seen that the mixture is black at the beginning (before printing). This is mainly due to the ferric chloride. Furthermore, a change in colour towards reddish brown could be observed during the heating. Figure 5.25 (b) shows the printing test (right) in comparison with printed fibres without ferric chloride additive. It can be observed here that the jet could not be kept stable. The parameters of printing are very different from the printing of pure polymer material. For this reason, no further analysis of the fibres was carried out in this thesis. A clear colouration of the fibres can be seen. Another difficulty of printing electroactive material via MEW 3D printing is the issue of arching. This was slightly recognized during printing and was one reason why the adjustment of printing was very complex.

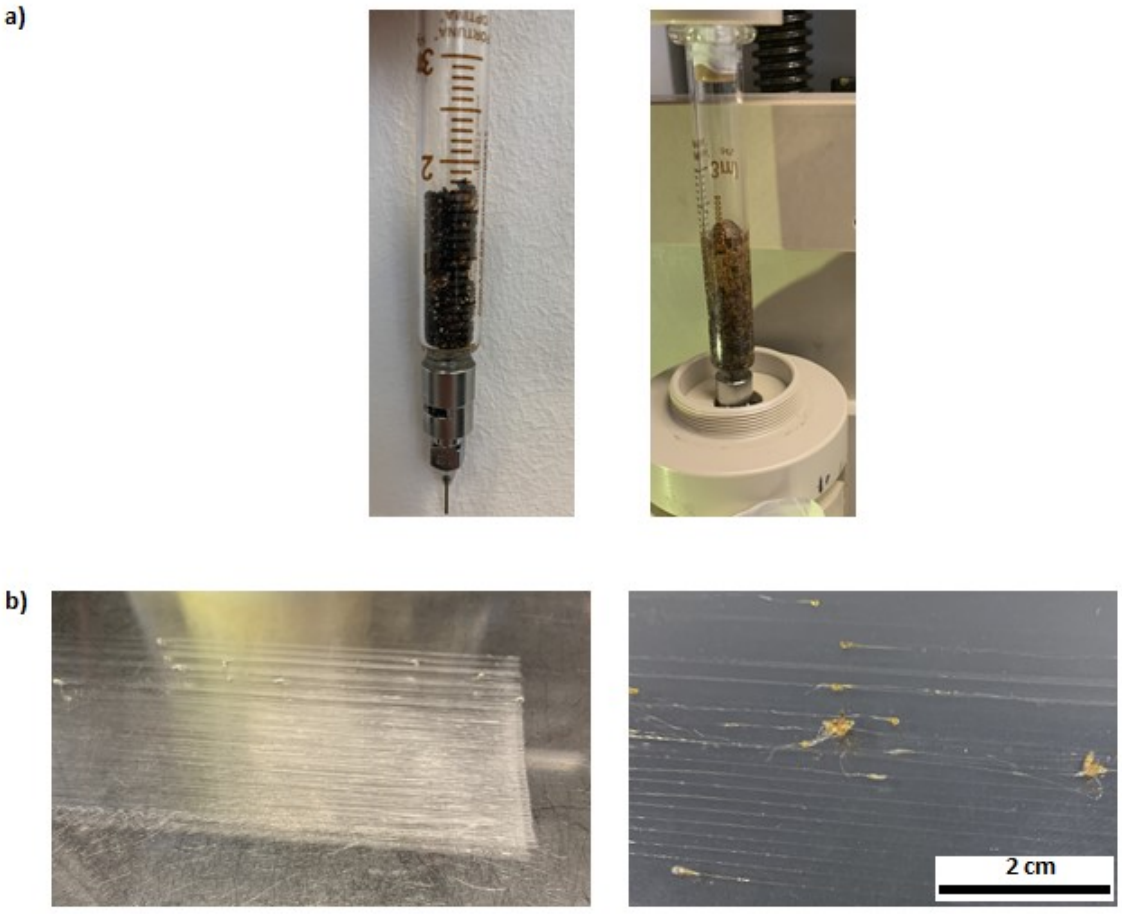


Figure 5.25 a) printing syringe filled with $FeCl_3$ and P2t3Ozi before and after heating for 2 hours, b) comparison of non-treated and with $FeCl_3$ additive printed fibres

This work was a part of a collaboration where coaxial 3D printing of 2 polymer types via MEW was a central objective. In this context, coaxial means the simultaneous printing of two materials in a core-shell format. For this purpose, the consideration was that an electroactive core should be surrounded by an insulating material during the printing process and thus 3D-printed fibres that can function analogously to nerves. Since coaxial printing is the focus of another work, only an outlook is presented here. Figure 5.26 shows the first attempt of coaxial printing with P2Th3Ozi and PVDF. An EDX analysis was useful here, as clear phase separation of the two polymers was possible due to the sulphur and fluorine atoms. Furthermore, it was also possible to distinguish the two polymers from each other purely optically. While P2Th3Ozi has the smooth surface as already shown above, the surface of PVDF was very rough and inhomogeneous.

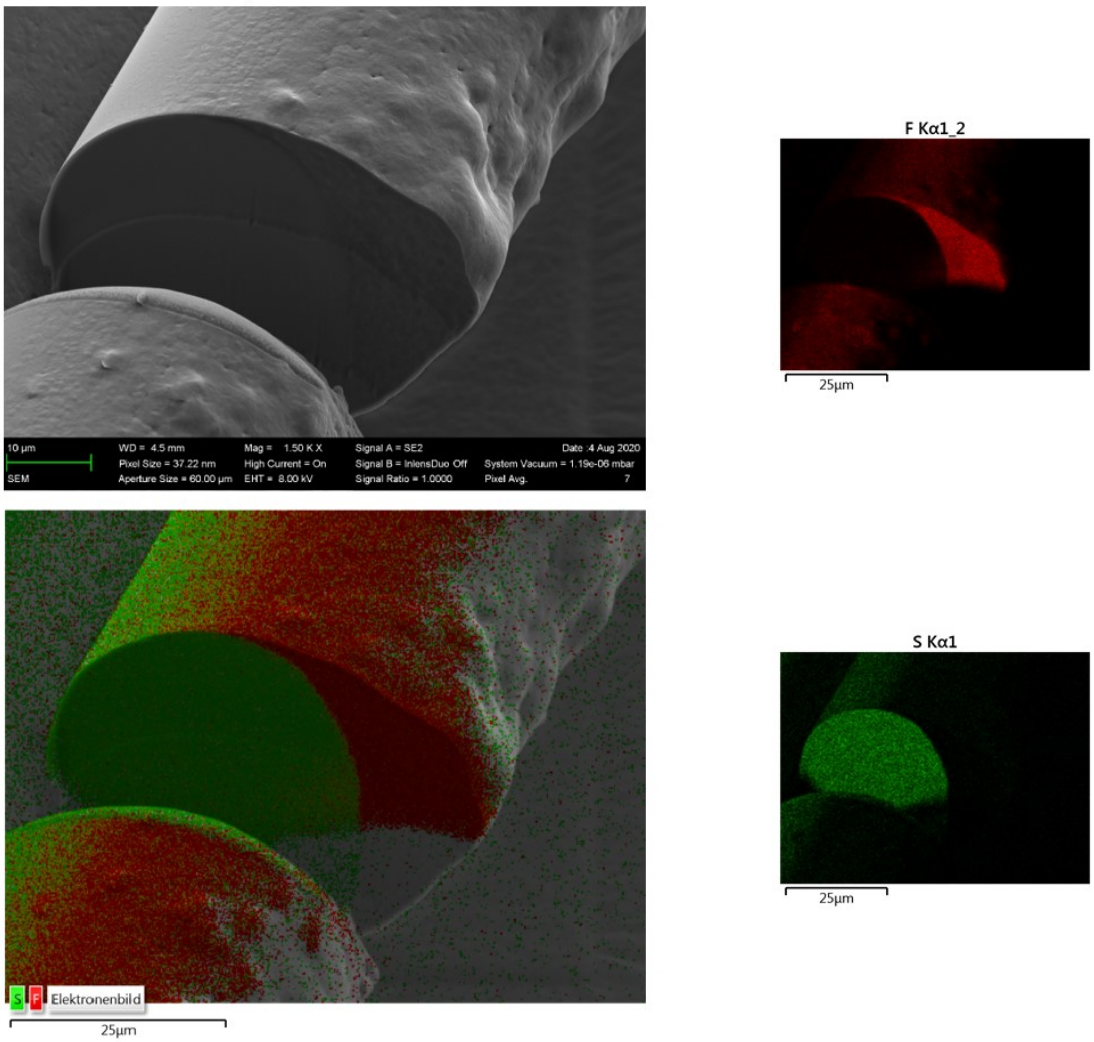


Figure 5.26 EDX SEM analysis of coaxial printed fibres with PVDF and P2t3Ozi

5.5 Conclusion

3D printing is of great importance for tailor-made treatments for patients in the biomedical environment. In addition to the synthesis and analysis of the PThOx and PThOzi platform, the printability of the

material was successfully demonstrated. A high level of accuracy could be achieved here. The printing temperature could be varied over a wide range. Furthermore, the coating of P2Th3Ozi with additional CP was successful and is proposed as a potential mechanism for increasing the overall conductivity.

It was shown that low molar mass P2Th3Ozi as well as their copolymers can be processed via MEW into box-like structures. While fluctuations at low CTS were observed, these could be compensated by printing at a CS above the fluctuation range. A strong influence of the T_g on the processing parameters was found. For instance, a processing temperature prediction corresponding chain length of the homopolymer has proven to allow processing for all polymers. It should be highlighted that the PThOzi and PThOx polymer system offers the straight-forward option for tuning the T_g, while minimizing changes in physiochemical properties like polarizability, thermal stability, chemical reactivity or dispersity. This makes the system an interesting candidate for an in-depth study on how the polymer properties influence MEW processing. The positive results for printing of P2Th3Ozi, indicate that a tuning of the polymer properties is in general possible and enables larger scale opportunities than what was discussed above. With an NT of between 120 – 150 °C, the P2Th3Ozi$_{15}$ homopolymer could be processed at the lowest printing temperature of all polymers. The printed fibres continue to be stable after printing over a time period of more than half a year. Since thermal degradation of CPs, this polymer platform shows long time stability during printing at elevated temperatures. Furthermore, the charge loading, which is essential for the jet forming was possible to keep constant by printing through a gap. The fibre diameter was around 35 µm and stacking of more than 20 layers was possible.

When studying new materials for use in the biomedical field, toxicological studies are essential. it was possible to show that the material was cytocompatible. In addition to toxicity, the affinity of cells in close proximity to the material is also of major concern. In this regard, it was successfully shown that clonal muscle cells were able to adhere, proliferate and grow over a period of more than ten days. In summary, the P2t3Ozi was found to be suitable for further investigations in the context of biomedical applications.

It was possible to control the pore formation during swelling. Furthermore, by treating the scaffold in cold water for 24 hours before swelling at ambient temperature, the structure can be stabilized. For determination of swelling by water, cryo-SEM analysis was performed and water was observed inside the pores. While there was no material change observed by other analysis methods, the swelling of the material is initiated by water.

Finally, it was shown that the post-print addition of CP was transferable to printed scaffolds. A qualitative proof of the electrical conductivity could be shown through SEM analysis. A CV and EIS analysis were omitted due to the fragile nature of the scaffolds. Future work on developing these scaffolds will focus on characterization of the mechanical properties and reinforcement through core-shell printing approaches to develop mechanically stable scaffolds that can be handled.

Chapter 6 – Summary and Outlook

Summary

The main objective of this thesis was to develop a novel material suitable for MEW 3D printing based on POx or POzi and containing electroactive elements from CPs. The focus for application of these new materials was biomedical scaffolds. This goal was achieved by a systematic investigation on the synthesis and characterisation of side-group functionalisation of POzi, POx and CPs based on thiophene. A novel polymer P2Th3Ozi was found to be promising for printed scaffold materials.

Motivated by the chemical versatility as well as the excellent biological properties of POx and POzi a new monomer system based on a thiophene side chain was developed and 8 different monomers were designed and realised. The properties of this material were specifically tailored for the processing by MEW printing. MEW is an emerging technology in the field of biofabrication and has found specific application in scaffold-based tissue engineering. The materials developed throughout this thesis have the potential to expand the number and type of material options employed for MEW printing, with a particular focus on introducing more hydrophilic and softer materials with electroactive components.

The initial chapter was focused on the synthesis of a library of thiophene-based monomers, which in the subsequent chapter, were examined for their ability to be polymerized. The first crystal structures of Ox and Ozi were synthesized and characterised. The polymers were then comprehensively studied to establish their physicochemical properties. It was shown that P2Th3Ozi offered an excellent opportunity for use in 3D printing due to its thermal properties and yield. Critical to the development of a new material with electroactive elements is the electrical performance. It was shown that these materials did not have conductivity comparable to neat CPs or other hybrid CP materials, as the thiophene units were not part of a doped, conjugated bond structure. As such a post-process modification was explored, with the aim of using the thiophene units to initiate growth of longer CP chains within the construct to impart higher conductivity. It was shown that the post-process polymerisation of EDOT could improve the conductivity of the P2Th3Ozi by an order of magnitude. With a focus on tissue engineering applications the biological properties of the bulk polymer were examined, including cytotoxicity through leachable studies. P2Th3Ozi was found to be non-toxic in a cell growth inhibition study following washing procedures to remove reagents used in the synthesis process.

Additive manufacturing is an emerging field in healthcare technologies that is aimed at producing patient specific solutions. The ability to print P2Th3Ozi was considered a critical design criterion, with a focus on MEW, to remove the need for solvents and increase the options available for fabrication of devices from these materials. The printing properties were quantified, and it was shown that both fibres and layered structures were able to be formed with high reliability. Fibres with a diameter of a 30 µm and

up to 20 layers were found to be reproducible. While swelling and pore formation were observed in environments that mimic biological conditions (100% humidity and 37°C), these properties could be controlled by post-fabrication thermal treatments. Controlled swelling was used to create pores of different sizes in the scaffold.

The ability for cells to interact with printed scaffolds of P2Th3Ozi was investigated through a direct contact assay with a skeletal muscle cell line. Cells were found to proliferate in close proximity to the scaffold, with some alignment observed when cells were in contact with the layered structured. The fine structure of the scaffolds were not maintained, as swelling and deformation occurred due to the increased temperature and aqueous environment. Despite evidence of deformation and erosion, there was no detectable impact on the cell growth.

In conclusion, a novel library of thiophene-based POx and POzi was developed within this thesis and found to be a promising platform for future investigations of biomedical electroactive materials. The physiochemical properties of P2Th3Ozi are widely adjustable and suitable for a broad application area. In the scope of this work, a fundamental understanding of this material class was achieved. To our knowledge, it was the first material with electroactive components that could be processed in 3D printing without additional materials such as solvents or plasticizers. Furthermore, either before printing or in post-modification steps, it was possible to control and improve the electrochemical properties and the pore sizes of the material. The understanding of the material properties developed in this work, build a broad platform for future work and the design of new electroactive materials.

Outlook

This work forms the basis for electroactive and printable materials. Because of the breadth of this class of molecules, there remains substantial outlook for future investigations and development. The main factor, which was only briefly explored in the context of this work and which should play an important role in future work, is the possibility of direct printing the more electroactive variant of the material. Further research should also include optimization of reaction conditions to enable upscaling, improvement of mechanical and electrical properties of the bulk material and scaffold structures, and an in-depth investigation of cell-material interactions.

While the focus of this work was on the investigation of P2Th3Ozi, the other polymers of thiophene-based POx and POzi class were not explored in latter chapters due to low yield. The improvement of the synthesis pathways to increase reaction efficiency and hence yield has the potential to enable a greater range of starting monomers for MEW printing. During the synthesis design and subsequent reactions it was found that the use of benzontrile as a solvent was not optimal. Although the solvent can be removed through careful purification steps, it has restrictions. By exploring other synthetic routes for the monomers, such as those reported by Aoi et al.[167], an optimization of the yield could be made possible.

Other synthetic routes could also allow the introduction of EDOT as a side group, such as the introduction of functional groups through the use of aldehydes. Taubman et al.[196] were able to introduce a wide variety of functional groups using this approach. Finally, it would be of interest whether the concept of thiophene-based side groups presented here can also be transferred to other polymerisation options such as RAFT polymerisation and thus open up further 3D printing methods such as DLS.

It is necessary to investigate the material properties and understand the available approaches for tuning or modifying these material characteristics. During these studies it was found that the P2Th3Ozi was quite brittle. A possible approach to improve these aspects, would be to blend or co-polymerise with other materials. This can be done either by simple mixing or by chemical means. For mechanical tuning, to improve flexibility copolymerisation would be of interest. Rietzau-Ried et al.[211] was able to make PEDOT oligomers significantly softer by copolymerizing with PCL. However, the introduction of components that are insulative will be of detriment to the electroactivity of the final scaffold. It is likely that there will need to be a trade-off between the desired scaffold properties to ensure that materials are both mechanically pliable and electroactive.

The electrical conductivity of both the bulk P2Th3Ozi and scaffold was found to be limited. Improving the electrical properties could be approached through the introduction of polymeric complexes that also dope the polymer, analogous to PEDOT:PSS.[287] As an alternative to PSS, various other polyanions can also be used.[288] In addition to the improving the electrical conductivity, this could also improve other physicochemical properties of the material,[289] by introducing mechanically flexible phases. A MEW print compatible polymer-based dopant should be chosen, with a focus on maintaining the macroscopic homogeneity of the material system during heating in the print head. Finally, acid-based or solvent-based additives could be used to improve conductivity. In this context, Lingstedt et al.[231] investigated the effect of DMSO on the conductivity of PEDOT:PSS. The authors found that even small amounts of solvent can improve the chain arrangement of the system and thus increase the conductivity. To further optimize the electrical conductivity, a quantitative investigation of doping and its influence on electrical conductivity is necessary.

Any change in the material properties has a direct influence on the printability of the material. Therefore, when material changes are made, the printing capabilities must also be adapted and can be optimised at the same time. Small changes in material compositions have a big impact on printability. The printing parameters such as pressure, tension and humidity also have a significant influence. Initial studies on other thiophene-based POx and POzi, which were during this thesis (but not presented), suggest that the principles for printing P2Th3Ozi apply to these polymers as well. In addition, different monomers can be combined in copolymers and thus significantly influence the properties in a targeted manner. In this context, it would be of great interest to introduce acrylic side groups to enable radical polymerisation and thereby further 3D printing technologies such as DLS. The use of small amounts of solvent could

be a good approach to improve the printability of the P2Th3Ozi. Guo et al.[290] were able to improve the printing properties of PLGA by using small amounts of DMSO, which could be reversibly removed after printing. This could also reduce the printing temperature and thus protect the material.

The use of solvents allows a wider range of printing techniques. Thus, other techniques might be developed with the thiophene-based POx and POzi. Park et al. were able to show that PEDOT:PSS could be processed via inkjet printing by using sorbitol. While the focus of 3D printing was on the MEW method within the scope of this work, it would also be of interest whether the new material could be used in other printing techniques such as FDM, SLS or SLM.

Since only an introductory cytotoxic examination and an alignment study were carried out, the next step would be to expand the biologically relevant analysis. For a targeted application in tissue engineering and regeneration, it would be interesting to use primary cell cultures in addition to the cell line. P2Th3Ozi offers a good platform for this, as the controlled pore shaping allows the surface area to be increased and the required material reduced while maintaining the same volume expansion. Consequently, tissue regeneration could be stimulated more efficiently due to the direct contact area. Even though it was shown that P2Th3Ozi is non-toxic, a non-toxic dopant must also be found to improve the conductivity for targeted electrical stimulation. Ultimately, it is proposed that through 3D printing, biomimetic structures can be created to initiate and guide muscle tissue regeneration. Targeted electrical stimulation in the literature has been shown to stimulate cell growth and thus enable faster regeneration. Patel et al.[291] showed that cell growth of C2C12 myoblasts in a laminin-based polydimethylsiloxane matrix could be promoted through electrical stimulation. Following the optimisation of electrical properties, the next phase of this project will focus on understanding the impact of electrical stimulation and its influence on cell growth.

Electrically active polymers have great potential for a wide variety of applications in both biomedical and technical fields. A well-founded and comprehensive analysis is essential to establish CPs as an alternative in the commercial environment. This work was able to successfully synthesize a new material class, present a detailed characterization, and, thus, enable a possible use of this material in future research projects. Future research efforts should stride to address the challenges related to the processibility of CPs without compromising their electroactive properties. The continued development of these technologies will be essential to realising their full potential and successful translation into impactful clinical technologies.

Chapter 7 Bibliography

[1] Ahmad, N.; Thomas, G.N.; Gill, P.; Chan, C.; Torella, F. Lower limb amputation in England: prevalence, regional variation and relationship with revascularisation, deprivation and risk factors. A retrospective review of hospital data. J. R. Soc. Med. **2014**, *107*(12), 483–489.

[2] Nerlich, A.G.; Zink, A.; Szeimies, U.; Hagedorn, H.G. Ancient Egyptian prosthesis of the big toe. Lancet **2000**, *356*(9248), 2176–2179.

[3] Binedell, T.; Meng, E.; Subburaj, K. Design and development of a novel 3D-printed non-metallic self-locking prosthetic arm for a forequarter amputation. Prosthetics Orthot. Int. **2021**, *45*(1), 94–99.

[4] Ghasemi-Mobarakeh, L.; Prabhakaran, M.P.; Morshed, M.; Nasr-Esfahani, M.H.; Baharvand, H.; Kiani, S.; Al-Deyab, S.S.; Ramakrishna, S. Application of conductive polymers, scaffolds and electrical stimulation for nerve tissue engineering. J. Tissue Eng. Regen. Med. **2011**, *5*(4), e17-35.

[5] Shah, A.M.; Kadir, M.R.A.; Razak, S.I.A. Novel PLA-Based Conductive Polymer Composites for Biomedical Applications. JOM **2017**, *69*(12), 2838–2843.

[6] Zhan, C.; Yu, G.; Lu, Y.; Wang, L.; Wujcik, E.; Wei, S. Conductive polymer nanocomposites: a critical review of modern advanced devices. J. Mater. Chem. C **2017**, *5*(7), 1569–1585.

[7] Pires, F.; Ferreira, Q.; Rodrigues, C.A.V.; Morgado, J.; Ferreira, F.C. Neural stem cell differentiation by electrical stimulation using a cross-linked PEDOT substrate: Expanding the use of biocompatible conjugated conductive polymers for neural tissue engineering. Biochim. Biophys. Acta - Gen. Subj. **2015**, *1850*(6), 1158–1168.

[8] Jin, L.; Wang, T.; Feng, Z.-Q.; Leach, M.K.; Wu, J.; Mo, S.; Jiang, Q. A facile approach for the fabrication of core–shell PEDOT nanofiber mats with superior mechanical properties and biocompatibility. J. Mater. Chem. B **2013**, *1*(13), 1818.

[9] Guo, B.; Glavas, L.; Albertsson, A.-C. Biodegradable and electrically conducting polymers for biomedical applications. Prog. Polym. Sci. **2013**, *38*(9), 1263–1286.

[10] Green, R.A.; Hassarati, R.T.; Goding, J.A.; Baek, S.; Lovell, N.H.; Martens, P.J.; Poole-Warren, L.A. Conductive hydrogels: mechanically robust hybrids for use as biomaterials. Macromol. Biosci. **2012**, *12*(4), 494–501.

[11] Green, R.A.; Lovell, N.H.; Poole-Warren, L.A. Impact of co-incorporating laminin peptide dopants and neurotrophic growth factors on conducting polymer properties. Acta Biomater. **2010**, *6*(1), 63–71.

[12] Wang, X.-S.; Tang, H.-P.; Li, X.-D.; Hua, X. Investigations on the Mechanical Properties of Conducting Polymer Coating-Substrate Structures and Their Influencing Factors. Int. J. Mol. Sci. **2009**, *10*(12), 5257–5284.

[13] Moser, M.; Ponder, J.F.; Wadsworth, A.; Giovannitti, A.; McCulloch, I. Materials in Organic Electrochemical Transistors for Bioelectronic Applications: Past, Present, and Future. Adv. Funct. Mater. **2019**, *29*(21), 1807033.

[14] Sun, K.; Zhang, S.; Li, P.; Xia, Y.; Zhang, X.; Du, D.; Isikgor, F.H.; Ouyang, J. Review on application of PEDOTs and PEDOT:PSS in energy conversion and storage devices. J. Mater. Sci. Mater. Electron. **2015**, *26*(7), 4438–4462.

[15] Green, R. Elastic and conductive hydrogel electrodes. Nat. Biomed. Eng. **2019**, *3*(1), 9–10.

[16] Ambrosio, L.; Santis, R. De; Nicolais, L. Composite hydrogels for implants. Proc. Inst. Mech. Eng. Part H J. Eng. Med. **1998**, *212*(2), 93–99.

[17] Kopecek, J. Hydrogels: From soft contact lenses and implants to self-assembled nanomaterials. J. Polym. Sci. Part A Polym. Chem. **2009**, *47*(22), 5929–5946.

[18] Giannetti, S.; Lauretti, L.; Fernandez, E.; Salvinelli, F.; Tamburrini, G.; Pallini, R. Acrylic hydrogel implants after spinal cord lesion in the adult rat. Neurol. Res. **2001**, *23*(4), 405–409.

[19] Teng, C.; Lu, X.; Ren, G.; Zhu, Y.; Wan, M.; Jiang, L. Underwater Self-Cleaning PEDOT-PSS Hydrogel Mesh for Effective Separation of Corrosive and Hot Oil/Water Mixtures. Adv. Mater. Interfaces **2014**, *1*(6), 1400099.

[20] Aggas, J.R.; Abasi, S.; Phipps, J.F.; Podstawczyk, D.A.; Guiseppi-Elie, A. Microfabricated and 3-D printed electroconductive hydrogels of PEDOT:PSS and their application in bioelectronics. Biosens. Bioelectron. **2020**, *168*, 112568.

[21] Wang, Y.; Zhu, C.; Pfattner, R.; Yan, H.; Jin, L.; Chen, S.; Molina-Lopez, F.; Lissel, F.; Liu, J.; Rabiah, N.I.; Chen, Z.; Chung, J.W.; Linder, C.; Toney, M.F.; Murmann, B.; Bao, Z. A highly stretchable, transparent, and conductive polymer. Sci. Adv. **2017**, *3*(3), e1602076.

[22] Heck, J.; Goding, J.; Lara, R.P.; Green, R. The Influence of Physicochemical Properties on the Processibility of Conducting Polymers: A Bioelectronics Perspective. Acta Biomater. **2021**.

[23] Lorson, T.; Lübtow, M.M.; Wegener, E.; Haider, M.S.; Borova, S.; Nahm, D.; Jordan, R.; Sokolski-Papkov, M.; Kabanov, A. V.; Luxenhofer, R. Poly(2-oxazoline)s based biomaterials: A comprehensive and critical update. Biomaterials **2018**, *178*, 204–280.

[24] Glassner, M.; Vergaelen, M.; Hoogenboom, R. Poly(2-oxazoline)s: A comprehensive overview of polymer structures and their physical properties. Polym. Int. **2018**, *67*(1), 32–45.

[25] Hu, C.; Hahn, L.; Yang, M.; Altmann, A.; Stahlhut, P.; Groll, J.; Luxenhofer, R. Improving printability of a thermoresponsive hydrogel biomaterial ink by nanoclay addition. J. Mater. Sci. **2021**, *56*(1), 691–705.

[26] Hahn, L.; Maier, M.; Stahlhut, P.; Beudert, M.; Flegler, V.; Forster, S.; Altmann, A.; Töppke, F.; Fischer, K.; Seiffert, S.; Böttcher, B.; Lühmann, T.; Luxenhofer, R. Inverse Thermogelation of Aqueous Triblock Copolymer Solutions into Macroporous Shear-Thinning 3D Printable Inks. ACS Appl. Mater. Interfaces **2020**, *12*(11), 12445–12456.

[27] Kade, J.C.; Dalton, P.D. Polymers for Melt Electrowriting. Adv. Healthc. Mater. **2021**, *10*(1), 2001232.

[28] Hochleitner, G.; Hümmer, J.F.; Luxenhofer, R.; Groll, J. High definition fibrous poly(2-ethyl-2-oxazoline) scaffolds through melt electrospinning writing. Polymer (Guildf). **2014**, *55*(20), 5017–5023.

[29] Nahm, D.; Weigl, F.; Schaefer, N.; Sancho, A.; Frank, A.; Groll, J.; Villmann, C.; Schmidt, H.-W.; Dalton, P.D.; Luxenhofer, R. A versatile biomaterial ink platform for the melt electrowriting of chemically-crosslinked hydrogels. Mater. Horizons **2020**, *7*(3), 928–933.

[30] Ma, C.; Jiang, L.; Wang, Y.; Gang, F.; Xu, N.; Li, T.; Liu, Z.; Chi, Y.; Wang, X.; Zhao, L.; Feng, Q.; Sun, X. 3D Printing of Conductive Tissue Engineering Scaffolds Containing Polypyrrole Nanoparticles with Different Morphologies and Concentrations. Materials (Basel). **2019**, *12*(15), 2491.

[31] Irimia-Vladu, M.; D. Glowacki, E.; S. Sariciftci, N.; Bauer, S. *Green Materials for Electronics*. Wiley-VCH Verlag GmbH & Co. KGaA: Weinheim, Germany, 2017.

[32] Molino, P.J.; Wallace, G.G. Next generation bioelectronics: Advances in fabrication coupled with clever chemistries enable the effective integration of biomaterials and organic conductors. APL Mater. **2015**, *3*(1), 014913.

[33] Jia, M.; Rolandi, M. Soft and Ion-Conducting Materials in Bioelectronics: From Conducting Polymers to Hydrogels. Adv. Healthc. Mater. **2020**, *9*(5), 1901372.

[34] Bolto, B.; McNeill, R.; Weiss, D. Electronic Conduction in Polymers. III. Electronic Properties of Polypyrrole. Aust. J. Chem. **1963**, *16*(6), 1090.

[35] Pron, A.; Rannou, P. Processible conjugated polymers: from organic semiconductors to organic

metals and superconductors. Prog. Polym. Sci. **2002**, *27*(1), 135–190.

[36] Zhu, Z.; Liu, C.; Xu, J.; Jiang, Q.; Shi, H.; Liu, E. Improving the electrical conductivity of PEDOT:PSS films by binary secondary doping. Electron. Mater. Lett. **2016**, *12*(1), 54–58.

[37] Jeong, S.-H.; Ahn, S.; Lee, T.-W. Strategies to Improve Electrical and Electronic Properties of PEDOT:PSS for Organic and Perovskite Optoelectronic Devices. Macromol. Res. **2019**, *27*(1), 2–9.

[38] Kaynak, A.; Rintoul, L.; George, G.A. Change of mechanical and electrical properties of polypyrrole films with dopant concentration and oxidative aging. Mater. Res. Bull. **2000**, *35*(6), 813–824.

[39] Leclerc, M.; Faid, K. Electrical and optical properties of Processable Polythiophene Derivatives: Structure-Property relationships. Adv. Mater. **1997**, *9*(14), 1087–1094.

[40] Dong, H.; Hu, W. Conducting Polymers: Applications in Electronics and Photovoltaics. In *Encyclopedia of Radicals in Chemistry, Biology and Materials*; John Wiley & Sons, Ltd: Chichester, UK, 2012; .

[41] Gustafsson, G.; Cao, Y.; Treacy, G.M.; Klavetter, F.; Colaneri, N.; Heeger, A.J. Flexible light-emitting diodes made from soluble conducting polymers. Nature **1992**, *357*(6378), 477–479.

[42] Onoda, M.; MacDiarmid, A.G. Light-emitting diodes using n-type conducting polymer. Synth. Met. **1997**, *91*(1–3), 307–309.

[43] Kim, W.H.; Mäkinen, A.J.; Nikolov, N.; Shashidhar, R.; Kim, H.; Kafafi, Z.H. Molecular organic light-emitting diodes using highly conducting polymers as anodes. Appl. Phys. Lett. **2002**, *80*(20), 3844–3846.

[44] Jiang, D.; Murugadoss, V.; Wang, Y.; Lin, J.; Ding, T.; Wang, Z.; Shao, Q.; Wang, C.; Liu, H.; Lu, N.; Wei, R.; Subramania, A.; Guo, Z. Electromagnetic Interference Shielding Polymers and Nanocomposites - A Review. Polym. Rev. **2019**, *59*(2), 280–337.

[45] Collins, G.E.; Buckley, L.J. Conductive polymer-coated fabrics for chemical sensing. Synth. Met. **1996**, *78*(2), 93–101.

[46] Lange, U.; Roznyatovskaya, N. V; Mirsky, V.M. Conducting polymers in chemical sensors and arrays. Anal. Chim. Acta **2008**, *614*(1), 1–26.

[47] Miasik, J.J.; Hooper, A.; Tofield, B.C. Conducting polymer gas sensors. J. Chem. Soc. Faraday Trans. 1 Phys. Chem. Condens. Phases **1986**, *82*(4), 1117.

[48] Onoda, M.; Abe, Y.; Tada, K.; Kawakita, Y.; Fujisato, T.; Uto, S. Conductive Polymers as Bioelectronic Materials. Electron. Commun. Japan **2013**, *96*(12), 24–31.

[49] Gnanasekaran, K.; Heijmans, T.; Bennekom, S. van; Woldhuis, H.; Wijnia, S.; With, G. de; Friedrich, H. 3D printing of CNT- and graphene-based conductive polymer nanocomposites by fused deposition modeling. Appl. Mater. Today **2017**, *9*, 21–28.

[50] Ruiz, J.; Gonzalo, B.; Dios, J.R.; Laza, J.M.; Vilas, J.L.; León, L.M. Improving the Processability of Conductive Polymers: The Case of Polyaniline. Adv. Polym. Technol. **2013**, *32*(S1), E180–E188.

[51] Rehahn, M. Elektrisch leitfähige Kunststoffe: Der Weg zu einer neuen Materialklasse. Chemie unserer Zeit **2003**, *37*(1), 18–30.

[52] Menke, K.; Roth, S. Metallisch leitfähige Polymere I. Chemie unserer Zeit **1986**, *20*(1), 1–10.

[53] Noelle Monique Wrubbel. Elektrisch Leitfähige Polymere Auf Basis von Flüssigkristallinen Thiophenderivaten, 2004.

[54] MacDiarmid, A.G. „Synthetische Metalle“: eine neue Rolle für organische Polymere (Nobel-Vortrag). Angew. Chemie **2001**, *113*(14), 2649–2659.

[55] Han, Y.; Fei, Z.; Lin, Y.-H.; Martin, J.; Tuna, F.; Anthopoulos, T.D.; Heeney, M. Anion-induced N-doping of naphthalenediimide polymer semiconductor in organic thin-film transistors. npj Flex. Electron. **2018**, *2*(1), 11.

[56] Wang, S.; Sun, H.; Ail, U.; Vagin, M.; Persson, P.O.Å.; Andreasen, J.W.; Thiel, W.; Berggren, M.; Crispin, X.; Fazzi, D.; Fabiano, S. Thermoelectric Properties of Solution-Processed n-Doped Ladder-Type Conducting Polymers. Adv. Mater. **2016**, *28*(48), 10764–10771.

[57] Lu, Y.; Wang, J.-Y.; Pei, J. Strategies To Enhance the Conductivity of n-Type Polymer Thermoelectric Materials. Chem. Mater. **2019**, *31*(17), 6412–6423.

[58] Le, T.-H.; Kim, Y.; Yoon, H. Electrical and Electrochemical Properties of Conducting Polymers. Polymers (Basel). **2017**, *9*(12), 150.

[59] Shirakawa, H.; Louis, E.J.; MacDiarmid, A.G.; Chiang, C.K.; Heeger, A.J. Synthesis of electrically conducting organic polymers: halogen derivatives of polyacetylene, (CH) x. J. Chem. Soc. Chem. Commun. **1977**, (16), 578.

[60] Zhang, Z. A convenient route to polyacrylonitrile/silver nanoparticle composite by simultaneous polymerization--reduction approach. Polymer (Guildf). **2001**, *42*(19), 8315–8318.

[61] Li, X.; Zhao, Y.; Feng, Z.; Xiang, X.; Wang, S.; Xie, X.; Ramani, V.K. Ring-opening metathesis polymerization for the preparation of polynorbornene-based proton exchange membranes with high proton conductivity. J. Memb. Sci. **2017**, *528*, 55–63.

[62] Yusof, N.; Ismail, A.F. Post spinning and pyrolysis processes of polyacrylonitrile (PAN)-based carbon fiber and activated carbon fiber: A review. J. Anal. Appl. Pyrolysis **2012**, *93*, 1–13.

[63] Park, C.-S.; Kim, D.H.; Shin, B.J.; Kim, D.Y.; Lee, H.-K.; Tae, H.-S. Conductive Polymer Synthesis with Single-Crystallinity via a Novel Plasma Polymerization Technique for Gas Sensor Applications. Mater. (Basel, Switzerland) **2016**, *9*(10).

[64] Bunting, R.K.; Swarat, K.; Yan, D.; Finello, D. Synthesis and Characterization of a Conducting Polymer: An Electrochemical Experiment for General Chemistry. J. Chem. Educ. **1997**, *74*(4), 421.

[65] Heinze, J.; Frontana-Uribe, B.A.; Ludwigs, S. Electrochemistry of Conducting Polymers—Persistent Models and New Concepts †. Chem. Rev. **2010**, *110*(8), 4724–4771.

[66] Hammerich, O.; Lund, H. (Eds). *Organic Electrochemistry*. CRC Press: , 2000.

[67] Zhou, M.; Pagels, M.; Geschke, B.; Heinze, J. Electropolymerization of Pyrrole and Electrochemical Study of Polypyrrole. 5. Controlled Electrochemical Synthesis and Solid-State Transition of Well-Defined Polypyrrole Variants. J. Phys. Chem. B **2002**, *106*(39), 10065–10073.

[68] Diaz, A.F.; Kanazawa, K.K.; Gardini, G.P. Electrochemical polymerization of pyrrole. J. Chem. Soc. Chem. Commun. **1979**, (14), 635.

[69] Diaz, A.F.; Rubinson, J.F.; Mark, H.B. Electrochemistry and electrode applications of electroactive/conductive polymers. 1988; 113–139.

[70] Chen, X.; Inganäs, O. Doping-induced volume changes in poly(3-octylthiophene) solids and gels. Synth. Met. **1995**, *74*(2), 159–164.

[71] Kumar, S.; Pande, S.; Verma, P. *In Factor Effecting Electro-Deposition Process*, 2015.

[72] Naseri, M.; Fotouhi, L.; Ehsani, A. Recent Progress in the Development of Conducting Polymer-Based Nanocomposites for Electrochemical Biosensors Applications: A Mini-Review. Chem. Rec. **2018**, *18*(6), 599–618.

[73] Chen, S.; Liu, H.; Wang, Y.; Xu, S.; Liu, W.; He, D.; Liu, X.; Liu, J.; Hu, C. Electrochemical Capacitance of Spherical Nanoparticles Formed by Electrodeposition of Intrinsic Polypyrrole onto Au Electrode. Electrochim. Acta **2017**, *232*, 72–79.

[74] Barisci, J.N.; Stella, R.; Spinks, G.M.; Wallace, G.G. Characterisation of the topography and surface potential of electrodeposited conducting polymer films using atomic force and electric force microscopies. Electrochim. Acta **2000**, *46*(4), 519–531.

[75] Rao, S. Adhesion molecule-modified biomaterials for neural tissue engineering. Front. Neuroeng. **2009**, *2*.

[76] Jyothibasu, J.P.; Lee, R.-H. Green synthesis of polypyrrole tubes using curcumin template for excellent electrochemical performance in supercapacitors. J. Mater. Chem. A **2020**, *8*(6), 3186–3202.

[77] Sabury, S.; Collier, G.S.; Ericson, M.N.; Kilbey, S.M. Synthesis of a soluble adenine-functionalized polythiophene through direct arylation polymerization and its fluorescence responsive behavior. Polym. Chem. **2020**, *11*(4), 820–829.

[78] Bandeira, R.M.; Silva, D.D. da; Khalid, M.; Tremiliosi-Filho, G. Synthesis of polyaniline/5-sulfosalicylic acid composite and it's electrochemical properties. Mater. Sci. Energy Technol. **2020**, *3*, 487–493.

[79] Khalid, H.; Yu, H.; Wang, L.; Amer, W.A.; Akram, M.; Abbasi, N.M.; Ul-Abdin, Z.; Saleem, M. Synthesis of ferrocene-based polythiophenes and their applications. Polym. Chem. **2014**, *5*(24), 6879–6892.

[80] Peng, H.; Sun, X.; Weng, W.; Fang, X. Synthesis and Design of Conjugated Polymers for Organic Electronics. In *Polymer Materials for Energy and Electronic Applications*; Elsevier, 2017; 9–61.

[81] MacDiarmid, A.G. "Synthetic metals": a novel role for organic polymers. Curr. Appl. Phys. **2001**, *1*(4–5), 269–279.

[82] Chiang, C.K.; Fincher, C.R.; Park, Y.W.; Heeger, A.J.; Shirakawa, H.; Louis, E.J.; Gau, S.C.; MacDiarmid, A.G. Electrical Conductivity in Doped Polyacetylene. Phys. Rev. Lett. **1977**, *39*(17), 1098–1101.

[83] Jeffries-EL, M.; Sauvé, G.; McCullough, R.D. In-Situ End-Group Functionalization of Regioregular Poly(3-alkylthiophene) Using the Grignard Metathesis Polymerization Method. Adv. Mater. **2004**, *16*(12), 1017–1019.

[84] Liu, J.; McCullough, R.D. End Group Modification of Regioregular Polythiophene through Postpolymerization Functionalization. Macromolecules **2002**, *35*(27), 9882–9889.

[85] Martin, K.L.; Nyquist, Y.; Burnett, E.K.; Briseno, A.L.; Carter, K.R. Surface Grafting of Functionalized Poly(thiophene)s Using Thiol–Ene Click Chemistry for Thin Film Stabilization. ACS Appl. Mater. Interfaces **2016**, *8*(44), 30543–30551.

[86] Bhatt, M.P.; Magurudeniya, H.D.; Sista, P.; Sheina, E.E.; Jeffries-EL, M.; Janesko, B.G.; McCullough, R.D.; Stefan, M.C. Role of the transition metal in Grignard metathesis polymerization (GRIM) of 3-hexylthiophene. J. Mater. Chem. A **2013**, *1*(41), 12841.

[87] Balint, R.; Cassidy, N.J.; Cartmell, S.H. Conductive polymers: Towards a smart biomaterial for tissue engineering. Acta Biomater. **2014**, *10*(6), 2341–2353.

[88] Kleis, J.; Schröder, E. Van der Waals interaction of simple, parallel polymers. J. Chem. Phys. **2005**, *122*(16), 164902.

[89] Xiao, S.; Nguyen, M.; Gong, X.; Cao, Y.; Wu, H.; Moses, D.; Heeger, A.J. Stabilization of Semiconducting Polymers with Silsesquioxane. Adv. Funct. Mater. **2003**, *13*(1), 25–29.

[90] Kim, D.Y.; Lee, J.Y.; Moon, D.K.; Kim, C.Y. Stability of reduced polypyrrole. Synth. Met. **1995**, *69*(1–3), 471–474.

[91] Hering, F. Sterische Und Elektronische Stabilisierung Niedervalenter Übergangsmetallverbindungen Durch N-Heterocyclische Carbene, 2014.

[92] Blinova, N. V.; Sapurina, I.; Klimovič, J.; Stejskal, J. The chemical and colloidal stability of polyaniline dispersions. Polym. Degrad. Stab. **2005**, *88*(3), 428–434.

[93] Ansari, R. Polypyrrole Conducting Electroactive Polymers: Synthesis and Stability Studies. E-Journal Chem. **2006**, *3*(4), 186–201.

[94] Qian, R.; Li, Y.; Yan, B.; Zhang, H. Electrochemical aspects of polypyrrole. Synth. Met. **1989**, *28*(1–2), 51–58.

[95] Debiemme-Chouvy, C.; Tran, T.T.M. An insight into the overoxidation of polypyrrole materials. Electrochem. commun. **2008**, *10*(6), 947–950.

[96] Kumar, A.; Singh, R.K.; Agarwal, K.; Singh, H.K.; Srivastava, P.; Singh, R. Effect of p - toluenesulfonate on inhibition of overoxidation of polypyrrole. J. Appl. Polym. Sci. **2013**, *130*(1), 434–442.

[97] Sah, C.; Yadav, A.K.; Venkataramani, S. Deciphering Stability of Five-Membered Heterocyclic Radicals: Balancing Act Between Delocalization and Ring Strain. J. Phys. Chem. A **2018**, *122*(24), 5464–5476.

[98] Thomas, C.A.; Zong, K.; Schottland, P.; Reynolds, J.R. Poly(3,4-alkylenedioxypyrrole)s as Highly Stable Aqueous-Compatible Conducting Polymers with Biomedical Implications. Adv. Mater. **2000**, *12*(3), 222–225.

[99] Groenendaal, L.; Jonas, F.; Freitag, D.; Pielartzik, H.; Reynolds, J.R. Poly(3,4-ethylenedioxythiophene) and Its Derivatives: Past, Present, and Future. Adv. Mater. **2000**, *12*(7), 481–494.

[100] Heywang, G.; Jonas, F. Poly(alkylenedioxythiophene)s—new, very stable conducting polymers. Adv. Mater. **1992**, *4*(2), 116–118.

[101] Green, R.A.; Hassarati, R.T.; Bouchinet, L.; Lee, C.S.; Cheong, G.L.M.; Yu, J.F.; Dodds, C.W.; Suaning, G.J.; Poole-Warren, L.A.; Lovell, N.H. Substrate dependent stability of conducting polymer coatings on medical electrodes. Biomaterials **2012**, *33*(25), 5875–5886.

[102] Thiéblemont, J.C.; Planche, M.F.; Petrescu, C.; Bouvier, J.M.; Bidan, G. Stability of chemically synthesized polypyrrole films. Synth. Met. **1993**, *59*(1), 81–96.

[103] Hagiwara, T.; Hirasaka, M.; Sato, K.; Yamaura, M. Enhancement of the electrical conductivity of polypyrrole film by stretching: Influence of the polymerization conditions. Synth. Met. **1990**, *36*(2), 241–252.

[104] Kanwat, A.; Jang, J. Extremely stable organic photovoltaic incorporated with WO x doped PEDOT:PSS anode buffer layer. J. Mater. Chem. C **2014**, *2*(5), 901–907.

[105] Kim, T.; Park, S.; Seo, J.; Lee, C.W.; Kim, J.-M. Highly conductive PEDOT:PSS with enhanced chemical stability. Org. Electron. **2019**, *74*, 77–81.

[106] Spanninga, S.A.; Martin, D.C.; Chen, Z. X-ray Photoelectron Spectroscopy Study of Counterion Incorporation in Poly(3,4-ethylenedioxythiophene) (PEDOT) 2: Polyanion Effect, Toluenesulfonate, and Small Anions. J. Phys. Chem. C **2010**, *114*(35), 14992–14997.

[107] Baek, S.; Green, R.A.; Poole-Warren, L.A. Effects of dopants on the biomechanical properties of conducting polymer films on platinum electrodes. J. Biomed. Mater. Res. Part A **2014**, *102*(8), 2743–2754.

[108] Tieke, B. *Makromolekulare Chemie - Eine Einführung*. Wiley-VCH Verlag GmbH & Co. KGaA: Weinheim, Germany, 2005; 368 pp.

[109] Singh, V.; Bougher, T.L.; Weathers, A.; Cai, Y.; Bi, K.; Pettes, M.T.; McMenamin, S.A.; Lv, W.; Resler, D.P.; Gattuso, T.R.; Altman, D.H.; Sandhage, K.H.; Shi, L.; Henry, A.; Cola, B.A. High thermal conductivity of chain-oriented amorphous polythiophene. Nat. Nanotechnol. **2014**, *9*(5), 384–390.

[110] Wang, X.; Zhang, X.; Sun, L.; Lee, D.; Lee, S.; Wang, M.; Zhao, J.; Shao-Horn, Y.; Dincă, M.; Palacios, T.; Gleason, K.K. High electrical conductivity and carrier mobility in oCVD PEDOT thin films by engineered crystallization and acid treatment. Sci. Adv. **2018**, *4*(9), eaat5780.

[111] Cameron, R.E.; Kamvari-Moghaddam, A. Synthetic bioresorbable polymers. In *Durability and Reliability of Medical Polymers*; Elsevier, 2012; 96–118.

[112] Flynn, J.H. Polymer degradation. In *Applications to Polymers and Plastics*; Elsevier, 2002; Vol. 3, , 587–651.

[113] Wang, R.-M.; Zheng, S.-R.; Zheng, Y.-P. Matrix materials. In *Polymer Matrix Composites and Technology*; Elsevier, 2011; 101–548.

[114] Aldissl, M. Chain Rigidity-Processability Correlation in Inherently Conducting Polymers. Polym. Plast. Technol. Eng. **1987**, *26*(1), 45–70.

[115] Franz Neufingerl, Otto Urban, M.V. *Chemie 1. Allgemeine und anorganische Chemie*. Jung und Volk: Wien, 2007.

[116] Lu, X.; Ng, H.Y.; Xu, J.; He, C. Electrical conductivity of polyaniline–dodecylbenzene sulphonic acid complex: thermal degradation and its mechanism. Synth. Met. **2002**, *128*(2), 167–178.

[117] Yang, C.Y.; Reghu, M.; Heeger, A.J.; Cao, Y. Thermal stability of polyaniline networks in conducting polymer blends. Synth. Met. **1996**, *79*(1), 27–32.

[118] Alam, M.; Ansari, A.A.; Shaik, M.R.; Alandis, N.M. Optical and electrical conducting properties of Polyaniline/Tin oxide nanocomposite. Arab. J. Chem. **2013**, *6*(3), 341–345.

[119] Biswas, M.; Roy, A. Thermal, stability, morphological, and conductivity characteristics of polypyrrole prepared in aqueous medium. J. Appl. Polym. Sci. **1994**, *51*(9), 1575–1580.

[120] Ju, H.; Kim, M.; Kim, J. Thermoelectric behavior of poly(3,4-ethylenedioxythiophene)/graphene composites depending on benzenesulfonate derivatives doped in polymer chains. J. Mater. Sci. Mater. Electron. **2015**, *26*(4), 2544–2554.

[121] Ray, S.; Cooney, R.P. Thermal Degradation of Polymer and Polymer Composites. In *Handbook of Environmental Degradation of Materials*; Elsevier, 2018; 185–206.

[122] Duc, C.; Stoclet, G.; Soulestin, J.; Samuel, C. Poly(ethylene oxide)/Poly(3,4-ethylenedioxythiophene):Poly(styrene sulfonate) (PEDOT:PSS) Blends: An Efficient Route to Highly Conductive Thermoplastic Materials for Melt-State Extrusion Processing ? ACS Appl. Polym. Mater. **2020**, *2*(6), 2366–2379.

[123] Li, H.; Mao, P.; Davis, M.; Yu, Z. PEDOT:PSS-polyethylene oxide composites for stretchable and 3D-Printed thermoelectric devices. Compos. Commun. **2021**, *23*, 100599.

[124] Ennis, B.C.; Truong, V.-T. Thermal and electrical stability of polypyrrole at elevated temperatures. Synth. Met. **1993**, *59*(3), 387–399.

[125] Ng, C.A.; Camacho, D.H. Polymer electrolyte system based on carrageenan-poly(3,4-ethylenedioxythiophene) (PEDOT) composite for dye sensitized solar cell. IOP Conf. Ser. Mater. Sci. Eng. **2015**, *79*, 12020.

[126] Bhadra, S.; Khastgir, D. Glass--rubber transition temperature of polyaniline: Experimental and molecular dynamic simulation. Synth. Met. **2009**, *159*(12), 1141–1146.

[127] Masuda, T.; Tang, B.Z.; Higashimura, T.; Yamaoka, H. Thermal degradation of polyacetylenes carrying substituents. Macromolecules **1985**, *18*(12), 2369–2373.

[128] Masuda, T.; Tang, B.Z.; Tanaka, A.; Higashimura, T. Mechanical properties of substituted polyacetylenes. Macromolecules **1986**, *19*(5), 1459–1464.

[129] Montes, I.; Lai, C.; Sanabria, D. Like Dissolves Like: A Guided Inquiry Experiment for Organic

Chemistry. J. Chem. Educ. **2003**, *80*(4), 447.

[130] WESSLING, B. Conductive polymers as organic nanometals. In *Handbook of Nanostructured Materials and Nanotechnology*; Elsevier, 2000; Vol. 5, , 501–575.

[131] Kaynak, A.; Foitzik, R. Synthesis and Characterization of Soluble Conducting Polymers. Res. J. Text. Appar. **2010**, *14*(2), 45–52.

[132] Lv, G.; Tian, H.; Shao, J.; Yu, D. Synthesis, characterization, and efficient electrohydrodynamic patterning with a high aspect ratio of a soluble oligomerpyrrole derivative. React. Funct. Polym. **2019**, *137*, 116–122.

[133] Lv, G.; Zhang, S.; Wang, G.; Shao, J.; Tian, H.; Yu, D. A methacryl ethyl-functionalized soluble polypyrrole: Synthesis, characterization, and potentiality in rapid fabrication of high-aspect-ratio pillar arrays. React. Funct. Polym. **2017**, *111*, 44–52.

[134] John, J.; Saheeda, P.; Sabeera, K.; Jayalekshmi, S. Doped polypyrrole with good solubility and film forming properties suitable for device applications. Mater. Today Proc. **2018**, *5*(10), 21140–21146.

[135] Ponder, J.F.; Österholm, A.M.; Reynolds, J.R. Designing a Soluble PEDOT Analogue without Surfactants or Dispersants. Macromolecules **2016**, *49*(6), 2106–2111.

[136] Hussin, H.; Gan, S.N.; Mohamad, S.; Phang, S.W. Synthesis of Water-soluble Polyaniline by Using Different Types of Cellulose Derivatives. Polym. Polym. Compos. **2017**, *25*(7), 515–520.

[137] Gribkova, O.L.; Saf'yanova, L. V.; Tameev, A.R.; Lypenko, D.A.; Tverskoi, V.A.; Nekrasov, A.A. A Water-Soluble Polyaniline Complex for Ink-Jet Printing of Optoelectronic Devices. Tech. Phys. Lett. **2018**, *44*(3), 239–242.

[138] Jang, K.S.; Lee, H.; Moon, B. Synthesis and characterization of water soluble polypyrrole doped with functional dopants. Synth. Met. **2004**, *143*(3), 289–294.

[139] Bae, W.J.; Kim, K.H.; Jo, W.H.; Park, Y.H. A Water-Soluble and Self-Doped Conducting Polypyrrole Graft Copolymer. Macromolecules **2005**, *38*(4), 1044–1047.

[140] Alizadeh, N.; Akbarinejad, A.; Hosseinkhani, S.; Rabbani, F. Synthesis of highly fluorescent water-soluble polypyrrole for cell imaging and iodide ion sensing. Anal. Chim. Acta **2019**, *1084*, 99–105.

[141] Green, R.; Abidian, M.R. Conducting Polymers for Neural Prosthetic and Neural Interface Applications. Adv. Mater. **2015**, *27*(46), 7620–7637.

[142] Novikov, A.; Goding, J.; Chapman, C.; Cuttaz, E.; Green, R.A. Stretchable bioelectronics: Mitigating the challenges of the percolation threshold in conductive elastomers. APL Mater. **2020**, *8*(10), 101105.

[143] Qu, J.; Ouyang, L.; Kuo, C.; Martin, D.C. Stiffness, strength and adhesion characterization of electrochemically deposited conjugated polymer films. Acta Biomater. **2016**, *31*, 114–121.

[144] Valentová, H.; Stejskal, J. Mechanical properties of polyaniline. Synth. Met. **2010**, *160*(7–8), 832–834.

[145] Cuenot, S.; Demoustier-Champagne, S.; Nysten, B. Elastic Modulus of Polypyrrole Nanotubes. Phys. Rev. Lett. **2000**, *85*(8), 1690–1693.

[146] Lang, U.; Naujoks, N.; Dual, J. Mechanical characterization of PEDOT:PSS thin films. Synth. Met. **2009**, *159*(5–6), 473–479.

[147] Sun, B.; Jones, J.J.; Burford, R.P.; Skyllas-Kazacos, M. Stability and mechanical properties of electrochemically prepared conducting polypyrrole films. J. Mater. Sci. **1989**, *24*(11), 4024–4029.

[148] Savagatrup, S.; Chan, E.; Renteria-Garcia, S.M.; Printz, A.D.; Zaretski, A. V.; O'Connor, T.F.; Rodriquez, D.; Valle, E.; Lipomi, D.J. Plasticization of PEDOT:PSS by Common Additives for

Mechanically Robust Organic Solar Cells and Wearable Sensors. Adv. Funct. Mater. **2015**, *25*(3), 427–436.

[149] Jamarani, R.; Erythropel, H.; Nicell, J.; Leask, R.; Marić, M. How Green is Your Plasticizer? Polymers (Basel). **2018**, *10*(8), 834.

[150] Ouyang, L.; Wei, B.; Kuo, C.; Pathak, S.; Farrell, B.; Martin, D.C. Enhanced PEDOT adhesion on solid substrates with electrografted P(EDOT-NH 2). Sci. Adv. **2017**, *3*(3), e1600448.

[151] Yan, H.; Jo, T.; Okuzaki, H. Highly Conductive and Transparent Poly(3,4-ethylenedioxythiophene)/Poly(4-styrenesulfonate) (PEDOT/PSS) Thin Films. Polym. J. **2009**, *41*(12), 1028–1029.

[152] Pang, H.; Xu, L.; Yan, D.-X.; Li, Z.-M. Conductive polymer composites with segregated structures. Prog. Polym. Sci. **2014**, *39*(11), 1908–1933.

[153] Cuttaz, E.; Goding, J.; Vallejo-Giraldo, C.; Aregueta-Robles, U.; Lovell, N.; Ghezzi, D.; Green, R.A. Conductive elastomer composites for fully polymeric, flexible bioelectronics. Biomater. Sci. **2019**, *7*(4), 1372–1385.

[154] Strakosas, X.; Wei, B.; Martin, D.C.; Owens, R.M. Biofunctionalization of polydioxythiophene derivatives for biomedical applications. J. Mater. Chem. B **2016**, *4*(29), 4952–4968.

[155] Mantione, D.; Agua, I. del; Sanchez-Sanchez, A.; Mecerreyes, D. Poly(3,4-ethylenedioxythiophene) (PEDOT) Derivatives: Innovative Conductive Polymers for Bioelectronics. Polymers (Basel). **2017**, *9*(12), 354.

[156] MacDiarmid, A.G.; Mammone, R.J.; Kaner, R.B.; Porter, S.J.; Pethig, R.; Heeger, A.J.; Rosseinsky, D.R. The Concept of `Doping' of Conducting Polymers: The Role of Reduction Potentials [and Discussion]. Philos. Trans. R. Soc. London. Ser. A, Math. Phys. Sci. **1985**, *314*(1528), 3–15.

[157] Tourillon, G.; Garnier, F. Effect of dopant on the physicochemical and electrical properties of organic conducting polymers. J. Phys. Chem. **1983**, *87*(13), 2289–2292.

[158] Patil, A.O.; Ikenoue, Y.; Wudl, F.; Heeger, A.J. Water soluble conducting polymers. J. Am. Chem. Soc. **1987**, *109*(6), 1858–1859.

[159] Bu, H.-B.; Götz, G.; Reinold, E.; Vogt, A.; Azumi, R.; Segura, J.L.; Bäuerle, P. "Click"-modification of a functionalized poly(3,4-ethylenedioxythiophene) (PEDOT) soluble in organic solvents. Chem. Commun. **2012**, *48*(21), 2677.

[160] Mantione, D.; Marquez, A.V.; Cruciani, F.; Brochon, C.; Cloutet, E.; Hadziioannou, G. Synthesis of Carboxyl-EDOT as a Versatile Addition and Additive to PEDOT:PSS. ACS Macro Lett. **2019**, *8*(3), 285–288.

[161] Zheng, C. Gradient copolymer micelles: an introduction to structures as well as structural transitions. Soft Matter **2019**, *15*(27), 5357–5370.

[162] Huynh, V.T.; Quek, J.Y.; Souza, P.L. de; Stenzel, M.H. Block Copolymer Micelles with Pendant Bifunctional Chelator for Platinum Drugs: Effect of Spacer Length on the Viability of Tumor Cells. Biomacromolecules **2012**, *13*(4), 1010–1023.

[163] Gaucher, G.; Dufresne, M.-H.; Sant, V.P.; Kang, N.; Maysinger, D.; Leroux, J.-C. Block copolymer micelles: preparation, characterization and application in drug delivery. J. Control. Release **2005**, *109*(1–3), 169–188.

[164] Blatz, T.J.; Fry, M.M.; James, E.I.; Albin, T.J.; Pollard, Z.; Kowalczyk, T.; Murphy, A.R. Templating the 3D structure of conducting polymers with self-assembling peptides. J. Mater. Chem. B **2017**, *5*(24), 4690–4696.

[165] Yagci, Y.; Toppare, L. Electroactive macromonomers based on pyrrole and thiophene: a versatile route to conducting block and graft polymers. Polym. Int. **2003**, *52*(10), 1573–1578.

[166] Sedlacek, O.; Bera, D.; Hoogenboom, R. Poly(2-amino-2-oxazoline)s: a new class of thermoresponsive polymers. Polym. Chem. **2019**, *10*(34), 4683–4689.

[167] AOI, K. Polymerization of oxazolines. Prog. Polym. Sci. **1996**, *21*(1), 151–208.

[168] Wiley, R.H.; Bennett, L.L. The Chemistry of the Oxazolines. Chem. Rev. **1949**, *44*(3), 447–476.

[169] Connon, R.; Roche, B.; Rokade, B. V.; Guiry, P.J. Further Developments and Applications of Oxazoline-Containing Ligands in Asymmetric Catalysis. Chem. Rev. **2021**, *121*(11), 6373–6521.

[170] Rossegger, E.; Schenk, V.; Wiesbrock, F. Design Strategies for Functionalized Poly(2-oxazoline)s and Derived Materials. Polymers (Basel). **2013**, *5*(3), 956–1011.

[171] Varanaraja, Z.; Kim, J.; Becer, C.R. Poly(2-oxazine)s: A comprehensive overview of the polymer structures, physical properties and applications. Eur. Polym. J. **2021**, *147*, 110299.

[172] Gabriel, S.; Heymann, T. Ueber Darstellung und Eigenschaften einiger Oxazoline. Berichte der Dtsch. Chem. Gesellschaft **1890**, *23*(2), 2493–2502.

[173] Penczek, S.; Pretula, J.; Slomkowski, S. Ring-opening polymerization. Chem. Teach. Int. **2021**, *3*(2), 33–57.

[174] Sahn, M.; Bandelli, D.; Dirauf, M.; Weber, C.; Schubert, U.S. Bifunctional Initiators as Tools to Track Chain Transfer during the CROP of 2-Oxazolines. Macromol. Rapid Commun. **2017**, *38*(19), 1700396.

[175] Luxenhofer, R.; Schulz, A.; Roques, C.; Li, S.; Bronich, T.K.; Batrakova, E. V.; Jordan, R.; Kabanov, A. V. Doubly amphiphilic poly(2-oxazoline)s as high-capacity delivery systems for hydrophobic drugs. Biomaterials **2010**, *31*(18), 4972–4979.

[176] Kourti, M.-E.; Fotinogiannopoulou, G.; Fega, E.; Pitsikalis, M. Statistical Copolymers of 2-Methyl- and 2-Phenyl-oxazoline by Metallocene-Mediated Cationic Ring-Opening Polymerization: Synthesis, Reactivity Ratios, Kinetics of Thermal Decomposition and Self-Assembly Behavior in Aqueous Solutions. J. Macromol. Sci. Part A **2015**, *52*(8), 630–641.

[177] Kobayashi, S.; Igarashi, T.; Moriuchi, Y.; Saegusa, T. Block copolymers from cyclic imino ethers: a new class of nonionic polymer surfactant. Macromolecules **1986**, *19*(3), 535–541.

[178] Sedlacek, O.; Monnery, B.D.; Hoogenboom, R. Synthesis of defined high molar mass poly(2-methyl-2-oxazoline). Polym. Chem. **2019**, *10*(11), 1286–1290.

[179] Pertel, S.S.; Zinin, A.I.; Seryi, S.A.; Kakayan, E.S. The study of the acid-catalyzed reaction between 2-methyl and 2-(2,2,2-trichloroethoxy) gluco-[2,1-d]-2-oxazolines. Synthesis of macrocyclic pseudo-tetrasaccharide derivative of d-glucosamine. Carbohydr. Res. **2021**, *499*, 108230.

[180] Nahm, D. Poly(2-Oxazine) Based Biomaterial Inks for the Additive Manufacturing of Microperiodic Hydrogel Scaffolds, 2021.

[181] Zhang, N.; Pompe, T.; Amin, I.; Luxenhofer, R.; Werner, C.; Jordan, R. Tailored Poly(2-oxazoline) Polymer Brushes to Control Protein Adsorption and Cell Adhesion. Macromol. Biosci. **2012**, *12*(7), 926–936.

[182] Oleszko-Torbus, N.; Utrata-Wesołek, A.; Bochenek, M.; Lipowska-Kur, D.; Dworak, A.; Wałach, W. Thermal and crystalline properties of poly(2-oxazoline)s. Polym. Chem. **2020**, *11*(1), 15–33.

[183] Zahoranová, A.; Luxenhofer, R. Poly(2-oxazoline)- and Poly(2-oxazine)-Based Self-Assemblies, Polyplexes, and Drug Nanoformulations—An Update. Adv. Healthc. Mater. **2021**, *10*(6), 2001382.

[184] Luxenhofer, R.; Huber, S.; Hytry, J.; Tong, J.; Kabanov, A. V.; Jordan, R. Chiral and water-soluble poly(2-oxazoline)s. J. Polym. Sci. Part A Polym. Chem. **2013**, *51*(3), 732–738.

[185] Lin, P.; Clash, C.; Pearce, E.M.; Kwei, T.K.; Aponte, M.A. Solubility and miscibility of poly(ethyl oxazoline). J. Polym. Sci. Part B Polym. Phys. **1988**, *26*(3), 603–619.

[186] Hoogenboom, R.; Schlaad, H. Thermoresponsive poly(2-oxazoline)s, polypeptoids, and polypeptides. Polym. Chem. **2017**, *8*(1), 24–40.

[187] Lambermont-Thijs, H.M.L.; Hoogenboom, R.; Fustin, C.-A.; Bomal-D'Haese, C.; Gohy, J.-F.; Schubert, U.S. Solubility behavior of amphiphilic block and random copolymers based on 2-ethyl-2-oxazoline and 2-nonyl-2-oxazoline in binary water-ethanol mixtures. J. Polym. Sci. Part A Polym. Chem. **2009**, *47*(2), 515–522.

[188] Pöppler, A.; Lübtow, M.M.; Schlauersbach, J.; Wiest, J.; Meinel, L.; Luxenhofer, R. Loading-Dependent Structural Model of Polymeric Micelles Encapsulating Curcumin by Solid-State NMR Spectroscopy. Angew. Chemie Int. Ed. **2019**, *58*(51), 18540–18546.

[189] Viegas, T.X.; Bentley, M.D.; Harris, J.M.; Fang, Z.; Yoon, K.; Dizman, B.; Weimer, R.; Mero, A.; Pasut, G.; Veronese, F.M. Polyoxazoline: Chemistry, Properties, and Applications in Drug Delivery. Bioconjug. Chem. **2011**, *22*(5), 976–986.

[190] la Rosa, V.R. de. Poly(2-oxazoline)s as materials for biomedical applications. J. Mater. Sci. Mater. Med. **2014**, *25*(5), 1211–1225.

[191] wyffels, L.; Verbrugghen, T.; Monnery, B.D.; Glassner, M.; Stroobants, S.; Hoogenboom, R.; Staelens, S. MPET imaging of the pharmacokinetic behavior of medium and high molar mass 89 Zr-labeled poly(2-ethyl-2-oxazoline) in comparison to poly(ethylene glycol). J. Control. Release **2016**, *235*, 63–71.

[192] Moreadith, R.W.; Viegas, T.X.; Bentley, M.D.; Harris, J.M.; Fang, Z.; Yoon, K.; Dizman, B.; Weimer, R.; Rae, B.P.; Li, X.; Rader, C.; Standaert, D.; Olanow, W. Clinical development of a poly(2-oxazoline) (POZ) polymer therapeutic for the treatment of Parkinson's disease – Proof of concept of POZ as a versatile polymer platform for drug development in multiple therapeutic indications. Eur. Polym. J. **2017**, *88*, 524–552.

[193] Lambermont-Thijs, H.M.L.; Woerdt, F.S. van der; Baumgaertel, A.; Bonami, L.; Prez, F.E. Du; Schubert, U.S.; Hoogenboom, R. Linear Poly(ethylene imine)s by Acidic Hydrolysis of Poly(2-oxazoline)s: Kinetic Screening, Thermal Properties, and Temperature-Induced Solubility Transitions. Macromolecules **2010**, *43*(2), 927–933.

[194] Hahn, B.T.; Tewes, F.; Fröhlich, R.; Glorius, F. Olefin-Oxazoline (OlefOx) - modulare, leicht zu variierende Liganden für die asymmetrische Katalyse. Angew. Chemie **2010**, *122*(6), 1161–1164.

[195] Podevyn, A.; Arys, K.; la Rosa, V.R. de; Glassner, M.; Hoogenboom, R. End-group functionalization of poly(2-oxazoline)s using methyl bromoacetate as initiator followed by direct amidation. Eur. Polym. J. **2019**, *120*, 109273.

[196] Taubmann, C.; Luxenhofer, R.; Cesana, S.; Jordan, R. First Aldehyde-Functionalized Poly(2-oxazoline)s for Chemoselective Ligation. Macromol. Biosci. **2005**, *5*(7), 603–612.

[197] A, S.; Manohara, S.R.; Gerward, L. Influence of polyvinylpyrrolidone on optical, electrical, and dielectric properties of poly(2-ethyl-2-oxazoline)-polyvinylpyrrolidone blends. J. Mol. Liq. **2017**, *247*, 328–336.

[198] Bussink, J.; Grampel, H.T. van de; Weber, M. Polymer Blends. In *Ullmann's Encyclopedia of Industrial Chemistry*; Wiley-VCH Verlag GmbH & Co. KGaA: Weinheim, Germany, 2017; 1–39.

[199] Kate, J. ten; Smit, G.; Breedveld, P. 3D-printed upper limb prostheses: a review. Disabil. Rehabil. Assist. Technol. **2017**, *12*(3), 300–314.

[200] Yang, J.L.; Su, L.; Ma, L.G.; Huang, Y. Colloidal Injection Moulding of Ceramics. Key Eng. Mater. **2002**, *224–226*, 667–672.

[201] Chen, D.X.B. Extrusion Bioprinting of Scaffolds: An Introduction. In *Extrusion Bioprinting of Scaffolds for Tissue Engineering Applications*; Springer International Publishing: Cham, 2019; 1–13.

[202] Hu, X.; Meng, X.; Xiong, J.; Huang, Z.; Yang, X.; Tan, L.; Chen, Y. Roll-to-Roll Fabrication of

Flexible Orientated Graphene Transparent Electrodes by Shear Force and One-Step Reducing Post-Treatment. Adv. Mater. Technol. **2017**, *2*(12), 1700138.

[203] Santos, G.H.; Gavim, A.A.X.; Silva, R.F.; Rodrigues, P.C.; Kamikawachi, R.C.; Deus, J.F. de; Macedo, A.G. Roll-to-roll processed PEDOT:PSS thin films: application in flexible electrochromic devices. J. Mater. Sci. Mater. Electron. **2016**, *27*(10), 11072–11079.

[204] Yoshioka, Y.; Jabbour, G.E. Desktop inkjet printer as a tool to print conducting polymers. Synth. Met. **2006**, *156*(11–13), 779–783.

[205] Wang, S.; Xu, J.; Wang, W.; Wang, G.-J.N.; Rastak, R.; Molina-Lopez, F.; Chung, J.W.; Niu, S.; Feig, V.R.; Lopez, J.; Lei, T.; Kwon, S.-K.; Kim, Y.; Foudeh, A.M.; Ehrlich, A.; Gasperini, A.; Yun, Y.; Murmann, B.; Tok, J.B.-H.; Bao, Z. Skin electronics from scalable fabrication of an intrinsically stretchable transistor array. Nature **2018**, *555*(7694), 83–88.

[206] Yuk, H.; Lu, B.; Lin, S.; Qu, K.; Xu, J.; Luo, J.; Zhao, X. 3D printing of conducting polymers. Nat. Commun. **2020**, *11*(1), 1604.

[207] Scordo, G.; Bertana, V.; Scaltrito, L.; Ferrero, S.; Cocuzza, M.; Marasso, S.L.; Romano, S.; Sesana, R.; Catania, F.; Pirri, C.F. A novel highly electrically conductive composite resin for stereolithography. Mater. Today Commun. **2019**, *19*, 12–17.

[208] Heo, D.N.; Lee, S.-J.; Timsina, R.; Qiu, X.; Castro, N.J.; Zhang, L.G. Development of 3D printable conductive hydrogel with crystallized PEDOT:PSS for neural tissue engineering. Mater. Sci. Eng. C **2019**, *99*, 582–590.

[209] Yu, M.; Ahn, K.H.; Lee, S.J. Design optimization of ink in electrohydrodynamic jet printing: Effect of viscoelasticity on the formation of Taylor cone jet. Mater. Des. **2016**, *89*, 109–115.

[210] Olvera, D.; Sohrabi Molina, M.; Hendy, G.; Monaghan, M.G. Electroconductive Melt Electrowritten Patches Matching the Mechanical Anisotropy of Human Myocardium. Adv. Funct. Mater. **2020**, 1909880.

[211] Ritzau-Reid, K.I.; Spicer, C.D.; Gelmi, A.; Grigsby, C.L.; Ponder, J.F.; Bemmer, V.; Creamer, A.; Vilar, R.; Serio, A.; Stevens, M.M. An Electroactive Oligo-EDOT Platform for Neural Tissue Engineering. Adv. Funct. Mater. **2020**, *30*(42), 2003710.

[212] Cuttaz, E.; Goding, J.; Vallejo-Giraldo, C.; Aregueta-Robles, U.; Lovell, N.; Ghezzi, D.; Green, R.A. Conductive elastomer composites for fully polymeric, flexible bioelectronics. Biomater. Sci. **2019**, *7*(4), 1372–1385.

[213] Spicer, C.D.; Booth, M.A.; Mawad, D.; Armgarth, A.; Nielsen, C.B.; Stevens, M.M. Synthesis of Hetero-bifunctional, End-Capped Oligo-EDOT Derivatives. Chem **2017**, *2*(1), 125–138.

[214] Liu, J.; Yan, C. 3D Printing of Scaffolds for Tissue Engineering. In *3D Printing*; InTech, 2018; .

[215] Gueye, M.N.; Carella, A.; Faure-Vincent, J.; Demadrille, R.; Simonato, J.-P. Progress in understanding structure and transport properties of PEDOT-based materials: A critical review. Prog. Mater. Sci. **2020**, *108*, 100616.

[216] Lemanski, G. Organikum. (20. Aufl.) VonH. G. O. Becker et al. J. A. Barth Verlag, Heidelberg, 1996. 813 S., geb. 88.00 DM.—ISBN 3-335-00492-2. Angew. Chemie **1997**, *109*(16), 1849–1849.

[217] Franke, C.; Olowu, R.; Waryo, T.; Wilson, L.; Williams, A.; Baker, G.; Iwuoha, E. Dendritic 7T-Polythiophene Electro-Catalytic Sensor System for the Determination of Polycyclic Aromatic Hydrocarbons. Int. J. Electrochem. Sci. Int. J. **2011**, *6*, 1949–1967.

[218] Krauklis, A.; Echtermeyer, A. Mechanism of Yellowing: Carbonyl Formation during Hygrothermal Aging in a Common Amine Epoxy. Polymers (Basel). **2018**, *10*(9), 1017.

[219] Ilkgul, B.; Gunes, D.; Sirkecioglu, O.; Bicak, N. Synthesis of 2-oxazolines via boron esters of N-(2-hydroxyethyl) amides. Tetrahedron Lett. **2010**, *51*(40), 5313–5315.

[220] Witte, H.; Seeliger, W. Cyclische Imidsäureester aus Nitrilen und Aminoalkoholen. Justus Liebigs Ann. Chem. **1974**, *1974*(6), 996–1009.

[221] Szkop, K.M.; Zhu, D.; Longobardi, L.E.; Heck, J.; Stephan, D.W. Interception of intermediates in phosphine oxidation by mesityl nitrile- N -oxide using frustrated Lewis pairs. Dalt. Trans. **2018**, *47*(27), 8933–8939.

[222] Koßmehl, G.; Budwill, D. Flüssig-kristalline Verbindungen aus der Thiophenreihe, Teil 2. Flüssig-kristalline Azomethine, Azine und Vinylene / Liquid Crystalline Compounds in the Thiophene Series 2. Liquid Crystalline Azomethines, Azines and Vinylenes. Zeitschrift für Naturforsch. B **1985**, *40*(9), 1199–1213.

[223] Holleman, A.F.; Wiberg, N.; Wiberg, E. *Lehrbuch der Anorganischen Chemie*. Walter de Gruyter: , 2007.

[224] Behr, A.; Agar, D.W.; Jörissen, J. *Einführung in die Technische Chemie*. Spektrum Akademischer Verlag: Heidelberg, 2010.

[225] Witte, H.; Seeliger, W. Simple Synthesis of 2-Substituted 2-Oxazolines and 5,6-Dihydro-4H-1,3-oxazines. Angew. Chemie Int. Ed. English **1972**, *11*(4), 287–288.

[226] Schwetlick, K.; Unverferth, K.; Mayer, R. Über die Reaktivität von Thiophen, Furan, Pyrrol und Benzol beim sauer katalysierten elektrophilen Wasserstoffisotopenaustausch. Zeitschrift für Chemie **2010**, *7*(2), 58–58.

[227] Martin, F.; Zipse, H. Charge distribution in the water molecule?A comparison of methods. J. Comput. Chem. **2005**, *26*(1), 97–105.

[228] Mathias, F.; Tahir, M.N.; Tremel, W.; Zentel, R. Functionalization of TiO 2 Nanoparticles with Semiconducting Polymers Containing a Photocleavable Anchor Group and Separation via Irradiation Afterward. Macromol. Chem. Phys. **2014**, *215*(7), 604–613.

[229] Zamborini, F.P.; Smart, L.E.; Leopold, M.C.; Murray, R.W. Distance-dependent electron hopping conductivity and nanoscale lithography of chemically-linked gold monolayer protected cluster films. Anal. Chim. Acta **2003**, *496*(1–2), 3–16.

[230] Shi, H.; Liu, C.; Jiang, Q.; Xu, J. Effective Approaches to Improve the Electrical Conductivity of PEDOT:PSS: A Review. Adv. Electron. Mater. **2015**, *1*(4), 1500017.

[231] Lingstedt, L. V.; Ghittorelli, M.; Lu, H.; Koutsouras, D.A.; Marszalek, T.; Torricelli, F.; Crăciun, N.I.; Gkoupidenis, P.; Blom, P.W.M. Effect of DMSO Solvent Treatments on the Performance of PEDOT:PSS Based Organic Electrochemical Transistors. Adv. Electron. Mater. **2019**, 1800804.

[232] Alishah, H.M.; Kazici, M.; Ongül, F.; Bozar, S.; Cantürk Rodop, M.; Kahveci, C.; Arvas, M.B.; Sahin, Y.; Gencten, M.; Kaleli, M.; Akyürekli, S.; Yilmaz, H.U.; Bayram, A.B.; Günes, S. Effect of UV exposure of ITO/PEDOT:PSS substrates on the performance of inverted-type perovskite solar cells. J. Mater. Sci. Mater. Electron. **2020**, *31*(10), 7968–7980.

[233] Lima, A.; Schottland, P.; Sadki, S.; Chevrot, C. Electropolymerization of 3,4-ethylenedioxythiophene and 3,4-ethylenedioxythiophene methanol in the presence of dodecylbenzenesulfonate. Synth. Met. **1998**, *93*(1), 33–41.

[234] Skompska, M.; Vorotyntsev, M.A.; Refczynska, M.; Goux, J.; Lesniewska, E.; Boni, G.; Moise, C. Electrosynthesis and properties of poly(3,4-ethylenedioxythiophene) films functionalized with titanocene dichloride complex. Electrochim. Acta **2006**, *51*(11), 2108–2119.

[235] Bouten, P.; Lava, K.; Hest, J. van; Hoogenboom, R. Thermal Properties of Methyl Ester-Containing Poly(2-oxazoline)s. Polymers (Basel). **2015**, *7*(10), 1998–2008.

[236] Meira, G.; Oliva, H. Molecular weight distributions in ideal polymerization reactors: An introductory review. Lat. Am. Appl. Res. **2011**, *41*, 389–401.

[237] Amella, A.D.; Patton, A.J.; Martens, P.J.; Lovell, N.H.; Poole-Warren, L.A.; Green, R.A. *In Freestanding, soft bioelectronics*, IEEE: 2015.

[238] Qi, Y.; Zhang, J.; Qiu, S.; Sun, L.; Xu, F.; Zhu, M.; Ouyang, L.; Sun, D. Thermal stability, decomposition and glass transition behavior of PANI/NiO composites. J. Therm. Anal. Calorim. **2009**, *98*(2), 533–537.

[239] Somboonsub, B.; Invernale, M.A.; Thongyai, S.; Praserthdam, P.; Scola, D.A.; Sotzing, G.A. Preparation of the thermally stable conducting polymer PEDOT – Sulfonated poly(imide). Polymer (Guildf). **2010**, *51*(6), 1231–1236.

[240] Hoogenboom, R. Poly(2-oxazoline): eine Polymerklasse mit vielfältigen Anwendungsmöglichkeiten. Angew. Chemie **2009**, *121*(43), 8122–8138.

[241] Shen, X.; Hu, W.; Russell, T.P. Measuring the Degree of Crystallinity in Semicrystalline Regioregular Poly(3-hexylthiophene). Macromolecules **2016**, *49*(12), 4501–4509.

[242] Oleszko-Torbus, N.; Wałach, W.; Utrata-Wesołek, A.; Dworak, A. Control of the Crystalline Properties of 2-Isopropyl-2-oxazoline Copolymers in Condensed State and in Solution Depending on the Composition. Macromolecules **2017**, *50*(19), 7636–7645.

[243] Das, S.; Chatterjee, D.P.; Ghosh, R.; Nandi, A.K. Water soluble polythiophenes: preparation and applications. RSC Adv. **2015**, *5*(26), 20160–20177.

[244] Chayer, M.; Faïd, K.; Leclerc, M. Highly Conducting Water-Soluble Polythiophene Derivatives. Chem. Mater. **1997**, *9*(12), 2902–2905.

[245] Sato, M.; Tanaka, S.; Kaeriyama, K. Soluble conducting polythiophenes. J. Chem. Soc. Chem. Commun. **1986**, (11), 873.

[246] Huggins, M.L. The Solubility of Nonelectrolytes. By Joel H. Hildebrand and Robert S. Scott. J. Phys. Chem. **1951**, *55*(4), 619–620.

[247] Dargaville, T.R.; Hollier, B.G.; Shokoohmand, A.; Hoogenboom, R. Poly(2-oxazoline) hydrogels as next generation three-dimensional cell supports. Cell Adh. Migr. **2014**, *8*(2), 88–93.

[248] Hahn, L.; Karakaya, E.; Zorn, T.; Sochor, B.; Maier, M.; Stahlhut, P.; Forster, S.; Fischer, K.; Seiffert, S.; Pöppler, A.-C.; Detsch, R.; Luxenhofer, R. An Inverse Thermogelling Bioink Based on an ABA-Type Poly(2-oxazoline) Amphiphile. Biomacromolecules **2021**, *22*(7), 3017–3027.

[249] Lu, B.; Yuk, H.; Lin, S.; Jian, N.; Qu, K.; Xu, J.; Zhao, X. Pure PEDOT:PSS hydrogels. Nat. Commun. **2019**, *10*(1), 1043.

[250] Segiet, D.; Stockmann, A.; Sadowski, J.; Katzenberg, F.; Tiller, J.C. Insights in the Thermal Volume Transition of Poly(2-oxazoline) Hydrogels. Macromol. Chem. Phys. **2021**, *222*(18), 2100157.

[251] Sánchez-Fernández, M.J.; Peerlings, M.; Félix Lanao, R.P.; Bender, J.C.M.E.; Hest, J.C.M. van; Leeuwenburgh, S.C.G. Bone-adhesive barrier membranes based on alendronate-functionalized poly(2-oxazoline)s. J. Mater. Chem. B **2021**, *9*(29), 5848–5860.

[252] Farooq, U.; Khan, I.; Ahmad, S.; Abas, M.; Zaib Khan, M.A.; Rahman, K. Fabrication of PEDOT: PSS conductive patterns on photo paper substrate through electro-hydrodynamic jet printing process. Int. J. Light. Mater. Manuf. **2019**, *2*(4), 318–329.

[253] Waltman, R.J.; Bargon, J. Electrically conducting polymers: a review of the electropolymerization reaction, of the effects of chemical structure on polymer film properties, and of applications towards technology. Can. J. Chem. **1986**, *64*(1), 76–95.

[254] Minudri, D.; Mantione, D.; Dominguez-Alfaro, A.; Moya, S.; Maza, E.; Bellacanzone, C.; Antognazza, M.R.; Mecerreyes, D. Water Soluble Cationic Poly(3,4-Ethylenedioxythiophene) PEDOT-N as a Versatile Conducting Polymer for Bioelectronics. Adv. Electron. Mater. **2020**, *6*(10), 2000510.

[255] McCullough, R.D. The Chemistry of Conducting Polythiophenes. Adv. Mater. **1998**, *10*(2), 93–116.

[256] Saberi, A.; Jabbari, F.; Zarrintaj, P.; Saeb, M.R.; Mozafari, M. Electrically Conductive Materials: Opportunities and Challenges in Tissue Engineering. Biomolecules **2019**, *9*(9), 448.

[257] Scherer, T. Einfluß Der Internen Architektur von Polymermikronetzwerken Auf Struktur Und Dynamik Konzentrierter Kolloid-Dispersionen, 2001.

[258] Lu, Y.; Santino, L.M.; Acharya, S.; Anandarajah, H.; D'Arcy, J.M. Studying Electrical Conductivity Using a 3D Printed Four-Point Probe Station. J. Chem. Educ. **2017**, *94*(7), 950–955.

[259] Begam, T.; Nagpal, A.K.; Singhal, R. A comparative study of swelling properties of hydrogels based on poly(acrylamide-co-methyl methacrylate) containing physical and chemical crosslinks. J. Appl. Polym. Sci. **2003**, *89*(3), 779–786.

[260] Kade, J.C.; Otto, P.F.; Luxenhofer, R.; Dalton, P.D. Melt electrowriting of poly(vinylidene difluoride) using a heated collector. Polym. Adv. Technol. **2021**, *32*(12), 4951–4955.

[261] Robinson, T.M.; Hutmacher, D.W.; Dalton, P.D. The Next Frontier in Melt Electrospinning: Taming the Jet. Adv. Funct. Mater. **2019**, *29*(44), 1904664.

[262] Eberle, F.; Gruska, A.-K.; Filippi, B.; Stahlhut, P.; Wallace, G.G.; Dalton, P.D.; Beirne, S. Hollow-Fiber Melt Electrowriting Using a 3D-Printed Coaxial Nozzle. Adv. Eng. Mater. **2022**, *24*(1), 2100750.

[263] Hochleitner, G.; Jüngst, T.; Brown, T.D.; Hahn, K.; Moseke, C.; Jakob, F.; Dalton, P.D.; Groll, J. Additive manufacturing of scaffolds with sub-micron filaments via melt electrospinning writing. Biofabrication **2015**, *7*(3), 035002.

[264] Zhang, Y. Post-3D printing modification for improved biomedical applications. Int. J. Bioprinting **2017**, *3*(2).

[265] Guo, H.; Lv, R.; Bai, S. Recent advances on 3D printing graphene-based composites. Nano Mater. Sci. **2019**, *1*(2), 101–115.

[266] Green, R.A.; Lovell, N.H.; Poole-Warren, L.A. Impact of co-incorporating laminin peptide dopants and neurotrophic growth factors on conducting polymer properties. Acta Biomater. **2010**, *6*(1), 63–71.

[267] Löblein, J.; Lorson, T.; Komma, M.; Kielholz, T.; Windbergs, M.; Dalton, P.D.; Luxenhofer, R. An initiator- and catalyst-free hydrogel coating process for 3D printed medical-grade poly(ε-caprolactone). Beilstein J. Org. Chem. **2021**, *17*, 2095–2101.

[268] Wolski, K.; Gruszkiewicz, A.; Zapotoczny, S. Conductive polythiophene-based brushes grafted from an ITO surface via a self-templating approach. Polym. Chem. **2015**, *6*(43), 7505–7513.

[269] Haigh, J.N.; Dargaville, T.R.; Dalton, P.D. Additive manufacturing with polypropylene microfibers. Mater. Sci. Eng. C **2017**, *77*, 883–887.

[270] Hochleitner, G.; Youssef, A.; Hrynevich, A.; Haigh, J.N.; Jungst, T.; Groll, J.; Dalton, P.D. Fibre pulsing during melt electrospinning writing. BioNanoMaterials **2016**, *17*(3–4).

[271] Hrynevich, A.; Elçi, B.Ş.; Haigh, J.N.; McMaster, R.; Youssef, A.; Blum, C.; Blunk, T.; Hochleitner, G.; Groll, J.; Dalton, P.D. Dimension-Based Design of Melt Electrowritten Scaffolds. Small **2018**, *14*(22), 1800232.

[272] Murphy, S.M.; Kiely, M.; Jakeman, P.M.; Kiely, P.A.; Carson, B.P. Optimization of an in vitro bioassay to monitor growth and formation of myotubes in real time. Biosci. Rep. **2016**, *36*(3).

[273] Kuete, V.; Karaosmanoğlu, O.; Sivas, H. Anticancer Activities of African Medicinal Spices and Vegetables. In *Medicinal Spices and Vegetables from Africa*; Elsevier, 2017; 271–297.

[274] Syed, O.; Walters, N.J.; Day, R.M.; Kim, H.-W.; Knowles, J.C. Evaluation of decellularization

protocols for production of tubular small intestine submucosa scaffolds for use in oesophageal tissue engineering. Acta Biomater. **2014**, *10*(12), 5043–5054.

[275] Cha, S.H.; Lee, H.J.; Koh, W.-G. Study of myoblast differentiation using multi-dimensional scaffolds consisting of nano and micropatterns. Biomater. Res. **2017**, *21*(1), 1.

[276] Berthold, J.; Olsson, R.J.O.; Salmén, L. Water Sorption to Hydroxyl and Carboxylic Acid Groups in Carboxymethylcellulose (CMC) Studied with NIR-spectroscopy. Cellulose **1998**, *5*(4), 281–298.

[277] Prolongo, S.; Jiménez-Suárez, A.; Moriche, R.; Ureña, A. Influence of Thickness and Lateral Size of Graphene Nanoplatelets on Water Uptake in Epoxy/Graphene Nanocomposites. Appl. Sci. **2018**, *8*(9), 1550.

[278] Marmorat, C.; Arinstein, A.; Koifman, N.; Talmon, Y.; Zussman, E.; Rafailovich, M. Cryo-Imaging of Hydrogels Supermolecular Structure. Sci. Rep. **2016**, *6*(1), 25495.

[279] Aston, R.; Sewell, K.; Klein, T.; Lawrie, G.; Grøndahl, L. Evaluation of the impact of freezing preparation techniques on the characterisation of alginate hydrogels by cryo-SEM. Eur. Polym. J. **2016**, *82*, 1–15.

[280] Guerzoni, L.P.B.; Bohl, J.; Jans, A.; Rose, J.C.; Koehler, J.; Kuehne, A.J.C.; Laporte, L. De. Microfluidic fabrication of polyethylene glycol microgel capsules with tailored properties for the delivery of biomolecules. Biomater. Sci. **2017**, *5*(8), 1549–1557.

[281] Chang, E.P.; Holguin, D. Electrooptical Light-Management Material: Low-Refractive-Index Hydrogels. J. Adhes. **2007**, *83*(1), 15–26.

[282] Mazánková, V.; Sťahel, P.; Matoušková, P.; Brablec, A.; Čech, J.; Prokeš, L.; Buršíková, V.; Stupavská, M.; Lehocký, M.; Ozaltin, K.; Humpolíček, P.; Trunec, D. Atmospheric Pressure Plasma Polymerized 2-Ethyl-2-oxazoline Based Thin Films for Biomedical Purposes. Polymers (Basel). **2020**, *12*(11), 2679.

[283] Sun, T.; Zhou, K.; Liu, M.; Guo, X.; Qu, Y.; Cui, W.; Shao, Z.; Zhang, X.; Xu, S. Loading of BMP-2-related peptide onto three-dimensional nano-hydroxyapatite scaffolds accelerates mineralization in critical-sized cranial bone defects. J. Tissue Eng. Regen. Med. **2018**, *12*(4), 864–877.

[284] Cameron, J.; Skabara, P.J. The damaging effects of the acidity in PEDOT:PSS on semiconductor device performance and solutions based on non-acidic alternatives. Mater. Horizons **2020**, *7*(7), 1759–1772.

[285] Singh, R.K.; Kumar, J.; Singh, R.; Kant, R.; Rastogi, R.C.; Chand, S.; Kumar, V. Structure–conductivity correlation in ferric chloride-doped poly(3-hexylthiophene). New J. Phys. **2006**, *8*(7), 112–112.

[286] Shanmugapriya, C.; Velraj, G. FT-IR Spectroscopy and SEM-EDX Studies on Nano Copper Doped Conducting Polymer. Adv. Mater. Res. **2012**, *584*, 541–545.

[287] Shahrim, N.A.; Ahmad, Z.; Wong Azman, A.; Fachmi Buys, Y.; Sarifuddin, N. Mechanisms for doped PEDOT:PSS electrical conductivity improvement. Mater. Adv. **2021**, *2*(22), 7118–7138.

[288] Xu, S.; Shi, X.-L.; Dargusch, M.; Di, C.; Zou, J.; Chen, Z.-G. Conducting polymer-based flexible thermoelectric materials and devices: From mechanisms to applications. Prog. Mater. Sci. **2021**, *121*, 100840.

[289] Hofmann, A.I.; Smaal, W.T.T.; Mumtaz, M.; Katsigiannopoulos, D.; Brochon, C.; Schütze, F.; Hild, O.R.; Cloutet, E.; Hadziioannou, G. An Alternative Anionic Polyelectrolyte for Aqueous PEDOT Dispersions: Toward Printable Transparent Electrodes. Angew. Chemie Int. Ed. **2015**, *54*(29), 8506–8510.

[290] Guo, T.; Lim, C.G.; Noshin, M.; Ringel, J.P.; Fisher, J.P. 3D printing bioactive PLGA scaffolds using DMSO as a removable solvent. Bioprinting **2018**, *10*, e00038.

[291] Patel, A.; Vendrell-Gonzalez, S.; Haas, G.; Marcinczyk, M.; Ziemkiewicz, N.; Talovic, M.; Fisher, J.S.; Garg, K. Regulation of Myogenic Activity by Substrate and Electrical Stimulation In Vitro. Biores. Open Access **2019**, *8*(1), 129–138.

Chapter 8 Appendices

POx-EDOT

Electrochemical characterization of POx-EDOT was investigated via cyclic voltammetry (CV) and impedance spectroscopy (EIS). A previous work by Cuttaz et al. was used as a guidline for the test specifications. The measurements took place under ambient atmospheric conditions. The conventional three electrode cell construction was used. The counter electrode was made of platinum. The isolated reference electrode was an Ag / AgCL electrode. Phosphate-buffered saline (PBS) was used as the electrolyte. EIS was examined with a sinusoidal voltage and a frequency range of 0.1 Hz - 10 kHZ between the working and reference electrodes. CV was examined in a voltage range of -0.6 - 0.8 V and a scan rate of 0.15 V / s. The current response was measured here. 11 cycles were performed. The last cycle was used for further investigation. The measurements were carried out on an AUTOLAB potentiostat-galvanostat (Multi Autolab / M101, Eco Chemie, Netherlands) and the associated software Nova 2.0. Area calculation of the CV was carried out using OriginLab. The relative charge storage capacity (CSC) was calculated over the area of the eleventh cycle. The electrodeposition was carried out at 1 mA / cm² for two minutes. All measurements were made on three independent samples.

For the investigation, POx-EDOT (Mw = 3100 g / mol) was used in various concentrations (1, 25, 50, 75, 100% POx-EDOT) with EDOT in a copolymerization. Visually, a noticeable change in the color and mechanical properties compared to pure PEDOT could be observed during the electrodeposition. A light gray / purple color and a very soft consistency could be observed. Figure XX shows the CV before and after the electrodeposition, as well as the CSC calculation. First of all, it should be noted that a successful electrode deposition with POx-EDOT was successful. A characteristic trapezoidal shape of the CV for the indication of capacitive and residual charge transfer could be determined in all samples. It should be noted, however, that the POx chain has an impact on the general CSC of PEDOT. The CSC compared to pure PEDOT is 7 times smaller. The wt 25% POx-EDOT sample showed the best CSC of approx. 3 mC / cm². This is significantly lower compared to PEDOT / Ce systems. These can have a CSC of approx. 100 mC / cm² at 15wt% CE.

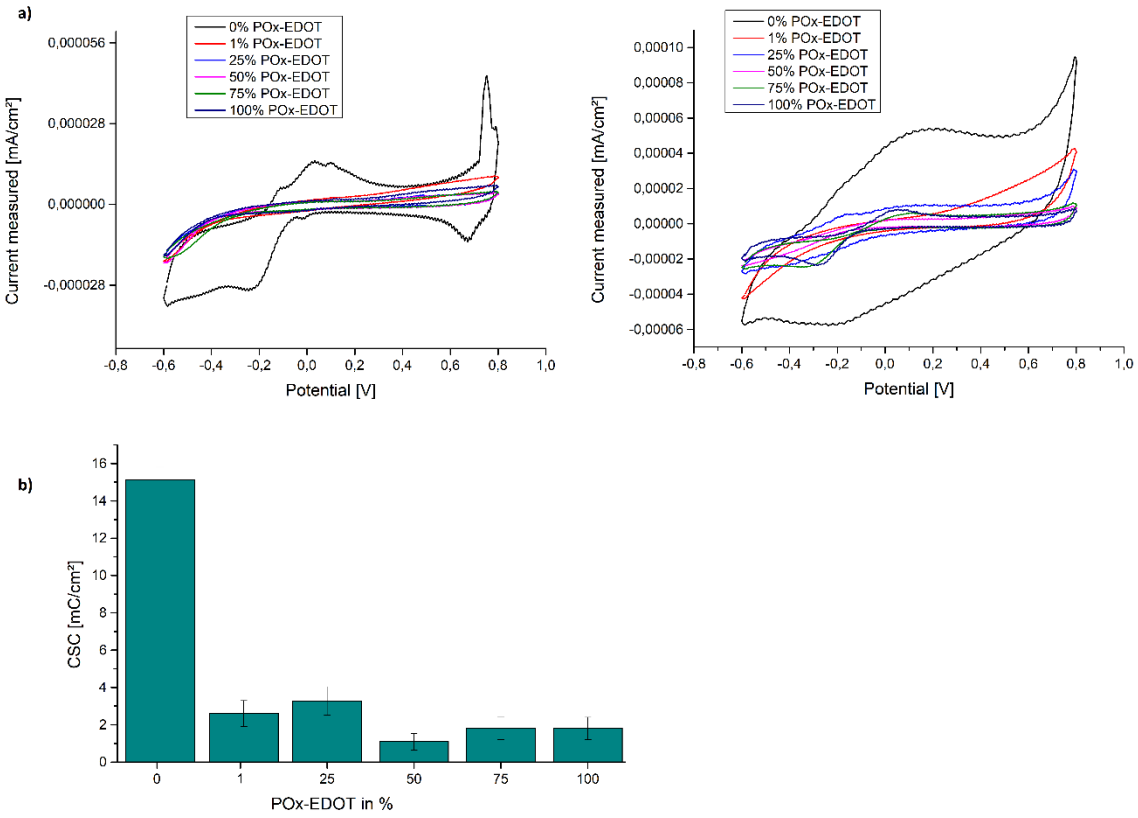
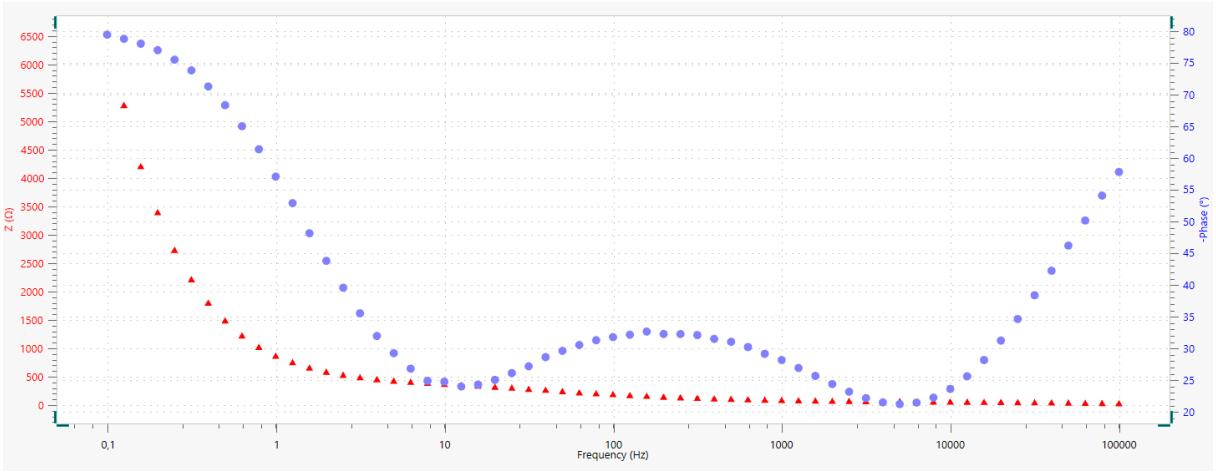
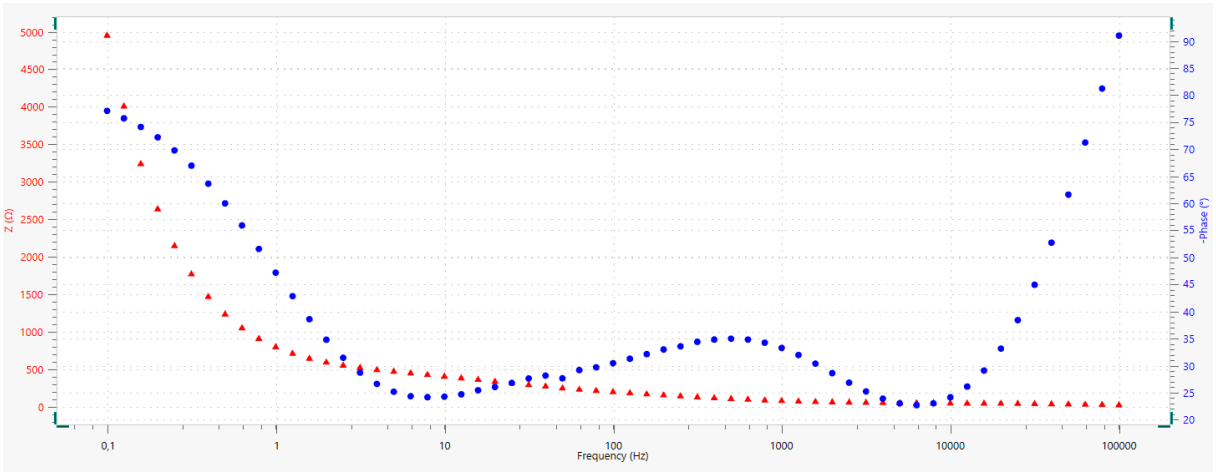


Figure 8.1 electrical properties analysis of end-functionalized PMeOx-EDOT

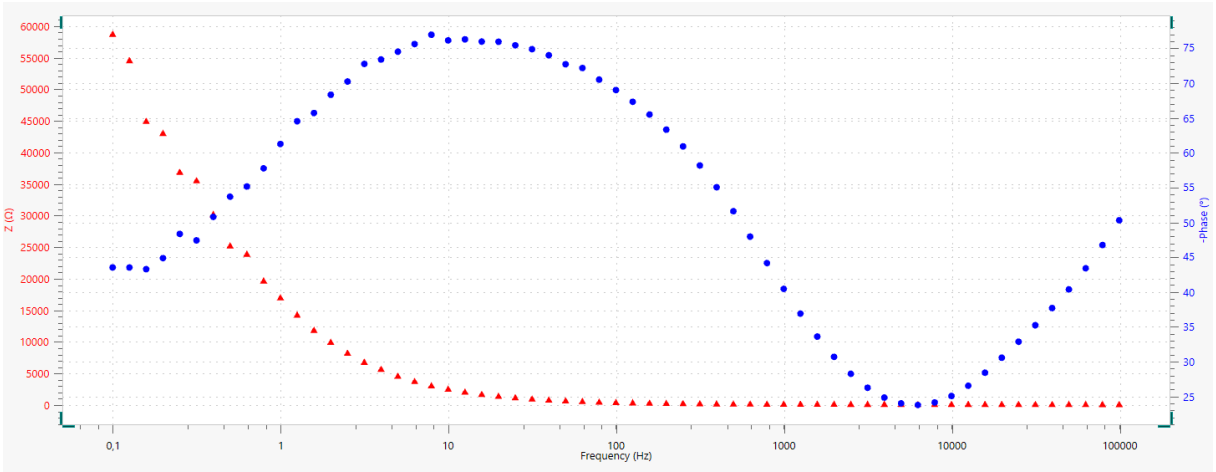
This fact could be due to the insulating properties of POx. A maximum distance of a few nanometers is necessary for intermolecular electron hopping. Due to the problems in the synthesis of the polymer already described in the previous chapter and the resulting poor electrochemical properties, a further investigation of this material was not carried out within the scope of this work. The raw data of the EIS measurement can be found in the appendix. It should also be mentioned here that for a subsequent application in 3D printing, electrochemical polymerization is only of limited use, since a larger amount of material is required for this and chemical oxidative polymerization is therefore more suitable. The advantage of electrodeposition lies in the coating of electrode materials.



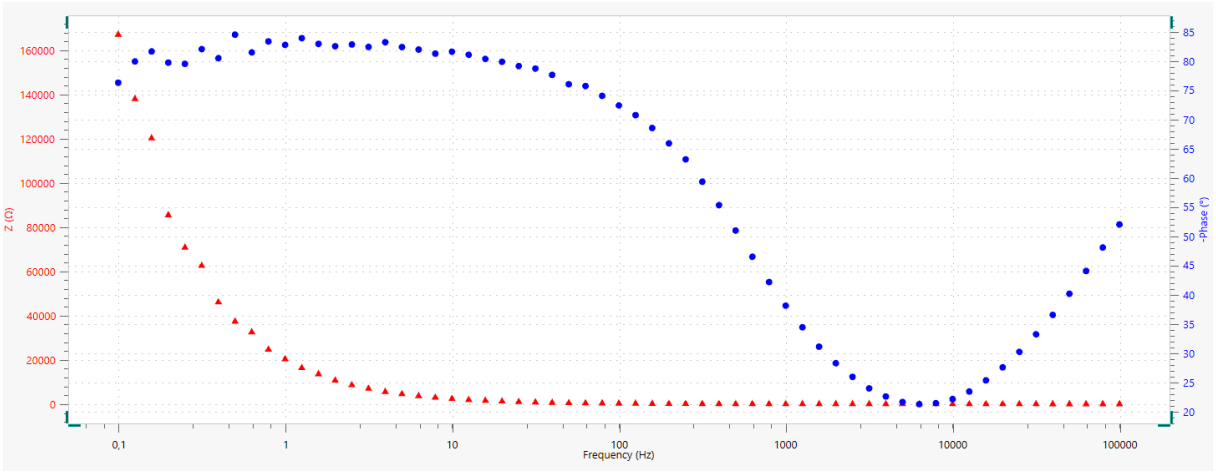
1% POx-EDOT EIS spectroscopy



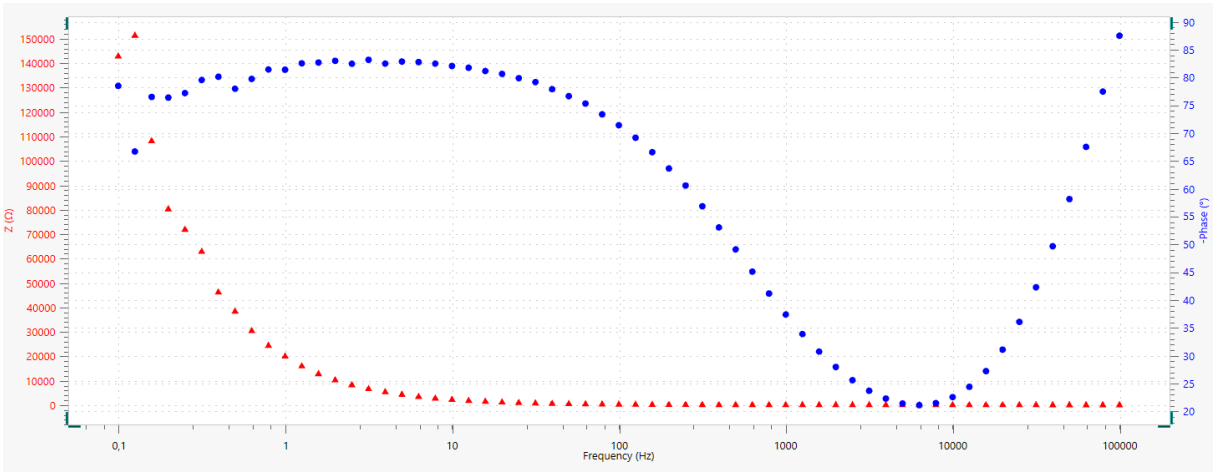
0% POx-EDOT EIS spectroscopy



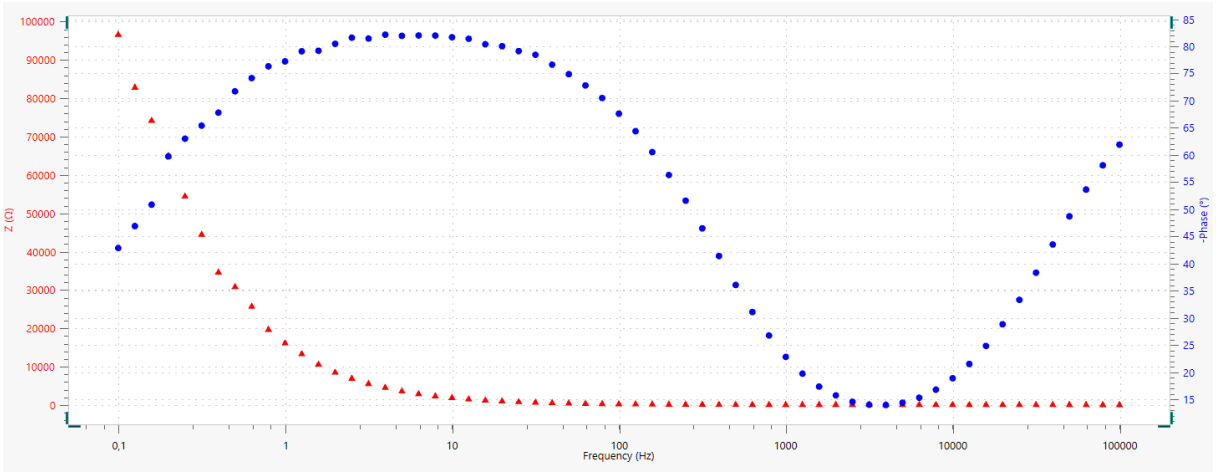
25% POx-EDOT EIS spectroscopy



50% POx-EDOT EIS spectroscopy

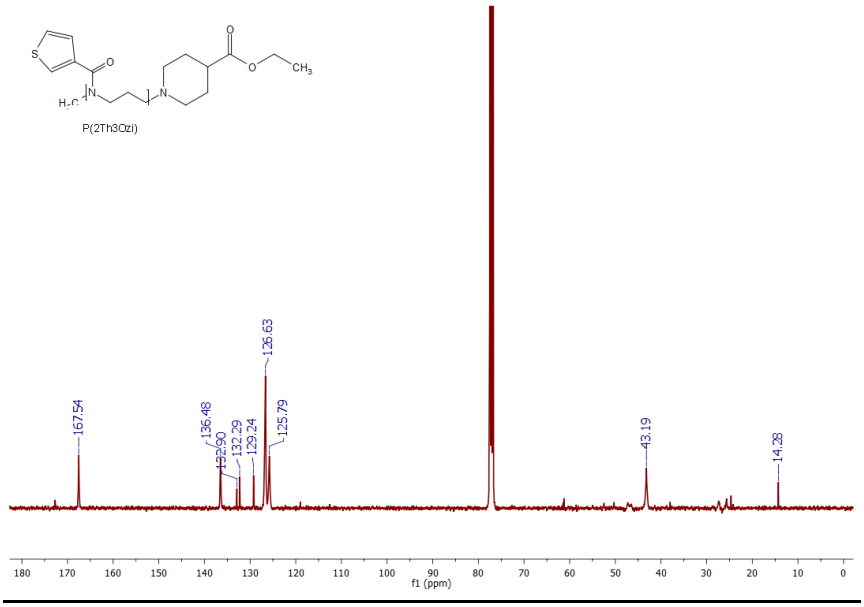


75% POx-EDOT EIS spectroscopy



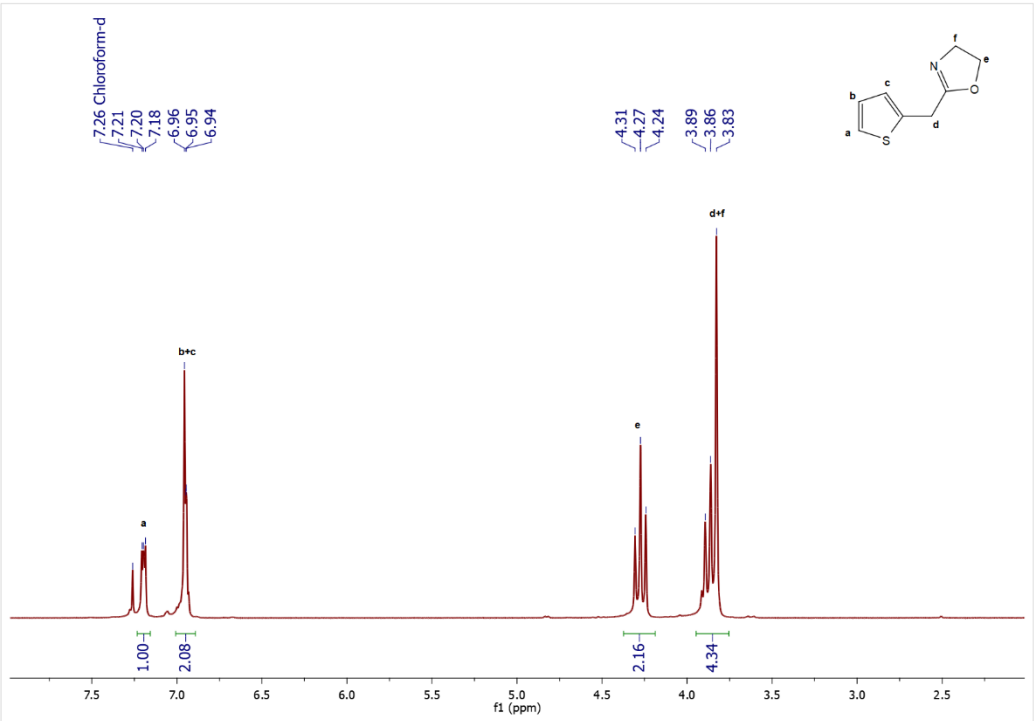
100% POx-EDOT EIS spectroscopy

13C-NMR spectroscopy P2Th3Ozi:

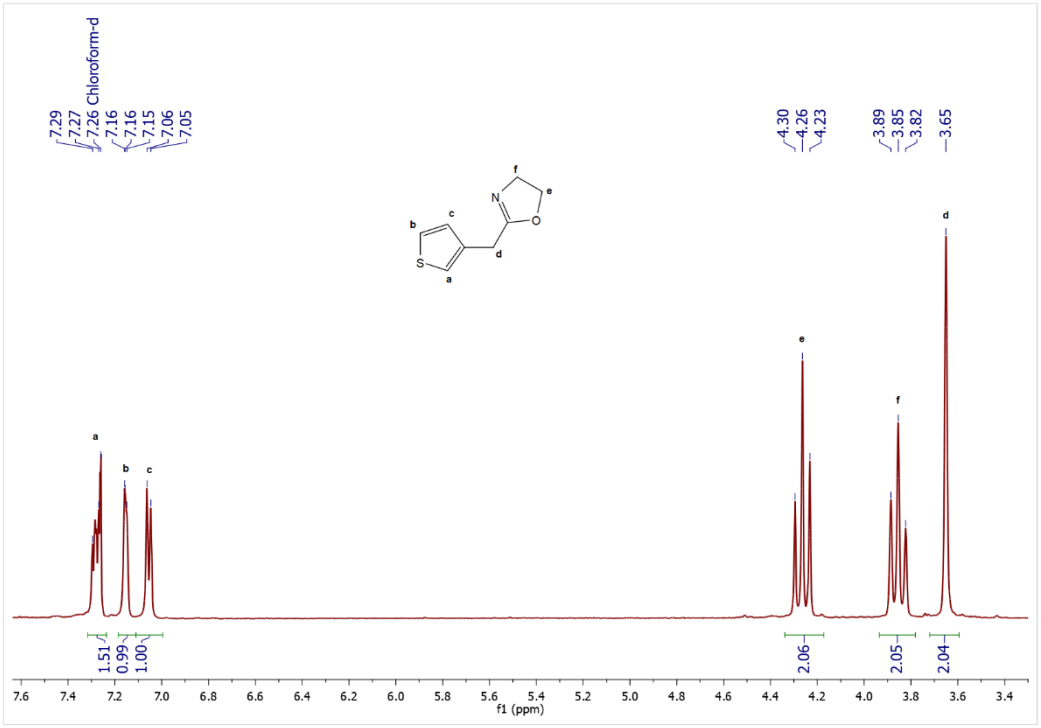


1H-NMR spectroscopy monomers:

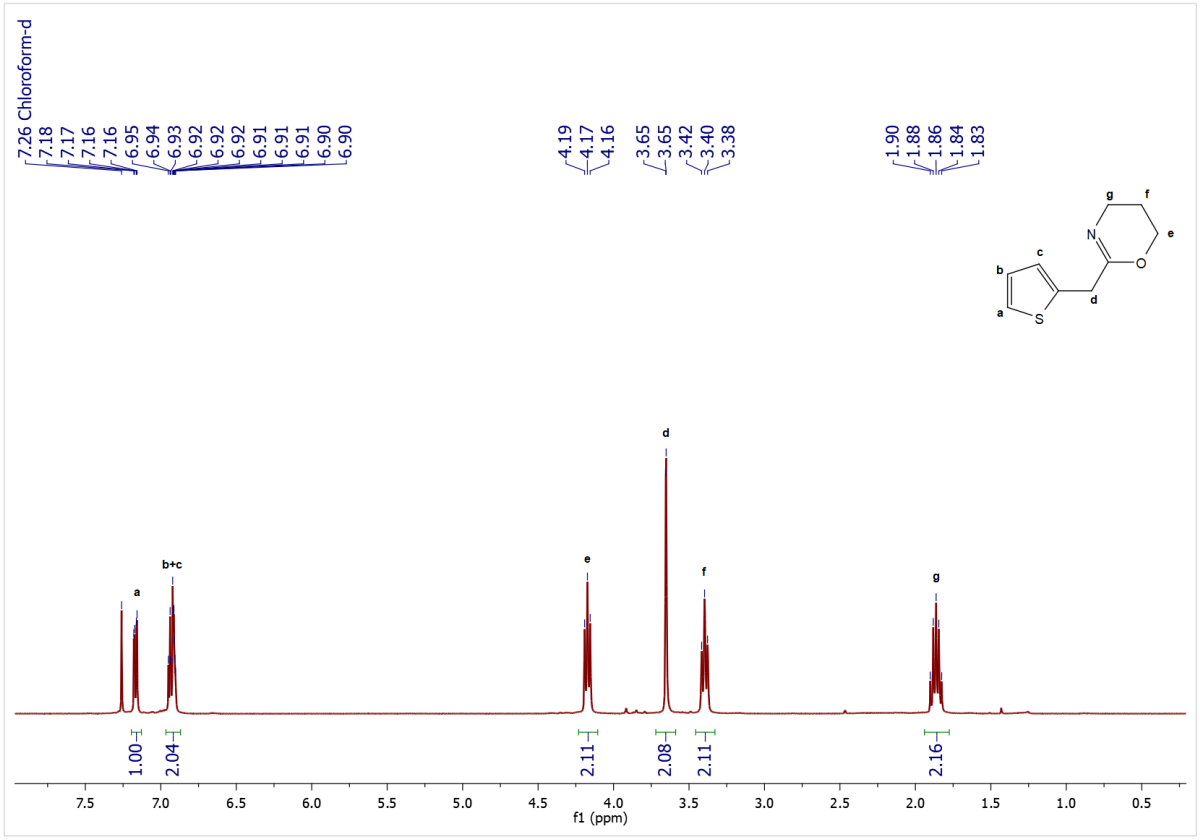
2At2Ox 2-acetothiophene-2-oxazoline



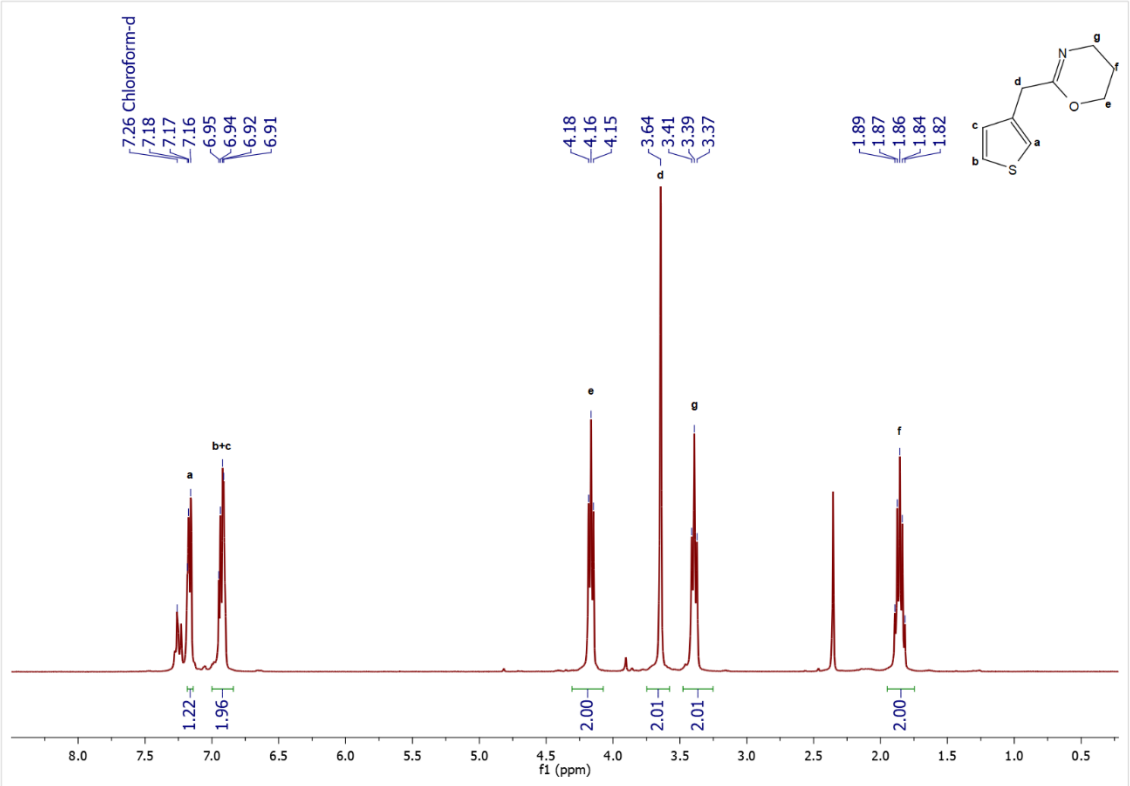
2At3Ox 2-acetothiophene-3-oxazoline



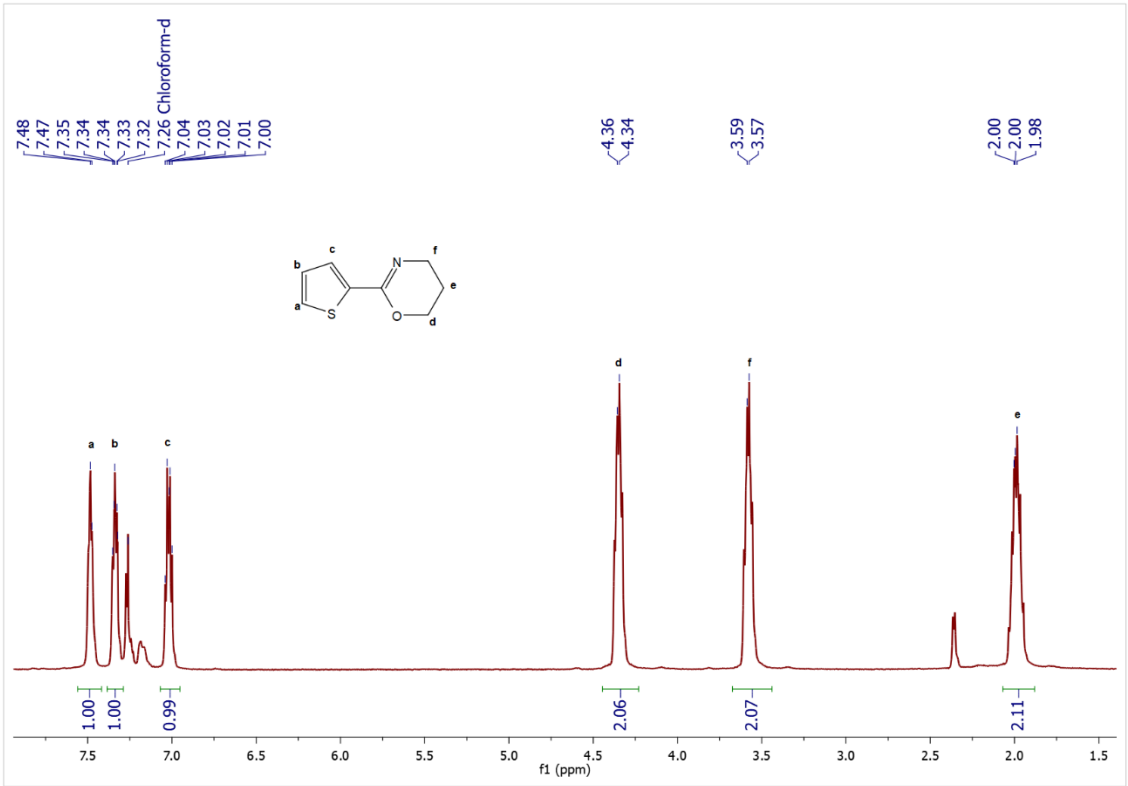
2At2Ozi 2-acetothiophene-2-oxazine



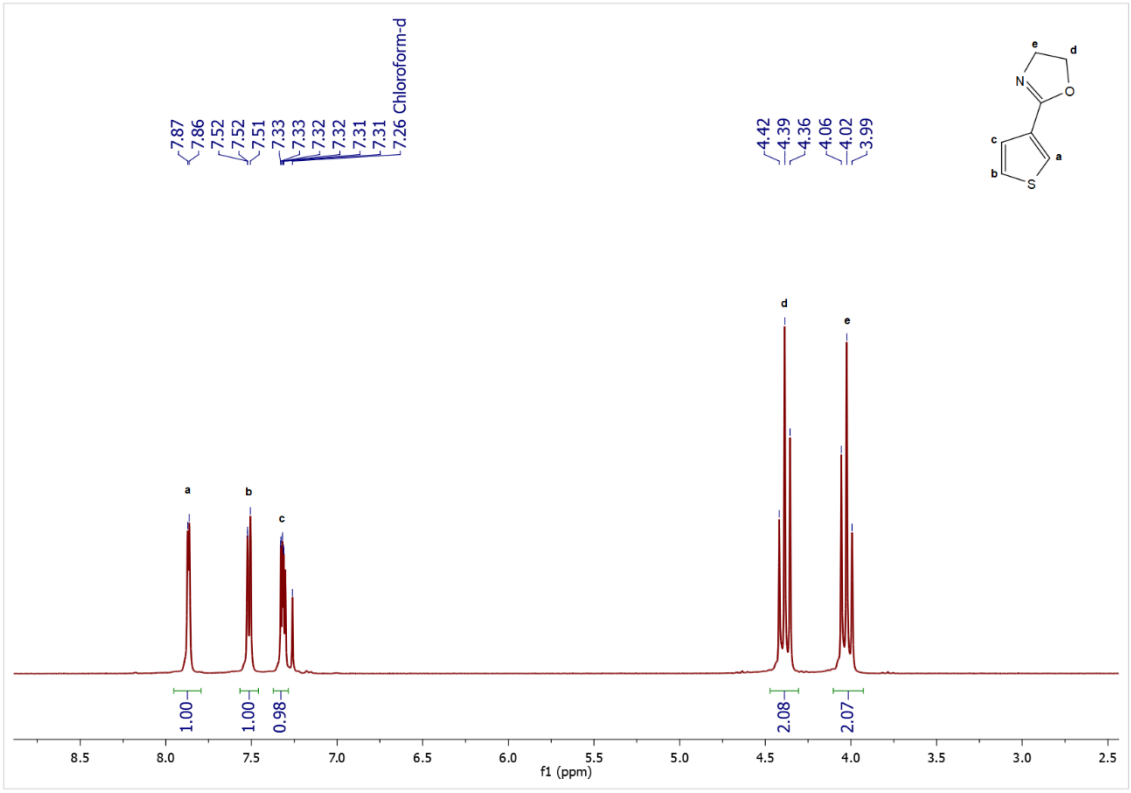
2At3Ozi 2-acetothiophene-3-oxazine



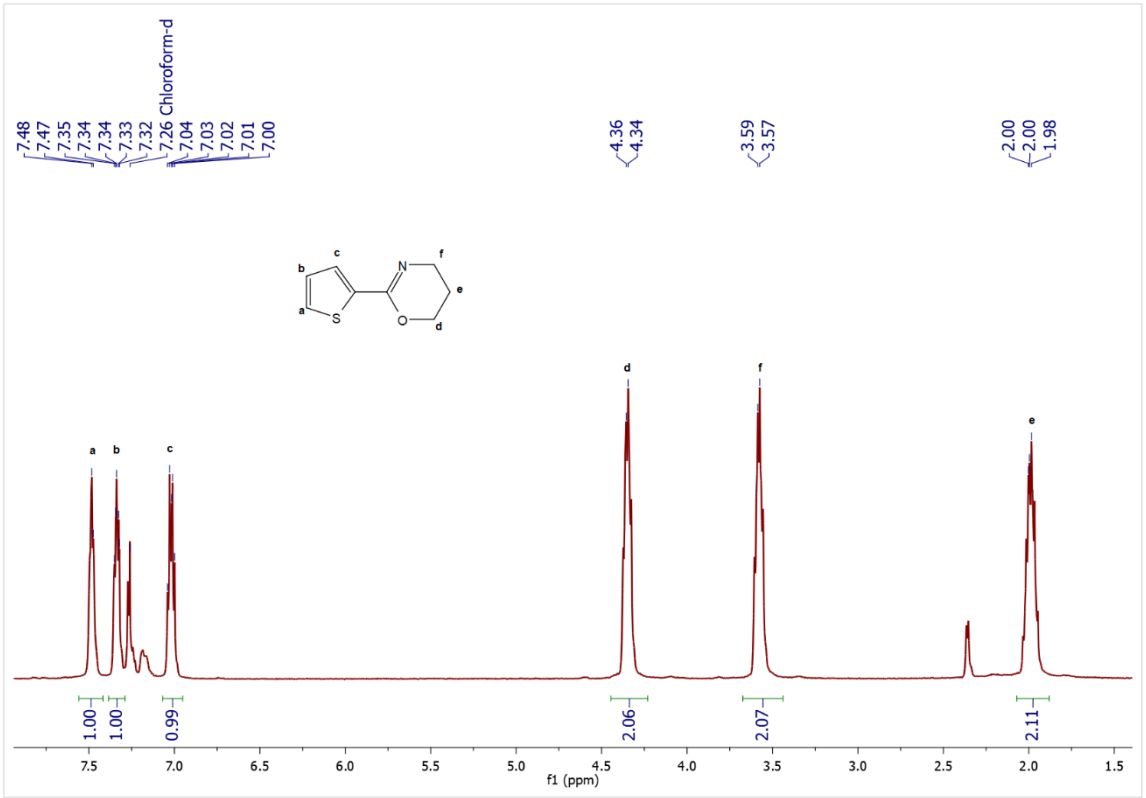
2Th2Ox 2-thiophene-2-oxazoline



2Th3Ox 2-thiophene-3-oxazoline



2Th2Ozi 2-thiophene-2-oxazine



2Th3Ozi 2-thiophene-3-oxazine

